

**THE ROLE OF BONE
MORPHOGENETIC PROTEINS AND
THEIR SIGNALLING IN HUMAN
CANCERS**

by

Sivan Bokobza

Metastasis & Angiogenesis Research Group

Cardiff University School of Medicine

Cardiff

May 2010

Thesis submitted to Cardiff University for the degree of Doctor of

Philosophy

UMI Number: U517328

All rights reserved

INFORMATION TO ALL USERS

The quality of this reproduction is dependent upon the quality of the copy submitted.

In the unlikely event that the author did not send a complete manuscript and there are missing pages, these will be noted. Also, if material had to be removed, a note will indicate the deletion.



UMI U517328

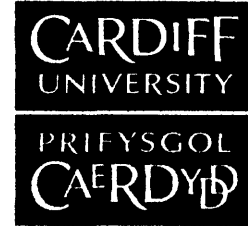
Published by ProQuest LLC 2013. Copyright in the Dissertation held by the Author.
Microform Edition © ProQuest LLC.

All rights reserved. This work is protected against
unauthorized copying under Title 17, United States Code.



ProQuest LLC
789 East Eisenhower Parkway
P.O. Box 1346
Ann Arbor, MI 48106-1346

**NOTICE OF SUBMISSION OF THESIS FORM:
POSTGRADUATE RESEARCH**



APPENDIX 1:

Specimen layout for Thesis Summary and Declaration/Statements page to be included in a Thesis

DECLARATION

This work has not previously been accepted in substance for any degree and is not concurrently submitted in candidature for any degree.

Signed Swag (candidate) Date 11/08/10

STATEMENT 1

This thesis is being submitted in partial fulfillment of the requirements for the degree of (insert MCh, MD, MPhil, PhD etc, as appropriate)

Signed Swag (candidate) Date 11/08/10

STATEMENT 2

This thesis is the result of my own independent work/investigation, except where otherwise stated. Other sources are acknowledged by explicit references.

Signed Swag (candidate) Date 11/08/10

STATEMENT 3

I hereby give consent for my thesis, if accepted, to be available for photocopying and for inter-library loan, and for the title and summary to be made available to outside organisations.

Signed Swag (candidate) Date 11/08/10

STATEMENT 4: PREVIOUSLY APPROVED BAR ON ACCESS

I hereby give consent for my thesis, if accepted, to be available for photocopying and for inter-library loans after expiry of a bar on access previously approved by the Graduate Development Committee.

Signed Swag (candidate) Date 11/08/10

Acknowledgements

Firstly, I would like to thank my supervisors Professor Wen G. Jiang and Professor Howard Kynaston for their guidance and support throughout the three years of my study. I greatly enjoyed being a part of the Metastasis and Angiogenesis Research Group and it was a privilege for me to pursue my PhD in this laboratory. I believe it will act as a great stepping stone for my future career. Furthermore, I'd especially like to thank Dr Lin Ye for his unwavering kindness, time, and help every step of the way, no matter how busy he was himself. This work would not have been possible without him and I owe him greatly. I am also grateful to Dr Andrew Sanders, Miss Astrid Escudero-Esparza, Miss Siobhan Webb, and Miss Kimberley Lewis for their wonderful friendship and support. Finally, I'd like to dedicate this work to my parents, whose belief, encouragement, and pride in everything I do, has gotten me to where I am today. They mean the world to me.

This work was kindly supported by the Desna Robins Jones Charitable Trust.

Publications

Full papers (published or accepted):

Bokobza S.M., Ye L., Kynaston H.E., Mansel R.E., Jiang W.G. (2009). Reduced expression of BMPR-IB correlates with poor prognosis and increased proliferation of breast cancer cells. *Cancer Genomics and Proteomics* **6(2):101-8.**

Bokobza, S.M., Ye, L., Jiang, W. G (2009). When BMP Signalling Goes Wrong: The Intracellular and Molecular Mechanisms of BMP Signalling in Cancer (review). *Current Signal Transduction Therapy* **4(3): 174-195(22)**

Ye L, **Bokobza S.M.,** Jiang W.G (2009). Bone morphogenetic proteins in development and progression of breast cancer and therapeutic potential (review). *Int J Mol Med* **24(5):591-7.**

L Ye, **Bokobza S.M.,** Jin Li, Moazzam Muhammad, Jinfeng Chen, Robert E. Mansel and Wen G. Jiang. Bone morphogenetic protein-10 (BMP-10) inhibits aggressiveness of breast cancer cells and correlates to poor prognosis in breast cancer. Accepted by Cancer Science.

Bokobza, S.M., Ye, L., Jiang, W.G, and Kynaston, H.GDF-9 promotes growth of prostate cancer cells by protecting them from apoptosis. Accepted by Journal of Cellular Physiology.

Bokobza, S.M., Ye, L., Jiang, W.G, and Kynaston, H. GDF-9 promotes adhesion and motility of prostate cancer cells via FAK and Paxillin by Smad-dependent pathway. Accepted by Oncology Reports.

Full papers submitted and in preparation:

Bokobza, S.M., Ye, L., Jiang, W.G, and Kynaston, H. GDF-9 induces epithelial mesenchymal transition (EMT) in prostate cancer cells. Submitted to *Molecular and Cellular Biochemistry*.

Abstracts and conference presentations

BMPR-II Mediates Positive Regulation on *in vitro* Cell Growth, the potential implications for Breast Cancer. December, 2009. **Bokobza, S.M., Ye, L., Jiang, W. G.** San Antonio Breast Cancer Symposium (SABCS), San Antonio, Texas, USA.

Reduced expression of BMPR-IB in breast cancer correlates with poor prognosis. **Bokobza, S.M., Ye, L., Jiang, W. G.** November, 2008. National Cancer Research Institute (NCRI), Birmingham, United Kingdom.

Reduced expression of BMPRIIB in breast cancer correlates with poor prognosis. **Bokobza, S.M., Ye, L., Jiang, W. G.** April, 2008. Wales Cancer Conference, Cardiff, Wales.

Growth and Differentiation Factor-9a (GDF-9a) promotes adhesion of the PC-3 prostate cancer cell line, an Electrical Cellular Impedance Sensing study. **Bokobza, S.M., Ye, L., Jiang, W. G.** August, 2007. British Prostate group (BPG), Bristol, United Kingdom.

Summary

The majority of advanced prostate cancers metastasise to the bone. Mediators of bone remodelling, the bone morphogenetic proteins (BMPs) have extensively been implicated in the progression and metastasis of prostate cancer. Due to the clear importance of BMPs in prostate cancer, this study aims to investigate the effects of GDF-9, a relatively unstudied member of this family, on prostate cancer cells.

Endogenous GDF-9 expression was altered by over-expression using cloning in PC-3 cells, and gene silencing using ribozyme transgenes, in both PC-3 and DU-145 cells. Functional assays were then carried out on these cells to determine any changes in their biological properties. Furthermore, recombinant GDF-9 (rh-GDF-9) was generated in order to treat the cells and confirm the effect it has on prostate cancer cell biological properties as well as any as any mechanisms and downstream signalling.

Both endogenous and exogenous GDF-9 led to a promotion in prostate cancer cell adhesion, invasion, motility, and growth. GDF-9 mediated growth promotion was shown to correlate with an increase in cell cycle progression via up-regulation of Cyclin D1, and protection from caspase 3 mediated apoptosis in a Smad-independent manner. Furthermore, GDF-9 associated cell adhesion, motility, and invasion, was shown to involve FAK, paxillin, and EMT and its associated inducers. These effects act to promote the aggressiveness of PC-3 cells, aiding in their progression and possibly metastasis.

These results suggest that GDF-9 is involved in prostate cancer progression via activation of a complex network of signalling pathways and molecules. This provides further proof of the importance of BMP signalling and suggests that perhaps novel treatments for prostate cancer based on BMPs should be investigated. In addition, it sheds some light on the use of BMPs as prognostic indicators of disease, aiding in diagnosis and treatment. Whether or not this would include GDF-9 requires further investigation.

CONTENTS

DECLARATION	i
ACKNOWLEDGEMENTS	ii
PUBLICATIONS AND PRESENTATIONS	iii
SUMMARY	vi
LIST OF FIGURES	xi
LIST OF TABLES	xvi
ABBREVIATIONS	xvii
Chapter 1 General Introduction	1
1.1 Prostate cancer	2
1.1.1 Epidemiology and risk factors	2
1.1.2 Biology, histology and function of the prostate	4
1.1.3 The biology of prostate cancer	8
1.1.4 Prostate cancer detection	9
1.1.5 Prostate cancer grading and staging system	14
1.1.6 Treatment and management of prostate cancer	20
1.2 Cancer metastasis	28
1.2.1 Local invasion	29
1.2.2 Cell matrix adhesion and ECM degradation	30
1.2.3 Cell migration and motility	31
1.2.4 Invasion and survival in the circulation	32
1.2.5 Extravasation and colonization of distant site	33
1.3 Prostate cancer metastasis	34
1.3.1 Why the bone?	34
1.3.2 Cell biology of bone development	35
1.3.3 Bone remodeling; bone formation and resorption	40
1.3.4 Bone metastases	44
1.4 The Transforming growth factor- β superfamily	48
1.4.1 The Bone morphogenetic protein family	49
1.4.2 BMP receptors and their structure	52
1.4.3 BMP signalling pathway	56
1.4.4 Regulation of the BMP pathway	66
1.4.5 Aberrant BMP signalling in prostate cancer	69
1.5 Growth and differentiation factor-9; a member of the BMP family	76
1.5.1 GDF-9 structure and signalling	76
1.6 Aims and objectives	79

Chapter 2 Materials and methods	81
2.1 General materials	82
2.1.1 Cell lines	82
2.1.2 Primers	82
2.1.3 Antibodies	86
2.2 Standard reagents and solutions	89
2.2.1 Solutions for use in cell culture	89
2.2.2 Solutions for use in molecular biology	89
2.2.3 Solutions for use in cloning	90
2.2.4 Solutions for use in protein work	91
2.2.5 Solutions for purification of His-tagged recombinant protein	92
2.2.6 Solutions for use in Immuno-cytochemical staining	93
2.3 Cell culture, maintenance and storage	93
2.3.1 Preparation of growth media and cell maintenance	93
2.3.2 Adherent cell trypsinisation and cell counting	94
2.3.3 Storing cells in liquid nitrogen and cell resuscitation	95
2.4 Methods for RNA detection	96
2.4.1 Total RNA isolation	96
2.4.2 RNA quantification	97
2.4.3 Reverse transcription of RNA for production of cDNA	98
2.4.4 Polymerase chain reaction (PCR)	99
2.4.5 Agarose gel electrophoresis and DNA visualisation	100
2.4.6 Gel extraction of DNA	101
2.4.7 Q-PCR	102
2.5 Methods for protein detection	107
2.5.1 Protein extraction and preparation of cell lysates	107
2.5.2 Protein quantification	108
2.5.3 Preparing immune-precipitates	109
2.5.4 SDS-PAGE	109
2.5.5 Western blotting	111
2.5.6 Protein staining	113
2.5.7 Protein detection using specific immune-probing	114
2.5.8 Chemiluminescent protein detection	115
2.5.9 Immuno-cytochemical staining	116
2.5.10 Immuno-flourescent staining	117
2.6 Alteration of gene expression	118
2.6.1 Knocking-down gene expression using ribozyme transgenes	118
2.6.2 Gene over-expression	120
2.7 TOPO TA gene cloning and generation of stable transfected cell lines	121
2.7.1 TOPO cloning reaction	123
2.7.2 Transformation of chemically competent <i>E.Coli</i>	123
2.7.3 Colony selection and analysis	124

2.7.4 Plasmid purification and amplification	125
2.7.5 Transfection of mammalian cell lines using electroporation	126
2.7.6 Establishment of a stable expression mammalian cell line	126
2.8 Generating human recombinant GDF-9	129
2.8.1 TOPO TA cloning	129
2.8.2 Collection of condensed media containing rh-GDF-9	129
2.8.3 Condensing rh-GDF-9 containing media	130
2.8.4 Purification of rh-GDF-9 using HiTrap chelating HP column	131
2.8.5 Desalting and buffer exchange	133
2.8.6 Quantification of rh-GDF-9	134
2.9 <i>In vitro</i> cell function assays	135
2.9.1 <i>In vitro</i> adhesion assay	135
2.9.2 <i>In vitro</i> invasion assay	136
2.9.3 <i>In vitro</i> cell growth assay	137
2.9.4 <i>In vitro</i> cell motility assay using cytodex-2 beads	138
2.9.5 ECIS	138
2.9.6 Analysing apoptosis with flow cytometry	139
2.9.7 Analysing the cell cycle using PI	140
2.9.8 Hoechst staining for apoptotic cells	141
2.9.9 The Smad3 inhibitor	141
Chapter 3 Altering the expression of GDF-9 in prostate cancer cells	142
3.1 Introduction	143
3.2 Materials and methods	145
3.3 Results	148
3.4 Discussion	163
Chapter 4 Effects of targeting GDF-9 on the proliferative, adhesive, invasive, and motile capacity of prostate cancer cells.	166
4.1 Introduction	167
4.2 Materials and methods	168
4.3 Results	170
4.4 Discussion	183
Chapter 5 Generating recombinant GDF-9	186
5.1 Introduction	187
5.2 Materials and methods	189
5.3 Results	191
5.4 Discussion	209

Chapter 6 GDF-9 promotes prostate cancer cell growth by protecting them from apoptosis	211
6.1 Introduction	212
6.2 Materials and methods	212
6.3 Results	214
6.4 Discussion	230
Chapter 7 GDF-9 promotes cell-matrix adhesion, invasion, and motility of prostate cancer cells by up-regulating adhesion and EMT molecules	232
7.1 Introduction	234
7.2 Materials and methods	234
7.3 Results	236
7.4 Discussion	258
Chapter 8 General discussion	262
8.1 Effect of altering expression of GDF-9 on prostate cancer cells	264
8.2 Effect of GDF-9 on cell cycle	265
8.3 Effect of GDF-9 on apoptosis	266
8.4 Signalling pathway of GDF-9 in prostate cancer cells	268
8.5 Effect of GDF-9 on FAK and paxillin mediated cell movement	270
8.6 Effect of GDF-9 on Rho GTPases and ROCK	271
8.7 Effect of GDF-9 on EMT associated molecules	272
8.8 Main findings/significance of this study	276
8.9 Future work	277
Bibliography	280
Appendix	319

List of Figures

Chapter 1:

- Figure 1.1: Number of deaths and age-specific mortality rates, prostate cancer.* 4
- Figure 1.2: schematic diagram of the different cell types present in the prostatic epithelium.* 8
- Figure 1.3: Schematic drawing of Gleason histological grading.* 15
- Figure 1.4: Diagram showing and explaining the three categories of TNM staging of prostate cancer.* 18
- Figure 1.5: Schematic diagram of the negative feedback loop in androgen production.* 27
- Figure 1.6: The process of metastasis is characterised by several basic steps.* 31
- Figure 1.7: Regulation of osteoclastogenesis that occurs during bone remodelling.* 43
- Figure 1.8: Mechanisms of osteoblastic metastases in prostate cancer.* 48
- Figure 1.9: Structural diagram of the type-I and type-II TGF- β receptors.* 54
- Figure 1.10: Structural diagram of the three Smad subtypes.* 58
- Figure 1.11: BMP signaling and its pathway.* 63

Chapter 2:

- Figure 2.1: Diagram showing function of the u-probe during DNA amplification using Q-PCR.* 105
- Figure 2.2: Detection of transcript levels from a range of standard samples using the iCycler^{IQ} thermal cycler.* 106
- Figure 2.3: Diagram depicting process of western blotting; the transferring of proteins onto a nitrocellulose membrane.* 113
- Figure 2.4: Secondary structure of hammerhead ribozyme with bound substrate.* 120
- Figure 2.5: Schematic of the pEF6 plasmid (taken from pEF6/V5-His TOPO TA Expression Kit protocol).* 122

<i>Figure 2.6: Flow chart summarising cloning and production of a stable expression mammalian cell line.</i>	128
<i>Figure 2.7: Diagram showing set-up of vivaflow 50 system.</i>	131
<i>Figure 2.8: Figure depicting vivaspin centrifugal concentrator system.</i>	134
<i>Figure 2.9: Schematic diagram showing in vitro invasion assay.</i>	137
Chapter 3:	
<i>Figure 3.1: LA-PCR products of GDF-9 coding sequence on agarose gel.</i>	151
<i>Figure 3.2: Agarose gel showing PCR of E.Coli analysis.</i>	152
<i>Figure 3.3: Purified GDF-9 SCD S-3 plasmid visualised on agarose gel.</i>	153
<i>Figure 3.4: Figure confirming extracted plasmid has GDF-9 sequence.</i>	154
<i>Figure 3.5: Ribozyme transgene synthesis.</i>	156
<i>Figure 3.6: Screen of different prostate cell lines for GDF-9 expression.</i>	159
<i>Figure 3.7: Verification of GDF-9 over-expression in PC-3 cells.</i>	160
<i>Figure 3.8: Verification of GDF-9 knockdown in PC-3 and DU-145 cells.</i>	161
<i>Figure 3.9: Verification of GDF-9 knockdown protein levels using ICC with an anti-GDF-9 antibody.</i>	162
Chapter 4:	
<i>Figure 4.1: Effect of GDF-9 on in vitro cell growth of PC-3 cells.</i>	174
<i>Figure 4.2: Effect of knocking-down GDF-9 on in vitro cell growth of DU-145 cells.</i>	175
<i>Figure 4.3: Effect of GDF-9 on in vitro cell adhesion of PC-3 cells.</i>	176
<i>Figure 4.4: Effect of knocking-down GDF-9 on in vitro cell adhesion of DU-145 cells.</i>	177
<i>Figure 4.5: Effect of GDF-9 on cell invasiveness of PC-3 cells.</i>	178
<i>Figure 4.6: Effect of GDF-9 on cell invasiveness of DU-145 cells.</i>	179
<i>Figure 4.7: Effect of GDF-9 on in vitro cell motility of PC-3 cells.</i>	180
<i>Figure 4.8: Effect of GDF-9 on cell motility of DU-145 cells.</i>	181
<i>Figure 4.9: Effect of GDF-9 on electrical resistance of PC-3 cells using ECIS.</i>	182
<i>Figure 4.10: Effect of GDF-9 on electrical resistance of DU-145 cells using ECIS.</i>	183

Chapter 5:

<i>Figure 5.1: LA-PCR product of GDF-9 NSCD coding sequence.</i>	193
<i>Figure 5.2: Agarose gel showing RT-PCR of E.Coli colony analysis.</i>	194
<i>Figure 5.3: Purified GDF-9 NSCD plasmids visualised on agarose gel.</i>	195
<i>Figure 5.4: Verification of GDF-9 over-expression in 3T3 transfected cells.</i>	196
<i>Figure 5.5: Western blot analysis verifying purification of rh-GDF-9.</i>	198
<i>Figure 5.6: Western blot analysis using anti-GDF-9 antibody to verify purification of rh-GDF-9.</i>	199
<i>Figure 5.7: Coomassie blue stained SDS-PAGE of rh-GDF-9 purification.</i>	200
<i>Figure 5.8: Graph showing quantification of rh-GDF-9.</i>	201
<i>Figure 5.9: Effect of rh-GDF-9 on in vitro cell growth of PC-3 cells.</i>	204
<i>Figure 5.10: Effect of rh-GDF-9 on in vitro cell growth of DU-145 cells.</i>	205
<i>Figure 5.11: Effect of rh-GDF-9 on in vitro adhesive capacity of PC-3 cells.</i>	206
<i>Figure 5.12: Effect of rh-GDF-9 on in vitro invasive capacity of PC-3 cells.</i>	207
<i>Figure 5.13: Effect of rh-GDF-9 on in vitro motile capacity of PC-3 cells.</i>	208

Chapter 6:

<i>Figure 6.1: Analysis of cell cycle in PC-3 cells using flow cytometry.</i>	217
<i>Figure 6.2: The effect of GDF-9 on Cyclin D1 expression in PC-3 cells.</i>	218
<i>Figure 6.3: Apoptotic analysis of PC-3 using flow cytometry.</i>	219
<i>Figure 6.4: Apoptotic analysis of rh-GDF-9 on PC-3 cells using flow cytometry.</i>	220
<i>Figure 6.5: Hoechst staining of PC-3 cells for apoptotic cells.</i>	221
<i>Figure 6.6: The effect of GDF-9 on caspase-3 protein levels using western blotting.</i>	222
<i>Figure 6.7: Downstream signalling of GDF-9.</i>	226
<i>Figure 6.8: GDF-9 signalling via MAPK pathway in PC-3 cells.</i>	227
<i>Figure 6.9: Growth assay analysing effect of Smad3 inhibitor on PC-3 cells.</i>	228
<i>Figure 6.10: Role of Smad3 in GDF-9 associated apoptosis.</i>	229

Chapter 7:

<i>Figure 7.1: Expression of FAK and paxillin in transfected prostate cancer cells.</i>	239
<i>Figure 7.2: ICC staining of FAK and paxillin in transfected PC-3 cells.</i>	240
<i>Figure 7.3: Expression of FAK and paxillin in response to rh-GDF-9.</i>	241
<i>Figure 7.4: Q-PCR quantifying mRNA levels of FAK and paxillin.</i>	242
<i>Figure 7.5: Effect of Smad3 inhibitor on the adhesive capacity of PC-3 cells.</i>	243
<i>Figure 7.6: Effect of Smad3 inhibitor on expression of FAK and paxillin in PC-3 cells.</i>	244
<i>Figure 7.7: Q-PCR quantifying mRNA levels of FAK and paxillin in response to Smad 3 inhibitor.</i>	245
<i>Figure 7.8: Immunofluorescent staining of EMT molecules in PC-3 cells.</i>	249
<i>Figure 7.9: Expression of EMT molecules in transfected prostate cancer cells.</i>	250
<i>Figure 7.10: Expression of cadherins in transfected prostate cancer cells.</i>	251
<i>Figure 7.11: Expression of EMT molecules in rh-GDF-9 treated PC-3 cells.</i>	252
<i>Figure 7.12: Q-PCR quantifying mRNA levels of ROCK-1 and RhoC.</i>	253
<i>Figure 7.13: Q-PCR quantifying mRNA levels of ROCK-1 in response to Smad3 inhibitor in PC-3 cells.</i>	254
<i>Figure 7.14: Q-PCR quantifying mRNA levels of E-Cadherin and N-Cadherin.</i>	255
<i>Figure 7.15: Q-PCR quantifying mRNA levels of SLUG and TWIST.</i>	256
<i>Figure 7.16: Western blot analysis demonstrating levels of EMT molecules.</i>	257
Appendix:	
<i>Figure A1: Effect of varying concentration of rh-GDF-9 on PC-3 cells.</i>	320

List of Tables:

Chapter 1:

<i>Table 1.1: Gleason grading system for prostate cancer.</i>	16
<i>Table 1.2: The 2002 TNM classification for adenocarcinoma of the prostate.</i>	19
<i>Table 1.3: All identified BMPs to date and their corresponding receptors and Smads.</i>	51

Chapter 2:

<i>Table 2.1: Details of cell lines used in this study.</i>	83
<i>Table 2.2: Primers for conventional RT-PCR and Q-PCR.</i>	84
<i>Table 2.3: Primers for amplifying GDF-9 coding sequence.</i>	85
<i>Table 2.4: Primers used for ribozyme synthesis.</i>	85
<i>Table 2.5: Primary antibodies used during the course of this study.</i>	86
<i>Table 2.6: Ingredients for resolving gel.</i>	110
<i>Table 2.7: Ingredient for stacking gel.</i>	111

Abbreviations

ActRI: activin A receptor, type I

ActRIB: activin A receptor, type IB

ActRIC: activin A receptor, type IC

ActRIIA: activin A receptor, type IIA

ActRIIB: activin A receptor, type IIB

ALK: Activin receptor-like kinase

ALP: Alkaline phosphatase

AMH: Anti-Mullerian hormone

AP-1: Activator protein-1

AR: Androgen receptor

ATCC: American Type Culture Collection

BAMBI: BMP and activin membrane bound inhibitor

BISC: BMP-induced signaling complexes

BM: Basement membrane

BMP: Bone morphogenetic protein

BMPR-1A: Bone morphogenetic protein receptor, type IA

BMPR-1B: Bone morphogenetic protein receptor, type IB

BMPR-II: Bone morphogenetic protein receptor, type II

Bp: Base pair

BPH: Benign prostatic hypertrophy

BSA: Bovine serum albumin

BSS: Balanced salt solution

CBP: cyclic AMP response element binding protein binding protein

CDKI: Cyclin-dependent kinase inhibitor

CDMP: cartilage-derived morphogenetic protein

CIP1/WAF1: CDKI P21

CO₂: Carbon dioxide

Co-Smad: Common mediator Smad

DD3/PCA3: Dihydrodiol dehydrogenase 3 also known as prostate cancer antigen 3

ddH₂O: Double-distilled water

DAPK: Death associated protein kinase

DEPC: Diethyl pyrocarbonate

DHT: Dihydrotestosterone

DMEM: Dulbecco's modified eagles medium

DMSO: Dimethyl sulphoxide

DNA: Deoxyribonucleic acid

dNTP: Deoxyribonucleoside triphosphate

DRE: Digital rectal examination

E. coli: Escherichia coli

ECACC: European Collection of Animal Cell Culture

ECD: Extracellular domain

ECL: enhanced chemiluminescence

ECM: Extracellular matrix

EDTA: Ethylene diaminetetraacetic acid
EGF: Epidermal growth factor
ELISA: Enzyme-linked immunoabsorbant assay
EMT: Epithelial-mesenchymal transdifferentiation/transformation
ERK: Extracellular regulated MAP kinase
ET-1: Endothelin-1
ETAR: Endothelin receptor type A
FBS: Foetal bovine serum
FGF: Fibroblast growth factor
FITC: Fluorescein isothiocyanate
FOXH1: Forkhead Box H1
G gravity's (unit of relative centrifugal force)
GADD45 β : Growth arrest and DNA-damage-inducible 45 β
GDF: Growth differentiation factor
GFP green fluorescent protein
H₂O₂: Hydrogen peroxide
HAT: Histone acetyl transferase
HCl: Hydrogen acid
HDAC: Histone deacetylase
HDR: High-dose rate
HEPES: N-hydroxyethylpiperazine-N'-2-ethansulphoxide
Hr: hour
HRP: horseradish peroxidase
ID-1/2/3: Inhibitor of differentiation factor
IF: Immunofluorescence
Ig: Immunoglobulin
IGF: Insulin-like growth factor
IGFBP: IGF binding protein
IL: interleukin
IMRT: Intensity-modulated radiotherapy
I-Smad: Inhibitory Smad
IP: Immunoprecipitation
JNK: Jun N-terminal kinases
Kb: kilo-base
kDa: kilo-dalton
LA-PCR: high fidelity long and accurate PCR
LB: Luria-Bertani
LDR: Low-dose rate
LH: Leutenising hormone
LHRH: LH releasing hormone
LIM Kinase 1: LIMK1
LRP: Laparoscopic radical prostatectomy
m: metre
M: Molar
mA: milli-amp
mAb: monoclonal antibody

MAD: Mothers against decapentaplegic homolog
MAPK: Mitogen-activated protein kinase
M-CSF: Macrophage colony-stimulating factor
ME: Mercaptoethanol
mg: Milligram
MH1: Mad homology 1
MH2: Mad homology 2
MIC: Macrophage inhibitory cytokine
MIS: Mullerian inhibiting substance
ml: milli litre
mM: milli molar
MMP: Matrix metalloproteinase
mRNA: Messenger ribonucleic acid
MW: Molecular weight
NaCl: Sodium chloride
NaOH: Sodium hydroxide
NF- κ B: Nuclear factor kappa B
ng: nano-gram
NiSO₄: Nickel Sulphate Heptahydrate
NLK: Nemo-like kinase
OP: osteogenic protein
OPG: osteoprotegerin
PAGE: polyacrylamide gel electrophoresis
Par-4: Prostate apoptosis response-4
PBS: Phosphate buffered saline
PBRT: Proton-beam radiotherapy
PCR: Polymerase chain reaction
PDF: Prostate derived factor
PDGF: Platelet-derived growth factor
PFC: Preformed hetero-oligomeric complexes
PI: Propidium iodide
PIA: Proliferative Inflammatory atrophy
PIN: Prostatic intraepithelial neoplasia
PI3K: Phosphoinositide 3-kinase
PKC: Protein kinase C
PLAB: Placental bone morphogenetic protein
PSA: Prostate specific antigen
PSMA: Prostate specific membrane antigen
PTHrP: Parathyroid hormone related protein
RALP: Robot-assisted LRP
RANK: Receptor activator of nuclear factor- κ B
RANKL: RANK ligand
Rb: Retinoblastoma
rh-BMP: Recombinant human BMP
Rho Guanine nucleotide exchange factor: Rho GEF
Rho GTP activating protein: Rho GAP.

RNA: Ribonucleic acid
 RNase: Ribonuclease
 rpm: Revolutions per minute
 RPMI: Roswell Park Memorial Institute
 R-Smad: Receptor-regulated Smad
 RT: Reverse transcription
 SARA: Smad-anchor for receptor activation
 SBE: Smad binding element
 SD: Standard deviation
 SDS: Sodium dodecyl sulphate
 SHIP: Src homology 2 (SH2) domain-containing 5' inositol phosphatase
 SIP-1: Stress-induced protein 1
 Ski: Sloan-Kettering retrovirus
 Sma: Small family member
 Smad: Sma and MAD
 Smurf: Smad ubiquitin regulatory factor
 SnoN: Ski related novel gene
 STAT: Signal transducer and activator of transcription
 TAB1/2/3: TGF- β activated binding protein
 TAE: Tris/acetate/EDTA electrophoresis buffer
 TAK1: MAPKKK TGF- β activated tyrosine kinase 1
 TBE: Tris/Borate/EDTA electrophoresis buffer
 TBS: Tris-buffered saline
 TE: Tris/EDTA buffer
 TEMED: N,N,N',N'-tetramethylethylenediamine
 TGFBR-I: Transforming growth factor, beta receptor I
 TGFBR-II: Transforming growth factor, beta receptor II
 TGFBR-III: Transforming growth factor, beta receptor III
 TGF- β : Transforming growth factor- β
 TGIF: TGF- β interacting factor
 TIEG: TGF- β inducible early gene
 TIMP: tissue specific inhibitor of matrix metalloproteinase
 TNF- α : Tumour necrosis factor-alpha
 TNM: Tumour, node and metastasis
 TRAF: TNF-receptor associated
 TRAIL: Tumour-necrosis factor-related apoptosis-inducing ligand
 Tob: Transducer of ErbB-2
 tPA: Tissue plasminogen activator
 Tris: Tris-(hydroxymethyl)-aminomethane
 TRITC: Tetra-Rhodamine Isothiocyanate
 TRUS: Trans-rectal ultrasonography
 μ g: microgram
 UICC: American Joint Committee on Cancer and International Union Against Cancer
 μ l: Microlitre
 μ M: Micro molar
 uPA: Urokinase plasminogen activator

UV: Ultraviolet

V: Volt

VEGF: Vascular endothelial growth factor

Wiskott-Aldrich syndrome protein: WASP

Wnt: Wingless-type

WT: Wild type

XIAP: X-linked inhibitor of apoptosis protein

Chapter 1

Introduction

1.1 Prostate Cancer

1.1.1 Epidemiology and risk factors

Prostate cancer is the primary male cancer in the developed world, accounting for 24% of all diagnosed male cancers, and is the second leading cause of death from cancer after lung cancer (Jemal *et al.*, 2009). Several risk factors have been recognized in the development of prostate cancer, the most significant of which include; age, race, diet, family history and place of birth (Wynder *et al.*, 1971).

Age is undoubtedly the most important and clear-cut of these factors with prostate cancer being most prevalent in men aged over 50. A consistent trend is present where clinical diagnosis of the disease increases directly with age. In the US for example, the probability of developing invasive prostate cancer is rare in men under the age of 39, with odds of only 0.01%, whereas this percentage increases to 2.43% in 40-59 year olds, 6.42% in 60-69 year olds and 15.78% in over 70 year olds (Jemal *et al.*, 2009). This trend remains in respect to mortality rates where 93% of prostate cancer deaths occur in men aged 65 and over, so much so that in men over the age of 85, the mortality rate even exceeds that of lung cancer (CR-UK, 2007) (Figure 1.1).

In terms of race, the highest incidence rates are seen in African American men with 60% more cases and double the mortality rate compared to that reported in white men of a similar age (DeChello *et al.*, 2006). Geographically, a variation is seen in the incidence rates of prostate cancer, with rates being far higher in the more developed countries as opposed to the less developed ones. North America has the highest prevalence with a rate of 119.9 per 100,000, followed by Australia and Western Europe with rates of 79.9 and 61.6, respectively. This is in comparison to the rates seen in places like Western Africa and Eastern Asia, where they reach 19.3 and 4.4 cases per 100,000, respectively. Despite this tendency, the more developed countries have much higher survival rates due to the larger proportion of early stage diagnoses and PSA testing that is performed (CR-UK, 2007). This geographical disparity is mainly

present due to dietary, racial, and environmental factors, as well as differences in cancer detection programmes and medical care in these countries.

Environmental and lifestyle factors found to be capable of contributing to prostate cancer development include diet. Several reports have found that high fat intake, dairy products, and butter, have a positive association with the risk of developing prostate cancer. This is thought to be due to the energy released from saturated fats (Whittemore *et al.*, 1995). Meanwhile, vitamins D and E, soy milk, selenium, and lycopene, a carotenoid found in tomatoes, have been reported to modify levels of male sex hormones, and hence inversely correlate with prostate cancer risk (Dagnelie *et al.*, 2004). This is one of the reasons why Asian populations with lower fat and higher soy protein intake than western populations, have lower incidence rates of prostate cancer.

Finally, there are also hereditary factors that have been found to influence the development of prostate cancer. A recent study demonstrated that early onset of prostate cancer risk was increased 2.3 fold in men who reported a history of the disease in either a father or brother (Chen *et al.*, 2008). Several candidate genes have been investigated in order to determine their role in hereditary prostate cancer development. Polymorphisms in genes such as E-cadherin, CDKN1B, CYP17 and the androgen receptor have been reported to have some influence on the risk of developing hereditary prostate cancer (Chang *et al.*, 2001; Chang *et al.*, 2002; Chang *et al.*, 2004; Jonsson *et al.*, 2004).

Although the BRCA genes have been identified as genetic markers for breast cancer, men carrying BRCA1/2 mutations were found to have more aggressive forms of prostate cancer of a higher Gleason score. For example, men with prostate cancer who carry BRCA2 mutations have been shown to have a shorter life expectancy than men with prostate cancer in the general population. It would therefore follow that BRCA1/2 mutations are prognostic indicators of

aggressive prostate cancer, and hence screening male carriers of these mutations for prostate cancer, would be of diagnostic use (Mitra *et al.*, 2008).

Number of deaths and age-specific mortality rates, prostate cancer, UK, 2007

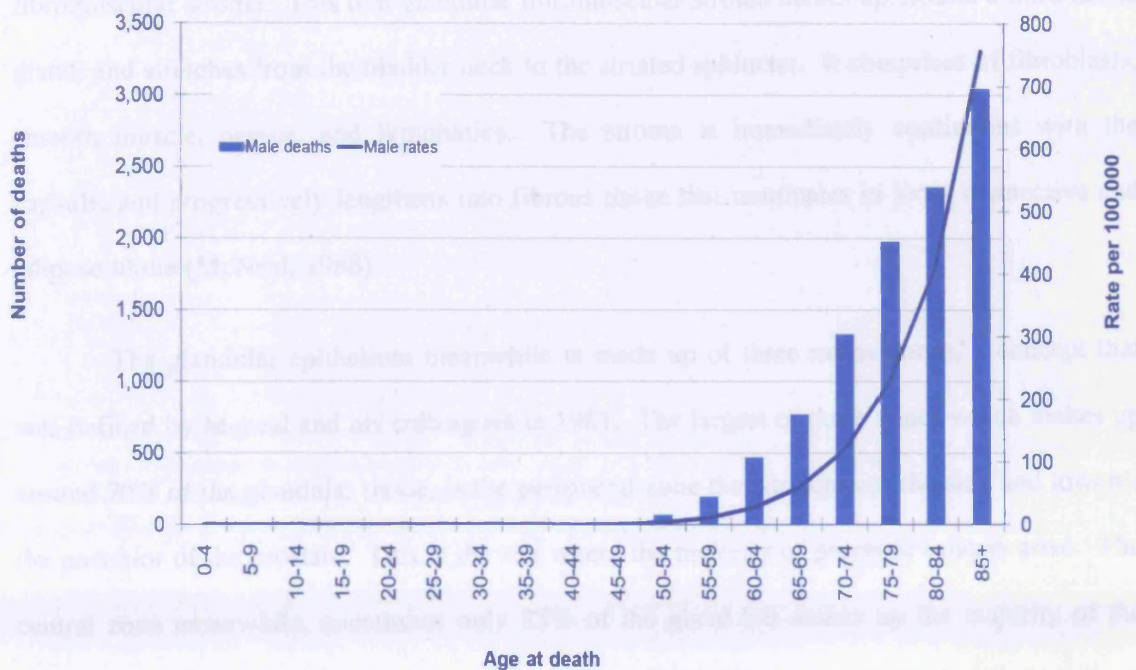


Figure 1.1: Number of deaths and age-specific mortality rates, prostate cancer, UK (taken from CR-UK, 2007).

1.1.2 Biology, histology, and function of the prostate

The prostate is a composite tubuloalveolar walnut-sized gland of the male reproductive system, which is situated within the pelvis at the base of the bladder, surrounding the urethra. The prostate is also surrounded posteriorly by the rectum, through which it can be felt, particularly when enlarged, during rectal examinations for prostate irregularities.

The prostate is covered by a capsule made up of collagen, elastin, and copious amounts of smooth muscle, involved in aiding the mechanical expulsion of semen during ejaculation following neural stimulation. Along with this function, the prostate also acts as a sex accessory

tissue by being responsible for storing and secreting a translucent, somewhat alkali fluid which acts to aid sperm motility by liquefying and protecting the sperm when passing through the hostile acidic conditions of the female vagina.

The prostate is mainly composed of glandular epithelium which is deposited in a fibromuscular stroma. This non-glandular fibromuscular stroma makes up around a third of the gland, and stretches from the bladder neck to the striated sphincter. It comprises of fibroblasts, smooth muscle, nerves, and lymphatics. The stroma is immediately continuous with the capsule, and progressively lengthens into fibrous tissue that terminates in loose connective and adipose tissue (McNeal, 1988)

The glandular epithelium meanwhile is made up of three major zones, a concept that was defined by Mcneal and his colleagues in 1981. The largest of these zones which makes up around 70% of the glandular tissue, is the peripheral zone that stretches to the side and towards the posterior of the prostate. This is the site where the majority of prostatic cancers arise. The central zone meanwhile, constitutes only 25% of the gland but makes up the majority of the prostatic base, and spreads cone-shaped around the ejaculatory ducts to the bladder base. Unlike the peripheral zone, only 1-5% of adenocarcinomas develop in the central zone. Finally, the transition zone makes up the smallest region at only 5% of total prostate volume, and is comprised of two small lobules that lie alongside the prostatic urethra. It is here where the bulk of Benign Prostatic Hyperplasia (BPH) originate, which are commonly of lower malignancy (McNeal, 1981).

On the whole, the prostatic glands are simply branched and tubuloalveolar in structure, lined with both cuboidal and columnar secretory epithelial cells, androgen-dependent for their growth. These terminally differentiated columnar cells are rich in secretory granules, keratin, and enzymes such as prostatic acid phosphatase, leucine amino peptidase, and PSA. They are tightly packed together via cellular adhesion molecules (CAMs), and attached to a basement

membrane through integrin receptors which connect them to the stromal cells via an extracellular matrix, enhancing epithelial cell growth. The apical luminal side of the cells contain microvilli, which aid in the secretion and drainage of seminal fluid from the acini into ducts linked to the urethra (Hallstrom and Laiho, 2008). Figure 1.2 is a schematic representation of the cell types present in the prostatic epithelium.

Along with these cells, the prostatic epithelium is made up of three other cell types; basal cells, transient amplifying epithelial cells, and neuroendocrine cells. The basal cells lie between the secretory cell layer and the basement membrane. Like the secretory epithelial cells, basal cells are also abundant in keratin but are much smaller and less plentiful. They are rounder and less differentiated with barely any secretory enzymes, and are independent of androgen for their growth. They do however contain large amounts of ATPase, implying that they may play a role in active transport. It has been shown that active DNA synthesis occurs only in this basal cell layer and so it is this layer that is thought to include the pluripotent prostate stem cells, which due to their high regenerative capacity, can act as progenitors for many neoplasms (Dermer, 1978).

Finally, neuroendocrine cells are scattered among the basal and secretory epithelial cell layers in the acini and ducts of the prostate. It is thought that there are three types of these neuroendocrine cells and that they may transmit narrow apical extensions into the lumen (McNeal, 1997). These cells can be characterised by their secretion of peptide hormones such as serotonin, somatostatin, and calcitonin (McNeal, 1997; Long *et al.*, 2005). The role they play in the prostate is still unclear, however it is believed that the cytokines they secrete may be involved in the growth and differentiation of the prostatic epithelium. They have also recently been linked to prostate carcinogenesis and may give rise to small cell carcinomas in the prostate (di Sant'Agnese, 1998).

Interactions between the stroma and the epithelium remain elusive but it has been recently suggested that the stroma is responsible for producing several growth factors vital for the growth and development of the normal as well as malignant prostate. Epidermal growth factor (EGF), basic fibroblast growth factor (bFGF), and transforming growth factor beta (TGF- β) for example, have been implicated in growth regulation of both the normal and benign prostate (Ware, 1993). It has been shown that prostatic epithelial cells but not stromal cells, express high levels of the EGF receptor. The TGF- β receptor on the other hand has the opposite expression pattern (Scher *et al.*, 1995). In addition, it has been demonstrated that the addition of fibroblasts to epithelial tumour cells, promotes their growth *in vivo* (Camps *et al.*, 1990). This suggests that it is indeed the stromal cells that act in a paracrine fashion to regulate the biological properties of the epithelial cells, and that cancer cells are capable of exploiting these pathways, and along with complex interactions between androgens and cellular communication, can lead to the progression and metastasis of prostate cancer. It is therefore of utter importance to understand the crosstalk between the epithelial and stromal components of the prostate in order to determine cancer aggressiveness.

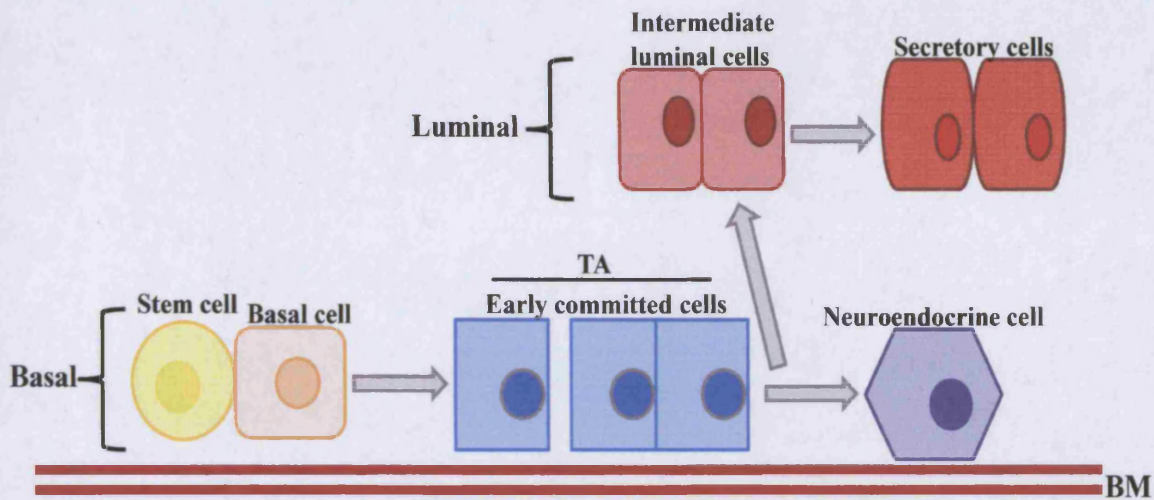


Figure 1.2: schematic diagram of the different cell types present in the prostatic epithelium (adapted from Hallstrom and Laiho, 2008).

1.1.3 The biology of prostate cancer

Around 95% of all prostate cancers are adenocarcinomas that arise from the prostatic epithelium. The remaining 5% of prostate cancers are very rare but are generally of the following types; sarcoma, squamous cell carcinoma, transitional carcinoma, signet-ring carcinoma, and neuroendocrine carcinoma. These rarer cancers are sometimes more difficult to distinguish between, and are usually less responsive to hormonal therapy (McWilliam *et al.*, 1997).

In prostate cancer, the genetic and epigenetic events that need to occur in order for a cell to become cancerous are elusive. However, it is believed that premalignant lesions are present that long precede prostate cancer development, as they are often found adjacent to prostate adenocarcinomas. There are several types of pre-malignant lesions, the most common being Prostatic Intraepithelial Neoplasia (PIN), which is a term that covers the expressions prostatic epithelial dysplasia and atypia (Haggman *et al.*, 1997). PIN is described as the appearance of morphological atypical or dysplastic epithelial cells surrounded by benign seeming glands and

acini, with a cell morphology that lies somewhere between that of a benign and a malignant cell. PIN is graded depending on the degree of basal cell layer disruption (with more disruption being present in high grade PIN) and a gradual reduction in keratin expression, and ranges from grade 1 (mild) to grades 2 and 3 (high grade or severe) (Bostwick, 1999).

Proliferative Inflammatory atrophy (PIA) is another form of premalignant lesion that is also found near adenocarcinomas and can fuse with high-grade PIN areas. PIA is normally triggered in response to tissue-detrimental chronic inflammation that causes oxidative stress, and is linked with rapid regenerative cell proliferation (Coussens and Werb, 2002; Palapattu *et al.*, 2005). Finally, BPH is a lesion associated with deregulated proliferation of stromal cells but is generally not believed to be a precursor of malignant transformation (McNeal, 1984).

1.1.4 Prostate cancer detection

The incidence of prostate cancer increases with age, with an incidence percentage of over 30% in men over the age of 50, and up to 80% by the age of 80. However, prostate cancer is typically a slow growing cancer, so much so that most never grow to the point where they cause symptoms, and the majority of men with prostate cancer die of other causes before the disease even impacts their lives. This lack of symptoms becomes problematic, as at the point of diagnosis around 75% of patients exhibit locally extensive or metastatic disease, resulting in a poor diagnosis of less than 15% 5 year survival rate (Foster, 1990).

Those that do display symptoms however, most commonly present with bladder outlet obstruction, nocturia, reduced urinary flow, and deficient bladder emptying-symptoms known as prostatism. However, these symptoms are more commonly associated with BPH, and this makes it difficult to distinguish between cancers of differing aggressiveness, adding another dilemma to the management of prostate cancer. In addition, there are currently no independent markers or cellular features that exist to aid in the prediction of the behavior of prostate cancer in a specific patient. However, patients with advanced prostate cancer present with symptoms

such as perineal pain, impotence, and hematuria, while those with metastatic disease exhibit symptoms of bone pain and fatigue (Foster and Abel, 1992).

Three main strategies exist in the detection of prostate cancer; serum prostate specific antigen (PSA) analysis, digital rectal examination (DRE), and trans-rectal ultrasound (TRUS) detection. It has been shown that if a combination of these methods are used, that higher prostate cancer detection rates can be achieved. PSA in combination with DRE for example, leads to a doubling in detection rates, in comparison to DRE alone (Littrup and Goodman, 1994).

1.1.4.1 PSA serum test

Prostate specific antigen (PSA) is a glycoprotein with serine protease activity which is located within the cytoplasm of both benign and malignant prostate cancers, and secreted exclusively by the prostatic epithelial cells. It generally functions as a liquefying agent in semen following ejaculation so as to aid sperm when traversing through the uterus (Catalona *et al.*, 1991).

Before the days of PSA testing, most prostate cancers were detected during DREs and TRUS, with prostatic acid phosphatase (PAP) being used as the main serum biomarker. PSA was first described in 1966, and was later found to be measurable, with increased levels demonstrated in clinical disorders of the prostate, such as; BPH, prostatitis, and prostate cancer (Habara *et al.*, 1966). However, it was only in 1991 that Catalona *et al.* first assessed PSA as a prostate cancer screening test (Catalona *et al.*, 1991).

PSA circulates in the blood stream in the form of three isoforms, both complexed and free, each of which can be measured separately. The lower the ratio of free-PSA:bound-PSA in the blood of a patient, the higher the risk of prostate cancer, with a ratio of 25% and less being used as a threshold for for instigating biopsies. There are three isoforms of free PSA, including: BPH-PSA, inactive PSA, and proenzyme-PSA, or pro-PSA. It has been demonstrated that in benign prostatic tissues, levels of both BPH-PSA and inactive PSA are more copious than pro-PSA,

whereas in prostate cancer tissues, there is 1.3-1.4 times more pro-PSA than BPH-PSA and inactive PSA (Loeb and Catalona, 2008). A PSA level of 4.0 ng/ml and above was believed to be indicative of possible prostate cancer, and hence was chosen as the threshold for initiating biopsies in prostate cancer diagnoses. Patients with PSA levels of between 0 and 3.99ng/ml were referred to as being within the normal range, and hence were normally not biopsied (Gann *et al.*, 1995).

The use of PSA serum testing altered the world of prostate cancer diagnosis and it became the most commonly used non-invasive method of screening for solid tumours of the prostate. Recently however, PSA testing has been shrouded with controversy as limitations to its specificity are being questioned. This is mainly due to data from several groups which showed that a significant number of men with PSA levels within the 'normal range' actually had prostate cancer, some even of a high grade. In addition, as BPH, prostatitis, and ejaculation can also cause an increase in PSA levels, patients who have PSA levels in the range of 4ng/ml-10ng/ml, sometimes have to undergo unnecessary and painful biopsies (Thompson *et al.*, 2005; De Angelis *et al.*, 2007).

For these reasons, several modifications have been made to PSA testing, including; age-specific PSA ranges (Dalkin *et al.*, 1993), transition zone PSA density (Catalona *et al.*, 1998), free to total PSA ratios (Catalona *et al.*, 1999), and PSA velocity (Carter *et al.*, 1992). In addition, extensive research is being carried out in order to find novel biomarkers for use in prostate cancer detection. Some of these include; prostate cancer gene 3 (PCA3), and early prostate cancer antigen (EPCA and EPCA-2), which are briefly mentioned below.

1.1.4.2 Novel potential biomarkers for prostate cancer

Due to the obvious flaws in PSA testing, research into improved biomarkers for the detection of prostate cancer has expanded and yielded numerous feasible candidates. An ideal biomarker would require several characteristics in order to be viable, the most important of which are;

disease specificity, high sensitivity, cost-effectiveness, user-friendliness, and having some sort of association to disease outcome.

Most of the targets that meet some of these requirements represent genes with altered expression levels in prostate cancer or epigenetic changes that lead to transcriptional changes in genes involved in prostate cancer progression (Lin, 2009). The most promising candidates include prostate-specific membrane antigen (PSMA), prostate cancer gene 3 (PCA3), and early prostate cancer antigen (EPCA).

PSMA is an essential cell-surface marker of prostate cancer, where its expression is specific and abundant. Recent development of PSMA-targeted prostate cancer therapies such as vaccines have entered clinical trials, demonstrating some promising results (Olson *et al.*, 2007). PCA3 meanwhile, was discovered in 1999 as a non-coding prostate-specific mRNA highly over-expressed in prostate cancer tissue compared to normal tissue (Bussemakers *et al.*, 1999). Recently, a non-invasive test called the Progenesa™ PCA3 test (Gen-probe, San Diego, CA, USA) has been developed, which uses PCR to amplify and quantify the ratio of PCA3 to PSA mRNA levels, following a DRE. This ratio gives a PCA3 score, which has been used to aid in better decision making when contemplating initial and secondary biopsies in patients with serum PSA levels between 2.5ng/ml and 10ng/ml (Kirby *et al.*, 2009).

Finally, EPCA and its isoform EPCA-2, are nuclear structural proteins specific to prostate cancer tissue which can be accurately measured with an ELISA assay that appears to be very precise in distinguishing between localized and high grade cancers (Getzenberg *et al.*, 1991). However, despite the promising advances seen in these novel biomarkers, a lot more work needs to be carried out before they can replace PSA testing in the detection of prostate cancer.

1.1.4.3 Digital rectal examination (DRE)

DRE was the first conventional method used in the detection of prostate cancer, popular in the days before PSA testing came about. The process involves an examiner inserting a gloved,

lubricated finger into the rectum in order to inspect the size, shape, and texture of the prostate, and any lumps or nodules that may be present. Areas deemed irregular then go through further evaluation to determine whether they are cancerous or not.

However, DRE only evaluates the posterior and lateral aspects of the prostate, and although the majority of cancers usually arise in this area, around 25-30% of cancers are not accessible to the examining finger and can be missed, therefore making the method insufficiently sensitive (McNeal *et al.*, 1986). The method also lacks in specificity, as a large proportion of examinations result in false-positives, with around 6-33% of asymptomatic men reporting positive values (Richie *et al.*, 1993). In addition, only prostate cancers which are more advanced can be felt by DRE, with only about 30% of those detected being organ confined and hence potentially curable. Any consequential treatment following DRE therefore typically proves less effective and for this reason the method is rarely used as a form of prostate cancer detection on its own (Narain *et al.*, 2002).

1.1.4.4 Trans-rectal ultrasonography (TRUS)

Trans-rectal ultrasonography was presented over 20 years ago and is the preferred method by which to obtain prostate needle biopsies. The process involves inserting an ultrasound probe into the rectum of the patient, and using the resulting image to direct spring loaded 18-gauge biopsy needles into abnormal areas of the prostate. The most commonly used technique is the six-core or sextant biopsy, with 8 to 10 being carried out to sample the prostate as it leads to significantly improved cancer detection rates (Chang *et al.*, 1998).

In TRUS, the typical prostate cancer appears as a hypoechoic nodule, with the larger ones being more visible on a sonogram. However, the method provides with very little information as a lot of cancers are not visible by sonography, and the 10-15% which are not blatant, despite the majority of the patients having an elevated PSA. Therefore, the low yield, high cost, difficulty,

and its rare detection of cancers, has led to the omission of TRUS as a screening test (Narain *et al.*, 2002).

1.1.5 Prostate cancer grading and staging system

In order to establish which treatment to provide a prostate cancer patient with, the cancer needs to be classified and graded using established grading systems such as the TNM staging system and the Gleason grading system.

1.1.5.1 The Gleason grading system

The most widely used grading system for prostate carcinomas is the Gleason grading system, which was initially described by Gleason and Mellinger in 1974. The grading is based on the histological pattern of the distribution and growth of the tumour cells in the prostatic stroma, as well as the degree of glandular differentiation in H&E stained prostatic tissue samples from either a biopsy, or if after radical prostatectomy, a whole prostate (Gleason and Mellinger, 1974).

The various growth patterns (shown in Figure 1.3) are combined to form 5 basic grade patterns ranging from 1 (least aggressive) to 5 (most aggressive). A histological score ranging from 2-10 is then generated, by the addition of the primary grade pattern; the prevailing one in that area, to the secondary pattern, which is the subsequently most widespread pattern. However, if only one grade is present, or if the second grade covers less than 3% of the total tumour, its value is doubled in order to give a corresponding Gleason score.

The most frequently observed pattern of prostatic adenocarcinoma growth is pattern 3, which is divided into three distinctive manifestations; A, B, and C. Patterns 4 and 5 meanwhile are only presented as forms A and B, whereas patterns 1 and 2 reveal only one outline. The cell arrangement seen in each Gleason pattern is described in Table 1.1, and ranges from the closely

packed well-differentiated carcinoma cells seen in pattern 1, to smooth rounded masses of necrotic and very poorly differentiated carcinoma cells in pattern 5 (Humphrey, 2004).

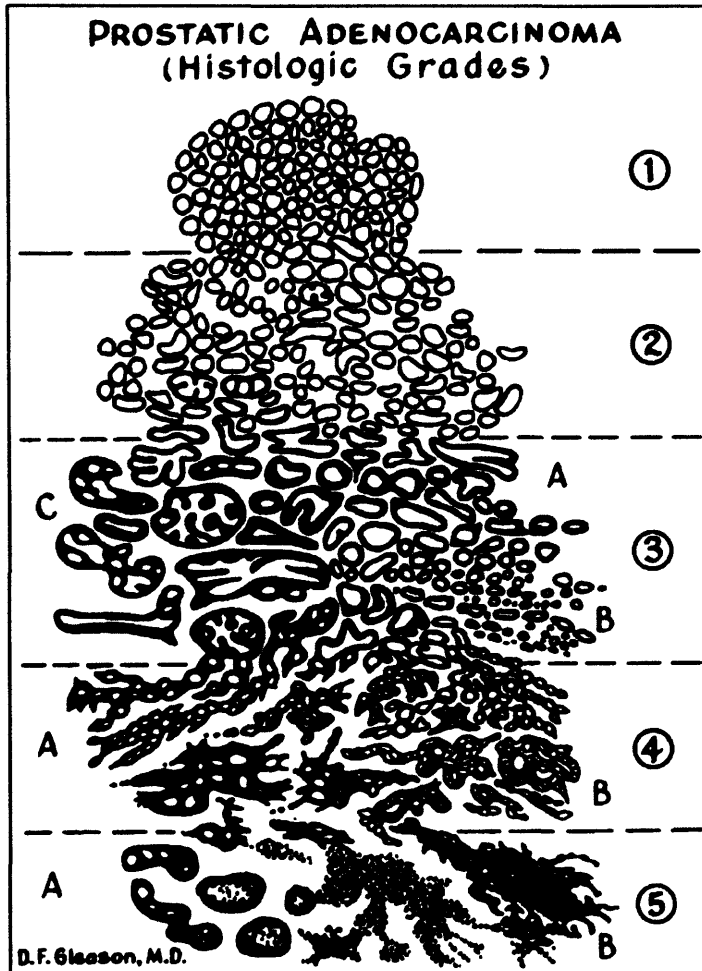


Figure 1.3: Schematic drawing of Gleason histological grading (Taken from Humphrey et al., 2004).

Pattern	Tumour shape	Stromal Invasion	Tumour cell distribution	Gland size
1	Nodular with well defined smooth edges	Pushing	Single, oval and closely packed cells, but detached glands	Medium
2	Less defined and constrained masses	Some gland separation at tumour peripheries	Single, separated, loosely packed oval glands, with more variation in their size and shape	Medium
3A	Indefinable infiltrating edges	Irregular extension	Single, detached glands of variable shape and size, with elongated and twisted forms and wide stromal separation	Medium
3B	Indefinable infiltrating edges	Irregular extension	As with 3A except with smaller glands	Small to very small
3C	Masses and cylinders with smooth round edges	Expansile	Papillary and cribriform epithelium without necrosis	Medium to large
4A	Raggedly infiltrative	Disseminated and permeative	Amalgamated glands in masses, cords, or chains	Variable
4B	Raggedly infiltrative	Disseminated and permeative	As 4A, but cells have cleared cytoplasm (hypernephromatoid)	Variable
5A	Smooth and rounded cylinders	Expansile	Papillary, cribriform or solid masses with central necrosis (comedocarcinoma)	Variable
5B	Raggedly infiltrative	Disseminated and permeative	Masses and sheets of anaplastic carcinoma, with some tiny glands or signet cells	Variable

Table 1.1: Gleason grading system for prostate cancer (adapted from Humphrey et al., 2004).

1.1.5.2 Tumour Nodal Metastasis (TNM) Classification

The TNM classification of the prostate was first established in the 1940s by Pierre Denoix, but was updated by the American Joint Committee on Cancer and International Union against Cancer (UICC), in 2002. The system is based on primary tumour (T), lymph node (N), and metastases (M) categories, with each one being built on a series of clinical examinations, radiological imaging, biopsies, and biochemical analyses (Greene and Sobin, 2002). Clinical T staging is the most important prognostic factor for clinically localised prostate cancer, and is

usually carried out using DRE. Regional lymph node metastases meanwhile are strong predictors of progression, and imaging using nomograms is essential for men who have a greater risk of developing metastases. Finally, staging for bone metastases has been widely used as the established norm for distinguishing outlying metastases of the axial skeleton, with MRI being the most reliable means of detection (Borley and Feneley, 2009). The staging is described in full detail in Table 1.2, and represented in diagram form in Figure 1.4 below.

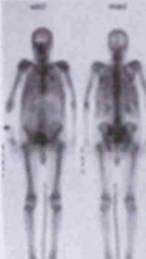
T1	T2	T3	T4
			
<p>T1 Clinically inapparent; tumor not palpable or visible by imaging</p> <p>T1a Incidental finding during transurethral resection of prostate; < 5% of tissue resected</p> <p>T1b Incidental finding during transurethral resection of prostate; > 5% of tissue resected</p> <p>T1c Tumor identified by needle biopsy (e.g. because of elevated PSA)</p>	<p>T2 Tumor confined within prostate (palpable or visible on TRUS)</p> <p>T2a Involves half of a lobe or less</p> <p>T2b Involves more than half of a lobe one lobe but not both lobes</p> <p>T2c Tumor involves both lobes</p>	<p>T3 Tumor extends through prostatic capsule, bladder neck or seminal capsule</p> <p>T3a Unilateral extracapsular extension</p> <p>T3b Bilateral extracapsular extension</p> <p>T3c Tumor invades seminal vesicle(s)</p>	<p>T4 The tumor has spread or attached to tissues next to the prostate (other than the seminal vesicles).</p> <p>T4a The tumor has spread to the neck of the bladder, the external sphincter (muscles that help control urination), or the rectum.</p> <p>T4b The tumor has spread to the floor and/or the wall of the pelvis.</p>
<p>N0-3</p> 	<p>M0-1</p> 	<p>N0 Cancer has not spread to any lymph nodes.</p> <p>N1 Cancer has spread to a single regional lymph node (inside the pelvis) and is not larger than 2 centimeters</p> <p>N2 Cancer has spread to one or more regional lymph nodes and is larger than 2 centimeters (¾ inch), but not larger than 5 centimeters</p> <p>N3 Cancer has spread to a lymph node and is larger than 5 centimeters</p> <p>M0: The cancer has not metastasized (spread) beyond the regional lymph nodes</p> <p>M1: The cancer has metastasized to distant lymph nodes (outside of the pelvis), bones, or other distant organs such as lungs, liver, or brain</p>	

Figure 1.4: Diagram showing and explaining the three categories of TNM staging of prostate cancer (Simon Kaiser, 2004).

Stage	Characterisation
Primary Tumour (T)	
TX	Primary tumour cannot be assessed
T0	Primary tumour not evident
T1	Tumour clinically inapparent, not palpable or visible by imaging
T1a	Tumour (non-palpable) as incidental histological finding at transurethral resection of prostate in 5% tissue resected.
T1b	Tumour (non-palpable) as incidental histological finding at transurethral resection of prostate in >5% tissue resected.
T1c	Tumour (non-palpable) identified by needle biopsy (for elevated serum PSA) includes bilateral non-palpable tumour on needle biopsy.
T2	Tumour confined within prostate (including prostatic apex and prostatic capsule) that is either palpable or visible on imaging, or (p-prefix) demonstrated in radical prostatectomy specimen.
T2a	Tumour involving one-half of one lobe or less.
T2b	Tumour involving more than one-half of one lobe or less.
T2c	Tumour involving both lobes.
T3	Tumour extends through prostatic capsule.
T3a	Extra-capsular extension (ECE).
T3b	Invasion of seminal vesicle(s)
T4	Tumour fixed, or invades adjacent structures: bladder neck, external sphincter, rectum, levator muscles, and pelvic wall.
Regional lymph nodes (N)	
NX	Regional lymph nodes cannot be assessed.
N0	No regional lymph node metastases.
N1	Regional lymph node metastases within true pelvis, below common iliac artery bifurcation, either unilateral or bilateral.
Metastases (M)	
MX	Distant metastases cannot be assessed.

M0	No distant metastases.
M1a	Non-regional lymph node metastasis.
M1b	Metastasis to bone(s).
M1c	Metastasis to other site(s).

Table 1.2: The 2002 TNM classification for adenocarcinoma of the prostate (adapted from Borley *et al.*, 2009).

1.1.6 Treatment and management of prostate cancer

1.1.6.1 Active surveillance

This method, also known as watchful waiting or expectant management, is the standard treatment for patients with T1 or T2 localised prostate cancer. Due to the fact that the natural history of patients with localised prostate cancer shows that few of them ever develop metastases or die from the disease, and that at present all active treatments for prostate cancer result in adverse effects, active surveillance can instead be employed as a less invasive form of treatment. This entails strict monitoring of a patient's progression by carrying out PSA serum tests, DREs, and tissue biopsies, until further action is carried out, if required (Wu *et al.*, 2004). The decision to undertake this method however, depends on several crucial factors including patient life expectancy, where active surveillance remains a reasonable option in older men with a life expectancy of less than 10 years. In the case of younger men however, this method is usually only undertaken for a period of around three years as the risk of metastasis increases. Other factors to consider include; tumour characteristics and aggressiveness, as well as the preference of the patient for a particular treatment regime after being informed of any possible adverse effects, efficiency, and issues concerning quality of life (Chodak *et al.*, 1994).

1.1.6.2 Radical prostatectomy

Complete surgical removal of the prostate, or prostatectomy, has been used as a treatment for prostate cancer for over a century, and is usually carried out on patients with either early stage

disease (T1-T2b), where the tumour is clinically confined to the prostate, or on those who have failed to respond to radiation therapy. However, it has also been advocated that its use in patients with locally advanced disease (T3-T4) alongside adjuvant radiation therapy, can prove beneficial. In contrast, the operation is rarely recommended for older men with a life expectancy of less than 10 years, as it proves to offer little benefit and can impose significant complications (Bill-Axelson *et al.*, 2005).

In the past, methods included a perineal approach, which was succeeded by the radical perineal tactic, where the surgeon removes the prostate through an incision in the perineum. In the 1940s however, this method was replaced by Millin's radical retropubic approach which, although slightly technically improved, remains the most commonly used form of prostatectomy to this day. The method entails the removal of the prostate through the pelvis above the pubic bone via an abdominal incision, and offers a considerable advantage over its perineal counterpart, as it is simpler to teach, and allows access to the pelvic lymph nodes, which is valuable for tumour staging (Millin *et al.*, 1949).

Other more modern methods include the less invasive Laparoscopic radical prostatectomy (LRP), or robotic assisted laparoscopic radical prostatectomy (RALP), which unlike the previously mentioned methods, do not require a large incision, and rely on modern technology such as fibre optics and miniaturisation (Smith *et al.*, 2007).

Prostatectomy is deemed curative only if the entire tumour is removed. However, it can come with several complications. In the past these included; impotence, incontinence, morbidity, and loss of erectile function. However, due to improved surgical techniques, these complications are less common, and morbidity for this procedure is low. The only time treatment failures can occur is when the cancer has previously spread to distant sites before the operation has taken place, or if the local tumour is not completely excised. For these patients, close monitoring is required in order to detect any recurrence (Garnick, 1993).

1.1.6.3 Radiation therapy

Radiotherapy is commonly used to treat all stages of prostate cancer or when surgery has failed. The method uses ionising radiation to damage cellular DNA, and although this occurs in both normal and cancer cells, the cancer cells are less capable of repairing the damage and therefore undergo apoptosis. Although initially attempted in the early twentieth century, radiotherapy only emerged as a principal treatment for prostate cancer in the 1950s. Nowadays, computer technology and advanced imaging has revolutionised the preparation and implementation of radiotherapy (Hanks *et al.*, 1997).

Two types of radiotherapy exist; external-beam radiotherapy, where the radiation is applied from an external source, or brachytherapy, where the radioactive source is implanted into the prostate. The development of treatment techniques for external-beam radiotherapy began in the 1950s by Bagshaw and colleagues (Bagshaw, 1969). They instigated the use of megavoltage linear accelerators as a means of directing a beam of high dose radiation (4,500-5,400 cGy) towards the prostate, with lower doses being applied to the surrounding tissue. The procedure is usually delivered using techniques such as intensity modulated (IMRT) or proton beam radiotherapy (PBRT), which act to amend the radiation beam to coincide with the shape of the tumour, so as to allow for higher doses to be applied to the prostate and seminal vesicles, while protecting the bladder and rectum from considerable damage (Zelefsky *et al.*, 2006). Treatment is generally given over a period several weeks, with daily 180 to 200 cGy portions 5 days per week, succeeded by a boost to the prostate to a total dose of 6600-7000 cGy. Possible side effects include inflammation of the bladder, rectum, and urethra, as well diarrhoea and dysuria (Bagshaw *et al.*, 1977).

Brachytherapy meanwhile, was introduced in 1983 by Holm and colleagues, who implemented the stereotactic perineal approach using TRUS guidance. The procedure involves the insertion of approximately 100 small radioactive rods ('seeds') with the use of a TRUS

guided needle through the perineum skin, directly into predetermined positions within the tumour, using catheters. The patient is placed in the dorsal lithomy position, and remains under general or spinal anaesthesia throughout the whole procedure. The radioactive source of the rods can either be of the low-dose rate (LDR), using Iodine-125 or palladium-103 as the source of energy, or as a high-dose rate (HDR) with Iridium-192. Currently, LDR is the most commonly used form of brachytherapy, with the seeds remaining permanently inserted within the prostate, until they eventually become inert and hence not posing a risk of radioactive exposure to any surrounding patients (Perez *et al.*, 1993).

Brachytherapy has been shown to cause less damage to external tissues when compared to external beam radiotherapy, but is also not as efficient at killing cancer cells that are situated outside the prostatic capsule. However, either one of the techniques can be used as a form of prostate cancer treatment instead or after surgery of early stage disease, or as a means of palliative treatment for painful bone metastases in metastatic prostate cancer patients. Hormonal therapy can sometimes be combined with either one, or both types of radiotherapy in patients with advanced prostate cancer, as this synergistic effect appears to improve patient survival (D'Amico *et al.*, 2004).

1.1.6.4 Androgen ablation therapy

The male sex hormones, or androgens, are essential for both normal prostate growth and maintenance, as well as for the development of early stage prostate cancer. Androgens are particularly important for the survival and growth of prostate cancer cells, and many groups have shown that their suppression results in an inhibition of tumour cell proliferation, activation of apoptosis, and a decrease in tumour size (Kyprianou *et al.*, 1990). The concept of using androgen ablation for prostate cancer treatment has been around for more than a century and is now used as a means for treating advanced and metastatic prostate cancer. However, androgen therapy is rarely curative. This is due to the androgen insensitive cells that are present within

the tumour, and although initial therapy will reduce tumour size, prolonged therapy can act as a selective pressure for the androgen independent cancer cells to thrive. These cells can then induce re-growth of a tumour which will no longer respond to hormonal therapy (Robson and Dawson, 1996).

In order to understand how androgen ablation therapy works, the complex feedback loops involved in androgen production need to first be explained (Figure 1.5). The vast majority of androgen production (95%) is produced by the testicles, with the remaining 5% being produced by the adrenal glands. Androgens are produced by a feedback loop that involves the testicles, hypothalamus, pituitary, as well as the adrenal and prostate glands. Androgens bind to androgen receptors (AR) within the hypothalamus, resulting in the stimulation of Luteinising-hormone-releasing-hormone (LHRH) production, which in turn travels to the pituitary where it binds to LHRH receptors, in order to produce Luteinising hormone (LH). LH then interacts with its receptors in the testes to induce the synthesis of testosterone from cholesterol.

Testosterone finally enters the prostate cells, where the enzyme 5α -reductase converts it to Dihydrotestosterone (DHT), which binds with high affinity to ARs. This complex then translocates to the nucleus of the prostate cells to activate the transcription of survival and growth genes. The whole process acts as a negative feedback loop, as high levels of testosterone inhibit production of LH and LHRH in order to maintain a balance of androgen levels in the blood. The adrenal glands also produce androgens which feed into the testicular androgen production loop (Denmeade and Isaacs, 2002).

Hormonal therapy acts to block testicular androgen production in order to prevent prostate cancer cells from using them for continued growth and survival, and this is carried out in one of two ways; surgical or chemical castration. Orchiectomy is the surgical procedure, in which either one or both (bilateral orchiectomy) of the testicals are removed. As the testicles are

responsible for the majority of androgen production, this results in a massive drop in testosterone levels, thereby preventing the prostate from producing DHT, and inhibits prostate cancer cell growth (Denmeade and Isaacs, 2002).

However, due to the obvious psychological effects this can have on a patient, there are alternative chemical methods available in order to induce castration. The first drug that was produced for chemical castration was the synthetic estrogen, diethylstilbestrol (DES). However, due to the toxicity issues and cardiovascular complications associated with this drug, other drugs were developed. The most commonly used are LHRH agonists, such as leuprolide and goserelin, which for the initial 7 days induce a transient increase in testosterone levels- referred to as 'testosterone flare'- which can cause considerable bone pain in 5-10% of patients.

However, with continued use, after around 2-3 weeks, the high levels of testosterone act to down-regulate LHRH receptors of the pituitary, resulting in a reduction in LH and testosterone levels (Vilchez-Martinez *et al.*, 1979). Side effects are rather mild and include; hot flashes, fatigue, reduced libido, impotence, and weight gain. This method therefore proves to be a successful form of chemical castration, and results compare to surgical and DES castration with significant reductions in PSA levels in 70-80% of patients, and a decrease in pain in 60-80% (Tolis *et al.*, 1982).

At the other side of the spectrum is the use of LHRH *antagonists* which include; Cetroxide, Abarelix, and Ganirelix that directly inhibit the LHRH receptor, resulting in a reduction of LH and testosterone levels comparable to that caused by LHRH agonists. However, they have an added benefit in that they do not cause the painful testosterone flare, characteristic of LHRH agonists (Schally *et al.*, 2000).

The final form of drugs for chemical castration is the anti-androgens, which competitively inhibit circulating androgens and DHT from binding to ARs, thereby preventing the downstream effects. Initially, the steroidal drug cyproterone acetate was used due to its bi-

functionality of acting as both an anti-androgen and a progesterone agonist, capable of binding the progesterone receptor in the pituitary in order to prevent the release of LH, and the corresponding increase in testosterone levels. The resulting effect proved to be equally effective as medical castration (Varenhorst *et al.*, 1982). However, due to its considerable side effects, novel non-steroidal drugs such as Flutamide, Bicalutamide, and Nilutamide were developed, due to their increased tolerance and lack of effect on libido. However, they were later found to be capable of crossing the blood-brain barrier and increasing LH and testosterone levels, making them a less effective therapy than conventional castration methods, in terms of overall patient survival (Chodak *et al.*, 1995).

As all these new agents were being developed, it became apparent that none of the castration methods alone were capable of curing patients with advanced prostate cancer. As mentioned above, the adrenal glands are also capable of secreting low levels of androgens alongside the testicles, and despite its controversial role in prostate cancer, it was thought that adrenal androgen production should be inhibited alongside testicular castration, resulting in a total androgen blockade. Adrenalectomy, the surgical removal of the adrenal glands, and hypophysectomy, the surgical removal of the pituitary, act as successful ways of inhibiting adrenal androgen synthesis, and have been shown to improve survival in prostate cancer patients who showed no improvement with testicular androgen ablation alone. Chemical methods to inhibit adrenal androgen production come in the form of drugs such as Aminoglutethimide and Ketoconazole (Labrie *et al.*, 1982).

When combined with LHRH-agonists, these anti-adrenal androgens prevent the testosterone flare reaction seen when LHRH-agonists are used on their own, and the gradual increase of testosterone seen when using anti-androgen drugs. This combined therapy showed reports of patients with slightly longer progression-free survival (Crawford *et al.*, 1989). In conclusion, while androgen-ablation presents patients with a means of significant palliative therapy, due to

the presence of androgen-independent cancer cells within the tumour, it is never curative, no matter how completely or early it is given.

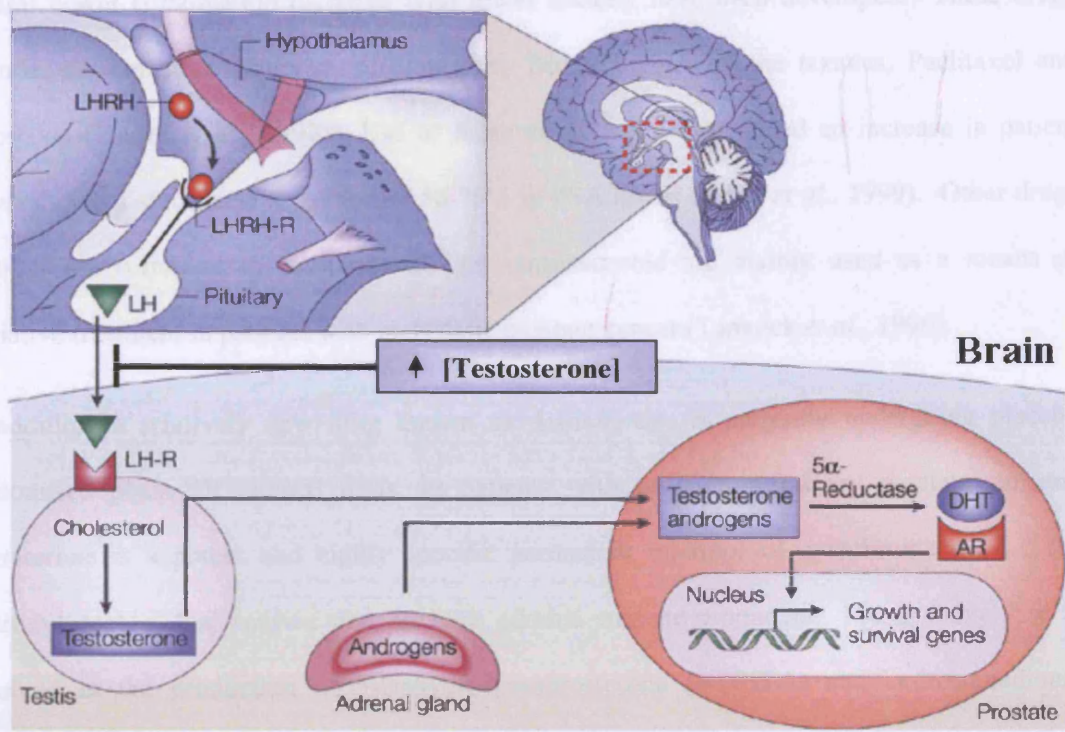


Figure 1.5: Schematic diagram of the negative feedback loop in androgen production. (Adapted from Denmeade *et al.*, 2002).

1.1.6.5 Cytotoxic chemotherapy (for hormone-refractory prostate cancers)

As mentioned in the previous section, androgen insensitivity poses problems when treating advanced prostate cancers. It has been proposed to occur by various mechanisms, including hypermethylation of the androgen receptor and hence silencing of androgen receptor gene expression, and during androgen ablation, through amplification of the AR gene, allowing the cancer cells to remain functional at lower concentrations of androgen (Kaarbo *et al.*, 2007). Despite this, some androgen-independent tumours will still respond to subsequent hormonal therapies. However, there exist some tumours which are hormone-refractory, and hence become completely unresponsive to continued hormonal manipulation.

For these tumours, treatment is possible in the form of cytotoxic chemotherapy. However, as these drugs are cytotoxic, they lead to the death of both cancer and normal cells, resulting in considerable toxicity and undesirable side effects. However, due to extensive research, several newer combination therapies with lower toxicity have been developed. These drugs include; Estramustine, Vincristine, Etoposide, Doxorubicin, and the taxanes, Paclitaxel and Docetaxel (Hudes *et al.*, 1997). Use of these drugs has demonstrated an increase in patient survival, and a significant reduction of 50-75% in PSA levels (Scher *et al.*, 1999). Other drugs such as Mitoxantrone in combination with corticosteroid are mainly used as a means of palliative treatment in patients with metastatic prostate cancer (Tannock *et al.*, 1996).

In addition, a relatively new drug known as Abiraterone is currently undergoing placebo randomised phase III clinical trials, in patients with hormone-refractory prostate cancers. Abiraterone is a potent and highly specific permanent inhibitor of cytochrome p-17 (17 α -hydroxylase), a dual enzyme that prevents adrenal enzyme production. 17 α -hydroxylase is involved in the production of 5-Dehydroepiandrosterone (5-DHEA) and androstenedione, which ultimately end up being metabolised into testosterone. Previous trials have shown that hormone-refractory patients treated with Abiraterone presented with a $\geq 50\%$ reduction in their serum PSA levels, and shrinkage in tumour size. MDV3100 is another novel AR antagonist that blocks nuclear translocation of AR and has shown promising results during clinical trials (Vishnu and Tan, 2010).

1.2 Cancer metastasis

Metastatic prostate cancer is responsible for the bulk of deaths associated with the disease, and as of yet no curative treatment has been discovered. For this reason the phenomenon of metastasis has become an intensively studied area, and it is anticipated that a more thorough understanding of the mechanisms behind the process will give rise to novel therapeutic targets, capable of delaying or preventing prostate cancer from metastasising.

Metastasis occurs as a multistage process in which cancer cells migrate from their site of origin, and colonise a secondary site in distant organs. The basic steps of the process include; local invasion, intravasation, survival in the circulation, adhesion and extravasation, and finally, colonisation of a secondary site (Figure 1.6). However, in order for cells to obtain metastatic abilities, they must undergo a series of genetic and epigenetic events to help them along this metastatic path. Firstly, in order for a primary tumour to develop, a normal cell needs to acquire initiating mutations bestowing it with unlimited proliferative potential, tolerance for replicative defects, and maintenance of progenitor phenotypes. The tumour slowly grows, but these mutations are not sufficient for metastatic competence and hence the cells need to undergo further transition (Nguyen *et al.*, 2009).

1.2.1 Local invasion

Local invasion is one of the most essential early steps of the metastatic process, as without it, the malignant cells are incapable of migrating from their site of origin. The cells need to acquire invasive and motile potential by down-regulating cell-cell, and cell-matrix adhesive components. The former, is mediated by cadherin-catenin complexes, the most important of which in the case of prostate cancer include, E-cadherin and β -catenin.

E-cadherin is a common tumour suppressor gene, and its loss induces cell detachment and invasive potential. Indeed, its expression has been found to be reduced in primary prostate cancers, and has been correlated with increased tumour grade, poor prognosis, and bone metastasis (Cheng *et al.*, 1996). In addition, it plays a critical role in the process of epithelial to mesenchymal transition (EMT), which cells are required to undergo in order to progress and metastasise. The transition involves the loss of cell polarity, and cell-cell binding, as the cells take on a mesenchymal phenotype and increase their expression of N-cadherin, granting them with the ability of invading the extracellular matrix (ECM) and migrating to remote sites. β -catenin meanwhile, links E-cadherin to intracellular actin, and its expression has been shown to

be significantly down-regulated in metastatic prostate cancer tissues, in comparison with primary tumours, suggesting that its loss of function plays a critical role early on in metastasis (Bryden *et al.*, 1999).

1.2.2 Cell-matrix adhesion and ECM degradation

Integrins are critical in mediating cell-matrix binding, and over-expression of some of their isoforms has been linked to increased invasion, perhaps due to their involvement in cell motility pathways and basement membrane (BM) attachment (Cress *et al.*, 1995). In addition, they have been demonstrated to work alongside ECM and BM degrading enzymes at metastatic sites. The most important of these enzymes include matrix metalloproteinases (MMPs), capable of digesting the collagen, laminin, and fibronectin, that make up these structures (Nagle *et al.*, 1994). MMPs are regulated by tissue inhibitors of metalloproteinases (TIMPs), and discrepancies in the MMP:TIMP ratio have been shown to induce invasiveness in tumour cells (Lokeshwar *et al.*, 1993). Urokinase-type plasminogen activator, an activator of the MMP cascade, is of particular importance in metastatic prostate cancer development (Hart *et al.*, 2002).

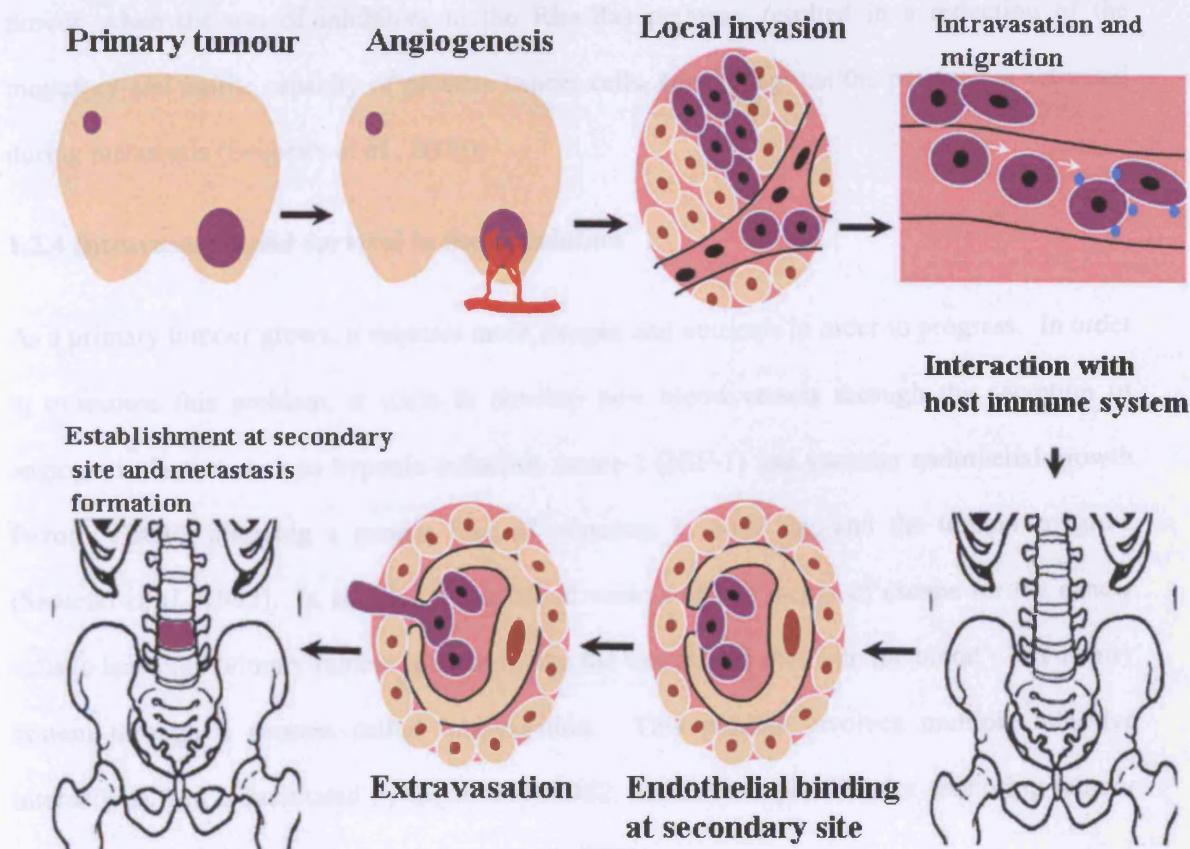


Figure 1.6: The process of metastasis is characterised by several basic steps; local invasion, intravasation, migration in the circulation, adhesion and extravasation, and finally colonisation of a secondary site (Adapted from (Clarke *et al.*, 2009)).

1.2.3 Cell migration and motility

In the prostate as well as other cancers, cell motility and migration depend on GTP-binding proteins such as Ras and Rho, which are involved in processes such as cytoskeletal construction, intracellular signalling, as well as whole cell, and cell membrane movement (Oxford and Theodorescu, 2003). Ras for example, regulates cell proliferation, gene transcription, apoptosis, and invasion, and is mutated in around 30% of solid tumours (Adjei, 2001). Rho GTPases act downstream of Ras, and regulate actin dynamics to lead cell growth and movement, important during cell migration and prostate metastasis. Their importance was

proven when the use of inhibitors to the Rho-Ras pathway resulted in a reduction of the migratory and motile capacity of prostate cancer cells, suggesting that the pathway is activated during metastasis (Sequeira *et al.*, 2008).

1.2.4 Intravasation and survival in the circulation

As a primary tumour grows, it requires more oxygen and nutrients in order to progress. In order to overcome this problem, it starts to develop new blood vessels through the secretion of angiogenic factors such as hypoxia-inducible factor-1 (HIF-1) and vascular endothelial growth factor (VEGF), allowing a greater flux of resources to build up, and the tumour to grow (Shweiki *et al.*, 1992). In addition, these blood vessels offer a means of escape for the cancer cells to leave the primary tumour, penetrate into the vessel, and shed into the blood's circulatory system through a process called intravasation. This process involves multiple adhesive interactions, and is facilitated by the loss of CD82, normally responsible for anchoring tumour cells to the endothelium (Bandyopadhyay *et al.*, 2006).

Alternatively, some tumour cells might also enter the circulation through the lymphatic system. Cancer cells can invade the lymphatics in the primary site, where they are drained into the lymph nodes, and enter the blood circulation either via efferent lymphatic vessels that end up in the venous system, or by newly formed blood vessels serving the lymph node metastases (Paget, 1889). Tumour cells are then disseminated throughout the body, where the vast majority are destroyed during cellular clearance from the circulation, mainly due to their large size. The 0.1% that do survive, probably do so by aggregating with platelets in the blood, concealing them from immune surveillance through the production of chemokines, cytokines, and growth factors (Im *et al.*, 2004). These cells need to survive long enough in order to colonise a distant site of preference.

1.2.5 Extravasation and colonisation of distant site

The idea that cancer cells 'home' to specific organs was first recognised by Paget over a century ago with his 'seed and soil' hypothesis, which states that selected cancer cells (seeds) will only readily grow at specific sites (soil) (Paget, 1989). The majority of prostate and breast cancers for example, choose the bone as their preferred metastatic site. More recent research however, has established that this is probably due to the efficiency of a particular type of cancer cell to grow in the microenvironment and molecular background of a specific organ, so 'the compatibility of the 'seed' with the 'soil'. Other factors that contribute to this homing phenomenon are the presence of chemokines and the availability of energy-rich sources (Fidler, 2001).

Upon arrival at the distant site, the cancer cells arrest on the endothelial surface of the blood vessel and undergo transendothelial migration, a process involving numerous adhesive interactions initially involving selectins and stabilised by integrin binding (Orr *et al.*, 1995). The cells then penetrate the endothelial junctions by a process known as extravasation. Endothelial cells aid in transmigration, as they retract following cancer cell attachment by the alteration of the expression, and localisation of adhesion molecules such as N-cadherin, VE-cadherin, and PECAM-1 (Voura *et al.*, 1998).

Once within the secondary site, the new micro-environment surrounding the metastatic cells is initially hostile and the survival of the cells depends on their molecular features and the ability to successfully engage in cross-talk with their surrounding environment. The cytoskeletal protein ezrin appears to facilitate this process by aiding the cells in resisting stress and linking them to the cytoskeleton (Khanna *et al.*, 2004). In addition, growth-factor receptor-ligand interactions between the cancer cells and host cells result in an interactive signalling loop, thereby up-regulating survival pathways and angiogenesis (Derynck *et al.*, 2001). These

processes allow the cells to survive and establish themselves in their new environment, developing a secondary tumour.

1.3 Prostate cancer metastasis

At the early stages of prostate cancer, the tumour remains confined within the prostatic capsule. However, once the cells acquire genetic changes to make them more aggressive, they begin to penetrate into surrounding tissues including; the erectile nerves, seminal vesicles, bladder, and rectum. Some cells meanwhile are disseminated around the body via either the lymphatic or vascular route. If via the former route, the prostate lymphatics drain into the periprostatic subcapsular network, with primary drainage occurring via the internal and external iliac, perivesical, obturator, and the presacral nodes, while secondary drainage transpires at the inguinal, common iliac, or para-aortic nodes (Cellini *et al.*, 2003). Surviving prostate cancer cells can then metastasise to preferred sites which include; the bones, lungs, liver, or brain. However as mentioned above, the red bone marrow of the axial skeleton is the preferred site for prostate cancer metastasis, with around 90% of advanced prostate cancer patients developing skeletal metastases (Taichman *et al.*, 2002)

1.3.1 Why the bone?

The reason why prostate cancers have a predilection for the bone is as of yet, unclear. One possible reason however, may be the high vascularity of the bone marrow, whose capillaries (sinusoids) are perhaps more permissive to circulating tumour cells due to the fenestrated endothelial cells that line them (Paku *et al.*, 2000). In addition, the prostate is surrounded by a rich venous plexus known as Batson's Plexus, which connects the gland to the venous drainage system of the spine, explaining the frequent occurrence of lumbosacral spinal metastases seen in advanced prostate cancer patients (Batson, 1995).

Another perhaps more important reason is the bone micro-environment, and the bone-derived growth factors released by bone cells, which may have proliferative effects on the cancer cells (Mundy, 1997). The chemokine receptor CXCR4 for example, has been shown to be involved in the motility and invasion of prostate cancer cells during metastatic implantation in the bone marrow. In addition, its expression increases with prostatic malignancy, with the highest expression levels being seen in highly aggressive and bone metastatic prostate cancer samples (Taichman *et al.*, 2002).

Another important stimulus appears to be the need of prostate cancer cells for a lipid source, which they require as a form of energy in order to carry out metabolism and tumour cell maintenance. This was demonstrated with PC-3 cells, which absorbed lipids and grew rapidly when lipids were present within the bone marrow (Brown *et al.*, 2006). The main reason why prostate cancer cells are thought to metastasise to the bone however, appears to be due to the genetic makeup of the cancer cell itself, allowing it to respond to the osteotropic factors present in the microenvironment of the bone, as described below.

1.3.2 Cell biology of bone development

The most common complication in advanced prostate cancer patients is morbidity from bone metastasis, with symptoms such as; bone pain, anaemia, pathologic fractures, and spinal cord compression. The few treatments that exist are merely palliative, as no cure has yet been discovered. For this reason, intensive research has gone into investigating the molecular mechanisms behind bone metastasis, and for this a thorough understanding of the biology of the bone is required.

1.3.2.1 The bone

The bone is a specialised, highly dynamic connective tissue, hardened by mineralisation with calcium phosphate that constantly undergoes remodelling. Its functions are mechanic in nature, by acting to sustain and protect body structures, offering rigidity and shape, and aiding in

locomotion. The vertebrate skeleton is made up of long bones and flat bones, of which there exist two major histological types of mature bone tissue. The compact or cortical bone is dense and organized in structure, and mostly found in long bone shafts and flat bone surfaces. It is composed of concentrically laid down bone, surrounding a network of blood vessels, lymphatics, nerves, and connective tissue (known as an osteon or Haversian system). Trabecular or cancellous bone meanwhile, is lighter, less dense, and irregular in structure, forming the edges of long bones and the inner segments of flat bones. It is made up of intersecting rods and plates (trabeculae) with interceding marrow, giving it a sponge-like structure. A typical bone is comprised of an outer layer of compact bone that is spread upon the surface of cancellous bone and the medullary cavity.

Compact bone makes up around 80% of the total skeleton, situated mainly in the peripheral bones, whereas cancellous bone is mainly found in the axial skeleton. However, despite making up the minority of the skeleton, due to the greater surface area of cancellous bone, it is the site where the majority of bone turnover occurs. This process involves four types of bone cells; the osteocytes which are rooted within the bone matrix, osteoblasts and osteoclasts, and finally, the bone lining cells which are located on the surface of bones (Datta *et al.*, 2008).

1.3.2.2 Osteoblasts

Osteoblasts derive from mesenchymal cells under the regulation of BMPs, osteoblast-stimulating factor (OSF-1), and IGF-I, amongst others (Yang *et al.*, 2001). The cells secrete a collagen-proteoglycan bone matrix known as osteoid, capable of binding calcium salts which thereby induces its mineralisation, converting it to bone. This bone matrix deposition occurs in both intramembraneous and endochondral bone formation, and is regulated with spatiotemporal coordination by a variety of endocrine, paracrine, and autocrine factors (Ducy *et al.*, 1999).

In addition, osteoblasts can regulate the differentiation of osteoclasts by the secretion of factors such as Macrophage colony-stimulating factor (M-CSF), Interleukins (IL-1,-6 and -11), tumour

necrosis factor (TNF), parathyroid hormone, and vitamin D, amongst others, and can also regulate osteoclast localisation by altering expression levels of adhesion molecules involved in osteoclast:bone matrix binding, allowing osteoblasts to recruit osteoclasts to sites of resorption (Athanasou, 1996).

Following bone formation, osteoblasts have one of four fates; to become encased in the bone matrix to form osteocytes, undergo apoptosis, trans-differentiate into chondroid or chondroid bone depositing cells, or finally, transform into dormant osteoblasts to become bone lining cells that cover the bone surface. These cells act as a blood-bone barrier, since they regulate the passage of ions in and out of the bone extracellular fluid. In addition, if exposed to parathyroid hormone or mechanical forces, they are capable of re-differentiating back into osteoblasts (Franz-Odenaal *et al.*, 2006).

1.3.2.3 Osteocytes

Osteocytes are terminally differentiated osteoblasts that have become enclosed within the bone matrix, and despite them being the most abundant cellular constituent in adult bone, making up 95% of all bone cells, little is known about this transformation. However, osteocyte phenotype and formation has been linked to type-I collagen cleavage, and a variety of cytoskeletal and matrix proteins (Holmbeck *et al.*, 2005).

What is known is that their bone forming capacity is much lower than that of the osteoblasts, but despite this they play a vital role in bone structure maintenance. Osteocytes interact with each other via a network of cellular processes which proceed inside lacuna-cannaliculi within the bone matrix. Recent data has shown that osteocytes act via these networks as mechanosensory cells, capable of sensing mechanical stress and strain and interacting with osteocytes in order to maintain bone structure and mass (Datta *et al.*, 2008).

1.3.2.4 Osteoclasts

Osteoclasts are multinucleated cells that originate from haematopoietic precursors of the monocyte lineage, similar to macrophages. Due to their lineage, osteoclasts have villous folded plasma membranes, resulting in their characteristic ruffled border that acts like a lysosome, allowing the cells to carry out phagocytosis, like their macrophage relatives (Ash *et al.*, 1980).

Osteoclasts enter the bone through blood vessels, where they bind to bone surfaces via integrin-mediated binding and occupy small depressions in the bone exterior known as Howship lacunae, to carry out the process of bone resorption. The osteoclasts secrete enzymes such as acid phosphatase as well as hydrogen ions via H⁺-ATPase pumps into the surrounding tissue, resulting in acidification and breakdown of the protein and inorganic portions that make up the bone matrix. This leads to bone demineralisation and the hollowing out of bone material to form the bone marrow cavity (Baron *et al.*, 1985).

In order to prevent any defects in bone resorption, the number and function of osteoclasts needs to be highly regulated, as, if their numbers are too high, too much bone dissolving will occur resulting in disorders like osteoporosis, and if too little bone resorption occurs the hollowing of the bones for the marrow does not occur, resulting in osteopetrosis (Tondravi *et al.*, 1997).

1.3.2.5 Bone Matrix

Bone is composed of 50-70% mineral mainly in the form of hydroxyapatite and small amounts of carbonate, magnesium, and acid phosphate, which provide the bone with mechanical rigidity and strength. The rest is made up of 20-40% organic matrix, 5-10% water, and 3% lipid. The bone matrix functions to provide elasticity and flexibility to bone, and is composed mainly of type-I collagen with trace amounts of types III and IV, as well as an inorganic fraction made up of crystalline mineral salts and hydroxyapatite (Brodsky and Persikov, 2005)

As mentioned above, bone matrix is deposited by osteoblasts as osteoid, and undergoes mineralisation to form bone. Matrix maturation correlates with alkaline phosphatase expression, which is secreted by the osteoblasts following mineralisation, and acts to precipitate hydroxyapatite which then facilitates calcium and phosphorus sequestration. In addition to the presence of collagen in the matrix, there exist a variety of non-collagenous calcium- and phosphate- binding proteins such as osteocalcin, osteopontin, and bone sialoprotein, which aid in the regulation of mineral deposition by controlling hydroxyapatite crystal size as well as in bone turn over and activity. The most abundant non-collagenous proteins however, are fibronectin and osteonectin, which are essential in regulating osteoblast differentiation, proliferation, and survival. Osteopontin on the other hand, affects the osteoclasts and is necessary for bone resorption (Clarke, 2008).

1.3.2.6 Bone marrow

The bone marrow is a highly specialised soft and diffusive connective tissue, known as myeloid. It is the source of blood cell production located within medullary cavities of long and spongy bone. There exist two types of bone marrow; red and yellow. Red marrow is the only present form in infants and is responsible for the production of red blood cells. As an individual ages, this red marrow is progressively substituted by the yellow marrow, where cells have become saturated with fat and are incapable of blood cell production.

There exist two types of stromal cells in the bone marrow; haematopoietic stem cells, which give rise to three classes of blood cells; leukocytes (white blood cells), erythrocytes (red blood cells), and thrombocytes (platelets), and mesenchymal stem cells located in the vicinity of the central sinus of the bone marrow. These pluripotent cells are the progenitors of osteoblasts, chondrocytes, and myocytes, amongst others. They are capable of self-maintenance throughout an individual's life, whose progeny make up tissues including; bone, tendon, ligament, and marrow stroma (Manolagas and Jilka, 1995).

1.3.3 Bone remodelling: bone formation and resorption

Bone is a dynamic tissue that constantly undergoes remodelling and is capable of enduring regeneration throughout life. In order to maintain bone mass, a tightly regulated balance exists between osteoblastic bone formation and osteoclastic bone resorption. Remodelling begins to occur before birth, and continues throughout a person's life. It involves the renewal of bone so as to sustain bone strength and mineral homeostasis. The process entails the continuous removal and resorption of old bone in order to prevent accumulation of bone microdamage, and replacing it with newly produced bone matrix that mineralises to form new bone (Clarke, 2008).

The process of remodelling involves four main steps; activation, resorption, reversal, and bone formation. Activation entails the recruitment of pre-osteoclasts from the circulation into bone, as well as their vitamin-D induced differentiation into mature osteoclasts which bind to the bone matrix. The activated osteoclasts then dig out a tunnel and resorb through old bone, closely followed by the osteoblasts that enter behind them. Reversal then occurs as the osteoclasts undergo apoptosis, and bone resorption is taken over by bone formation carried out by the osteoblasts, which line the bone surface and start to deposit layers of matrix into the cavity. The signals that link the end of bone resorption with the start of bone formation are thought to be triggered by growth factors including; transforming growth factor- β (TGF- β), bone morphogenetic proteins (BMPs), Insulin growth factors (IGFs), and fibroblast growth factors (FGFs), as all are induced during bone turnover (Sims and Gooi, 2008).

Bone formation is followed by matrix mineralisation to form new bone, a process regulated by the osteoblasts that release small vesicles to induce accumulation of calcium and phosphate as well as destroying mineralisation inhibitors such as pyrophosphate and proteoglycans. Some of the osteoblasts become enclosed by the newly formed bone to become osteocyte or bone lining cells, while the rest undergo apoptosis. The tunnel gradually becomes filled with concentric layers of new bone, leaving only a narrow central canal with a capillary that sprouts down the

centre of it. This canal acts as a means of access for osteoclasts and osteoblasts, while the blood vessel transports and supplies the bone cells with nutrients which they require in order to survive (Jaworski *et al.*, 1981).

This process is tightly regulated by a variety of hormones, and involves the combined efforts of osteoblasts, osteoclasts, osteocytes, and bone marrow stromal cells. The most established cellular interaction is between the osteoclasts and osteoblasts, the key players in bone remodelling. Osteoclast differentiation, activation, and resorption is dependent on receptor activator of nuclear factor- κ B ligand (RANKL), osteoprotegerin (OPG), macrophage colony-stimulating factor (M-CSF), parathyroid hormone (PTH), and 1,25-dihydroxyvitamin D₃.

RANKL and M-CSF are secreted by both osteoblasts and bone marrow stromal cells, and both are critical in regulating osteoclastogenesis. M-CSF is critical for osteoclast precursor proliferation, differentiation, survival, and cytoskeletal rearrangement, essential for bone resorption. RANKL meanwhile, is required for osteoclast activation by inducing receptor activator of nuclear factor- κ B (RANK). In fact, with low levels of M-CSF, RANKL is essential and sufficient for the complete differentiation of osteoclast precursors into mature osteoclasts (Lacey *et al.*, 1998).

As the reversal from bone resorption to formation is such a critical step during bone remodelling, it makes sense that the osteoblasts control osteoclast activity. Therefore, RANKL exists both in a membrane-bound form on the surface of osteoblastic and stromal cells, as well as in a soluble form, secreted by these cells. In order to initiate its effects, RANKL needs to bind to its receptor RANK, present on the surface of pre-osteoclastic cells. The same is true for M-CSF, which is also secreted by the osteoblasts and needs to bind to its own receptor c-fms, also expressed on osteoclast precursors. RANK activation by RANK-L binding results in its interaction with downstream TNF-receptor associated (TRAF) family members such as; NF- κ B, c-fos, Jun N-terminal kinases (JNK), and Akt/PKB, inducing transcription of genes vital for

osteoclast activation and differentiation (Khosla, 2001). These genes include the monocyte-chemokines MCP-1 and RANTES, which are critical in the fusion of RANK⁺ mononuclear precursors and hence formation of multi-nucleated osteoclastic cells (Kim *et al.*, 2006).

Osteoblasts also secrete osteoprotegrin (OPG), a soluble decoy receptor of the TRAF superfamily that binds to RANKL with high-affinity thereby inhibiting its effects on the RANK receptor (Cohen, 2006). On the other side of the spectrum, osteoblasts can also *promote* osteoclast survival by secreting IL-6, which activates NF- κ B and induces osteoblast RANK-L expression. Other pro-resorptive cytokines include TNF- α and IL-1 which act mainly by promoting M-CSF production and increasing RANKL expression, whereas TGF- β released from the bone matrix, has the opposite effect, by up-regulating OPG expression (Takai *et al.*, 1998).

Systemic hormones also play a role in bone remodelling and include PTH, vitamin D₃, and glucocorticoids, which are capable of increasing RANKL production or decreasing OPG secretion, whereas estrogen increases OPG production (Hofbauer *et al.*, 1999; Lee and Lorenzo, 1999). Finally, a more physical means by which osteoblasts can promote bone resorption is by secreting collagenase and tissue plasminogen, which can digest the unmineralised organic matrix that covers bone surfaces, and it is under these circumstances that osteoclasts resorb most efficiently (Chambers *et al.*, 1985).

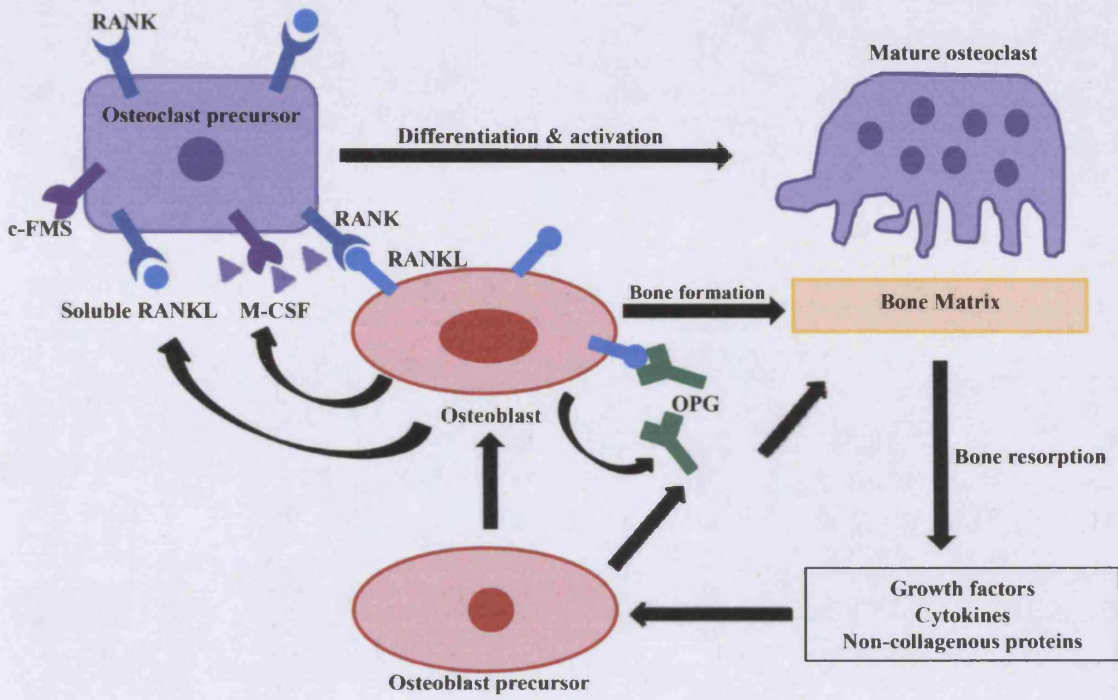


Figure 1.7: Regulation of osteoclastogenesis that occurs during bone remodelling. Adapted from (Khosla, 2001).

1.3.4 Bone metastases

In order for a malignant cell to establish itself in a secondary site, it requires several genetic changes to allow it to adapt and take advantage of the nutrients in its novel micro-environment. Metastasis to the bone occurs in a comparable fashion to the process described in section 1.2.6. However, in order to invade this secondary site, the tumour cells need to acquire the capacity to migrate through the sinusoidal wall, invade the marrow stroma, and induce angiogenesis. Once a prostate cancer cell develops into micro-metastases within the bone marrow space, it results in an interruption of the osteoblast-fibroblast microenvironment, inducing osteoclast-mediated bone resorption and the discharge of stimulatory cytokines from the bone surface.

This in turn sets off a cycle of resorption and tumour stimulation, which as the metastasis progresses results in an imbalance of bone resorption and formation, ensuing in a simultaneous acceleration of the two processes and hence growth of the bone metastases (Clarke *et al.*, 2009). Depending on the balance of bone resorptive and bone formation factors, the tumour cells stimulate either osteoclast or osteoblast cell formation, which ultimately decides the type of metastatic lesion that arises.

1.3.4.1 Osteolytic metastases

Unlike the bone metastases seen in breast and lung cancers, the majority of the metastases that arise from prostate cancer are osteoblastic in nature. However, a crucial first step during prostate cancer cell initial migration is the activation of osteoclast-mediated bone resorption. This acts as a means of de-bulking the bone, thereby allowing the tumour cells to penetrate into the bone matrix and stimulate the release of survival and growth factors that promote tumour progression.

Tumour cells induce bone resorption by recruiting osteoclast precursors by the release of chemokines such as M-CSF, and induce their differentiation into mature osteoclasts by the

production of soluble RANK-L and parathyroid hormone-related protein (PTHrP). Increased levels of PTHrP have been demonstrated in the PC-3 prostate cancer cell line that is derived from bone metastases lesions (Iwamura *et al.*, 1994). Osteolysis carried out by the osteoclasts, results in the release of growth factors that act both as autocrine and paracrine effectors of tumour cell survival, and later on, cytokines that promote bone formation. The former includes TGF- β , which in breast cancer is capable of increasing PTHrP tumour cell expression, resulting in a vicious cycle whereby PTHrP increases bone resorption, inducing a greater release of growth factors capable of inducing its own production and thereby promoting tumour cell growth (Mundy, 2002).

Osteolysis also promotes production of interleukins-8 and -11 (IL-8, -11) secreted by osteoblasts and bone marrow cells, which are chemokines capable of inducing osteoclast differentiation (Bendre *et al.*, 2005). Meanwhile, family members IL-11 and IL-6 act as important mediators of pathological bone loss, and hence can stimulate osteoclast formation and activity. In addition, IL-6 can regulate the expression of members of the T family including RANK and OPG (Yang *et al.*, 2005).

1.3.4.2 Osteoblastic metastases

As mentioned above, prostate cancer bone metastasis mainly results in the formation of osteoblastic lesions. Symptoms arising from this include; anaemia, increased vulnerability to infection, bone pain, pathological fractures, and spinal-cord compression. In order for these osteoblastic metastases to develop, bone resorption needs to occur so as to allow the tumour cells to invade the bone matrix, and eventually tip the neighbouring cytokine environment in favour of bone formation. The interactions between tumour cells, bone cells, and the bone matrix, form a cycle of osteoblastic lesion development (Figure 1.8). The mature osteoblasts proliferate and deposit new matrix for bone formation, and this un-mineralised matrix supplies the tumour cells with a fertile environment full of growth factors and non-collagenous proteins,

which aid in tumour cell survival and proliferation. The tumour cells then in turn activate more osteoblasts, resulting in a cycle of bone formation and tumour growth (Clark and Torti, 2003).

The switch between osteolysis and bone formation is thought to occur due to the secretion of OPG by the tumour cells. As mentioned previously, OPG is a decoy receptor that can inhibit RANK-L secreted by the tumour cells, and thereby inhibits osteoclastogenesis and bone resorption. In addition, OPG acts as a survival factor by binding to monocyte-induced Tumour-necrosis factor-related apoptosis-inducing ligand (TRAIL) thereby protecting it from TRAIL-induced apoptosis. Therefore, over-expression of OPG by prostate cancer cells may explain the osteoblastic phenotype of the resulting bone metastases (Holen *et al.*, 2002).

In addition, prostate cancer cells secrete a variety of osteogenic factors including endothelins (ETs), TGF- β 1, BMPs, IGFs, FGFs, platelet-derived growth factors (PDGFs), urokinase-type plasminogen activator (uPA), and PSA, which by inducing bone formation provide a fertile environment for prostate cancer cells, allowing for their survival and proliferation. Endothelins for example, are important factors in the regulation of bone formation, synthesised in vascular endothelial cells. When applied exogenously to prostate cancer cells, ETs act via the Endothelin-A receptor (ETAR), to enhance cell proliferation and osteoblast over-stimulation, along with promotion of the mitogenic effects of other growth factors such as IGFs, making it an essential intermediary of osteoblastic metastasis (Guise *et al.*, 2003). Treatment with ETAR agonist Atrasentan, has demonstrated promising results, with patients displaying reduced skeletal morbidity as well as a prevention of osteoblastic lesions in mice (Carducci *et al.*, 2003).

Levels of IGFs (IGF-1 in particular), are locally increased within the bone micro-environment, and mitogenically stimulate osteoblasts and decrease collagen degradation as well as supporting the survival and growth of prostate cancer cells. This local increase in IGF-1 levels correlates with an increase in the concentration of uPA and IGF-binding proteins, resulting in a release of active IGF-1, and hence an enhancement in IGF-receptor mediated

osteoblast and prostate cancer cell proliferation (Koutsilieris and Polychronakos, 1992). It therefore comes as no surprise that IGF-I levels have been demonstrated to be associated with increased risk of prostate cancer, with low levels of IGF binding protein 3 (IGFBP-3) being present in patients with bone metastasis (Chan *et al.*, 1998).

FGFs meanwhile, are vital in the regulation of processes such as migration, proliferation and differentiation, and in the bone both the FGF-1 and FGF-2 isoforms can induce proliferation of immature osteoblasts, while decreasing the proliferation of mature osteoblasts. In addition, FGF-2 can inhibit osteoclastogenesis, suggesting that both isoforms can induce multiple and complex effects on bone cells (Valta *et al.*, 2006). PDGF isoforms can act as potent osteotropic factors that can contribute to osteoblastic migration and proliferation (Yi *et al.*, 2002).

PSA is a highly secreted prostate cancer protein with kallikrein serine protease activity. It acts to cleave osteolytic PTHrP into osteoblastic fragments capable of inducing bone formation due to their homology to ET-1, and capability of activating ETAR. Like uPA, PSA is also capable of cleaving IGFBP3 to release IGF-1, which promotes osteoblast proliferation. In addition, it can activate osteoblastic growth factors, including TGF- β . This again helps explain the osteoblastic phenotype of prostate cancer metastases (Cohen *et al.*, 1994).

Finally, although several members of the TGF- β family promote osteoclastogenesis, TGF- β 2 is expressed by prostate cancer cells and is capable of inducing osteoblastic metastases. Constituents of the BMP subfamily, including BMP-2, -6, and -7, have high expression levels in prostate cancers and induce a similar bone-inducing effect. BMP-2 for example, promotes bone formation and regulates mineralization by synergizing with the Wnt pathway. BMP-6 meanwhile has the opposite effect as it can enhance PTH and vitamin-D induced osteocalcin expression, which is vital in the regulation of osteoclasts (Masuda *et al.*, 2003).

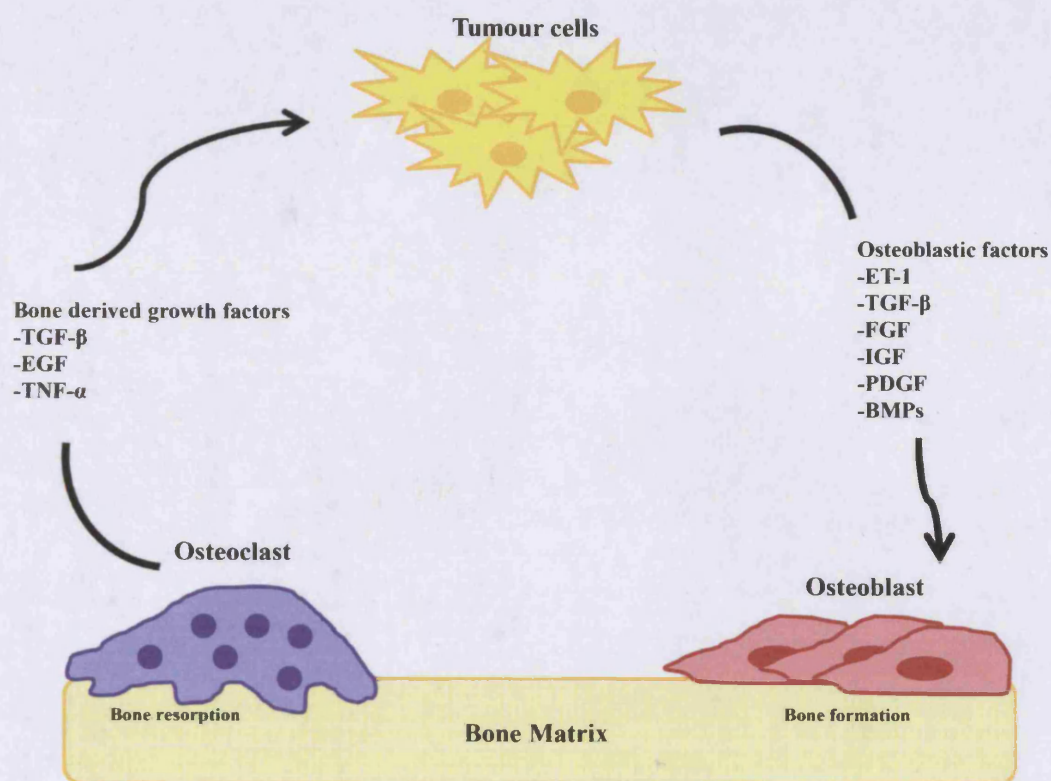


Figure 1.8: Mechanisms of osteoblastic metastases in prostate cancer. Tumour cells and the bone microenvironment interact to constitute a vicious cycle that contributes to the predominant osteoblastic lesions that form in metastatic prostate cancers (Adapted from (Fili *et al.*, 2009)).

It is believed that with thorough understanding of the many complex pathways that occur in the bone, that anti-survival factors capable of inhibiting the pathways that aid in the growth of the cancer cells in this microenvironment can be developed. This would therefore allow for the production of drugs that can prevent or inhibit the metastasis of prostate cancer. The family of growth factors that this project focuses on is the bone morphogenetic protein family whose role in prostate cancer remains elusive to this day.

1.4 The Transforming Growth Factor- β (TGF- β) superfamily

The Transforming Growth Factor- β (TGF- β) superfamily is one of the biggest and most influential, ubiquitous family of proteins. To date, more than 30 structurally related growth

factors have been identified in the TGF- β superfamily, including: TGF- β s, Activins, Inhibins, Bone and Morphogenetic Proteins (BMPs), Growth and Differentiation Factors (GDFs), and Mullerian Inhibiting Substance (MIS) (Heldin *et al.*, 1997). Members of this family are dimeric pleiotropic proteins that are ubiquitously expressed in a wide range of different cell types, tissues, and species. They play an important role during embryonic development and regulate a wide variety of cellular processes including; proliferation, growth, migration, differentiation, apoptosis, and extracellular matrix production (Schmierer and Hill, 2007).

1.4.1 The Bone Morphogenetic Protein (BMP) family

The BMP subfamily contains over 20 members, which were initially described as inducers of bone formation by Urist *et al.* in 1965 (Granjeiro *et al.*, 2005). Table 2.1 summarises the BMPs identified to date, along with the receptors they bind to. Like other members of the TGF- β superfamily, BMPs are synthesised as large precursor proteins, which following dimerisation, are proteolytically cleaved by a furin peptidase at the consensus sequence Arg-X-X-Arg. This leads to the formation of biologically active mature dimers, 110 to 140 amino acids in length. BMPs form either homo- or hetero-dimers linked by disulphide bonds, which is necessary for their biological activity. The active domain of BMPs contains a conserved motif of seven cysteines, six of which form a structure known as a cysteine knot, and this is involved in dimerisation (Massague *et al.*, 1994).

Active BMP and TGF- β ligands signal through two types of serine/threonine transmembrane receptors; seven type-I and five type-II TGF- β receptors. Activation of these receptors leads to downstream signalling via two independent pathways; the Smad-dependent and Smad-independent pathways. Smads are the downstream signalling molecules used by TGF- β family members to alter the expression of their responsive genes, leading to changes in cellular properties (Miyazawa *et al.*, 2002).

TGF- β ligands can also interact with coreceptors that can either promote or impede receptor kinase signalling. Endoglin and the proteoglycan betaglycan (TGF- β RIII) for example, are capable of regulating TGF- β signalling. More specifically, TGF- β RIII mediates both ligand dependent and independent signalling via smad and non-smad signalling pathways. Its ligands include; TGF- β 1, 2, and 3, inhibin, and BMP-2, -4, and -6. In most cases, presentation of these ligands by TGF- β RIII increases their binding to their type-I and type-II receptors, and thereby promotes smad signalling. As TGF- β signalling is often growth inhibitory, this synergisation may be one of the reasons why TGF- β RIII is often lost in cancers. However, when bound to inhibin, the type-III receptor can lead to inhibition of BMP and TGF- β signalling (Gatza *et al.*, 2010).

BMP	Alternative names	Type-I receptors	Type-II receptors	Smads	References
BMP-2	BMP-2a	ALK 3/6	BMPRII ActRIIA	1/5/8	(Koenig <i>et al.</i> , 1994),(Liu <i>et al.</i> , 1995), (Yamaji <i>et al.</i> , 1994)
BMP-3	Osteogenin	ALK 4	ActRIIA	2/3	(Daluisi <i>et al.</i> , 2001)
BMP-3B	GDF-10				
BMP-4	BMP-2B	ALK 3/6	BMPRII ActRIIA	1/5/8	(ten Dijke <i>et al.</i> , 1994; Regazzoni <i>et al.</i> , 2001)
BMP-5	-	ALK 3		1/5/8	(Beck <i>et al.</i> , 2001) (Mailhot <i>et al.</i> , 2008)
BMP-6	Vrg1, Dvr6	ALK 1/2/3/6	ActRIIA ActRIIB BMPRII	1/5	(Ebisawa <i>et al.</i> , 1999; Ahmed <i>et al.</i> , 2001)
BMP-7	OP-1	ALK2/3/6	BMPRII ActRIIA	1/5/8	(Liu <i>et al.</i> , 1995; Aoki <i>et al.</i> , 2001; Nakagawa <i>et al.</i> , 2004)
BMP-8A	OP-2	ALK 3/6			(Zhao <i>et al.</i> , 2001)
BMP-8B	OP-3				
BMP-9	GDF-2	ALK 1	ActRIIA ActRIIB BMPRII	1/5	(Brown <i>et al.</i> , 2005; Lopez-Coviella <i>et al.</i> , 2006)
BMP-10	-	ALK 3/6	BMPRII ActRIIA	1/5/8	(Mazerbourg <i>et al.</i> , 2005)
BMP-11	GDF-11	ALK 4	ActRIIA ActRIIB	2/3	(Oh <i>et al.</i> , 2002; Andersson <i>et al.</i> , 2006)

BMP	Alternative names	Type-I receptors	Type-II receptors	Smads	References
BMP-12	GDF-7, CDMP-3	ALK 3/6	BMPII ActRIIA		(Zhao <i>et al.</i> , 2001)
BMP-13	GDF-6	ALK 3/6	BMPII ActRIIA	1/5/8	(Gordon and Blobe, 2008) (Zhao <i>et al.</i> , 2001)
BMP-14	GDF-5	ALK 3/6	BMPII ActRIIA	1/5/8	(Chen <i>et al.</i> , 2006)
BMP-15	GDF-9B	ALK 6	BMPII	1/5/8	(Moore <i>et al.</i> , 2003)
GDF-1	-	ALK 4	ActRIIB	2/3	(Cheng <i>et al.</i> , 2003)
GDF-3	-	ALK 4/7	ActRIIA ActRIIB	2/3	(Andersson <i>et al.</i> , 2007; Andersson <i>et al.</i> , 2008)
GDF-8	-	ALK 4/5	ActRIIB	2/3	(Rebbapragada <i>et al.</i> , 2003)
GDF-9	-	ALK 5	BMPII	2/3	(Mazerbourg and Hsueh, 2006)
GDF-15	PDF, MIC-1, PLAB, NAG-1, PTGFB		TGF- β RII	2/3	(Xu <i>et al.</i> , 2006; Johnen <i>et al.</i> , 2007)

Table 1.3: All identified BMPs to date, and their corresponding type-I and type-II receptors as well as the R-Smads they activate. Empty boxes mean receptors/smads have not yet been identified.

1.4.2 Bone Morphogenetic receptors and their structure (BMPRs)

Members of the TGF- β superfamily bind to two diverse subfamilies of receptors in order to mediate their cellular activity. These receptors termed type-I and type-II, are transmembrane serine/threonine kinase receptors. Both receptor types are required for downstream signalling

to occur; the type-I receptors are unable to bind their ligands without the presence of the type-II receptors, while the latter is incapable of signalling without their type-I counterparts (Wrana *et al.*, 1994). Seven type-I TGF- β receptors have been described in humans (Table 1.3), known as Activin Like Kinase Receptors 1-7 (ALK), of which all bind BMPs except for ALK-7. In the case of type-II Receptors, five receptors have been identified of which only 3 bind BMPs; BMP Receptor type-II (BMPRII), Activin A Receptor type IIB (ActRIIB) and ActRIIA. TGF- β receptors type-II and -III are the type-II receptors used by TGF- β ligands (Moustakas and Heldin, 2009).

Both types of receptors are conformationally conserved and are made up of an amino terminal extracellular ligand binding domain, a single transmembrane domain, and a large serine/threonine kinase domain at their carboxyl-terminal (Attisano *et al.*, 1994). Figure 1.9 shows a structural diagram of both the type-I and type-II receptors.

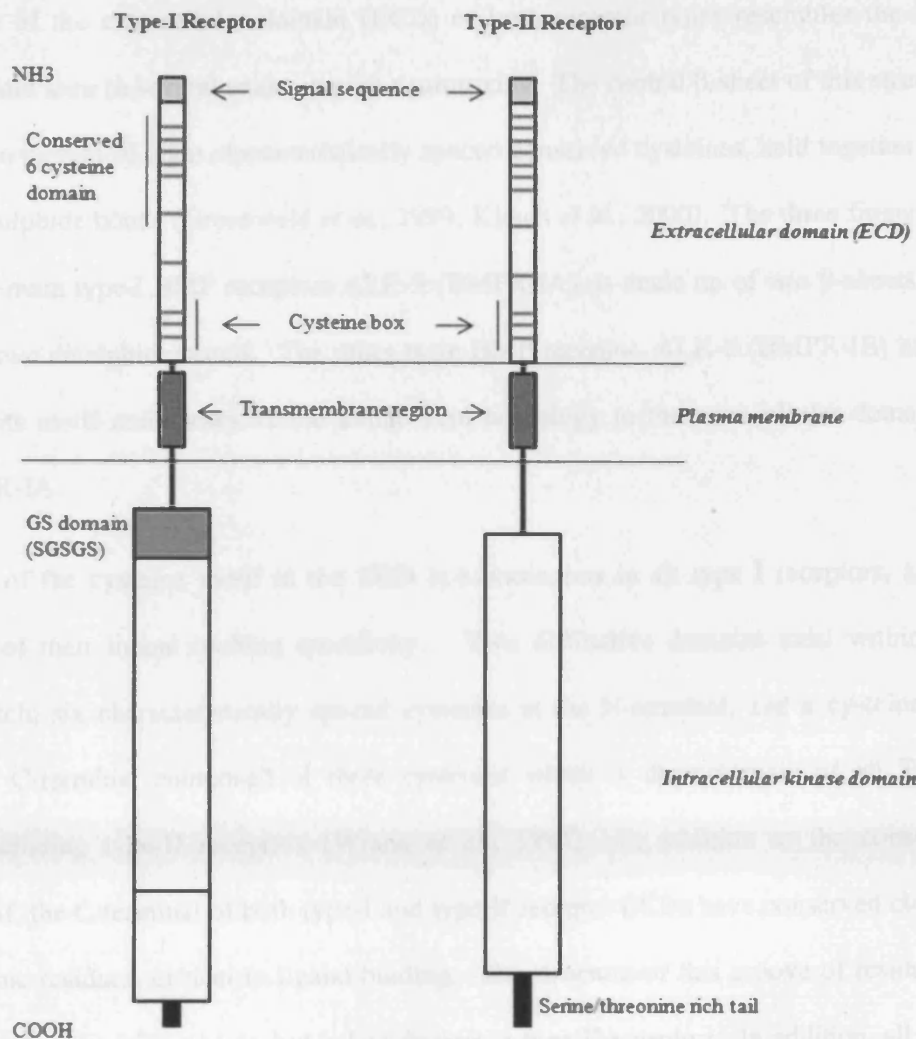


Figure 1.9: Structural diagram of the type-I and type-II TGF- β receptors which are very similar to the BMP receptors. The boxes represent the conserved domains of most of the receptors of this family and the horizontal lines in the ECD represent the extracellular conservedly spaced cysteines. Adapted from (Kingsley, 1994).

1.4.2.1 Receptor extracellular ligand binding domain

The structure of the extracellular domain (ECD) of both receptor types resembles the three finger toxin fold seen in several snake venom neurotoxins. The central β -sheet of this structure has a common pattern of eight characteristically spaced conserved cysteines, held together by a cluster of disulphide bonds (Greenwald *et al.*, 1999; Kirsch *et al.*, 2000). The three finger fold of one of the main type-I BMP receptors ALK-3 (BMPR-IA), is made up of two β -sheets, one α -helix, and two disulphide bonds. The other main BMP receptor, ALK-6 (BMPR-IB) has 10 cysteines in its motif and shows 42.1% amino acid homology to the extracellular domain of human BMPR-IA.

The spacing of the cysteine motif in the ECD is homologous in all type I receptors, and is independent of their ligand binding specificity. Two distinctive domains exist within this cysteine stretch; six characteristically spaced cysteines at the N-terminal, and a cysteine box motif at the C-terminal composed of three cysteines which is characteristic of all TGF- β receptors, including type-II receptors (Wrana *et al.*, 1994). In addition to the conserved cysteine motif, the C-terminal of both type-I and type-II receptor ECDs have conserved clusters of hydrophobic residues, critical in ligand binding. The structure of this groove of residues is common in both types of receptors, but is less distinct in type-II receptors. In addition, all type-I receptors apart from ALK-1, have a large protruding hydrophobic residue on the core α -helix which fits into a hydrophobic pocket of the ligand. This process is known as the 'knob into hole' motif of type-I receptor ligand binding (Kirsch *et al.*, 2000).

The ECD of ActRIIA, ActRIIB, and BMPR-II, on the other hand, does not include an α -helix, and is made up of three anti-parallel β -sheets held together by four disulphide bonds. The first finger of the type-II receptor three finger toxin fold is the least conserved and shows most variability suggesting that it may act as a docking site for ligands and determines binding specificity (Kirsch *et al.*, 2000).

1.4.2.2 Receptor kinase domain

The intracellular cytoplasmic region of both types of receptors consists of an enzymatic serine/threonine kinase domain critical in transducing the downstream signal of BMPs. The kinase domains of the type-I receptors are highly conserved, but only share 40% homology with the amino acid sequence of the type-II kinase domain (Kingsley, 1994). Type-I receptors have a highly preserved region of 30 amino acids rich in serine and glycine, juxtamembrane and near to the N-terminal of their kinase domain (Wrana *et al.*, 1994). This SGSGS motif is known as the GS domain and functions as a substrate for phosphorylation by the type-II receptors. This transphosphorylation is critical as it is required for activation of the type-I receptor, and hence downstream signalling.

In addition, type-I receptors have a 9 amino acid segment in their kinase domains known as the L45 loop, that along with an L3 loop in the C-terminal of Smads, is responsible for establishing the specificity of receptor-Smad interactions (Chen *et al.*, 1998). The type-II receptor kinase domain on the other hand, is constitutively active and hence does not require any activational phosphorylation event (Mace *et al.*, 2006). In addition, type-II receptors have a short serine-threonine rich tail at the C-terminal of their kinase domains, not seen in type-I receptors (Attisano *et al.*, 1994).

1.4.3 The BMP signalling pathway

1.4.3.1 Ligand binding

TGF- β and BMP receptor mediated signalling involves ligands binding and activating specific multi-subunit receptor complexes to trigger a cytosolic kinase cascade (Wrana *et al.*, 1994). Each ligand subunit is responsible for recruiting one type-I and one type-II receptor to form a receptor complex composed of six polypeptide chains containing the two ligand subunits and two pairs of each receptor type. In order to compensate for the outnumbering of receptors by ligands, receptors are capable of binding multiple ligands. Binding affinity is dependent on the

energetic stability of the hydrophobic and electrostatic interactions between ligands and the receptor ECD (Allendorph *et al.*, 2006).

In the case of TGF- β , the ligand binds to the knuckles of the three finger toxin fold of the receptor, where a sequential binding model is apparent, with TGF- β initially binding to its high affinity type-II receptor as a pre-existing homodimer allowing for the recruitment of the type-I receptor. This induces a conformational change in either the ligand or the receptor, resulting in an increased cross-linking ability between the two. This leads to activation of the Smad pathway via Smads 2 and 3.

As opposed to other TGF- β members, BMPs bind to the concave surface of the curved fingers of the receptor and have higher affinity for the type-I rather than the type-II receptor. BMPs can activate two different pathways depending on the way they oligomerise to the same types of receptors. If BMPs bind to preformed heteromeric complexes (PFC) of type-I and type-II receptors simultaneously, the Smad-dependent pathway is activated. On the other hand, if BMPs initially bind to their high-affinity type-I receptor and then recruit the type-II receptor into a heteromeric complex known as the BMP-induced signalling complex (BISC), this leads to activation of the Smad-independent pathway (Nohe *et al.*, 2002).

1.4.3.2 The Smads

Smads are the downstream cytoplasmic signalling molecules of type-I TGF- β and BMP receptors. They are homologues of the originally identified mothers against decapentaplegic (Mad) and Sma proteins, found in *Drosophila* and *C. Elegans*, respectively (Heldin *et al.*, 1997). To date, 8 Smads have been identified in mammals. Smads are grouped into three subfamilies based on their structure and function; the receptor-regulated Smads (R-Smads); Smads 1, 2, 3, 5, and 8, common-partner Smad 4 (Co-Smad), and inhibitory Smads (I-Smads); Smads 6 and 7 (Moustakas *et al.*, 2001). Figure 1.10 is a structural diagram of the three Smad subtypes showing their conserved domains and functions. R-Smads are direct substrates of the

type-I serine/threonine receptors and are phosphorylated at their C-terminal Ser-Ser-X-Ser (SSXS) motif by these receptors, resulting in R-Smad activation. Of the R-Smads, Smads 2 and 3 are known as TGF- β /activin activated Smads, whereas Smads 1, 5, and 8 are the BMP activated Smads (Miyazawa *et al.*, 2002).

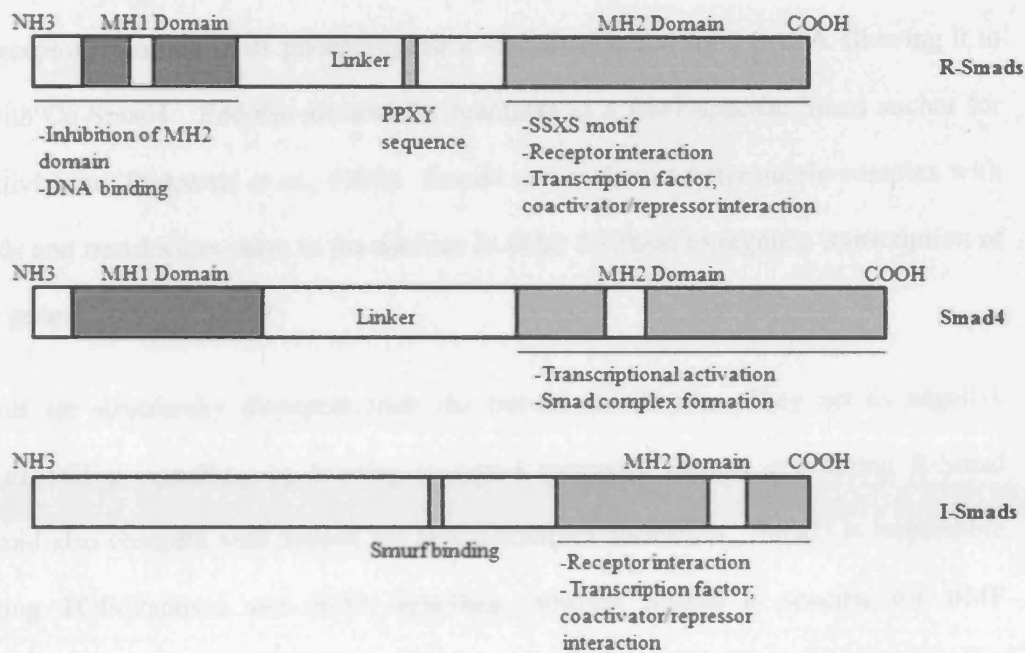


Figure 1.10: Structural diagram of the three Smad subtypes showing areas of homology (filled boxes) as well as conserved areas of functionality. In the case of the R-Smads, Smad2 doesn't have DNA binding activity while Smad3 has an extra nuclear localisation signal (KKLKK). The SSXS motif at the C-terminal of R-Smads is a substrate for phosphorylation by type-I receptors. Smad4, unlike the R-Smads can't bind to the receptors and lacks this motif and instead uses the MH2 domain to interact with the R-Smads.

Smad2/3 has been shown to colocalise to the cell membrane via a FYVE domain Smad interacting protein known as Smad-anchor for receptor activation (SARA). Phosphoinositide 3 kinase (PI3K) phosphorylates membrane phosphoinositides (PtdIns). PtdIns3P for example, is a PtdIns that is specifically located on membranes associated with the endocytic pathway. The FYVE domain is a cysteine rich region that binds two zinc ions, and proteins containing this domain are recruited to PtdIns3 rich membranes via a basic patch within the FYVE region (Gillooly *et al.*, 2001). During induction of TGF- β signalling, SARA acts to recruit Smad2 to its type-I receptor, resulting in its phosphorylation and dissociation from SARA allowing it to complex with Co-Smad4. Endofin meanwhile, functions as a BMP-specific Smad anchor for receptor activation (Tsukazaki *et al.*, 1998). Smad4 acts to form a heteromeric complex with the R-Smads and translocates them to the nucleus in order for them to regulate transcription of their target genes.

The I-Smads are structurally divergent from the rest of the Smads. They act as negative regulators of TGF- β signalling by binding to type-I receptors, thereby preventing R-Smad activation and also compete with Smad4 for hetero-complex formation. Smad7 is responsible for inhibiting TGF- β /activin and BMP signalling, whereas Smad6 is specific for BMP signalling (Hayashi *et al.*, 1997; Hata *et al.*, 1998).

The R-Smads are around 400-500 amino acids in length and are all structurally similar. They are composed of three distinct and conserved domains; an N-terminal Mad homology (MH1) domain, a non-conserved proline rich linker region, and a C-terminal MH2 domain. The MH1 domains of the R- and Co-Smads are around 130 amino acids in length, and are highly conserved. This domain forms a compact globular fold composed of six small β -strands, three α -helices, and five loops (Heldin *et al.*, 1997). The MH1 domain regulates transcription by interacting with other transcription factors and contains a highly conserved β -hairpin eleven residues in length, which can directly bind to DNA through the major groove. This hairpin is displaced in Smad2 making it incapable of binding DNA (Attisano and Lee-Hoeflich, 2001).

In the case of the I-Smads, the MH1 domain is very short, with highly distinct sequences and hence also can not bind DNA. Furthermore, the MH1 domain of inactive Smads acts as a repressor of the MH2 domain, by preventing it from forming a complex with Smad4. Phosphorylation of the C-terminal by the type-I receptor appears to unfold the two domains and alleviates the inhibition by MH1 (Heldin *et al.*, 1997). In Smad3, basic helix 2 consists of a KKLKK sequence that acts as a nuclear localisation signal and hence is critical during Smad3 nuclear translocation (Attisano and Lee-Hoeflich, 2001).

The MH2 domain is around 200 residues in length, and consists of a sandwiched core of anti-parallel β -sheets, with three α -helices on one end, and a loop/helix region composed of three loops and an α -helix on the other end. This domain is multifunctional and provides the Smads with their specificity and selectivity as well as transcriptional activity. A 17 amino acid region protruding from the Smad MH2 domain, known as the L3 loop, is responsible for mediating specific receptor interaction. In addition, three sulphates within the L3 loop are critical in oligomer formation, and when activated, Smads can form homo-oligomeric complexes by interacting through their MH2 domains (Lo *et al.*, 1998). The interface of this complex is formed by the helix bundle of one subunit, and the loop/helix end of the other subunit (Chen *et al.*, 2002).

Finally, the MH2 domain is also responsible for specific interactions with type-I receptors. This is due to a pocket of basic residues that acts as a docking site for the phosphorylated GS domains of these receptors (Chen *et al.*, 2002). Smad4 however, does not interact with the receptors as it has an insertion element preventing it from doing so and instead acts as a docking site for other R-Smads.

The linker region of Smads meanwhile, is variable in sequence and length and also contributes to the oligomerisation of Smads. In addition, phosphorylation of four PXS/TP motifs within the linker region by mitogen-activated protein kinase (MAPK), acts as a mechanism to prevent the

accumulation of Smads in the nucleus (Kretschmar *et al.*, 1999). Finally, a proline rich PPXY (PY) sequence allows for interaction with WW motif containing proteins involved in Smad degradation (Zhang *et al.*, 2001).

1.4.3.3 The Smad dependent pathway

Unlike TGF- β receptors, 30-40% of type-I BMPRs are found at the cell surface in the form of preformed heteromeric complexes (PFCs) with BMPR-II, in the absence of ligand binding, increasing to 50-60% upon ligand binding. This is thought to be due to an intrinsic affinity that the receptors have for each other, that is enhanced by ligand binding. When a BMP ligand binds to the receptor complex, it causes a conformational change, resulting in complex activation.

This conformational change is thought to expose a common structural motif of type-I receptors required for signalling specificity, known as the L45 loop. This loop is slightly different when comparing TGF- β and BMP ligands, and is responsible for them binding different sets of R-Smads (Smads2 and 3 being TGF- β specific, while Smads1, 5, and 8 are BMP specific). The conformational change that occurs when BMPs bind the PFC, is thought to be necessary in order to make the L45 loop accessible to Smads. In addition, it is thought that BMP ligand binding to the type-I receptor alone is insufficient to expose the loop, or that BMPR-II recruitment may conceal it, thereby preventing Smad binding. This additional form of receptor binding allows for a higher variability and flexibility in receptor responses to various ligands, compared to their TGF- β counterparts (Nohe *et al.*, 2002).

Therefore, during the Smad dependent pathway, dimeric ligand binding induces receptor complex formation, resulting in the type-II receptor trans-phosphorylating, and thereby activating the type-I receptor at their GS domains. The activated type-I receptor is then responsible for phosphorylating and activating its corresponding R-Smads at their SSXS motif.

These activated R-Smads are then rapidly released from the type-I receptors and interact with Smad4 to form a hetero-oligomeric complex which translocates from the cytoplasm to the nucleus, where they can then alter transcription of target genes (Miyazawa *et al.*, 2002; Nohe *et al.*, 2004). Figure 1.11 illustrates both the Smad dependent and Smad independent pathways.

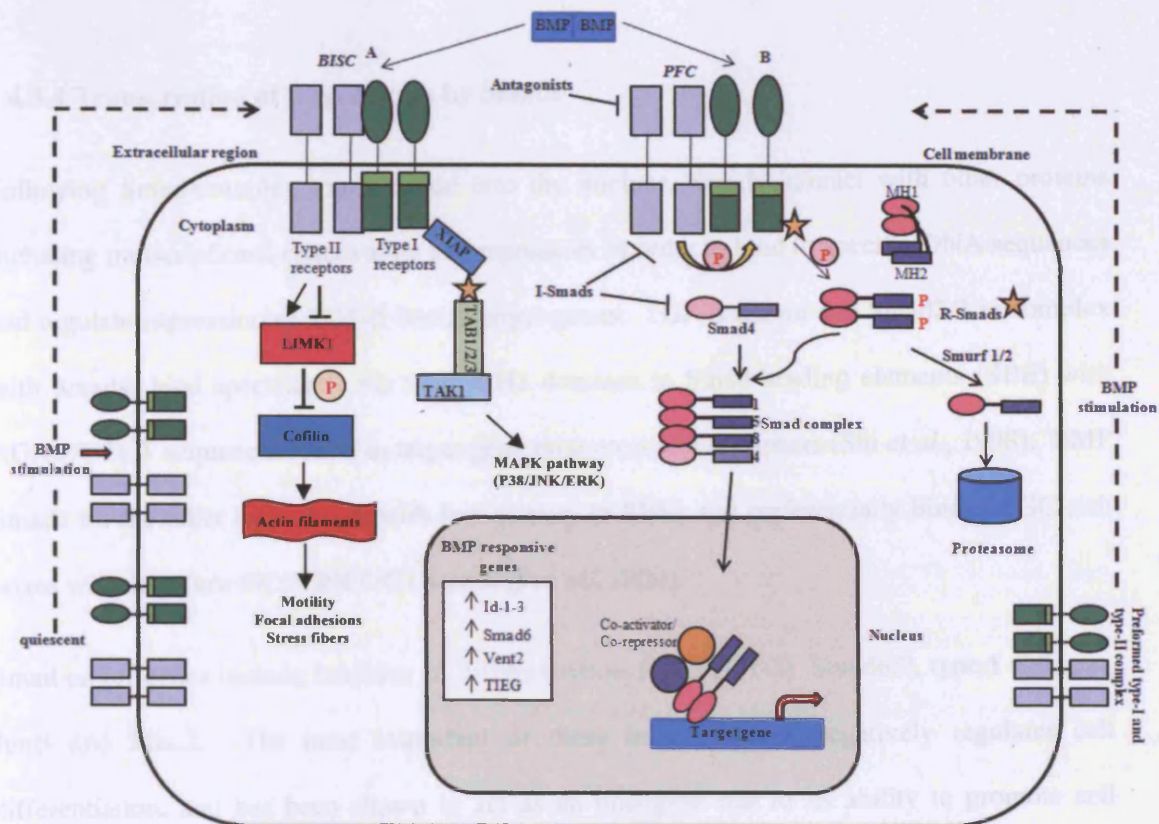


Figure 1.11: BMP signalling and its pathway. Modified from (Moustakas and Heldin, 2009). Active proteins are demonstrated by a star. The letter P in a circle refers to phosphorylation. **A.** Dimeric BMP ligand can bind to a homo-oligomeric type-I receptor and then recruits the type-II receptor into a BMP induced Signalling Complex (BISC), resulting in activation of the Smad independent P38 MAPK pathway. Alternatively, LIMK1 has been shown to bind to the tail region of BMPRII, thereby regulating depolymerisation factor cofilin and its associated effects on the actin cytoskeleton. Whether or not this interaction with BMPRII activates or inhibits LIMK1 activity, remains undecided, with one study claiming LIMK1 activation (Lee-Hoeflich *et al.*, 2004), and another claiming the opposite (Foletta *et al.*, 2003). **B.** If the ligand binds to a preformed complex (PFC) of the type-I and type-II receptors, the Smad pathway is activated. The type-II receptor activates and trans-phosphorylates the type-I receptor which in turn phosphorylates R-Smads 1, 5, and 8, causing a conformational change where the MH1 domain no longer inhibits the MH2 domain. These R-Smads then form a complex with Smad4 which translocates to the nucleus and along with co-activators and co-repressors, alters the expression of BMP target genes.

1.4.3.4 Transcription of target genes by Smads

Following Smad-complex translocation into the nucleus, Smads interact with other proteins including transcriptional coactivators and repressors in order to bind to specific DNA sequences and regulate expression of TGF- β family target genes. TGF- β /activin and Smad2/3 in complex with Smad4, bind specifically via their MH1 domains to Smad binding elements (SBE) with AGAC/GTCT sequences found in target gene promoters and enhancers (Shi *et al.*, 1998). BMP Smad1 on the other hand, binds with low affinity to SBEs and preferentially binds to GC-rich boxes with sequence GCCGNCGC (Kusanagi *et al.*, 2000).

Smad target genes include Inhibitor of differentiation-1 to 3 (Id1-3), Smad6/7, type-I collagen, JunB and Mix.2. The most important of these is Id-1 which negatively regulates cell differentiation, and has been shown to act as an oncogene due to its ability to promote cell growth, survival, invasion, angiogenesis, and metastasis in various cancers (Ling *et al.*, 2006). TGF- β growth inhibition results in upregulation of Cyclin dependant kinase inhibitors (CDKI) P21 and P15, and Smad3 repression of C-myc expression (Miyazawa *et al.*, 2002). Finally, TGF- β potently enhances expression of plasminogen activator inhibitor-1 (PAI-1). This process involves a positive feedback loop and interaction with activator protein 1 (AP-1), SP-1, P15, and P21 (Keeton *et al.*, 1991; Datto *et al.*, 1995).

1.4.3.5 Smad interacting proteins

As Smads generally bind SBEs with low affinity, they need to interact with and be recruited by several other transcription factors. Most of the proteins identified refer to interaction with Smad3 as opposed to BMP Smads. This is due to the fact that the MH2 domain of Smad3 is richer in charged amino acids and acidic residues in its upper N-terminal region, resulting in more efficient interactions with other proteins (Nicholls *et al.*, 1991). The first of these proteins to be identified was Forkhead box HI (FOXHI) which specifically recruits activated Smad2/4 to promoters (Germain *et al.*, 2000). Others include P53 (Cordenonsi *et al.*, 2007), Runx

transcription factors (Miyazono *et al.*, 2004), Smad interacting protein-1 (SIP-1) (Feng *et al.*, 2000), Activating transcription factor-2 (ATF-2) (Sano *et al.*, 1999), and YY1 transcription factors which repress expression of genes including PAI-1 and Id-1 (Kurisaki *et al.*, 2003).

In addition, Smads also interact with transcriptional co-activators and repressors. P300/CBPs are histone acetyl transferase (HAT) proteins that interact with Smads to enhance transcription of their target genes by increasing the accessibility of the transcriptional machinery (Miyazono *et al.*, 2000). The repressors include TGF- β interacting factor (TGIF), C-Sloan-Kettering retrovirus (C-Ski), and Ski related novel gene (SnoN) which bind with Smad3/4 to their SBES and recruit histone deacetylases (HDACs) to repress target gene expression. Induction of TGF- β signalling, results in C-Ski and SnoN degradation, allowing Smad3/4 to induce transcription (Massague and Chen, 2000; Zhao *et al.*, 2001)

1.4.3.6 Smad degradation

The concentration of available Smads in the intracellular pool is regulated by HECT type E3 ligases known as Smad Ubiquitination Regulatory Factors (Smurf) 1 and 2. The WW motifs of Smurfs interact with the PY domain in the linker region of R-Smads, inducing their degradation by the proteasome, which results in inhibition of TGF- β family signalling.

In addition, Smurfs are responsible for the translocation of I-Smads from the nucleus into the cytoplasm, and enhance I-Smad interaction with the type-I receptors (Ebisawa *et al.*, 2001). This also results in Smurf-dependent ubiquitin degradation of the type-I receptors, leading to a down-regulation of cell surface receptor expression. On the other side of the spectrum, TGF- β signalling is amplified by the Ring type E3 ligase Arkadia, which induces the ubiquitination of Smad7 but not type-I receptors (Koinuma *et al.*, 2003).

1.4.3.7 Smad independent pathway

The alternative route that BMP signalling can take is Smad-independent, and is known as the P38 Mitogen-activated protein kinase (MAPK) pathway. During this cascade, the X-linked inhibitor of apoptosis protein (XIAP) acts as a positive regulator of the downstream components, linking the type-I receptor and the TGF- β activated binding protein (TAB1/2/3) (Shibuya *et al.*, 1996). This protein activates TGF- β activated tyrosine kinase-1 (TAK1), which is a member of the MAPKK family and is capable of activating kinases including; P38 MAPK, Jun N-terminal kinases (JNK), Nemo-like kinase (NLK) and Nuclear Factor- κ B (NF- κ B) (Yamaguchi *et al.*, 1995; Shirakabe *et al.*, 1997; Ishitani *et al.*, 1999; Lee *et al.*, 2002). TAK1 normally induces apoptosis by activating JNK or P38 MAPK pathways. However, in *Xenopus* embryos, the BMP signal was shown to interact with XIAP to inhibit TAK1 associated apoptosis by impeding the action of caspases (Yamaguchi *et al.*, 1999).

Alternatively, LIM Kinase 1 (LIMK1), a key regulator of actin dynamics, has been shown to colocalise with the tail region of BMPR-II, independently of the Smads. LIMK1 is a downstream effector of Rho GTPases and is responsible for phosphorylating and inactivating cofilin, an actin depolymerising factor. Whether or not interaction with BMPR-II stimulates or inhibits LIMK1 has been debated. One study demonstrated that BMPR-II prevents LIMK1 from inactivating cofilin, an effect that was alleviated by BMP-4 binding (Foletta *et al.*, 2003), while another showed that LIMK1 interaction with BMPR-II synergises with Rho GTPases to activate LIMK1 catalytic activity and cofilin inactivation (Lee-Hoeflich *et al.*, 2004).

1.4.4 Regulation of BMP pathway

Both negative and positive mechanisms are responsible for modulating BMP signal transduction at an extracellular and intracellular level. Extracellularly, the pathway is impeded by secreted proteins known as the BMP antagonists, and include; Noggin, Follistatin, Chordin, Gremlin, and Cerberus, amongst others. They mainly act by competing for receptor binding

with the BMP ligands either by binding to the receptors or ligands themselves (Canalis *et al.*, 2003). BMP activin membrane bound inhibitor (BAMBI) acts as a pseudoreceptor and inhibits BMP signalling. It contains a similar ECD to type-I BMP receptors, but lacks a kinase domain and acts by competing for BMP binding. BAMBI and most of the aforementioned antagonists function on a negative feedback loop, with BMPs up-regulating their expression (Onichtchouk *et al.*, 1999).

Intracellular mechanisms of regulation include the I-Smads, as well as C-Ski and Smurfs, which are responsible for Smad degradation, whose functions have been previously mentioned. As I-Smads are targets of BMP signalling, the expression of I-Smads functions as a negative feedback loop (Ebisawa *et al.*, 2001). In addition, there exists an intracellular antagonist known as transducer of ErbB2 (Tob), which binds Smads 1, 4, 5, and 8, and blocks transcription of their target genes (Yoshida *et al.*, 2000).

1.4.4.1 Cross talk between BMP signalling and other pathways

Despite the extensive amount of knowledge on BMP signalling, the signalling itself doesn't provide us with an explanation for the complex functions of BMPs, in the right perspective. Recently it has become clear that this has to do with cross talk between BMP signalling and several other important signalling pathways, as well as the proteins that BMPs recruit. Hox proteins for example, are downstream BMP pathway transcription factors that are involved in morphological development as well as cell differentiation.

Smads are responsible for regulating Hox transcriptional activities, with Smads 1, 4, and 6 being shown to mainly repress Hox transcriptional activation (Zhou *et al.*, 2008). Hox proteins control processes such as cell death, proliferation, adhesion, and cell specification, but the effect they have is greatly dependant on cell type. BMPs regulate *Hox* gene expression, and due to the huge variety of cell type dependant functions that Hox proteins carry out, partially explains the contradicting effects that BMPs play on cells (Foronda *et al.*, 2009).

Additionally, signals induced by BMP and TGF- β /activin act antagonistically to each other. For example, as both ligand types require Smad4 for their signalling, its limited availability in the cytoplasm suggests that these ligands may compete for Smad4 during complex formation. In addition, the I-Smads, irrespective of which ligand induced their expression inhibit both BMP and TGF- β signals (Candia *et al.*, 1997).

Furthermore, various MAPK pathways have been shown to interact with BMP signalling, including the p38 MAPK pathway, activated by BMPs themselves. Smads 6 and 7 not only inhibit BMP Smad signalling, but also p38 kinase. Smad6 has been shown to physically interact with and block TAK1, which in turn may interact with other transcription factors to alter TGF- β gene expression (Kimura *et al.*, 2000). Extracellular regulated MAPK (ERK) is capable of phosphorylating the linker region of R-Smads, inhibiting nuclear accumulation of Smad1, and hence BMP signalling (Kretschmar *et al.*, 1997).

On the other hand, BMP-2 Smad signalling stimulates activation of Ras and ERK, which enhance Smad1 transcriptional activity in osteoblastic cells (Suzawa *et al.*, 2002; Nohe *et al.*, 2004). Other Smads phosphorylated by kinases at their linker region include Smad2/3 by JNK and Hepatocyte growth factor (HGF), and Smad1 by FGF and IGF (Pera *et al.*, 2003; Mori *et al.*, 2004). JNK for example, has been shown to phosphorylate Smad3, aiding in its activation by receptor complexes and its nuclear translocation thereby enhancing Smad3 signalling. This cross talk between Smad3 and JNK has been shown to be interdependent, with Smad-dependent signalling being required for sustained JNK activity (Engel *et al.*, 1999).

IFN- γ acting through the JAK-STAT pathway induces Smad7 expression and hence inhibits BMP signalling (Ulloa *et al.*, 1999). Additionally, signal transducer and activator of transcription 3 (STAT3) has been reported to complex with Smad1, translocate into the nucleus and with P300, activate target gene expression (Nakashima *et al.*, 1999). Finally, other pathways shown to antagonise or synergise BMP signalling include Calmodulin which binds

Smad4, Notch and Wnt/ β -catenin signalling, and most recently oestrogen, which has been reported to interfere with BMP-2, -6, and -7 Smad transcriptional activity, and inhibit BMP gene expression in the breast (Zimmerman *et al.*, 1998; Nishita *et al.*, 2000; Itoh *et al.*, 2004; Helms *et al.*, 2005).

1.4.5 Aberrant BMP signalling in prostate cancer

Due to the complexity and importance of the BMP signalling pathway, alterations such as mutations or expressional changes can occur at any stage, and although heavily regulated, misregulations in the pathway have been implicated in many different diseases. These include developmental syndromes, cardiovascular diseases, and most commonly cancer. The role of TGF- β and BMP ligands in cancer has been extensively studied and reviewed, but the function that their receptors and downstream molecules have is less clear (Gordon and Blobe, 2008).

In terms of cancer, TGF- β has been shown to potently inhibit the growth of most cell types, especially breast cancer cells (Chang *et al.*, 2007). In the prostate, TGF- β plays a critical role in controlling androgen dependence, and has been shown to induce loss of sensitivity to hormone mediated growth inhibition, and hence has been implicated in prostate cancer progression. The role of BMP signalling in prostate cancer has been thoroughly researched and elucidated and is explained below.

1.4.5.1 BMP expression in prostate cancer

BMPs specifically, have been implicated in the pathogenesis of a number of cancers including: prostate, colorectal, osteosarcomas, myelomas, and breast cancer (Ye *et al.*, 2007). For example, over-expression of BMP-4 and -7 has been shown in breast cancer cells, with BMP-7 promoting the motility and invasiveness of breast cancer cell lines (Alarmo *et al.*, 2007; Alarmo *et al.*, 2009). Contrastingly, in the normal prostate, expression of BMP-2 and -4 is predominant, but considerable amounts of BMP-5, -6, and -7 are also present. When comparing to prostate cancer tissues, expression of BMP-2 and -4 is slightly reduced, but BMP-7

expression is significantly lower than in normal prostate samples (Bobinac *et al.*, 2005). Additionally, we have recently shown that expression of BMP-9 and -10 is decreased or absent in prostate cancer tissues, especially in those of a higher grade (Ye *et al.*, 2008).

Growth and differentiation factors (GDFs) are members of the BMP family that have also been implicated in prostate cancer. GDF-15, for example, is also reduced in prostate cancer tissues and appears to be dependent on the presence of androgen, as its expression is higher in LNCaP, an androgen-dependent cell line, than the androgen insensitive PC-3 and DU-145 cell lines. This loss of expression of BMP-7 and GDF-15 seen in prostate cancer tissues may be due to the prostate cancer cells shifting from an androgen-dependent phenotype, to an independent one. However, both appear to be re-expressed in metastatic prostate cancer tissues suggesting that they may aid in the metastatic process (Kakehi *et al.*, 2004). BMP-6 meanwhile, is expressed at low levels in localized prostate cancers, but its expression is significantly increased in samples from metastatic prostate cancers and bone lesions, suggesting that like BMP-7 and GDF-15, it may play a role in prostate cancer progression and metastasis (Haudenschild *et al.*, 2004).

1.4.5.2 Expression of BMPRs and BMP signalling molecules in prostate cancer

In normal prostate tissue, the expression of BMPRs including BMPR-IA, BMPR-IB, and BMPR-II, has been shown to be localised to the epithelial compartment. In contrast, prostate cancer tissues often exhibit loss of BMPR expression, and their expression significantly correlates with tumour grade, tumour stage, and clinical stage. Expression of the BMPRs was lower in prostate cancer tissues with worsening Gleason scores and tumour grade in prostate cancer tissues with poor prognosis (Kim *et al.*, 2000). In well differentiated tumours (Gleason score 4), loss of expression of BMPR-IA and BMPR-IB was seen in 17% of cases, while negative BMPR-II expression was detected in 33%. In poorly differentiated tumours (Gleason scores 8-10) however, expression of BMPRs was lost in around 80% of the tissues. However,

only BMPR-II down-regulation was shown to significantly correlate with 5 year survival rates and a higher rate of recurrence (Kim *et al.*, 2004).

In reference to prostate cancer cell lines, expression of the BMPRs is contradictory. The laboratory has recently shown expression of BMPR-IB and BMPR-II in prostate cancer cell lines; PC-3, DU-145, CAHPV10, and LNCaP, as well as in immortalised prostate epithelial cell lines PZHPV7, PNT1A, and PNT2C2. BMPR-IB expression was high in all the mentioned cell lines but BMPR-II expression was lower in the prostate cancer cell lines compared to the epithelial cell lines. Furthermore, expression levels of both the receptors increased in response to HGF (Ye *et al.*, 2007). In contrast, a different study showed expression of all three BMPRs in LNCaP, DU-145, PC-3, and PC-3M (Kim *et al.*, 2004), whereas another showed no BMPR-IA expression in LNCaP, DU-145, or PC-3, and BMPR-IB expression in only LNCaP (Brubaker *et al.*, 2004).

In the case of the Smads, the laboratory has recently shown that there is no significant change in the expression of Smads 1, 2, 3, 5, 6, and 8, when comparing prostate cancer cell lines and prostate epithelial cell lines (cell lines mentioned above). However, expression of Smad4 and 7 was barely detectable in the three highly metastatic prostate cancer cell lines PC-3, DU-145, and LNCaP, but showed higher expression levels in the less invasive CAHPV10 cell line and the prostate epithelial cell lines (Ye *et al.*, 2008). Likewise, Smad4 expression was shown to be significantly down-regulated in high grade prostatic intraepithelial neoplasia and prostate cancer tissue, compared to tissue of benign prostate hyperplasia origin (Zeng *et al.*, 2004).

However, in prostate cancer cells, BMP signalling events downstream of BMPRs are also dependent upon the type of BMPs initiating the process. For example, BMP-9 acts on PC-3 cells via the Smad dependent pathway, whereas BMP-10 signals via the Smad independent pathway in the same cells (Ye *et al.*, 2008; Ye *et al.*, 2009). Cross talk between androgen receptor (AR) signalling and Smad mediated signalling within the prostate has been shown. In

PC-3 and LNCaP cells, Smad3 treatment can induce activation of the AR, promoting tumour growth. In contrast, loss of Smad4 expression is needed to up-regulate AR activation, and when it is co-transfected with Smad3, AR activation is inhibited (Kang *et al.*, 2002). Meanwhile, in the rat normal and malignant prostate, up-regulation of activated Smad2, as well as expression of Smads 3, 4, 6, and 7, was observed following androgen deprivation after castration. This makes cells more responsive to TGF- β , whose action and duration is regulated by the I-Smads which are also over-expressed. Expression of Smads 1 and 5 was barely detectable in both the normal and cancerous prostate, but pSmad2, Smad3, TGF- β RI and TGF- β RII expression, was up-regulated in the tumours in response to oestrogen stimulation, suggesting that oestrogen makes prostate cells more susceptible to BMP signalling (Brodin *et al.*, 1999).

1.4.5.3 Role of BMPs in prostate cancer

Due to the alterations in BMP expression in prostate cancers, substantial research has gone into elucidating the role that BMPs play during the development and progression of this disease. Indeed, several groups have shown that BMPs play a profound role on the biological properties of prostate cancer cells, especially during bone metastasis. Despite this, finding the precise mechanisms by which they exert their effects remains unclear. However, with the development of recombinant human BMPs as well as methods of altering their expression, it is now possible to investigate these mechanisms *in vitro*.

1.4.5.4 Role of BMPs on prostate cancer cell proliferation

TGF- β is well known for its growth inhibitory effects on a variety of cell types, including prostate cancer cells (Massague *et al.*, 2000). The role of BMPs on cell proliferation however, remains unclear. Despite this, several BMPs have been shown to have an effect on the proliferation of prostate cancer cells. BMP-6 and BMP-2 for example, were shown to inhibit the growth of prostate cancer cells including LNCaP and DU-145 (Brubaker *et al.*, 2004). BMP-7 meanwhile, has been shown to inhibit the proliferation of androgen-independent PC-3

and DU-145, inducing a G1 cell cycle arrest by up-regulating the expression of CDKI-P21^{CIP1/WAF1} (Miyazaki *et al.*, 2004).

However, the effect of BMPs on prostate cancer cell growth has been shown to be dependent on the concentration of fetal bovine serum (FBS) present, as BMP-7 failed to inhibit the growth of PC-3 cells in the presence of 10% FBS. In addition, BMP-7 mediated Smad1/5 phosphorylation and Id-1 expression was reduced in cells grown in 10% FBS, in comparison to those grown in only 1%. This suggests that FBS may contain or induce expression of, BMP antagonists such as noggin or chordin, resulting in the inhibition of BMP-7 activity (Ide *et al.*, 1997).

In addition, the effect of BMPs is also dependent on the presence of androgen, as well as receptor type. When using the prostatic cell line LNCaP, signalling via BMPR-IA or -IB was shown to have opposite effects on the growth rate of these cells. When LNCaP was cultured in the presence of rh-BMP-2 and androgen, it led to an increase in BMPR-IB expression and inhibited the growth rate of the cells. In contrast, when androgen was absent, the opposite was true and the cells showed increased growth via BMPR-IA. As BMP-2 can signal via BMPR-IA or -IB in concordance with BMPR-II, it is feasible that when BMP-2 signals via BMPR-IA it leads to growth promotion of prostate cancer cells, while signalling via BMPR-IB leads to growth inhibition (Ide *et al.*, 1997). Meanwhile, expression of a constitutively active form of BMPR-IB in PC-3 cells led to an inhibition of cell growth *in vitro*, and decreased the growth of prostate tumours *in vivo* when these cells were injected into nude mice (Miyazaki *et al.*, 2004).

1.4.5.5 BMPs and apoptosis of prostate cancer cells

Cancer cells usually become resistant to apoptotic signals from the cell signalling pathways by altering the expression of pro-apoptotic and anti-apoptotic factors. Smad signalling regulates the expression of several genes involved in apoptosis. These include, growth arrest and DNA-damage-inducible 45 β (GADD45 β), Bim, Death-associated protein kinase (DAPK), Src

homology domain 2 (SH2)-containing 5' inositol phosphatase (SHIP), and TGF- β inducible early gene-1 (TIEG-1) (Pardali and Moustakas, 2007). Smad3 for example, depending on its expression levels, can determine whether or not epithelial cells undergo apoptosis in response to TGF- β , by interacting with and blocking Akt/PKB (Conery *et al.*, 2004). In addition, in the normal and malignant prostate, there was an up-regulation in the expression of phosphorylated Smad2, as well as in non-phosphorylated Smad3, 4, 6, and 7, after castration. Expression of these Smads was particularly present within apoptotic cells, suggesting that the TGF- β pathway is activated in the prostate after castration, resulting in the up-regulation of pro-apoptotic factors. The TGF- β pathway regulated apoptosis *in vivo* and hence may be deregulated during the progression of prostate cancers (Brodin *et al.*, 1999).

Several BMPs have been shown to induce apoptosis. The laboratory has recently shown that BMP-9 signals via BMPR-IB and BMPR-II to inhibit the growth of prostate cancer cells by inducing apoptosis via Smad1, 5, and 8 mediated up-regulation of pro-apoptotic factor Par-4 (Ye *et al.*, 2008). In addition, it also previously demonstrated that BMP-10, as well as decreasing *in vitro* cell growth, adhesion, invasion, and migration of prostate cancer cells, can also induce apoptosis by signalling via BMPR-IB in a Smad-independent manner leading to activation of XIAP and ERK, which are involved in the promotion of apoptosis (Ye *et al.*, 2009).

1.4.5.6 Role of BMPs in prostate cancer bone metastasis

Due to the role of BMPs as potent osteoinductive agents with a crucial role during skeletal development and fracture repair, the notion that they may also be involved in the development of osteoblastic lesions associated with prostate cancer metastasis, does not seem farfetched. One possible mechanism by which BMPs have been shown to induce this process, is by the activation of VEGF, which given its role in angiogenesis, osteoblastic differentiation, and chemotaxis, may be a key downstream player of BMP-mediated regulation of osteoblastic

metastases. Indeed BMP-2, -4,-6, and -7 induced VEGF mRNA and protein expression in an osteoblastic cell line (Dai *et al.*, 2004). In contrast, BMP-9, when signalling via ALK-1 and BMPR-II in endothelial cells, activates Smad1/5 downstream signalling to block VEGF mediated angiogenesis (Scharpfenecker *et al.*, 2007).

Another mechanism by which BMPs can aid in prostate cancer metastasis is by promoting the motile and invasive capacity of tumour cells. BMP-7 and GDF-15 for example, were shown to be re-expressed in bone metastatic lesions, and BMP-2 alongside BMP-7, is capable of stimulating the migration and invasion of prostate cancer cells, an effect which was reversed when these cells were treated with the BMP antagonist, noggin. Furthermore, *in vivo* development of osteoblastic lesions associated with prostate cancer, was inhibited by the over-expression of noggin, suggesting that BMPs do play a role during bone metastasis, and that the blocking of BMP activity may be a useful potential therapeutic treatment by acting to decrease the pain associated with metastatic lesions. Additionally, BMP-2, and to a lesser extent BMP-4, can also stimulate the migration of PC-3 cells in a dose dependent manner, an effect also inhibited by noggin (Feeley *et al.*, 2005). Finally, BMP-2 alongside BMP-6, promotes the invasive capacity of prostate cancer cells *in vitro*, and when mice were treated with anti-BMP-6, osteoblastic activity and bone production was reduced, implying that prostate cancer can encourage osteoblastic function through BMP-6 (Dai *et al.*, 2005).

Despite the clear importance of BMP signalling in bone metastasis, other cross-talking pathways and cytokines present in the bone microenvironment have been shown to aid in the process. For example, both the osteoclastic PC-3 cell line which expresses osteoclast-associated cytokines including RANKL, IL-1, and TNF- α , and the osteoblastic LAPC-9 which expresses OPG, an inhibitor of osteoclastogenesis and minimal amounts of the aforementioned cytokines, secrete BMP-2, -4, and -6, which are associated with bone formation (Lee *et al.*, 2003). HGF, along with its receptor, meanwhile, are up-regulated in prostate cancer cells, and in androgen-independent prostate cancer cells, promotes their invasive capacity as well as

formation of bone metastases. HGF was recently shown to up-regulate expression of BMPR-IB and BMPR-II in these cells, and as the bone has high levels of BMP, an up-regulation of its receptors would provide the prostate cancer cells with a growth and survival advantage within the bone microenvironment, aiding in osteoblastic metastasis. These results suggest that BMPR-IB and BMPR-II along with HGF play a role during the bone metastasis of prostate cancer cells (Ye *et al.*, 2008).

1.5 Growth and Differentiation Factor-9 (GDF-9); a member of the BMP family

Due to the obvious importance of BMPs in the development and progression of prostate cancer, a novel member of this family always sparks up interest. GDF-9 (or GDF-9a) is a member of the BMP family that has been identified as an oocyte growth factor which plays an important role in the regulation of folliculogenesis and ovulation (Su *et al.*, 2008). However, its role in cancer has scarcely been studied. Therefore, based on the obvious importance of BMPs in prostate cancer, and significant findings observed in previous projects carried out in the laboratory on BMPs in this disease (Ye *et al.*, 2008; 2009), we are the first to investigate the role of GDF-9 in prostate cancer.

1.5.1 GDF-9 structure and signalling

As previously mentioned, TGF- β and BMPs are produced as precursors made up of a longer N-terminal pro-region, signal peptide, and a shorter functionally active C-terminal mature polypeptide. Dimers of these precursor proteins are linked by disulphide bonds via conserved cysteine residues in the pro-region and mature peptide sequence. Once in the secretory pathway, the mature and pro-region are cleaved apart by furin proteases. The protein dimers are then secreted in order for them to bind their cell surface receptors. However, the TGF- β pro-region known as latency-associated peptide (LAP), remains non-covalently attached to the mature peptide, acting as a chaperone during complex exocytosis and preserving the ligand in an inactive state (Moustakas and Heldin, 2009). Additionally, LAP also mediates TGF- β

deposition in the ECM by covalently linking to large secreted proteins and ECM proteins such as fibronectin (Rifkin, 2005). This LAP interaction of TGF- β ligands is conserved in the BMPs, but instead of acting as means of extracellular antagonism, restricts ligand availability by regulating mature ligand stability, processing, and degradation (Moustakas and Heldin, 2009).

GDF-9 and BMP-15 (GDF-9B) are oocyte secreted factors that are processed in a similar fashion to their BMP relatives, being secreted as cleaved mature and proregion proteins. In addition, non-covalent interactions between the mature and proregion proteins were identified in both GDF-9 and BMP-15. Furthermore, the GDF-9 mature protein was also found to associate with the BMP-15 pro-region, which acted to regulate and immunoneutralise BMP-15/GDF-9 cooperativity (McIntosh *et al.*, 2008). Before secretion however, their bioactivity is tightly regulated through phosphorylation by Golgi Casein Kinase (GCK) that occurs in the Golgi apparatus before secretion. This phosphorylation acts as a means of regulating protein bioactivity, with the dephosphorylated isoforms acting as antagonists of their phosphorylated counterparts (Tibaldi *et al.*, 2010).

In addition, they also differ from other BMPs when it comes to post-translation. Members of the TGF- β family contain a characteristic conserved 7 cysteine knot within their mature region. The fourth cysteine is required for disulphide bond formation for covalent linking between monomers, to form dimers. GDF-9 and BMP-15 however, lack this fourth cysteine as it is replaced by a serine residue. Therefore, it is thought that these BMPs either form non-covalent bound dimers, or biologically active monomers (Liao *et al.*, 2003).

Despite this difference in their structure, GDF-9 and BMP-15 still use BMP receptors in order to initiate their downstream signalling. GDF-9 has been shown to have highest affinity for TGF- β RI (ALK-5) and BMPRII, thereby activating the TGF- β associated Smads, 2 and 3 (Mazerbourg *et al.*, 2004). BMP-15 meanwhile, also uses BMPRII as a type II receptor, but

BMPR-IB (ALK-6) as its type I receptor, and hence activates the BMP associated Smads, 1, 5, and 8 (Moore *et al.*, 2003). This difference in receptors suggests that these related proteins may have different functions, with GDF-9 acting more like its TGF- β relatives, as opposed to the BMPs, like BMP-15. However, it has recently been shown that BMP-15 and GDF-9 act together to stimulate granulosa cell growth by signalling via BMPR-II (Edwards *et al.*, 2008)

1.5.1.1 GDF-9 function

Expression of GDF-9 and BMP-15 has been described in oocytes of species including; rodents, ovine, and humans, and both have been shown to play a critical role in ovarian function. Mice lacking the *GDF-9* gene demonstrated a block at an early stage of follicular development, making them infertile. This suggests that GDF-9 may play an important role in early follicular development. BMP-15 deficient mice on the other hand, exhibit only reduced fertility, whereas sheep with homozygous naturally occurring BMP-15 mutations (Inverdale sheep) are infertile. Both BMPs have been shown to co-operate during ovarian follicular development and ovulation rate and can promote cholesterol biosynthesis in cumulus cells (Su *et al.*, 2008).

More specifically, GDF-9 is expressed throughout follicular development in the mammalian oocyte and can stimulate granulosa cell proliferation, pre-antral follicle growth, and cumulus cell expansion, partly by inhibiting FSH-induced cAMP production and steroidogenesis (Vitt *et al.*, 2000). Meanwhile, treating human follicles with GDF-9 results in a greater percentage of viable cells in organ culture, suggesting it also plays a role in follicular survival. Furthermore, it has been demonstrated to act as an anti-apoptotic factor in pre-antral follicles, by preventing granulosa cells from undergoing apoptosis through activation of the PI3K/AKT pathway (Orisaka *et al.*, 2006).

1.6 Aims and objectives

From all the studies carried out on BMPs and their function in cancer, it is clear that they are important regulators during cancer progression and metastasis. In addition, due to the significant role they play in the bone, it can be implied that they may be vital in the process of bone metastasis, especially that of prostate cancer. Indeed, we have previously shown that BMP-9 and -10 have an inhibitory effect on the growth and motility of prostate cancer cells (Ye *et al.*, 2008; 2009).

Despite the established importance of GDF-9 in female fertility, knowledge of its role in human cancer has been limited, and only recently have there been papers published on its expression in cancer. The laboratory has previously shown that GDF-9 inhibits the invasiveness of breast cancer cells, and that high expression of both GDF-9 and BMP-15 is present in tumour samples with good prognosis (Hanavadi *et al.*, 2007). The only other study to suggest a role for GDF-9 in cancer, demonstrated an up-regulation in its expression in an oral squamous carcinoma cell line, suggesting that in this type of cancer GDF-9 may aid in tumour progression and metastasis, opposite to its effects in breast cancer (Zhuang *et al.*, 2010). However, a clear role for this protein in human cancer is still unclear.

Therefore, due to the importance of BMPs both in prostate cancer development and bone metastasis, as well as several studies indicating the potential of GDF-9 as a molecular marker in cancers, this study aims to be the first to characterise a role for GDF-9 in the development of prostate cancer. If clear mechanisms are established for the functionality of GDF-9 in prostate cancer, it may aid in the development of innovative treatments to either prevent the progression and metastasis of prostate cancer, or treat bone metastases of which to date there exist only palliative therapies.

The specific aims of this study are:

1. To establish the expression profile of GDF-9 and its associated downstream molecules in a variety of prostate cancer cell lines.
2. By producing a plasmid construct of GDF-9, to force-express and knock-down its expression in prostate cancer cell lines, respectively. This would then allow for the effect that GDF-9 has on biological properties of cancer cells including adhesion, invasion, proliferation, motility, and migration, to be studied.
3. Generate recombinant human GDF-9 (rh-GDF-9) which can be used to treat the cells in order to support the effects seen with endogenous GDF-9, and determine its downstream signalling pathway.
4. Although the BMP receptors that GDF-9 activates to initiate its downstream signalling have been identified as ALK-5 and BMPR-II in the ovary, it is unclear as to whether this is the case in the prostate. Therefore, by carrying out phosphorylation studies, using a Smad3 inhibitor, and treating the cells with rh-GDF-9, it can be determined how GDF-9 downstream signalling allows it to exert its effects on prostate cancer cells. This includes determination of any downstream target genes and mechanisms involved in its functions.

Chapter 2

Materials and Methods

2.1 General materials

2.1.1 Cell lines

This current study made use of seven prostatic cell lines; PC-3 acquired from the European Collection of Animal Cell Culture (ECACC, Salisbury, UK), DU-145, CA-HPV10, LNCaP, and PZHPV-7, which were all obtained from the American Type Culture Collection (ATCC, Rockville, Maryland, USA), and PNT-1A and PNT-2C2 which were generously given to us by Professor Norman Maitland (University of York, England, UK). Full details of these cell lines are supplied in Table 2.1. DMEM-F12 Media supplemented with 10% foetal bovine serum (FBS) and antibiotics was used to maintain the cells. The cells were kept for approximately 8-10 passages in order to retain cellular integrity, before being discarded. Due to improper freezing of cell stocks, attempts to culture the prostatic epithelial cell lines PNT-1A, PNT-2C2, and PZ-HPV-7, were unsuccessful. However, this study did have access to RNA and protein samples procured from these cells.

2.1.2 Primers

All the primers used in this current study were designed with the use of the Beacon Design programme (Palo Alto, California, USA) and were synthesised by Invitrogen (Paisley, UK). The forward and reverse primers used for conventional RT-PCR and Quantitative PCR (Q-PCR) are provided in Table 2.2, those used for amplifying the GDF-9 coding sequence in Table 2.3, and primers used for generating hammerhead ribozymes are detailed in Table 2.4.

Cell line	Origin	Cell morphology	Tissue type	Metastatic site	Features
PC-3	62 year old Caucasian male	Epithelial	Adenocarcinoma (highly tumourogenic)	Bone	Tumour stage: grade IV Isolation date: 1979 Antigen expression: HLA A1, A9 Androgen receptor negative Adherent cells
DU-145	69 year old Caucasian male	Epithelial	Carcinoma	Brain	Isolation date: 1978 Antigen expression: Blood type O; Rh+ Androgen receptor negative
LNCaP	50 year old Caucasian male	Epithelial	Carcinoma	left supraclavicular lymph node	Isolation date: 1977 Androgen and Estrogen receptor positive Cellular products: PSA, human prostatic acid phosphatase Adherent cells
CA-HPV-10	63 year old Caucasian male	Epithelial	Non tumourogenic cell line derived from prostatic adenocarcinoma, transformed through HPV18 transfection	—	Isolation date: 1994 Gleason grade: IV Adherent cells Cellular products: KLK3, PSA
PZHPV-7	70 year old Caucasian male	Epithelial	Non tumourogenic epithelial cell line transformed through HPV18 transfection	—	Derived from normal adult prostatic epithelial cells
PNT1A	35 year old Caucasian male	Epithelial	Normal prostatic epithelial cell line, transfected and immortalised with SV40 DNA with a defective replication origin.	—	Derived from human prostate epithelium of the peripheral zone
PNT-2C2	33 year old Caucasian male	Epithelial	Normal prostatic epithelial cell line, immortalised with SV40 DNA	—	

Table 2.1: Details of cell lines used in this study.

Table 2.2: Primers for conventional RT-PCR and Q-PCR (Primers were designed by Beacon Design programme (Palo Alto, California, USA) and were synthesised by Invitrogen (Paisley, UK)).

Gene	Primer name	Primer sequence (5'-3')	Annealing temperature	Product size (bps)
GDF-9	GDF-9aF8	TGTTTTCTATTAGCCTTGG	55°C	466
	GDF-9aR8	ATTTGACAGCAGAGGAAAAA		
GDF-9	GDF-9aF9	GCGCTTTTCAAAGTTCTATC	56°C	432
	GDF-9aR9	GGTCACATCAATCTGAATCC		
GDF-9	GDF-9aF1	GCAGAGGTCAGGAACTGT	55°C	100
	GDF-9aZR1	ACTGAACCTGACCGTACAATGGAG CTCACACTCATTTTT		
β-actin	BACTF	ATGATATCGCCGCGCTCG	55°C	580
	BACTR	CGCTCGGTGAGGATCTTCA		
B-actin	BACTINZF	GGACCTGACTGACTACCTCA	55°C	117
	BACTINZR	ACTGAACCTGACCGTACAAGCTTC TCCTTAATGTCACG		
Rock-1	ROCK1F10	CATCTCGCATTCTACAAGTG	55°C	473
	ROCK1R10	TAAAAACATGCCAGAGAGGT		
FAK	FAKF1	AACAGGTGAAGAGCGATTAT	55°C	99
	FAKZR1	ACTGAACCTGACCGTACACAGTAT GATCGCCGTTTTT		
Paxillin	PAXF1	CAATCCTTGACCCCTAGA	55°C	115
	PAXZR1	ACTGAACCTGACCGTACATTGGAG ACACTGGAAGTTTT		
SNAI1	SNAF	ACTATGCCGCGCTCTTTCC	55°C	798
	SNAR	TCAGCGGGGACATCCTGAGC		
RhoC	RHOCF8	GAGAAGTGGACCCAGAG	55°C	117
	RHOCZR	ACTGAACCTGACCGTACACTTCAT CTTGCCACGCTC		

E- Cadherin	ECADF8	CAGAAAGTTTTCCACCAAAG	55°C	106
	ECADZR	ACTGAACCTGACCGTACAAAATGT GAGCAATTCTGCTT		
N- Cadherin	NCADF1	ATTCTCAACCCCATCT	55°C	110
	NCADZR1	ACTGAACCTGACCGTACATTCTCC ACTTGATTTCATT		

Table 2.3: Primers for amplifying GDF-9 coding sequence.

Gene	Primer name	Primer sequence (5'-3')	Annealing temperature	Product size (bps)
GDF-9a	GDF-9aExF1	ATGGCACGTCCCAACAAAT	60-65°C	1362
	GDF-9aExR1	ATTTGACAGCAGAGGAAAAA		
	GDF-9aExR2	TTAACGACAGGTGCACTTTGTAGC		
	T7F	TAATACGACTCACTATAGGG		
	BGHR	TAGAAGGCAGTCGAGG		

Table 2.4: Primers used for ribozyme synthesis.

Gene	Primer name	Primer sequence (5'-3')
GDF-9 ribozyme-2	GDF-9aRIB2F	CTGCAGTAAGTGTTCAACGGTAGT AATGCCTGATGAGTCCGTGAGG
	GDF-9aRIB2R	ACTAGTGGAAGTCTATTTAACCT GGATTTTCGTCTCACGGACT
GDF-9 ribozyme-3	GDF-9aRIB3F	CTGCAGCTGTGATAAGCCTGAGCA CTTGTGTCATTCAAATATAACTGA TGAGTCCGTGAGGA
	GDF-9aRIB3R	ACTAGTTTTAACATGACTCTGGTG TCCCCCTCACTGATTTTCGTCTCAC GGACT
	T7F	TAATACGACTCACTATAGGG
	BGHR	TAGAAGGCAGTCGAGG

	RBBMR	TTCGTCCTCACGGACTCATCAG
	RBTPF	CTGATGAGTCCGTGAGGACGAA

2.1.3 Antibodies

2.1.3.1 Primary antibodies

Full details of the spectrum of primary antibodies used in this study are provided in Table 2.5.

2.1.3.2 Secondary antibodies

The secondary antibodies used for western blotting were horseradish peroxidase (HRP) conjugated anti-goat IgG, goat anti-rabbit IgG, and rabbit anti-mouse IgG antibodies, all supplied by Sigma (Poole, Dorset, UK). Those used for immunofluorescent studies are either goat anti-rabbit IgG TRITC conjugated secondary antibodies (Sigma, Poole, Dorset, UK), or FITC conjugated sheep anti-mouse, and rabbit anti-goat IgG, supplied by Santa-Cruz Biotechnology (Santa-Cruz, California, USA).

Table 2.5: Primary antibodies used during course of study

Antibody name	Source	Molecular weight (kDa)	Supplier	Product code
Anti-GDF-9	Goat polyclonal antibody	17.5/40/57/70	SANTA CRUZ BIOTECHNOLOGY, INC.	SC-12244
Anti-TGF- β RI	Goat polyclonal antibody	53	SANTA CRUZ BIOTECHNOLOGY, INC.	SC-33933
Anti-Smad1	Mouse monoclonal antibody	52/56	SANTA CRUZ BIOTECHNOLOGY, INC.	SC-7965
Anti-p-smad1	Goat polyclonal antibody	52/56	SANTA CRUZ BIOTECHNOLOGY, INC.	SC-12353

Anti-Smad2	Goat polyclonal antibody	55-60	SANTA CRUZ BIOTECHNOLOGY, INC	SC-6200
Anti-Smad3	Mouse monoclonal antibody	54	SANTA CRUZ BIOTECHNOLOGY, INC	SC-110154
Anti-p-Smad3	Rabbit polyclonal antibody	54	SANTA CRUZ BIOTECHNOLOGY, INC	SC-130218
Anti-ROCK-1	Goat polyclonal antibody	160	SANTA CRUZ BIOTECHNOLOGY, INC	SC-6056
Anti-FAK	Mouse monoclonal antibody	125	BD Transduction Laboratories	610088
Anti-p-FAK	Rabbit polyclonal antibody	125	SANTA CRUZ BIOTECHNOLOGY, INC	SC-101680
Anti-Paxillin	Mouse monoclonal antibody	68	BD Transduction Laboratories	610051
Anti-p-Paxillin	Rabbit polyclonal antibody	68	SANTA CRUZ BIOTECHNOLOGY, INC	SC-101774
Anti-SNAI1	Mouse monoclonal antibody	29	SANTA CRUZ BIOTECHNOLOGY, INC	SC-10433
Anti-RhoC	Goat polyclonal antibody	24	SANTA CRUZ BIOTECHNOLOGY, INC	SC-26481
Anti-E-cadherin	Goat polyclonal antibody	120/135	SANTA CRUZ BIOTECHNOLOGY, INC	SC-7870
Anti-JNK	Mouse monoclonal antibody	46/54	SANTA CRUZ BIOTECHNOLOGY, INC	SC-137018
Anti-ERK1/2	Mouse monoclonal antibody	42/44	SANTA CRUZ BIOTECHNOLOGY, INC	SC-135900

Anti-Actin	Mouse monoclonal antibody	42	SANTA CRUZ BIOTECHNOLOGY, INC	SC-8432
Anti-His-Probe	Mouse monoclonal antibody	Dependent on protein	SANTA CRUZ BIOTECHNOLOGY, INC	SC-8036
Anti-Phosphoserine /threonine	Rabbit polyclonal antibody	Dependent on protein	Abcam plc	ab17464
Anti-GAPDH	Goat polyclonal antibody	37	SANTA CRUZ BIOTECHNOLOGY, INC	SC-20358
Anti-rabbit (whole molecule) IgG peroxidise conjugate	Goat polyclonal antibody	Dependent on primary	Sigma	A-9169
Anti-goat (whole molecule) IgG peroxidise conjugate	Rabbit polyclonal antibody	Dependent on primary	Sigma	A-5420
Anti-mouse (whole molecule) IgG peroxidise conjugate	Rabbit polyclonal antibody	Dependent on primary	Sigma	A-9044

2.2 Standard reagents and solutions

2.2.1 Solutions for use in cell culture

0.05M EDTA

1g KCl (Fisons Scientific Equipment, Loughborough, UK), 5.72g Na₂HPO₄ (BDH Chemical Ltd., Poole, England, UK), 1g KH₂PO₄ (BDH Chemical Ltd., Poole, England, UK), 40g NaCl (Sigma-Aldrich, Inc., Poole, Dorset, England, UK) and 1.4g EDTA (Duchefa Biochemie, Haarlem, The Netherlands) was dissolved in 5L distilled water, adjusted to a pH of 7.4, autoclaved, and stored until further use.

Trypsin (25mg/ml)

This solution was made up by dissolving 500mg trypsin in the 0.05M EDTA, before being mixed, and then filtered through a 0.2µm minisart filter (Sartorius, Epsom, UK). This solution was then aliquoted into samples of 250µl and stored at -20°C until further use. When required for cell culture work, one of these aliquots was further diluted in 10ml 0.05M EDTA and used to detach the cells.

Balanced Saline Solution (BSS)

79.5g NaCl, 2.1g KH₂PO₄, 2.2g KCl and 1.1g of Na₂HPO₄, was dissolved in 10L of distilled water, and the pH amended to 7.2, using 1M NaOH (Sigma-Aldrich, Inc., Poole, Dorset, England, UK).

100x Antibiotic cocktail mix

5g streptomycin, 3.3g penicillin and 12.5mg amphotericin B in DMSO, were dissolved in BSS and filtered. 5ml was then added to a 500ml bottle of DMEM media.

2.2.2 Solutions for use in molecular biology

Tris-Boric-Acid-EDTA (TBE)

5xTBE solution (1.1M Tris; 900mM Borate; 25mM EDTA; pH 8.3) was made up by dissolving 540g Tris-Cl (Melford Laboratories Ltd, Suffolk, UK), 275g Boric acid (Duchefa Biochemie, Haarlem, The Netherlands) and 46.5g of EDTA in 10L of distilled water. The pH was adjusted to 8.3 using NaOH, and then stored at room temperature until further needed for use in agarose gel electrophoresis, when it was further diluted in water to a 1X concentrate.

DEPC water

Prior to being autoclaved, 250ml of Diethyl Pyroncarbonate (DEPC) (Sigma-Aldrich, Inc., Poole, Dorset, England, UK) was supplemented to 4.75ml of distilled water.

Loading buffer (used for DNA electrophoresis)

25mg of bromophenol blue (Sigma-Aldrich, Inc., Poole, Dorset, England, UK) and 4g sucrose (Fisons Scientific Equipment, Loughborough, UK) was dissolved in 10ml of distilled water and stored at 4°C in order to avoid mould growth.

Ethidium Bromide

A stock solution of 10mg/ml ethidium bromide was prepared by dissolving 200mg of ethidium bromide powder (Sigma-Aldrich, Inc., Poole, Dorset, England, UK) in 20ml distilled water. In order to protect the solution from sunlight, it was then placed in a tube and covered in aluminium foil before being safely stored.

2.2.3 Solutions for use in cloning

LB agar

LB agar was prepared by dissolving 10g tryptone (Duchefa Biochemie, Haarlem, The Netherlands), 5g yeast extract (Duchefa Biochemie, Haarlem, The Netherlands), 15g agar, and 10g NaCl, in 1L of distilled water, before adjusting the pH to 7.0, and autoclaving the solution. As soon as it was further needed, the solution was melted and left to cool, before adding antibiotics and pouring the solution into 10cm² Petri dishes (Bibby Sterilin LTd., Staffs, UK). These were left to cool and harden before being inverted and stored at 4°C.

LB broth

10g tryptone, 10g NaCl and 5g yeast extract was dissolved in 1L of distilled water. The pH of the solution was then adjusted to 7.0, and after being autoclaved was left to cool. Antibiotics were then added and the solution stored at room temperature.

2.2.4 Solutions for use in protein work

Lysis Buffer

This was made up by dissolving 2mM CaCl₂, 0.5% Triton X-100, 1mg/ml aprotinin, 1mg/ml leupeptin and 10mM Sodium Orthovanadate in 50ml distilled water. The solution was then stored at 4°C until further use.

10% Ammonium Persulphate (APS)

1g APS was dissolved in 10ml distilled water before being aliquoted into fractions of 2.5ml. This was then stored at 4°C until further use.

Tris Buffered Saline (TBS)

24.228g Tris and 80.06g NaCl was dissolved in 1L of distilled water in order to make a 10x TBS (0.5M Tris, 1.38 M NaCl, pH 7.4) stock solution. The pH was then adjusted to 7.4 using HCl and stored until further use.

10x Running buffer (for SDS-PAGE)

10x running buffer (0.25M Tris, 1.92M glycine, 1% SDS, pH8.3) was prepared by dissolving 303g of Tris, 1.44kg of Glycine (Melford Laboratories Ltd., Suffolk, UK) and 100g SDS (Melford LaboratoriesLtd., Suffolk, UK) in 10L of distilled water. Prior to use this solution was further diluted to a 1x concentrate.

Transfer buffer

15.5g Tris and 72g glycine was dissolved in 4L distilled water before 1L of methanol (Fisher

Scientific, Leicestershire, UK) was added to make a final volume of 5L.

Ponceau S stain

Supplied directly by Sigma.

Coomassie blue stain

100g Coomassie Brilliant Blue (Sigma-Aldrich, Inc., Poole, Dorset, England, UK) was dissolved in 100ml acetic acid (Fisher Scientific, Leicestershire, UK) and 250ml ethanol (Fisher Scientific, Leicestershire, UK), which was then added to 650ml distilled water.

Coomassie blue destain

500ml of methanol was mixed with 100ml acetic acid (Fisher Scientific, Leicestershire, UK) and then added to distilled water to make up a final volume of 1L.

2.2.5 Solutions for purification of histidine-tagged recombinant protein

8x Phosphate buffer (PBS), pH 7.4

1.42g $\text{Na}_2\text{HPO}_4 \cdot 2\text{H}_2\text{O}$ (177.99g/mol), 1.11g $\text{NaH}_2\text{PO}_4 \cdot \text{H}_2\text{O}$ (137.99g/mol), and 23.38g NaCl (58.44g/mol) was dissolved in 100ml distilled water, adjusted to the correct pH, and filtered through a 0.45 μm filter.

2M imidazole, pH 7.4

13.62g imidazole was added to 100 ml distilled water, adjusted to the correct pH, and filtered.

0.1M NiSO_4

2.63g $\text{NiSO}_4 \cdot 6\text{H}_2\text{O}$ was dissolved in 100ml distilled water and filtered.

Binding buffer

In order to make up 24ml binding buffer, 3ml 8x PBS was mixed with 0.12ml 2M imidazole, and topped up to 24ml with distilled water.

Elution buffer

To prepare 8ml elution buffer, 1ml 8x PBS was mixed with 2ml 2M imidazole and topped with distilled water to a volume of 8ml. The pH was then adjusted to pH 7.4-7.6, and the final solution filtered.

2.2.6 Solutions for use in immunocytochemical staining

Diaminobenzidine (DAB) chromagen

2 drops of wash buffer, 4 drops of DAB (Vector Laboratories, Inc., Burlingame, USA) and 2 drops of H₂O₂ were added to 5ml of distilled water and shaken well before use.

ABC Complex

The ABC complex is prepared by using a kit provided by Vector Laboratories Inc. (Burlingame, USA). 4 drops of reagent A and B were added to 20ml of wash buffer before being mixed thoroughly and left at room temperature for 30 minutes before being used.

2.3 Cell culture, maintenance, and storage

2.3.1 Preparation of growth media and cell maintenance

- Dulbecco's Modified Eagle's medium (DMEM/ Ham's F-12 with L-Glutamine; E15-813, PAA Laboratories, Somerset, UK), pH 7.3 containing 2mM L-glutamine and 4.5mM NAHCO₃, supplemented with 10% heat inactivated Foetal Bovine Serum (PAA Laboratories, Somerset, UK) and an antibiotic cocktail, was used to routinely culture the cells used in this study.
- Cell lines transfected with the pEF6/His plasmid were originally cultured in 5µg/ml blasticidin S (Melford laboratories ltd, Suffolk, UK) selection media until they were ready to be transferred into 0.5µg/ml blasticidin S maintenance media.

- All the cell lines were cultured in 25cm² and 75cm² culture flasks (Greiner Bio-One Ltd, Gloucestershire, UK) with a loosely fitted cap in incubator at 37°C, 98% humidification, and 5% CO₂.
- Cell confluency was visually assessed using a light microscope and approximating the percentage of cells covering the surface of the tissue culture flasks. If needed for experimental work, the cells were left to grow until they reached sub-confluency (2-3 days). All handling of cells was carried out aseptically, using a Class II Laminar Flow Cabinet with autoclaved and sterile equipment. Cells were routinely sub-cultured when they had reached a confluency of 80-90% (5-7 days), as explained in section 2.3.2.

2.3.2 Adherent cell trypsinisation (detachment) and cell counting

- As mentioned above, once the cells had reached a confluency of approximately 80-90%, the medium was aspirated before being briefly rinsed with sterile EDTA in order to remove any remaining serum which has an inhibitory effect on the action of trypsin.
- Adherent cells were then detached from the tissue culture flask using 1-2ml of Trypsin/EDTA (0.01% trypsin and 0.05% EDTA in BSS buffer) by incubating the cells at 37°C for approximately 5 minutes.
- Once detached, the cell suspension was then poured into 20ml universal containers (Greiner Bio-One Ltd, Gloucestershire, UK) before being centrifuged at 1,600rpm for 5 minutes in order to pellet the cells.
- The excess liquid was then aspirated and the cell pellet resuspended in an appropriate amount of medium, and the cells were either counted for use in immediate experimental procedures, or transferred into fresh tissue culture flasks for re-culturing.
- Cells were counted using a Neubauer haemocytometer counting chamber (Mod-Fuchs Rosenthal, Hawksley, UK) using an inverted microscope at a magnification of 10x10 (Reichert, Austria). A haemocytometer allows for the calculation of the number of

cells in a predetermined volume of fluid in order to obtain the quantity of cells per millilitre, and an accurate estimation of cell density for use in *in vitro* and *in vivo* cell function assays.

- The haemocytometer chamber is divided into 16 squares with dimensions of 1mm x 1mm x 0.2mm. For consistency of cell density, two of these 16 squared areas were counted. This allowed for determination of cell number by using the following equation:

$$\text{Cell number/ml} = (\text{number of cells in two 16 squares} \div 2) \times (1 \times 10^4)$$

2.3.3 Storing cells in liquid nitrogen and cell resuscitation

Cell stocks of low passage number that needed to be stored were done so in liquid nitrogen.

- Cells were trypsinised as described in section 2.3.2 and resuspended in medium with 10% Dimethylsulphoxide (DMSO; Fisons, UK) at a cell density of 1×10^6 cells/ml.
- This cell suspension was then divided into 1ml aliquots and transferred into pre-labelled 1.8ml cryopreserve tubes (Nunc, Fisher Scientific, Leicestershire, UK) before being wrapped in protective tissue paper, stored overnight at -80°C , and then transferred to liquid nitrogen tanks for long term storage until required.
- In order to resuscitate the cells, they were removed from liquid nitrogen and left to rapidly thaw before being transferred into a universal container containing 10ml pre-warmed medium, and incubated for 10 minutes at 37°C .
- This was followed by centrifugation at 1,600rpm for 5 minutes to remove any excess DMSO, before re-suspending the pellet in 5ml media, transferring the suspension into a fresh 25cm^2 tissue culture flask and maintaining it in an incubator.

2.4 Methods for RNA detection

2.4.1 Total RNA isolation

There are three main types of Ribonucleic acid (RNA) in the cytoplasm known as; ribosomal (rRNA), transfer (tRNA), and messenger RNA (mRNA). Despite its critical role of carrying the genetic information required for specific protein formation, cellular mRNA only constitutes 1-2% of the total cellular RNA. It is this type of RNA that is normally used in research, and indeed is used in this study.

- The protocol followed for RNA isolation was carried out using the ABgene Total RNA Isolation Reagent (TRIR) kit (ABgene, Surrey, UK).
- Cells were grown in a monolayer of 85-90% confluency before the medium was aspirated and replaced with RNA reagent (1ml per $5-10 \times 10^6$ cells), in order to induce cell lysis.
- This homogenate was passed through a transfer pipette, transferred into a 1.8ml eppendorf, and stored at 4°C for 5 minutes, to allow for complete nucleoprotein complex dissociation.
- This was followed by the addition of 0.2ml (per 1ml of RNA reagent) chloroform (Sigma-Aldrich, Inc., Poole, Dorset, England, UK), 15 seconds of vigorous shaking, and incubation at 4°C for 5 minutes.
- The resulting homogenate was then centrifuged at 12,000rpm for 15 minutes at 4°C (Boeco, Wolf laboratories, York, UK). Under these acidic conditions, the homogenate is separated into three phases; a lower organic phase containing protein, an interphase containing DNA, and finally an upper aqueous phase containing the RNA.
- This aqueous phase which should constitute around 40-50% of the total volume, was then carefully removed and transferred into a fresh eppendorf, before adding an equal volume (usually around 0.5ml) of isopropanol (Sigma-Aldrich, Inc., Poole, Dorset,

England, UK), and incubating for 10 minutes at 4⁰C. After centrifuging the samples at 12,000rpm for 10 minutes at 4⁰C, the RNA precipitate forms as a white pellet on the bottom of the eppendorf.

- The supernatant was then discarded, and the RNA pellet washed twice with 75% ethanol (3:1 ratio of pure ethanol and DEPC water). Each wash was carried out by adding 1ml 75% ethanol, vortexing, and subsequently centrifuging the samples at 7,500rpm for 5 minutes at 4⁰C.
- After the final wash, the RNA pellet was briefly dried at 55⁰C for 5-10 minutes, in a Techne, Hybridiser HB-1D drying oven (Wolf laboratories, York, UK), so as to remove any remaining traces of ethanol.
- The final step was to dissolve the RNA pellet in 50-100 μ l (depending on pellet size) of DEPC water by vortexing for a short while. DEPC is used, as it is a histidine specific alkylating agent and inhibits the effect of RNAases, which require histidine active sites to carry out their function.

2.4.2 RNA Quantification

- Once RNA isolation was completed, the concentration and purity of the resulting RNA was measured with the use of a UV1101 Biotech Photometer (WPA, Cambridge, UK). This spectrophotometer had been previously set to detect ssRNA (μ g/ μ l) at a dilution of 1:10 by measuring the difference in absorbance between the RNA sample and DEPC water (used as a blank) at a wavelength of 260nm.
- By using a ratio of A260nm/A280nm an estimation of the purity of the RNA can be determined, with pure RNA reaching an optical density of 2.0, and RNA contaminated with ethanol or protein, reaching optical density values of less than 1.5.
- The samples were measured using Starna glass cuvettes (Optiglass limited, Essex, UK). The RNA samples were then either placed at -80⁰C for long term storage or used immediately for reverse transcription (RT).

2.4.3 Reverse Transcription of RNA for production of cDNA

Reverse transcription (RT) is a simple and sensitive technique for mRNA analysis and acts as an enhanced and more rapid alternative to the more conventional methods of RNA examination.

- In this study RT is carried out by converting 0.25µg/µl of RNA into complementary DNA (cDNA) using the iScript™ cDNA Synthesis Kit (Bio-Rad Laboratories, California, USA). The protocol that was carried out is outlined below:
- Each reaction was set up in thin-walled 200µl PCR tubes (ABgene, Surrey, UK) as follows:

<i>Component</i>	<i>Volume per reaction</i>
5x iScript Reaction Mix	4µl
iScript Reverse Transcriptase	1µl
Nuclease-free water	xµl
RNA template (0.25µg/µl)	xµl
<i>Total Volume:</i>	<i>20µl</i>

- The complete reaction was mixed and then incubated in a T-Cy Thermocycler (Creacon Technologies Ltd, The Netherlands) at the following temperatures:

5 minutes at 25°C

30 minutes at 42°C

5 minutes at 85°C

- Once the process was completed, the cDNA was diluted 1 in 3 with PCR water, and either used immediately as a template for conventional PCR, or stored at -20°C until further use.

2.4.4 Polymerase Chain Reaction (PCR)

Polymerase chain reaction (PCR) was initially devised in 1983 by Karey Mullis as a compelling method for detecting and amplifying a specific target sequence of nucleic acid.

- In this study, a particular gene of interest was amplified by PCR using the REDTaq™ ReadyMix PCR Reaction mix (Sigma, Dorset, UK). The reactions were set up in thin walled PCR tubes in aliquots of 12µl as follows:

<i>Component</i>	<i>Volume</i>
cDNA template	1µl
Forward primer (working concentration of 1 µM)	1µl
Reverse primer (working concentration of 1 µM)	1µl
2×REDTaq™ ReadyMix	6µl
PCR H ₂ O	3µl

A negative control containing PCR water instead of the template (cDNA) was run alongside all the test samples to ensure there was no contamination.

- The PCR reactions were then briefly mixed before being placed in a T-Cy Thermocycler set to the following conditions;

Initial denaturation– 94°C for 5-10 minutes

Followed by 30-42 cycles of:

Denaturation – 94°C for 1 minute

Annealment – gene/primer specific temperature for 30-40 seconds

Extension – 72⁰C for 1-1.5 minutes

And finally:

Final extension – 72⁰C for 7-10 minutes

The cycling conditions are dependent, and vary, according to different sets of primers and the size of the PCR product.

- The primer binding sites along with the predicted product sizes were determined using the Primer3 (v.0.4.0) software available online (<http://frodo.wi.mit.edu/>), and the products were verified and visualised using agarose gel electrophoresis (as explained in section 2.4.5) and staining with ethidium bromide. In order to demonstrate a representative and reliable expression pattern, each RT-PCR was triplicated.

2.4.5 Agarose gel electrophoresis and DNA visualisation

Agarose gel electrophoresis is the most simple and common method of DNA separation and analysis. It works by using an electrical current to separate the amplified DNA according to charge and size. Depending on the product size, the samples were either run on a 0.8% agarose gel (used for large DNA fragments 1-10kb in size) or a 2% gel (used for smaller fragments less than 1kb in size).

- The agarose gels were prepared by adding the required amount of agarose (Melford Chemicals, Suffolk, UK) to 400ml of TBE solution before being heated to completely dissolve the agarose. An appropriate amount of this solution was then poured into electrophoresis cassettes (Scie-Plas Ltd., Cambridge, UK) containing well forming combs, before the gel was left to set at room temperature for 30-40 minutes.
- Once set, TBE buffer was poured over the gel until it reached to a level 5mm above the gel surface. The comb was removed, and approximately 8µl of 1Kb DNA ladder (Cat

No. 15615-016; Invitrogen, Paisley, Scotland), or 6-10 μ l of each PCR reaction, was loaded into the wells by placing the gel loading tip just over the well and dispensing the product into it.

- A power pack (Gibco BRL, Life Technologies Inc.) was then used to run the samples electrophoretically through the gel at a constant voltage of around 100V for approximately 30-50 minutes until the samples had migrated to around two thirds down the gel or as far as required for that particular product size.
- The DNA was then visualised by the addition of ethidium bromide which acts as a DNA intercalator and fluoresces, thereby absorbing invisible UV light and transmitting the energy into visible orange light. The gel was placed in ethidium bromide stain diluted in the TBE buffer and left for 15 minutes with constant agitation to ensure even staining, before being visualised under UV light using a UV illuminator (UVitech, Cambridge, UK).
- Images could then be captured with the use of a UV camera imaging system (UVitech, Cambridge, UK), and printed with a Mitsubishi thermoprinter (Mitsubishi UK, London, UK) or saved as a TIFF file. If insufficient staining was found, the gel was returned to the ethidium bromide stain for additional staining, or if destaining to remove any background staining was required, the gel was placed in water.

2.4.6 Gel extraction of DNA

PCR products of interest were extracted from the agarose gels using the GelElute™ Gel Extraction Kit (Sigma-Aldrich, Inc., Poole, Dorset, England, UK) the protocol of which was carried out as follows:

- Once the DNA electrophoresis had been completed, the required PCR products were excised from the gel using a sharp scalpel. The gel slice was then placed in an eppendorf and weighed, while the excess bits of gel were discarded.

- This was followed by the addition of 300µl/100mg of Gel Solubilisation solution, and incubation at 55°C for 10 minutes or until the gel had dissolved entirely. The gel mixture was routinely vortexed in order to aid in the dissolving process. If the resulting solution was not yellow in colour, then an appropriate amount of 3M sodium acetate buffer (pH 5.2) was added until this colour had developed.
- While this was happening, the binding column was prepared by placing the GenElute Binding Column G into a 2ml collection tube as provided, and adding 500µl of Column Preparation solution to the binding column. This was then centrifuged for 1 minute, and the flow-through liquid discarded.
- The solution containing the dissolved gel was then placed into the binding column, centrifuged for 1 minute and the resulting flow-through discarded once more. This was followed by the addition of 700µl of wash solution before being briefly centrifuged, discarding the flow-through and re-centrifuging so as to dry and rid the column completely of wash buffer.
- The binding column was subsequently placed into a fresh collection tube, and the PCR products eluted using 50µl of elution solution or PCR water. The resulting product was then either used immediately or stored at -80°C.

2.4.7 Quantitative RT-PCR (Q-PCR)

Unlike conventional RT-PCR, which only allows for semi-quantification, Q-PCR is a method of detecting extremely small amounts of cDNA template within a sample while also determining an accurate and reliable value of the template copy number in each sample. This method works due to the use of a sequence specific DNA based fluorescent reporter probe which only quantifies the levels of DNA containing the probe sequence, thereby greatly increasing specificity.

This current study uses the Ampliflour™ Uniprimer™ Universal system (Intergen company®, New York, USA) to quantify transcript copy number. The ampliflour probe consists of a 3' region specific to the Z-sequence (ACTGAACCTGACCGTACA) present on the target specific primers, and a 5' hairpin structure labelled with a flourophore (FAM). When in this hairpin structure, the flourophore is linked to, and hence is in close proximity to, an acceptor moiety (DABSYL) which acts to quench the fluorescence emitted by the flourophore, preventing any signal from being detected.

During PCR however, the probe becomes incorporated and acts as a template for DNA polymerisation in which DNA polymerase uses its 5'-3' exonuclease activity to degrade and unfold the hairpin structure, thereby disrupting the energy transfer between flourophore and quencher, allowing sufficient fluorescence to be emitted and hence detected. The fluorescent signal emitted during each PCR cycle can then be directly correlated to the amount of DNA that has been amplified. This process is illustrated in Figure 2.1.

- Each reaction to be amplified was set up as follows:

<i>Component</i>	<i>Volume</i>
Forward Z primer	0.3µl (1pmol/µl)
Reverse primer	0.3µl (10pmol/µl)
Precision™ mastermix	5µl
(Primer design Ltd., Southampton, UK)	
Ampliflour probe	0.3µl (10pmol/µl)
cDNA and PCR H ₂ O	4µl

- Each sample was then loaded into a 96 well plate (BioRad laboratories, Hemel Hempstead, UK), alongside standards (ranging from copy numbers of 10¹-10⁸), covered

with optically clear Microseal® (Biorad laboratories, California, USA) and this was placed in an iCycler^{IQ} thermal cycler and detection software (BioRad laboratories, Hemel Hempstead, UK) at the following conditions:

Initial denaturation– 94⁰C for 5 minutes

Followed by 80-90 cycles of:

Denaturation– 94⁰C for 10 seconds

Annealment– 55⁰C for 15 seconds

Extension – 72⁰C for 20 seconds

- The fluorescent signal is detected at the annealing stage by a camera where its geometric increase directly correlates with the exponential increase of product. This is then used to determine a threshold cycle (TC) for each reaction and the transcript copy number depends on when the fluorescence detection reaches this specific threshold.
- The degree of fluorescence emitted by a range of standards of a known transcript copy number is then used to compare to the amount emitted by each sample, allowing for the transcript copy number in each sample to be accurately calculated.
- Furthermore, the transcript copy number of each sample was then normalised against the detection of β -actin or GAPDH copy numbers. The procedure was repeated at least three times, and representative data is demonstrated as expressional trends. Figure 2.2 shows how transcript levels are quantified.

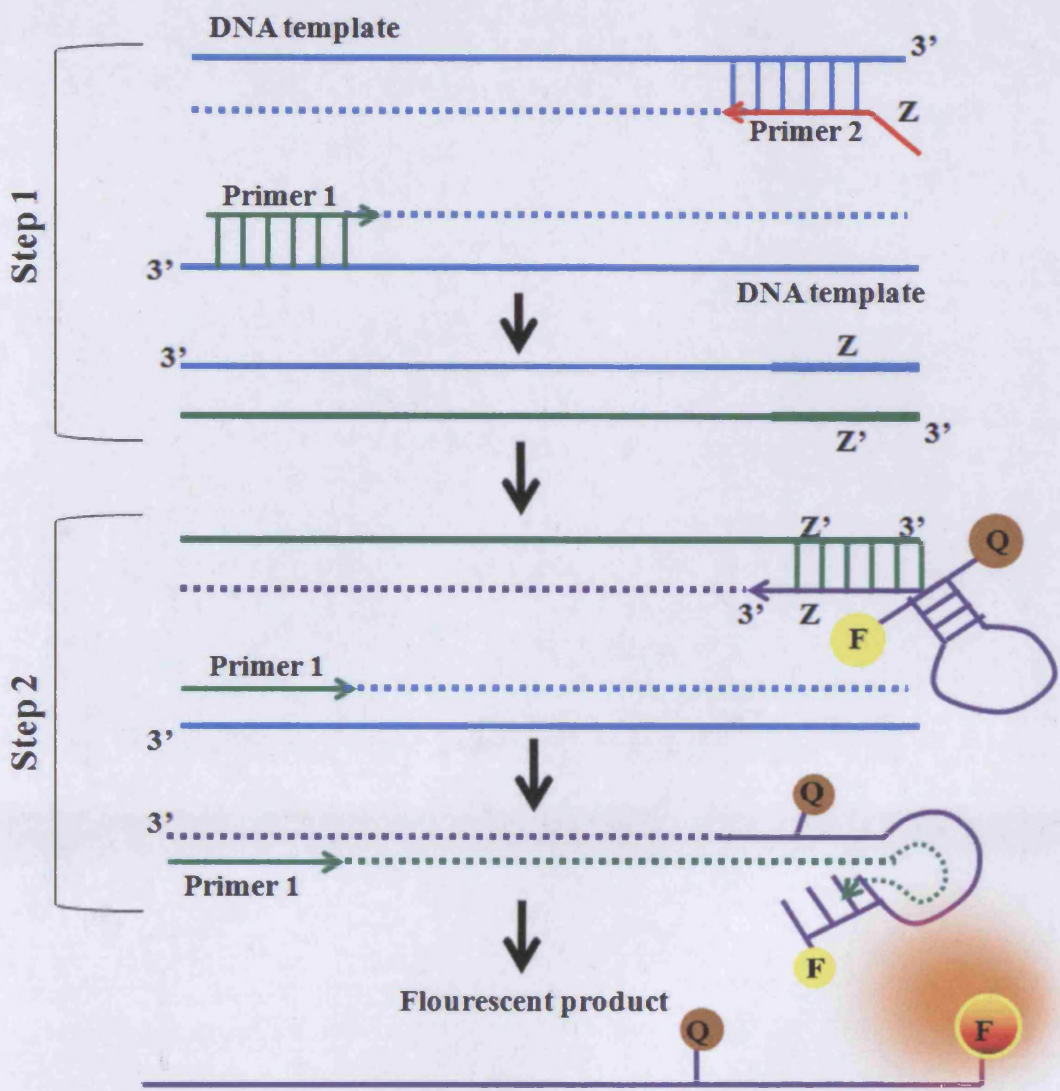
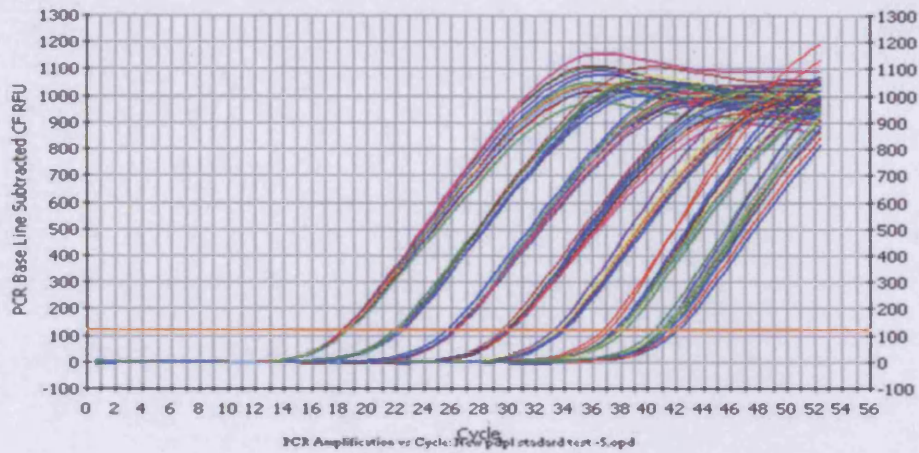


Figure 2.1: Diagram showing function of the u-probe during DNA amplification using Q-PCR.

(A)



(B)

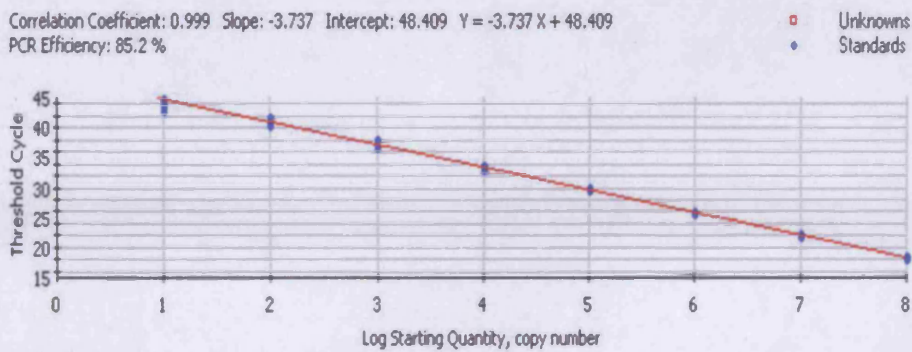


Figure 2.2: (A) Detection of transcript levels from a range of standard samples (108 to 102 copy number) using the iCycler^{IQ} thermal cycler. (B) Subsequent generation of a standard curve from these samples.

2.5 Methods for protein detection

2.5.1 Protein extraction and preparation of cell lysates

- Once cells had reached an adequate confluency, the cell monolayer was scraped off using BSS and a cell scraper. The cell suspension was then transferred into a universal tube.
- This was followed by centrifugation at 2,000rpm for 5 minutes before the supernatant was poured off, and the cell pellet resuspended in 200-300µl (depending on pellet size) of lysis buffer.
- This was transferred into a 1.8ml eppendorf tube and placed for an hour at room temperature on a Labinco rotating wheel (Wolf laboratories, York, UK) to allow for cell lysis.
- The resulting suspension was then centrifuged at 13,000rpm for 15 minutes so as to pellet any unwanted cell debris. The supernatant was transferred to a fresh eppendorf tube, and the pellet discarded.
- The protein samples were then either quantified for SDS-PAGE as explained below, or stored at -20°C until further use.

2.5.2 Protein quantification and preparation of samples for SDS-PAGE

In order to standardise the protein sample concentration for western blotting, the amount of protein in each sample was quantified by following the protocol outlined in the Bio-Rad DC Protein Assay kit (Bio-Rad laboratories, Hemel Hempstead, UK).

- In a 96 well plate, 10mg/ml of bovine serum albumin (BSA) standard (Sigma, Dorset, UK) was serially diluted in lysis buffer to a concentration of 0.005mg/ml and used to set up a standard curve of protein concentration.

- 5 μ l of either protein sample or standard was then pipetted into fresh wells, before 25 μ l of 'working reagent A' (prepared by adding 20 μ l of reagent S per millilitre of reagent A), and 200 μ l of reagent B was added to each well.
- After mixing the samples, the plate was left at room temperature for 30-45 minutes in order to allow the colorimetric reaction to take place. Once this was complete, the absorbance of each of the wells was measured at 620nm using the ELx800 plate reading spectrophotometer (Bio-Tek, Wolf laboratories, York, UK).
- Using the absorbance of the standards, a standard curve was set up, and by comparing this to the absorbences of the samples, sample concentration was determined. The samples were then diluted in an appropriate amount of lysis buffer in order to normalise them to the required final concentration of 1.0-1.5mg/ml.
- This was then further diluted with 2x Lamelli sample buffer concentrate (Sigma-aldrich, St Louis, USA) in a ratio of 1:1 before the samples were denatured by boiling at 100 $^{\circ}$ C for 5 minutes, and either loaded onto an SDS-PAGE gel or stored at -20 $^{\circ}$ C until further use.

2.5.3 Preparing immunoprecipitates

Immunoprecipitation (IP) can be used for analysing intracellular phosphorylation that occurs in downstream signalling cascades. The process involves adding a specific antibody targeted against a protein of interest within a cell lysate. This is then mixed with sepharose or agarose bonded staphylococcal protein A, protein G, or both, in order to collect the ensuing protein-antibody complexes. These complexes are then centrifuged to induce precipitation, run on an SDS-PAGE gel, and evaluated using immunoprobng. The process was carried out as follows:

- Antibody targeted against a protein of interest was added to the cell lysate samples before being incubated at 4 $^{\circ}$ C for 1 hour on a Labinco rotating wheel.

- Following incubation, 50µl of conjugated A/G protein agarose beads (Santa Cruz Biotechnology, supplied by Insight Biotechnologies Inc, Surrey, England, UK) was added to each sample and placed back on the wheel for another hour in order to allow for the antibody-protein complexes to bind to the beads.
- Centrifuging at 8,000rpm for 5 minutes then acts as a way of removing any unbound protein or excess antibodies present in the supernatant. The protein pellet was subsequently washed twice with 300µl lysis buffer before being resuspended in 40-60µl of 2x sample buffer, and boiled for 5 minutes. The resulting samples were then run on SDS-PAGE gels as explained below.

2.5.4 Sodium Dodecyl Sulphate Polyacrylamide Gel Electrophoresis (SDS-PAGE)

- The system used to carry out SDS-PAGE in this study was the OmniPAGE VS10 vertical electrophoresis system. Resolving gels of a required percentage (depending on protein size) were prepared in 15ml aliquots (enough for 2 gels) by adding all the constituents at the amounts indicated below:

Component	8% Resolving gel (50-100kDa proteins)	10% Resolving gel (20-90kDa proteins)
Distilled water	6.9ml	5.9ml
30% acrylamide mix (Sigma-Aldrich, St Louis, USA)	4.0ml	5.0ml
1.5M Tris (pH 8.8)	3.8ml	3.8ml
10% SDS	0.15ml	0.15ml
10% Ammonia persulphate	0.15ml	0.15ml
TEMED (Sigma-Aldrich, St Louis, USA)	0.009ml	0.006ml

Table 2.6: Ingredients for resolving gel.

- The resulting mixture was then poured in between two glass plates held in place by a loading cassette, until a level 1cm below the top of the plate, and in order to prevent gel oxidation, the top of the resolving gel was covered with a 0.1% SDS solution.
- The gels were then left to polymerise at room temperature for approximately 30 minutes, or until fully set. The excess SDS solution was then poured off before adding a sufficient amount of stacking gel in its place, prepared as shown below:

Component	Stacking gel
Distilled water	3.4ml
30% acrylamide mix (Sigma-Aldrich, St Louis, USA)	0.83ml
1.0M Tris (pH 6.8)	0.63 ml
10% SDS	0.05ml
10% Ammonia persulphate	0.05ml
TEMED (Sigma-Aldrich, St Louis, USA)	0.005ml

Table 2.7: Ingredients for stacking gel.

- Immediately after the addition of the stacking gel, a well forming Teflon comb is inserted before allowing the gel to polymerise at room temperature for around 20 minutes.
- Once set, the loading cassette was transferred into an electrophoresis tank and covered with 1X running buffer before removing the well comb, and by use of a 50 μ l syringe (Hamilton), loading 6-8 μ l of ColorPlus Prestained Protein Marker (New England BioLabs Ltd., Herts, UK), followed by 10-15 μ l of the required protein samples.
- The gels were then run at 125V, 40mA, and 50W for a length of time appropriate for the size of the protein of interest, in order to separate the proteins according to charge and molecular weight.

2.5.5 Western blotting: transferring proteins from gel to nitrocellulose membrane

- Once SDS-PAGE was completed, the protein samples were transferred onto a nitrocellulose membrane by western blotting. The electrophoresis equipment was

disassembled and the gel pried out from in between the two glass plates before discarding of the stacking gel. The resolving gel was then placed on the bottom graphite base electrode in a SD20 SemiDry Maxi System blotting unit (SemiDRY, Wolf Laboratories, York, UK) on top of 3 pieces of 1x transfer buffer pre-soaked filter paper (Whatman International Ltd., Maidstone, UK), and 1 sheet of Hybond nitrocellulose membrane (Amersham Biosciences UK Ltd., Bucks, UK).

- An additional 3 sheets of pre-soaked filter paper were placed on top of the gel to form a sandwich arrangement of paper: membrane: gel: paper, as shown in Figure 2.3. Electroblotting was then carried out at 15v, 500mA, and 8W for around 45 minutes to an hour. Once the proteins had been sufficiently transferred, the membranes were blocked over night at 4°C in 10% skimmed dry milk solution (10% milk powder and 0.1% polyoxyethylene (20) sorbitan monolaurate (Tween 20) (Sigma-Aldrich, St Louis, USA) in 50ml TBS. This acts to block the proteins onto the membrane for subsequent antibody probing.

SD20 Semi-Dry Blotting Unit

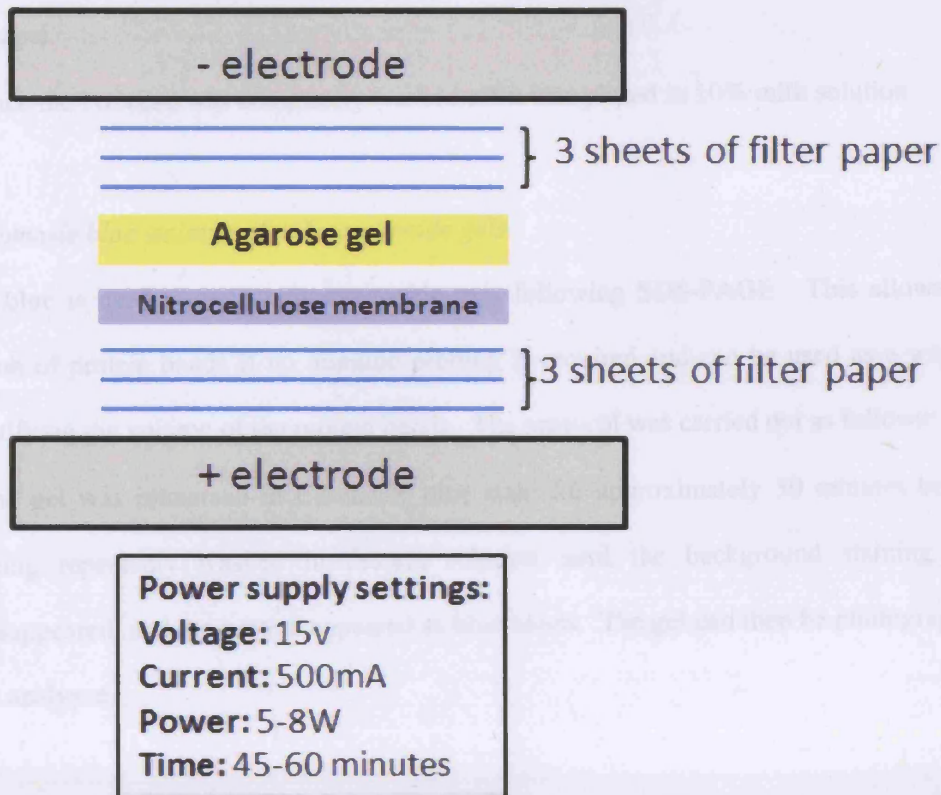


Figure 2.3: Diagram depicting process of western blotting; the transferring of proteins onto a nitrocellulose membrane.

2.5.6 Protein staining

2.5.6.1 Staining membranes in Ponceau S

Ponceau S is a reversible and re-usable protein stain that does not interfere with any subsequent immuno-probing. Its main use is to confirm that protein transfer from the polyacrylamide gel to the nitrocellulose membrane has been successful, but can also be used to aid in membrane sectioning for multiple immune-probing. The protocol was carried out as follows:

- After the transfer was completed and before probing began, the membrane was immersed in Ponceau S solution for a few minutes at room temperature.

- The solution was then washed off with distilled water until the bands become visible. If required, the membrane was then cut into several sections using a sharp and clean scalpel.
- Once the Ponceau was completely washed off it was placed in 10% milk solution.

2.5.6.2 Coomassie blue staining of polyacrylamide gels

Coomassie blue is used to stain polyacrylamide gels following SDS-PAGE. This allows for visualisation of protein bands if no immuno-probing is required and can be used as a way of semi-quantifying the volume of the protein bands. The protocol was carried out as follows:

- The gel was immersed in Coomassie blue stain for approximately 30 minutes before being repeatedly washed in destain solution until the background staining had disappeared, and the protein appeared as blue bands. The gel can then be photographed or analysed.

2.5.7 Protein detection using specific Immuno-probing

- Once any staining was completed, the membrane was transferred into 50ml falcon tubes (Nunc, Fisher-Scientific, Leicestershire, UK) ensuring that the membrane surface that had been in contact with the gel was facing upwards. 10% milk blocking solution was then added to the membranes and incubated for an hour at room temperature on a roller mixer (Stuart, Wolf-Laboratories, York, UK).
- Once this was done, the 10% milk solution was poured off and replaced with 10ml of 3% milk solution (3% milk powder, 0.1% Tween 20 in TBS) for 15 minutes. This was followed by incubation of the membranes for an hour at room temperature, with primary antibody diluted 1:200 in 5mls of 3% milk solution.
- After pouring off the primary antibody solution, any remaining unbound antibody was washed off three times in 3% milk solution at 15 minute intervals.

- Once washing was completed, the membranes were further incubated with 5ml of 1:1000 HRP conjugated secondary antibody (of the same species) diluted in 3% milk. This was carried out for an hour at room temperature on a roller mixer.
- This was followed by two 15 minute washes in 10ml of 3% milk solution, and two 15 minute washes with Tween TBS (0.1% Tween 20 in TBS), in order to wash off any unbound secondary antibody.
- A final two 15 minute washes with solely TBS was carried out so as to remove any residual detergent, before placing the membrane in weighing boats containing TBS solution, ready for chemiluminescent detection.

2.5.8 Chemiluminescent protein detection

Chemiluminescent protein detection was carried out using the Supersignal™ West Dura system (Pierce Biotechnology, Inc., Rockford, IL, USA), which consists of a highly sensitive chemiluminescent substrate that detects the horseradish peroxidase (HRP) used during the western blot procedure. The protocol was carried out as follows:

- The two reagents provided were added in a 1:1 ratio (normally 4ml of each for a mini gel) into the weighing boat containing the membrane to be analysed. After 5 minutes incubation at room temperature with constant agitation, the membrane was carefully removed from the solution using forceps.
- Any excess solution on the membrane was then drained over a piece of tissue paper and transferred into a fresh weighing boat. The chemiluminescent signal was detected using an UVITech Imager (UVITech Inc., Cambridge, UK) which contains both an illuminator and a camera linked to a computer, which then captures and stores the image.
- Each membrane was subjected to varying exposure times until the protein bands were sufficiently visible. These images were then captured and further analysed with the

UVIband software package (UVITEC, Cambridge, UK), which allows for protein band quantification.

- In this study, β -actin was used as a housekeeping gene and run alongside any other proteins to be detected, so as to allow for additional normalisation of the samples, and to compensate for any other negligible inaccuracies which may have occurred during the process. The cytoskeletal protein β -actin is used due to its highly abundant and conserved nature within eukaryotic cells, and is one of the most widely employed and accepted internal controls in scientific research.
- In order to confirm reliability of the results, each western blot was carried out three times and the protein bands quantified and standardised separately, followed by calculation of mean values and graphical presentation of the results.

2.5.9 Immunohistochemical staining

This study uses a previously reported method of Immunohistochemical staining (Jiang *et al.* 2005) and was carried out as follows:

- 20,000 cells in 200 μ l DMEM media were seeded into chamber slides (Nalge, NUNC International, LAB-TEK®, USA) and left to incubate overnight at 37^oC, with 5% CO₂.
- The cells were then fixed in ice-cold pure ethanol for 30 minutes at 4^oC, before being rehydrated with BSS for an hour at room temperature.
- This was followed by cell permeabilisation in 0.1% TritonX100 in TBS for 5-10 minutes at room temperature. This causes the cell membranes to rupture, releasing intracellular proteins.
- Permeabilisation was followed by blocking of the cells with horse serum (Vector Laboratories Inc., Burlingame, USA) in OptiMax Wash Buffer (BioGenex, San Ramon, USA) for 30 minutes at room temperature. 1-2 drops of horse serum per 5ml of wash buffer was diluted 1:20 in distilled water and used as the blocking solution.

- After blocking, the cells were washed four times with wash buffer before being incubated for an hour at room temperature with primary antibody diluted 1:100 (depends on antibody used) in blocking solution.
- Any unbound antibody was subsequently washed off with wash buffer. This was repeated 4 times before incubating the cells for a further 30 minutes at room temperature, with the corresponding secondary antibody diluted 1:1000 in blocking solution.
- After 4 washes with wash buffer, the cells were incubated with 200µl of working VECTASTAIN® Universal ABC complex (Vector Laboratories Inc., Burlingame, USA). The ABC complex was made up 30 minutes before use by mixing 4 drops of the supplied reagent A, with 4 drops of reagent B.
- The ABC solution was subsequently removed by washing four times with wash buffer before a few drops of DAB chromogen (Vector Laboratories Inc., Burlingame, USA) were added to the cells and left to incubate for 5 minutes in darkness. DAB was made up as follows; 2 drops of the provided buffer (pH 7.5), 4 drops of DAB, and 2 drops of hydrogen peroxide diluted in 5ml of distilled water.
- Following DAB addition, the solution should turn brown and once this had occurred, the DAB was washed off using distilled water before the cells were counterstained with Mayer's haematoxylin for approximately 1 minute.

2.5.10 Immunofluorescent staining

The method used in this study for fluorescent staining was carried out as previously reported (Jiang *et al.*, 1999). 20,000 cells in 200µl DMEM media were seeded into chamber slides (Nalge, NUNC International, LAB-TEK®, USA) and left to incubate overnight at 37°C, with 5% CO₂.

- After incubation cells can be treated with protein of interest if need be. The media was aspirated and the cells fixed with 200µl ice-cold pure ethanol for 20 minutes at 4°C.
- Following fixation, the cells were rehydrated with 200µl BSS for a minimum of 30 minutes at room temperature.
- The cells were permeabilised with 0.1% Tritonx100 in TBS for 5-10 minutes at room temperature before being blocked with horse serum in OptiMax Wash Buffer (BioGenex, San Ramon, USA) for 30 minutes at room temperature as explained in section 2.5.9.
- Blocking was followed by four washes with wash buffer before the cells were incubated for an hour at room temperature with primary antibody diluted 1:100 (depending on antibody used) in blocking solution.
- After a further four washes with wash buffer, the cells were incubated with the corresponding secondary antibody labelled with either FITC or TRITC diluted 1:100 in blocking serum.
- The secondary antibodies were subsequently washed off twice using wash buffer before the slides were mounted with Flouoro-Save (CalBiochem, Nottingham, England) and viewed under a fluorescent microscope (Olympus). Photos were taken and analysis carried out using the Cell Analyser software (Olympus).

2.6 Alteration of gene expression

2.6.1 Knocking down gene expression using Ribozyme Transgenes

In order to knockdown the expression of GDF-9, it was targeted at the mRNA level using hammerhead ribozyme transgenes that specifically target and cleave the GDF-9 mRNA transcript. The hammerhead ribozyme was first described by Forster and Symons in 1987 as a self-cleaving region in the RNA genome of various plant viroids and virusoids. The

hammerhead motif was subsequently integrated into short synthetic oligonucleotides, transforming it into a turnover catalyst capable of cleaving various RNA targets (Uhlenbeck, 1987; Haseloff and Gerlach, 1988).

Hammerhead motifs contain a conserved secondary structure that consists of three helical stems (I, II, and III) enclosing a junction known as the catalytic core, typified by various invariant nucleotides. The best codons demonstrated to be suitable for cleavage are AUC, GUC and UUC (Figure 2.4). In order to generate a ribozyme transgene specific to GDF-9, primers were designed using Zuker's RNA mFold programme (Zuker, 2003) according to the secondary structure of the gene. Subsequently, an appropriate GUC ribozyme target site was chosen from within GDF-9's secondary structure and the ribozyme created to specifically bind the sequence adjacent to this GUC codon. This made it possible for the hammerhead catalytic region of the ribozyme to bind to and specifically cleave the GUC sequence within the target mRNA transcript.

Following ribozyme design, the sequences were ordered from invitrogen as sense/antisense strands (as shown in Table 2.4) and joined to the transgene by carrying out touchdown PCR under the following conditions:

Initial denaturation– 94°C for 5 minutes

Followed by 8 cycles of each annealing temperature (total of 48 cycles):

Denaturation – 94°C for 10 seconds

Various annealment steps– 70°C for 15 seconds, 65°C for 15 seconds,

60°C for 15 seconds, 57°C for 15 seconds, 54°C for 15 seconds and 50°C for 15 seconds.

Extension – 72°C for 20 seconds

And finally:

Final extension – 72°C for 7 minutes

- Subsequently, the transgenes were run on a 0.8% agarose gel in order to verify their presence as well as size before being cloned into the pEF6/His plasmid as described in section 2.7.

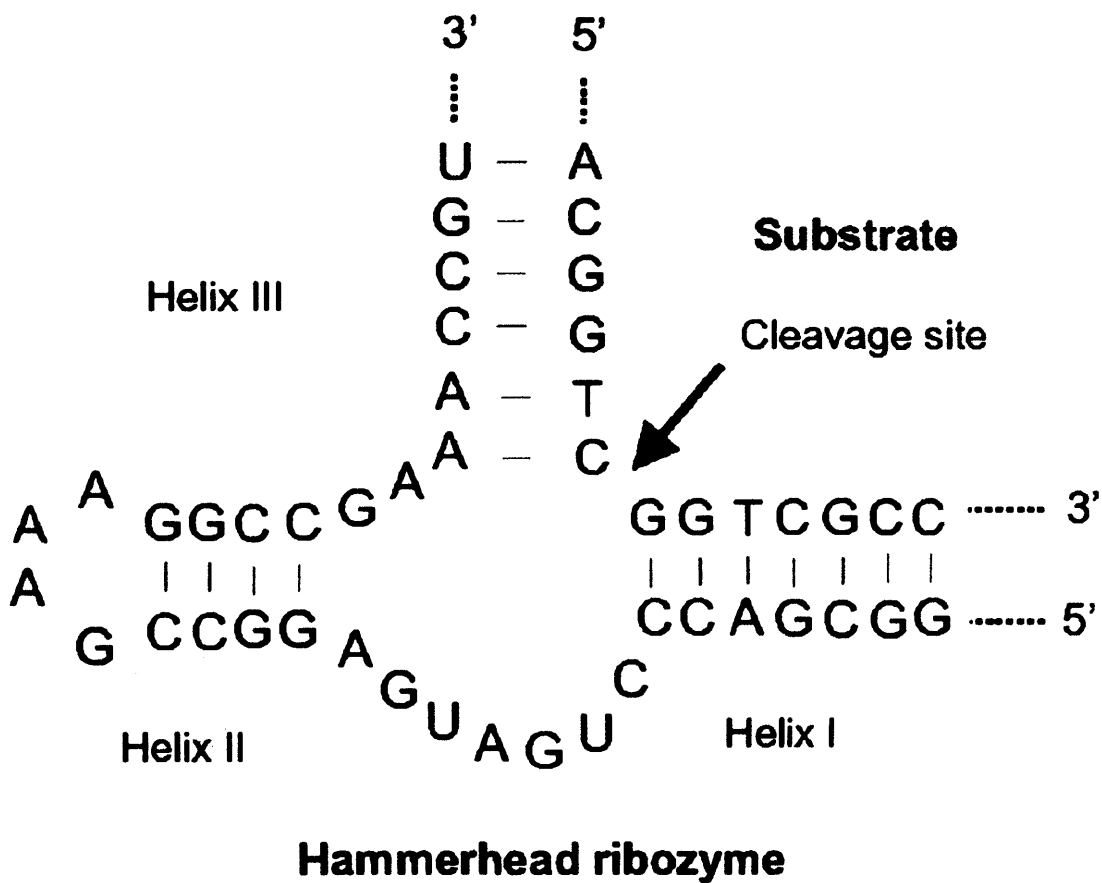


Figure 2.4: Secondary structure of hammerhead ribozyme with bound substrate.

2.6.2 Gene over-expression

Primers capable of amplifying the complete coding sequence of GDF-9 with or without stop codon, were designed according to the GDF-9 mRNA sequence. High fidelity and accurate

PCR (LA-PCR) was carried out using the DuraScript™ RT-PCR kit (Sigma-Aldrich, Inc., Poole, Dorset, England, UK) and cDNA from normal prostate tissue (previously shown to highly express GDF-9).

- The reaction was carried out at the following conditions:

Initial denaturation – 93°C for 2 minutes

Followed by 42 cycles of:

Denaturation – 93°C for 20 seconds

Annealment – 58°C (for SCD sequence) and 62°C (for NSCD sequence) for 20 seconds

Extension – 68°C for 1.5 minutes

And finally:

Final extension – 68°C for 10 minutes

- The resulting products were then run on a 2% agarose gel before being excised using the gel extraction kit (section 2.4.6) and then cloned into a pEF6/His plasmid as described in the following section.

2.7 TOPO TA gene cloning and generation of stable transfectants

The TOPO TA expression system provides a highly efficient and simple one step cloning approach without the requirement of ligases, specific PCR primers, or any post PCR procedures. The process involves the direct insertion of *Taq* polymerase amplified PCR products into a plasmid vector suited for high level and constitutive expression in mammalian host cell lines, following transfection.

This current study uses the pEF6/V5-His-TOPO plasmid vector (Invitrogen Inc., Paisley, UK) which is provided linearised with a single 3' Thymidine (T) overhangs for TA cloning, and a

covalently bound Topoisomerase (Figure 2.5). Due to its template independent terminal transferase activity, *Taq* polymerase catalyses the addition of a single deoxyadenosine (A) to the ends of PCR products. This allows for efficient ligation of the PCR product into the plasmid vector due its 3' T overhang mentioned above (the process of cloning is summarised in figure 2.6).

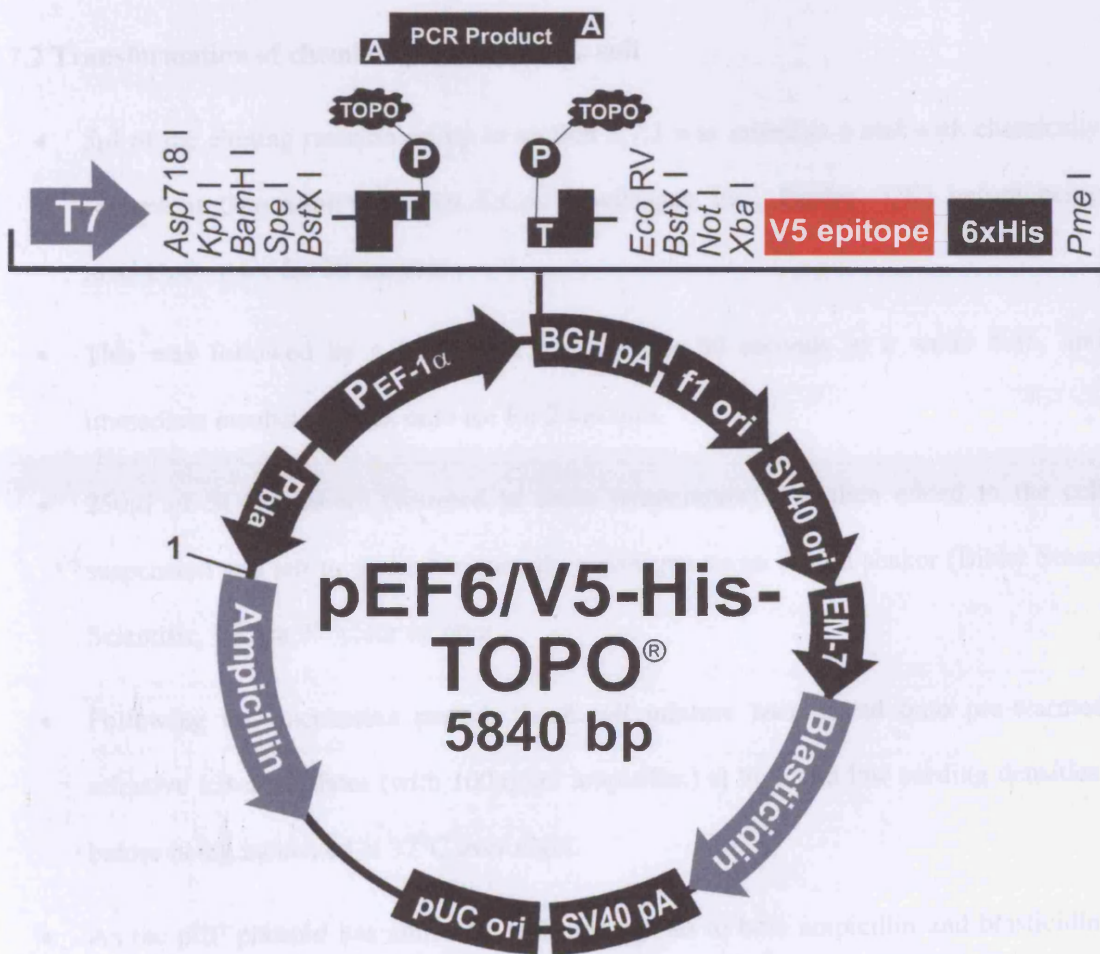


Figure 2.5: Schematic of the pEF6 plasmid (taken from pEF6/V5-His TOPO TA Expression Kit protocol).

2.7.1 TOPO cloning reaction

- The following reagents were placed in a pre-labelled eppendorf tube and mixed gently before being incubated for 5 minutes at room temperature.
 - 4ul of PCR product
 - 1ul salt solution
 - 1ul TOPO vector

2.7.2 Transformation of chemically competent *E. coli*

- 5µl of the cloning reaction set up in section 2.7.1 was mixed in a vial with chemically competent One Shot™ TOP10 *E.Coli* (Invitrogen Inc., Paisley, UK) before being incubated on ice for 30 minutes
- This was followed by a heat-shock at 42°C for 30 seconds in a water bath, and immediate incubation back onto ice for 2 minutes.
- 250µl of SOC medium (warmed to room temperature) was then added to the cell suspension and left to shake horizontally at 200rpm on an orbital shaker (Bibby Stuart Scientific, UK) at 37°C for an hour.
- Following this incubation period, the *E.coli* mixture was spread onto pre-warmed selective LB-agar plates (with 100µg/ml ampicillin) at high and low seeding densities, before being incubated at 37°C over night.
- As the pEF plasmid has antibiotic resistance genes to both ampicillin and blasticidin, only the cells that contain the plasmid are capable of growing on the agar. This is a way of selecting only the colonies positive for the plasmid containing your gene of interest. However, to confirm that the gene sequence has been inserted in the correct orientation, the colonies need further testing.

2.7.3 Colony selection and analysis

- In order to ensure that a viable product will be produced, the colonies were analysed to verify that the gene expression sequence had been ligated into the vector in the correct orientation.
- This was done by carrying out PCR on around 10 colonies, with three different sets of primers. The first reaction uses a forward primer specific for the primer (T7F or BGHR) and a reverse primer specific for the sequence. T7F starts around 90bp before the beginning of the insert and so if the insert has been ligated in the correct orientation, the resulting product should be around 100bp bigger than the predicted product size. The second reaction contains T7F and a forward primer specific for the sequence. If a product is seen following amplification, then the insert is in the wrong orientation. If a band is seen for both reactions then the colonies contain a mixture of plasmids with both correctly and incorrectly inserted sequences. Finally, in order to verify that the full sequence has been inserted without degradation, a further reaction with T7F and BGHR is carried out on the colonies.
- Individual colonies were examined by lightly touching a labelled colony with a pipette tip, and mixing it into each PCR reaction before specific amplification of the desired sequence. The thermal cycler was set to the following conditions:

Initial denaturation – 94°C for 10 minutes

Followed by 35 cycles of:

Denaturation – 94°C for 30 seconds

Annealment – 56°C for 40 seconds

Extension – 72°C for 1.5 minutes

And finally:

Final extension – 72°C for 7 minutes

2.7.4 Plasmid purification and amplification

- Following colony analysis, the ones deemed to have the insert in the correct orientation were picked off the plate and inoculated in 10ml of LB broth with 100µg/ml ampicillin, before being incubated at 37°C over night with constant agitation.
- The amplified *E.coli* were then pelleted by centrifugation at 4°C for 15 minutes at 6,000rpm, and then used for plasmid extraction. This was carried out using the Sigma GenElute Plasmid MiniPrep Kit (Sigma-Aldrich, USA) according to the provided protocol, outlined below.
- The bacterial pellet was first resuspended in 200µl of resuspension fluid (containing RNase A) before being mixed thoroughly, and transferred into the provided 2ml collection tubes.
- This was followed by the addition of 200µl lysis solution and mixing by inverting the tubes 5-6 times. The resulting mixture was left at room temperature for 5 minutes before adding 350µl of neutralisation solution.
- The tubes were inverted several times again, and centrifuged at 12,000rpm for 10 minutes. The resulting supernatant was then transferred into a fresh collection tube containing a Mini Spin Column, which binds the plasmid DNA after centrifugation at 12,000rpm for 1 minute.
- The flow through was discarded before the column was washed with 700µl of wash solution (containing ethanol) and centrifuging at 12,000rpm for 1 minute. The flow through was discarded once more, before the column was dried by another minute of centrifugation.

- The column was then transferred into a fresh collection tube for elution. This was carried out by adding 50-100µl of elution solution and centrifuging at 12,000rpm for 1 minute. The resulting flow through containing the purified plasmid was collected, and around 4µl run on a 0.8% agarose gel in order to confirm the presence and purification of the plasmid.

2.7.5 Transfection of mammalian cells using electroporation

- Following plasmid extraction, the empty plasmid, and the plasmid containing the ribozyme transgene was used to transfect both the PC-3 and DU-145 prostate cancer cell lines respectively, while the plasmid with the GDF-9 coding sequence was transfected into the PC-3 cells alone. As DU-145 cells already express such high endogenous levels of GDF-9, only GDF-9 knock-down was attempted in this cell line.
- The method of transfection used in this study was electroporation using an electroporator (Easyjet, Flowgene, Surrey, UK).
- Once the cells had reached confluency they were detached from their tissue culture flasks, counted, and approximately 2×10^6 cells were resuspended in 1ml of media.
- 500µl of the cell suspension was then added into an electroporation cuvette (Eurgenetech, Southampton, UK), and following the addition of 3-5µl of plasmid, left at room temperature for 5 minutes.
- The cuvette was placed into the electroporator and subjected to an electrical pulse of 310V before immediately being transferred into a fresh tissue culture flask containing media.

2.7.6 Establishment of a stable expression mammalian cell line

- Following transfection, in order to obtain a stable cell line expressing the gene of interest, the cultured cells needed to be selected so as to yield only the population of cells containing the required plasmid, and hence expressing the desired molecule.

- As mentioned before, the pEF plasmid contains a resistance gene against blasticidin, and this is used as a form of mammalian cell selection. Therefore, the cells were cultured in selection media containing 5µg/ml blasticidin S for around 1-2 weeks so that those cells that did not contain the plasmid were killed off, allowing only the cells containing the plasmid to survive.
- Following selection, the cells were transferred into maintenance media containing 0.5µg/ml blasticidin, in which they were cultured in, indefinitely. In order to verify that the cells were actually expressing the gene of interest, the cells were analysed by carrying out RT-PCR and western blotting.
- Once the cells had been verified to stably express the desired molecule, they were subjected to various *in vitro* assays in order to test the effect of altering the expression of that molecule on the biological properties of the cells. These assays are outlined in section 2.9.

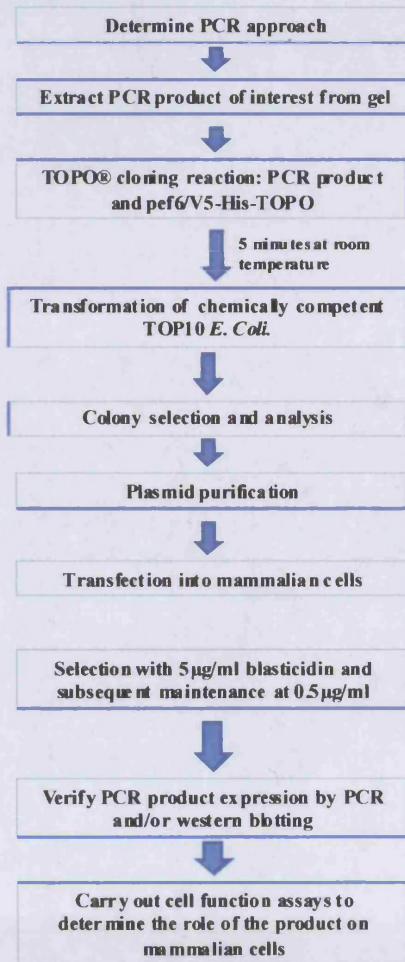


Figure 2.6: Flow chart summarising cloning and production of a stable expression mammalian cell line.

2.8 Generating human recombinant protein (rh-GDF-9)

2.8.1 TOPO TA cloning

The process of cloning carried out for recombinant protein production was identical to the one previously mentioned in section 2.7, except that the primers used for plasmid design had a deleted stop codon (ATC), in order to allow for production of a histidine-tagged version of the protein of interest.

Once the ideal parameters for carrying out PCR were determined, the resulting PCR product was cloned into a pEF6/V5-His-TOPO vector using the exact method as previously described. This was followed by *E.coli* transformation, plasmid amplification, and finally plasmid purification using the GenElute™ Plasmid Miniprep Kit (Sigma-Aldrich, Inc.). The purified transgene and empty plasmid were then transfected into 3T3 cells (murine fibroblastic cell line, obtained from ATCC), respectively. After a few weeks of selection with 5µg/ml blasticidin, stable GDF-9 transfectants were established and used to produce rh-GDF-9.

2.8.2 Collection of condensed media containing recombinant protein

Following verification of the 3T3 cell line with the plasmid coding for histidine-tagged GDF-9, the cells were grown to large numbers, seeded into a 5L roller bottle, and left to grow at 37°C, while rotating on a wheaton bench top roller (Cole Parmer, Illinois, USA). Once the cells had adhered to the roller bottle, and reached sufficient confluency, the cells were left to grow in 20ml serum free DMEM F12 media for 6-8 hours. This media was then collected and spun down for 5 mins at 6,000rpm, in order to remove any cell debris. The cells were then left to grow over-night in 10% DMEM F12 media containing 0.5µg/ml blasticidin, before being returned to serum free media as before. This process was continued until sufficient media was collected for protein purification, which was filtered before use. The cells were trypsinised off

the roller bottle and spun down for 5 mins at 6,000rpm, to form a cell pellet, which was then lysed in SDS-free lysis buffer.

2.8.3 Condensing of rh-GDF-9 containing media

Before the conditioned media could be passed through a chelating column, it needed to be condensed down to 50ml. This was carried out using the Vivaflow 50 system (Sartorius Vivascience AG, Hannover, Germany), which is a modular tangential system that allows for fast concentration performance. Polyethersulfone membranes with various pore sizes retain 90% of the molecules of that size or larger in the solution, thereby providing a molecular weight cut off point (MWCO). Several of these filters of varying MWCOs can be used in order to condense the media, and concentrate a protein of a desired size. The system is run by the use of a peristaltic pump (Masterflex pump™, Sartorius AG, Germany), that pumps the media through the connected filters, with the flow through ending up in two separate flasks, one containing the protein of the desired size, and the other containing proteins larger or smaller than the desired size.

- The components of the system were set up as shown in Figure 2.7 and rinsed, firstly with ethanol, and then distilled water, for 30 minutes each before use.
- The solution to be purified was then placed in the sample reservoir and the liquid was pumped through the system at a recirculation rate of 200-400ml/min, with the pressure indicator reading no higher than 2.5.
- When the desired volume was reached, the recirculation rate was reduced to 20-40ml/min, and the concentrated solution re-circulated through the system in order to maximise recovery.
- Once completed, the system was rinsed thoroughly with ethanol and distilled water before re-use.

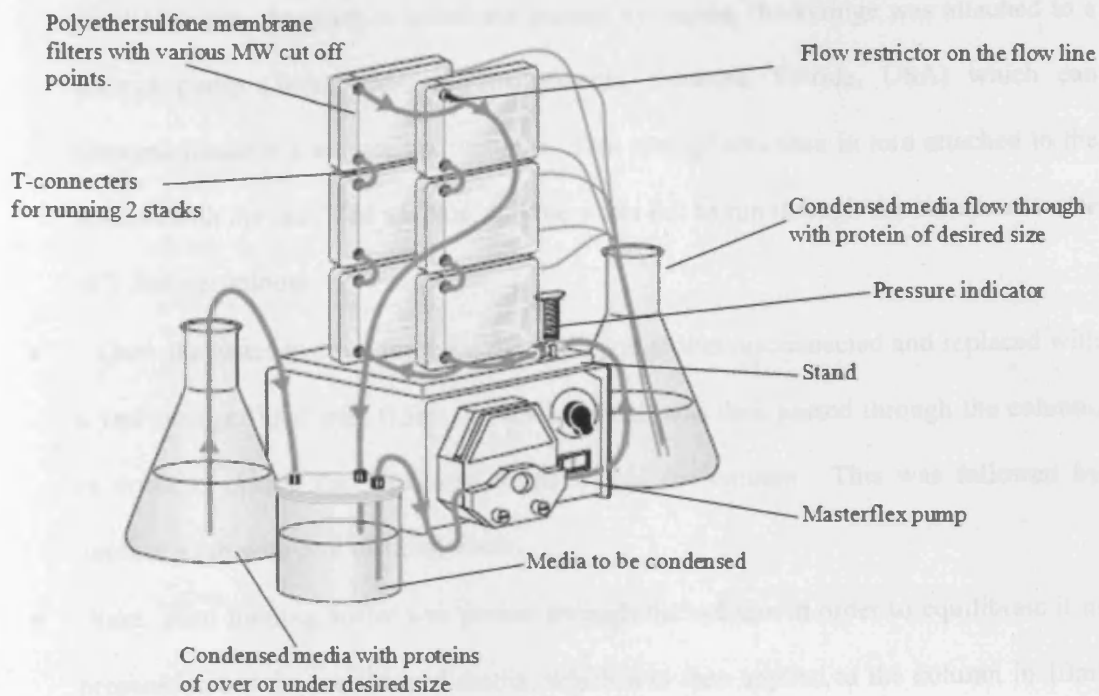


Figure 2.7: Diagram showing set-up of vivaflow 50 system.

2.8.4 Purification of rh-GDF-9 using the HiTrap chelating HP column

The rh-GDF-9 that should be present in the media collected above, carries a 6 residue histidine-tag at one end of the protein. This histidine-tag binds with high affinity to metals such as nickel, and this characteristic can be manipulated in order to purify the protein of interest. This current study uses a HiTrap™ purification kit (Amersham Bioscience UK Ltd., Buckinghamshire, UK). This kit comes with a ready-to-use HiTrap™ Chelating HP 1ml column, which when charged with Ni^{2+} ions, will selectively bind proteins with histidine residues exposed on their surface, by the process of immobilised metal affinity chromatography. This process allows for a quick one-step highly concentrated purification of the protein of interest.

- Firstly, the twist off end was removed from the column, and a 5ml syringe filled with distilled water. In order to substitute manual syringing, the syringe was attached to a syringe pump (World precision instruments, Sarasota, Florida, USA) which can dispense liquid at a set rate and volume. This syringe was then in turn attached to the column with the provided adaptor, and the water left to run through the column at a rate of 1-3ml per minute.
- Once the water had run through, the 5ml syringe was disconnected and replaced with a 1ml syringe filled with 0.5ml of NiSO₄, which was then passed through the column, in order to charge the sepharose beads within the column. This was followed by another wash with 5ml distilled water.
- Next, 10ml binding buffer was passed through the column in order to equilibrate it in preparation for the conditioned media, which was then applied to the column in 10ml aliquots at a flow rate of 1-3ml per minute. The flow through was collected as it may still contain some unbound protein.
- Once all the media had been passed through the column, it was washed with 10ml binding buffer, whose flow through was also kept as it contains imidazole and hence may have eluted some of the protein.
- The final step is elution and this was carried out with 5ml elution buffer. In order to prevent dilution of the eluate, this was done by collecting it in 1ml fractions with varying concentrations of imidazole (in this case 0, 1,5,10 and 20mM), allowing for varying binding affinities of the protein.
- The purification of each of the eluates was then run on an SDS-PAGE in order to see which aliquot contains the highest concentration of the recombinant protein, which in most cases would be the second or third eluate. This also acted as a means of assessing recombinant protein purification.

- After the protein had finished eluting, the column was regenerated by being washed with start buffer making it ready for a new run of purification of the same protein, without the need to reload with nickel.

2.8.5 Desalting and buffer exchange

Before the recombinant protein could be used in any further experiments, any remaining imidazole needed to be removed as it may have an effect on the cells, once treated. This can be done in one of two ways; buffer exchange using dialysis, or centrifugal concentrators which was the method carried out and explained in this study.

This study uses Vivaspin centrifugal concentrators (Sartorius AG, Goettingen, Germany) which use ultrafiltration vertical membranes to combine protein filtration and recovery, avoiding any lengthy dialysis steps. The ultrafiltration membrane allows proteins to be retained while letting salts pass through freely, independently of protein concentration or molecular weight. The concentration of the protein of interest therefore remains unchanged and can be diluted back to the original volume with water or a salt-free buffer, such as PBS. However, it is also possible to dilute the protein with a new buffer, thereby completely exchanging the buffering substance. The process is carried out as follows:

- Firstly, the protein eluate was diluted 1 in 10 before a centrifugal concentrator of the appropriate molecular weight and volume was selected, and filled up to the maximum level with the diluted protein.
- The concentrator then underwent centrifugation for the recommended amount of time at an appropriate spin speed for the vivaspin model. In the case of the vivaspin 6 (maximum of 6ml), 4000xg for 30 minutes.
- The flow through was then discarded and the concentrator refilled with an appropriate sample to the maximum level. This process was continued until the desired concentration of salt was reached.

- Once this was achieved, the concentrated, desalted sample was retrieved from the bottom of the concentrate pocket, with a pipette.

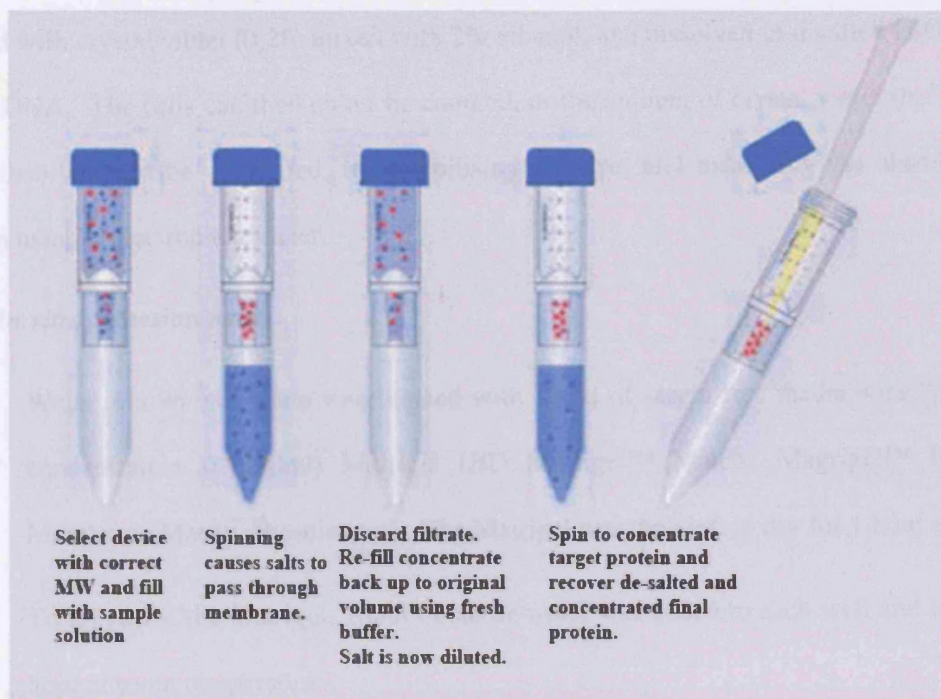


Figure 2.8: Figure depicting vivaspin centrifugal concentrator system (adapted from Sartorius GA manual).

2.8.6 Quantification of recombinant protein

Once the concentration of imidazole was reduced to a negligible amount, the resulting protein was run on another SDS-PAGE alongside a serial dilution of BSA standard starting at a concentration of 50 μ g. The volume of the recombinant protein band was then compared to a similar sized band of a known concentration of BSA, in order to determine the approximate concentration of the recombinant protein. This was carried out using the UViband software package (UVITEC, Cambridge, UK) which allows for protein band quantification.

2.9 *In vitro* cell function assays

These assays can be used to quantify cell density as they adhere to multi-well plates, with or without Matrigel (a basement membrane substitute). After a set amount of time, the cells are stained with crystal violet (0.2% mixed with 2% ethanol, and dissolved in distilled H₂O), which stains DNA. The cells can then either be counted, or the amount of crystal violet that the cells have absorbed can be quantified, by solubilising the dye, and measuring the absorbance at 540nm using a spectrophotometer.

2.9.1 *In vitro* adhesion assay

- Wells in a 96 well plate were coated with 100ul of serum free media with 5µg (stock concentration 0.5mg/ml) Matrigel (BD Matrigel™ Matrix, Magrigel™ Basement Membrane Matrix, Biosciences). The Matrigel was then left to dry for 1 hour at 55°C.
- To rehydrate the Matrigel, 100ul of sterile water was added to each well and left for an hour at room temperature.
- The media was aspirated and 30,000 to 40,000 cells diluted in 200µl DMEM, were seeded into each well and left to adhere at 37°C, with 5% CO₂ for 40 minutes.
- The media was discarded, and the wells washed with BSS to remove any unbound cells. The cells that had remained adhered after washing were fixed in 4% formalin for 10-20 minutes, and then stained with 0.5% crystal violet for 10 minutes. The dye was washed off and the plates left to dry, before the stained cells were photographed and counted using a microscope. Due to the fluid dynamics within the small sized wells of a 96 well plate, matrigel sets unevenly, causing cell aggregation around the edges of the well. Therefore, in order to avoid these areas, only the cells which had adhered to the centre of the well were counted, making sure that the same area of the well was assessed for each sample.

2.9.2 *In vitro* invasion assay

- 8µm pore Transwell inserts (FALCON®, pore size 8.0µm, 24 well format, Greiner Bio one, Germany) were placed into wells of a 24 well plate (NUNC™, Greiner Bio one, Germany), using forceps in order to prevent contamination.
- Each insert was subsequently coated with 100µl serum free media with 50µg Matrigel, and left to dry for several hours at 55°C.
- The Matrigel was then rehydrated with 200µl sterile water for an hour at room temperature.
- The water was discarded, and 30,000 cells aliquoted in 200µl DMEM were seeded into each insert. 600µl media was then added to each well, surrounding the inserts, and the cells were incubated for a maximum of 96 hours, with 5% CO₂ at 37°C. This set up is shown in figure 2.9.
- After 96 hours incubation, the invasive cells migrate through the Matrigel, and the porous membrane to the other side of the insert. The Matrigel layer and the non-invasive cells were then removed from inside the insert using some tissue paper. If this step is not carried out, the Matrigel would also be stained with crystal violet, making it difficult to distinguish between the background and invading cells.
- The invasive cells were then fixed for 10-20 minutes with 4% formalin, and then stained with 0.5% crystal violet for 10 minutes. The crystal violet was washed off, the plates left to dry, and the stained cells photographed and counted under a microscope.

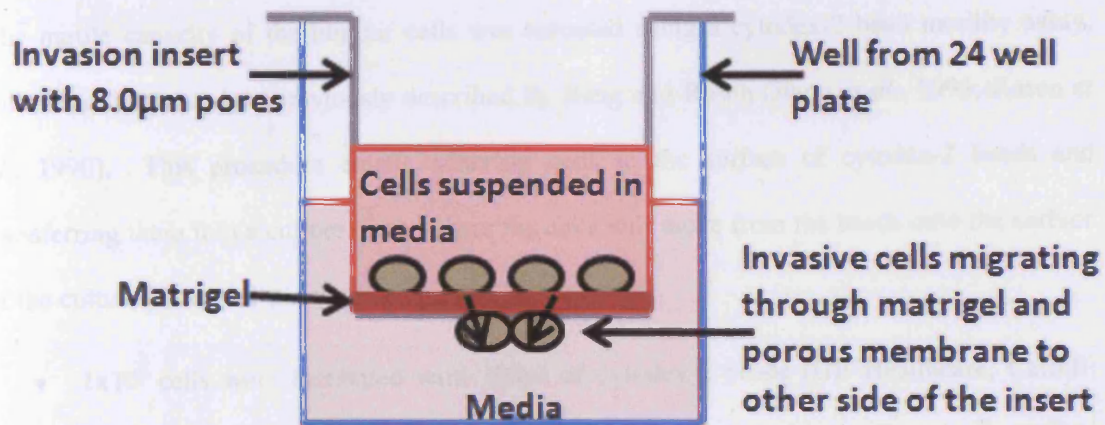


Figure 2.9: Schematic diagram showing *in vitro* invasion assay.

2.9.3 *In vitro* cell growth assay

- The protocol by Jiang et al. was followed (Jiang *et al.*, 2005). 200 μl of media containing 3,000 cells was seeded into four 96 well plates and if required, were treated with a protein of interest in serum free media.
- These plates were then left to incubate at 37°C, with 5% CO₂, for a period of 24 hours, 48 hours, 72 hours, and 120 hours, respectively.
- After incubation, the media was discarded, and the cells fixed with 4% formalin for 10-20 minutes, before being subsequently stained with 0.5% crystal violet for 10 minutes. The dye was washed off with water, and the plates left to dry.
- The dye was then solubilised using 100 μl acetic acid, and cell growth was assessed by measuring the absorbance at 540nm using a spectrophotometer (BIO-TEK, Elx800, UK). The growth rate was calculated as a percentage, using the absorbance taken at 24 hours as a baseline.

2.9.4 *In vitro* motility assay using Cytodex-2 beads

The motile capacity of the tumour cells was assessed using a cytodex-2 bead motility assay, following the procedure previously described by Jiang and Rosen (Jiang *et al.*, 1995; Rosen *et al.*, 1990). This procedure entails adhering cells to the surface of cytodex-2 beads and transferring them into a culture plate, where the cells will move from the beads onto the surface of the culture plate, and can then be counted and assessed.

- 1×10^6 cells were incubated with 100 μ l of cytodex-2 beads (GE Healthcare, Cardiff, UK) for 3.5 hours in 10ml of media in order to allow the cells to adhere to the surface of the beads.
- The beads were subsequently washed twice using 5ml of media so as to remove any non-adherent or dead cells.
- Following the second wash, the cells were resuspended in 1ml of media, 200 μ l of which was then transferred in triplicates, into a 24 well plate containing a further 800 μ l of media, and left to incubate over night.
- The following day, the cells that had migrated from the cytodex-2 beads and adhered to the surface of the culture plate, were washed with BSS several times, in order to remove any remaining cytodex-2 beads.
- The cells were then fixed using 4% formaldehyde for 5 minutes, stained with 0.5% crystal violet for 10 minutes, and counted using a microscope at 40x magnification. At least 4 random fields were counted per well, and the procedure was carried out three independent times in order to obtain statistical relevance.

2.9.5 Electrical cellular impedance sensing (ECIS)

Electrical Cellular Impedance Sensing (ECIS) is a novel method used as an alternative to the conventional function assays mentioned above. It works using an array of 8 wells, each containing a gold electrode. These measure the current and voltage across this electrode,

calculating the impedance and resistance. From the impedance changes, effects on cell attachment and motility can be examined.

- Using 8W10E arrays (ECIS™ cultureware, Applied Biophysics, Inc., NY, USA), each well was stabilised at room temperature for around 20 minutes using 200µl electrode stabilising solution (ECIS™, Applied Biophysics, Inc., NY, USA).
- The solution was then aspirated and replaced with 200µl DMEM F12 media containing Hepes buffer (Lonza, Verviers, Belgium) and left until further needed.
- The media was aspirated, and 400,000 cells diluted in 400µl DMEM were seeded into each well, and treated with a protein of interest if required.
- The array was then placed into an ECIS™ CO₂ incubator (RS biotech 9600, R galaxy R+) which is connected to the ECIS™ Model 9600 Controller (Applied Biophysics, Inc., NY, USA). The software was set up so that resistance to the current flow was measured at 400Hz. Data was normalised using resistance from the first time point.

2.9.6 Analysing apoptosis with flow cytometry

Phosphatidylserine (PS), a phospho-lipid component of the cell membrane is normally located on the cytoplasmic side of cell membranes in normal live cells. However, when the cells become apoptotic, PS translocates from the inner to the outer leaflet of the cell membrane, resulting in it being exposed to the external cellular surroundings. In leukocytes, this functions as a trigger for macrophages to phagocytose the apoptotic cells.

In order to detect apoptosing cells, this current study uses the Vybrant® Apoptosis Assay Kit (Invitrogen, Inc., Paisley, UK) to carry out an apoptosis assay. This kit works due to the fact that it contains recombinant Fluorescein conjugated annexin V (FITC annexin V) and Propidium Iodide (PI) solution. The calcium dependent phospholipid-binding protein annexin V, binds to PS with a high affinity, and hence when labelled with a fluorophore or biotin, can be used to detect apoptotic cells by binding to the PS on the outer leaflet of the cell membrane.

PI on the other hand, is a red-flourescent intercalating dye, capable of permeating only through cell membranes of non-viable cells, and binding to their nucleic acids. Therefore, any cells that have lost their membrane integrity will be stained red by the PI, whereas the apoptotic cells, which are impermeable to PI, will be stained green by the FITC annexin V. Any live cells present in the solution will show little or no fluorescence. This partial staining allows for easy identification with the Partec CyFlow® SL flow cytometer and the accompanying FloMax software package (Partec GmbH, Munster, Germany). The protocol was carried out as follows:

- Both the adherent cells and those floating in the culture medium, were harvested and washed in PBS. The cell solution was then centrifuged, before 1×10^6 cells were resuspended in 1X annexin-binding buffer, sufficient for 100µl per assay.
- 5µ of FITC annexin V and 1µl of PI working solution (100µg/ml) was subsequently added to each 100µl cell fraction, and the cells were left to incubate for 15 minutes.
- Following incubation, 400µl of 1X annexin binding buffer was added and mixed gently, before being placed on ice.
- Immediately after, the stained cells were analysed using the flow cytometer and FlowMax software package, by measuring any fluorescence emission at 530nm (FL1) and >575nm (FL3).

2.9.7 Analysing the cell cycle using PI

- Following harvestation of both adherent and floating cells (including detached mitotic, apoptotic and dead cells), the cells were centrifuged before being washed twice with PBS, and counted.
- 1×10^6 cells were subsequently resuspended in 500µl of PBS, and fixed with 4.5ml of 70% ethanol for 2 hours at 4°C.
- Following fixation, the cells were washed with PBS, and subsequently stained with 1ml of PI in a solution including Tritonx100, used to additionally permeabilise the cells, and

RNase A used to digest any double stranded RNA which can also bind to PI, so as to increase the specificity of DNA binding.

- After an incubation period of 30 minutes at room temperature, any fluorescence emitted by PI was detected with the flow cytometer and cell cycle analysis carried out using the FlowMax software.

2.9.8 Hoechst DNA stain for detection of apoptosis

The cells were firstly incubated either with DMEM with 10% FCS, or serum free, for a period of 48 hours before both the adherent cells and those floating in the culture medium, were harvested and washed in PBS. The cells were counted, and 20,000 cells were spun down before the cell pellet was resuspended in 20ng/ml Hoechst 33342 solution, and incubated in darkness for 15 minutes. The cells were centrifuged again, and resuspended with BSS before being mounted onto a cover slip, and visualised using a microscope under fluorescent light. Hoechst stains DNA, and can help identify apoptotic cells due to their condensed chromatin. Apoptotic cells were counted and using the total number of cells, a percentage for the amount of apoptotic cells was calculated.

2.9.9 The Smad3 inhibitor

The Smad3 inhibitor (566405 Calbiochem, EMD Chemicals Inc., Gibbstown, USA) was first characterised by Jinnin et al. in 2006 (Jinnin *et al.*, 2006). It is a cell-permeable pyrrolopyridine compound (7-Dimethoxy-2-((2E)-3-(1-methyl-2-phenyl-1H-pyrrolo[2,3-b]pyridin-3-yl-prop-2-enoyl))-1,2,3,4-tetrahydroisoquinoline) that selectively inhibits TGF- β 1-dependent Smad3 phosphorylation and Smad3-mediated cellular signalling, without having any effect on Smad2, p38 MAPK, ERK, or PI3K signalling.

The cells were treated with 3ng/ml Smad3 inhibitor, which was previously found to be the minimum working concentration (Jinnin *et al.*, 2006). Treatment was carried out for 4 days in the case of a growth assay, 40 minutes for an adhesion assay, and 2 hours for RNA and protein extraction.

Chapter 3

**Altering the expression of GDF-9 in
prostate cancer cells**

3.1 Introduction

Growth and Differentiation Factor 9 (GDF-9) is a member of the TGF- β superfamily and BMP subfamily, identified in 1993 by McPherron and Lee (McPherron and Lee, 1993). GDF-9 expression was initially found to be exclusive to the ovary but has recently been detected in a variety of tissues including the breast, prostate, and oral squamous carcinomas (Hanavadi *et al.*, 2007; Zhuang *et al.*, 2010). It is now known to be an oocyte derived growth factor vital in follicular development, so much so that mice lacking the *GDF-9* gene exhibit a block at an early stage of follicular development, thereby making them infertile (Su *et al.*, 2008).

BMPs have been implicated in the pathogenesis of a number of cancers, including; colorectal, osteosarcomas, myelomas, breast cancers, and most specifically, prostate cancer and associated osteoblastic lesions (Ye *et al.*, 2007). The expression profile of BMPs and their signalling counterparts has been shown to be variable in prostate cancer cells. In addition, BMPs have an effect on a range of biological properties of prostate cancer cells such as growth, apoptosis, angiogenesis, and migration.

Although most BMPs have been shown to inhibit the growth of prostate cancer cells, several studies have shown that the effect that BMPs have on *in vitro* cell growth depends on their choice of receptors, the presence of androgen, and foetal bovine serum. BMP-2 for example, when signalling via BMPR-IA, has been shown to promote prostate cancer cell growth, but inhibit growth when signalling through BMPR-IB (Ide *et al.*, 1997).

Similarly to its family members, apart from its oocyte specific functions, GDF-9 has more recently been shown to play a role in various human cancers. The laboratory has previously shown that GDF-9 can inhibit breast cancer cell invasiveness, with high levels of GDF-9 expression correlating with good prognosis (Hanavadi *et al.*, 2007). Another study demonstrated up-regulation of GDF-9 expression in an oral squamous carcinoma cell line, suggesting that unlike in breast cancer, GDF-9 may promote tumour progression in this cancer

type (Zhuang *et al.*, 2010). A clear role for GDF-9 in the progression of human cancer however, remains to be established, but it is plausible that like many other BMPs, GDF-9 may also be a factor in prostate cancer.

TGF- β has been shown to play a complicated role in regulating the autonomous, local, and systemic cellular responses that together control the development, progression, and prognostic outcome of human cancers. In prostate cancer, the cellular phenotypes of the tumour cells are induced and maintained by complex cross-talking networks between intracellular signalling pathways of the prostatic epithelial cells and their adjacent stroma. This intimate communication between prostate cancer cells and their microenvironment drives mutual stromal reactions to the prostate tumour epithelium, resulting in a vicious cycle that involves the microenvironment and cancer epithelium, which additionally promote the tumour epithelium to develop malignant properties, and may be responsible for carcinogenesis and bone metastasis (Sung and Chung, 2002).

In addition, once established, tumour cells undergo genetic modifications which allow them to secrete soluble factors that act in an autocrine fashion to promote the vicious cycle independently of the surrounding stroma. One of these factors is TGF- β , which is released by tumour epithelial cells, which along with VEGF secreted by both the epithelial and stromal cells can drive tumour progression (Stover *et al.*, 2007). BMPs have also been shown to be capable of autocrine signalling due to their regulated processing and secretion, as well as interactions with components of their microenvironment. BMP-2, -6, and -7 for example, have been shown to be involved in the cycle of osteoblastic lesion development in prostate cancer bone metastases (Clark and Torti, 2003).

No previous studies have investigated a possible role for GDF-9 in this vicious cycle of prostate cancer progression. Therefore, based on the established implications of their BMP relatives in carcinogenesis, as well as the success of previous projects carried out in the laboratory based on

BMPS in prostate cancer, this study aims to establish a role for GDF-9, by altering its expression levels in two prostate cancer cell lines. As GDF-9 has been shown to be processed and secreted in the ovary in a similar fashion to BMPs, and the laboratory has previously shown GDF-9 expression in both normal and malignant prostate epithelial cells (unpublished data), it was proposed that prostate epithelial cells could secrete GDF-9. Therefore, by altering the endogenous expression levels of GDF-9 in prostate cancer cell lines, it was hypothesised that GDF-9 secretion by prostate cancer cells would be modified accordingly, allowing the effect this would have on the aggressiveness of the prostate cancer cells to be analysed in the form of functional assays based on the associated biological properties of these cells.

In this study, GDF-9 expression plasmids and ribozyme transgenes were generated in order to over-express and/or silence GDF-9 expression in PC-3 cells, respectively. GDF-9 expression was further down-regulated in another prostate cancer cell line, DU-145 which expresses high levels of GDF-9. Following transfection with the plasmids, GDF-9 expression was verified using both mRNA and protein based methods. The remaining chapters in this study then aim to investigate the effect of altering GDF-9 expression on the biological properties of prostate cancer cells in order to elucidate the function of GDF-9 in this cancer.

3.2 Materials and methods

3.2.1 Materials

Polyclonal goat anti-GDF-9 antibody (SC-12244) was obtained from Santa Cruz Biotechnology (Santa Cruz, California, USA). All the primers used were synthesised and provided by Invitrogen (Paisley, UK). Primer sequences are located in Tables 2.2 to 2.4.

3.2.2 Cell lines

PC-3 and DU-145 were the cell lines used to investigate the effects of targeting GDF-9, and were cultured in DMEM-F12 medium as described in section 2.3.

3.2.3 Amplification of GDF-9 coding sequence

Amplification of the GDF-9 coding sequence was carried out using high fidelity and accurate PCR (LA-PCR) with the DuraScript™ RT-PCR kit (Sigma-Aldrich, Inc., Poole, Dorset, England, UK). Primers capable of amplifying the complete coding sequence of GDF-9 with or without stop codon were designed according to the GDF-9 mRNA sequence (Table 2.3) and cDNA from normal prostate tissue (previously shown to highly express GDF-9) was used as a template. LA-PCR was then carried out at the following conditions; 93°C for 2 minutes, followed by 42 cycles of 93°C for 20 seconds, 58°C for 20 seconds, and 68°C for 1.5 minutes, ending with a final extension period of 10 minutes at 68°C. After running and visualising the PCR product on a 0.8% agarose gel, the corresponding bands were extracted as described in section 2.4.6.

3.2.4 Generation of GDF-9 ribozyme transgenes

Hammerhead ribozymes targeting GDF-9 were designed using Zuker's RNA mFold programme (Zuker, 2003), based on the secondary structure of GDF-9 mRNA. Primers containing restriction sites were then generated (Table 2.4), and used for ribozyme synthesis by carrying out touch-down PCR at the following conditions; 94°C for 5 minutes, followed by 8 cycles at each annealing temperature (total of 48 cycles): 94°C for 10 seconds, 70°C, 65°C, 60°C, 57°C, 54°C, and 50°C for 15 seconds, 72°C for 20 seconds, and a final extension of 7 minutes at 72°C. Subsequently, the transgenes were run on a 2% agarose gel in order to verify their presence as well as size, before being cloned into the pEF6/His plasmid.

3.2.5 TOPO TA cloning of GDF-9 fragments or transgenes into a pEF6/His TOPO plasmid vector

Following verification, either the GDF-9 transgene or coding sequence was cloned into a pEF6/V5-His-TOPO plasmid (Invitrogen Inc., Paisley, UK), followed by transformation of constructed plasmid into *E.Coli*. Colonies of transformed *E.Coli*. were analysed by carrying out

RT-PCR, using the T7F primer coupled either with RbBMR and RbTPF primers in the case of the transgenes, or BGHR and a GDF-9 specific primer in the case of the coding sequence. The correct colonies were then amplified, and the plasmids extracted using the Sigma GenElute Plasmid MiniPrep Kit (Sigma-Aldrich, USA).

3.2.6 Prostate cancer cell transfection and generation of stable transfectants

Following plasmid verification using DNA electrophoresis, the plasmids were transfected into PC-3 and/or DU-145 cells by electroporation at 310V, and were put through selection with 5µg/ml blasticidin for up to two weeks. Empty plasmid vectors were also used to transfect the same cells in order to act as controls. Following selection, the surviving cells were grown to large numbers and verified for either GDF-9 knock-down or force expression, using RT-PCR, western blotting, and ICC. Full details of the cloning process are given in section 2.7.

3.2.7 RNA isolation, cDNA synthesis, and RT-PCR

RNA was isolated from the cells using the ABgene Total RNA Isolation Reagent (TRIR) kit (ABgene, Surrey, UK), and converted into cDNA by reverse transcription using the iScript™ cDNA Synthesis Kit (Bio-Rad Laboratories, California, USA), as described in section 2.4. This was then used as a template for RT-PCR, which was carried out at the following conditions; 94°C for 5 minutes, followed by 30 to 42 cycles of 94°C for 30 seconds, 56°C for 30 seconds, and 72°C for 1 minute, and a final extension of 7 minutes at 72°C. The products were run on an agarose gel and visualised using ethidium bromide.

3.2.8 Protein extraction, SDS-PAGE, and Western blot analysis

Protein was extracted following cell lysis, and was then quantified using the DC Protein Assay kit (BIO-RAD, USA). Following SDS-PAGE, the proteins were transferred onto nitrocellulose membranes which were blocked, and probed with the specific primary (anti-GDF-9 1:200) and the corresponding peroxidase-conjugated secondary antibodies (1:1000). All of the antibodies

used in this study are listed in Table 2.5. The protein bands were eventually visualised using the Supersignal™ West Dura system (Pierce Biotechnology, USA).

3.2.9 Immunoprecipitation

Following cell lysis, the lysates were treated with GDF-9 specific antibody. The resulting immune complexes were then collected using protein A and G beads attached to sepharose, which bind these complexes. The complexes then underwent precipitation by centrifugation, and were separated using SDS-PAGE and visualised by immuno-probing.

3.2.10 Immunocytochemistry

Immunocytochemical staining of GDF-9 in prostate cancer cells was carried out using specific primary antibody for the protein, followed by secondary antibody. For detailed ICC procedure refer to Section 2.5.9.

3.3 Results

3.3.1 Amplifying the coding sequence of GDF-9

In order to assess the effects of over-expressing human GDF-9 in prostate cancer cells, a mammalian expression construct had to be generated. For this purpose, the entire coding sequence of GDF-9 containing a 3' ATC stop codon was amplified using specially designed primers and the Extensor Long Range Durascript PCR master mix™, which contains a proof reading enzyme that ensures amplification of large products with minimum mistakes. Gradient PCR was then carried out in order to determine the optimal annealing temperature for each pair of primers. Finally, using prostate tissue cDNA as a template and an optimal annealing temperature of 58°C, a final PCR was carried out and the products were run on an agarose gel (Figure 3.1A). Products of the right size (1365bp) corresponding to the GDF-9 coding sequence were excised from the gel and extracted using the GelElute™ Gel Extraction Kit (Sigma-Aldrich, Inc., Poole, Dorset, England, UK). In order to verify that the band was

successfully extracted and that it indeed contained the GDF-9 sequence, it was run on an agarose gel alongside an RT-PCR product containing the excised band as a template with GDF-9 specific primers (Figure 3.1B).

3.3.2 TOPO TA cloning of GDF-9 into a pEF6 plasmid

Once the GDF-9 coding sequence was prepared, it was cloned into a pEF/His plasmid vector. After the newly constructed plasmid was transformed into TOP10 *E.Coli*, the colonies were analysed to ensure not only that they contained the GDF-9 plasmid, but that the plasmids had incorporated the fragment in the correct orientation.

This was done by carrying out several PCR reactions. The first pairs the plasmid specific T7F primer, and a reverse primer specific for GDF-9. As T7F is located about 90bp upstream of the GDF-9 insert, considering the insert is ligated in the correct orientation, the resulting product should be approximately 520bp in length. The following reaction pairs T7F with a forward primer specific for GDF-9 and hence if a product of around 300bp is detected for a colony following amplification, the insert is ligated in the wrong orientation and hence cannot be used. If a colony has products for both of the aforementioned reactions, then the colony contains a mixture of correctly and incorrectly aligned inserts. Finally, in order to determine whether the entire sequence of GDF-9 has been inserted without degradation, a concluding reaction containing both T7F and BGHR was carried out which generates a product size of around 1700bp. Figure 3.2A shows the analysis of various colonies using these three reactions.

The positive colonies (colony 1) were then further amplified, before being pelleted and undergoing plasmid extraction. Figure 3.2B shows the three aforementioned PCR reactions carried out on the extracted plasmid in order to ensure the correct plasmid was extracted. Furthermore, so as to determine plasmid integrity, the purified plasmid was run on an agarose gel as well as used as a template in an RT-PCR using GDF-9 specific primers to ensure correct insert orientation (Figure 3.3). This plasmid was then sent off to Geneservice Ltd. (Source

Bioscience, Cambridge, UK) for sequencing, in order to ultimately verify that the insert within the plasmid was genuinely GDF-9. The results showed a match between the sequence cloned into plasmid vector and the human GDF-9 precursor sequence (Figure 3.4).

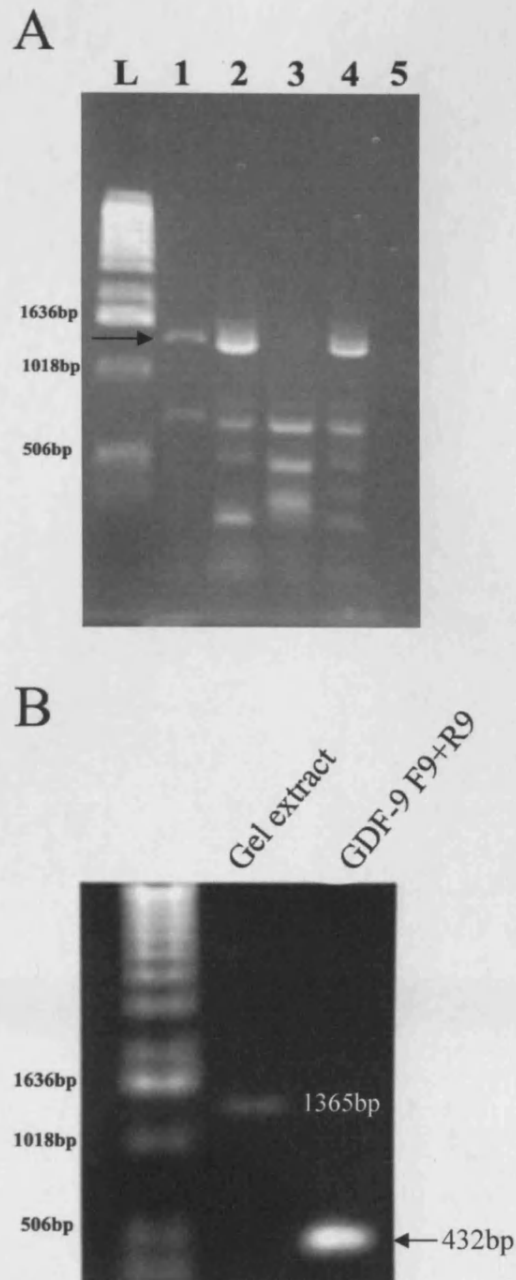


Figure 3.1: A. LA-PCR products of GDF-9 coding sequence visualised on an agarose gel. L is the DNA ladder and the annealing temperatures for LA-PCR in lane 1, 2, 3 and 4 are; 58°C 60°C, 62°C and 64°C, respectively. The correct size of extracted product is 1365bp as indicated by the arrow. B. Left lane: In order to confirm that the gel extract from the previous gel contained the GDF-9 coding sequence, it was run on an agarose gel, showing up as a band of the correct size at 1365bp. Right lane: This gel extract was further used as a template for a PCR using GDF-9 specific primers GDF-9 F9+R9, in order to ensure that the gel extract contained the correct GDF-9 sequence (product size 432bp).

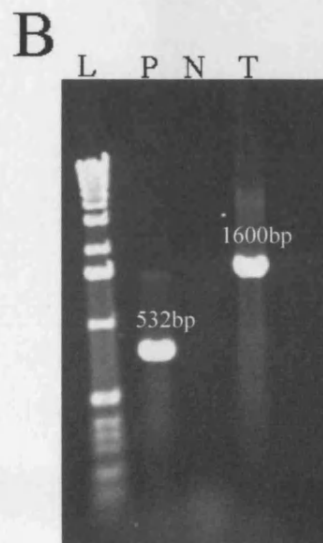
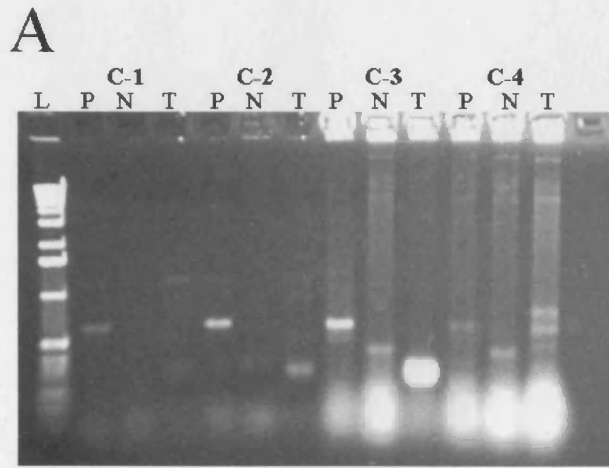


Figure 3.2: **A.** Agarose gel showing PCR of *E.coli* colony analysis. L is the ladder, P stands for correct orientation of GDF-9, where the product sized at 532bp is a result of a PCR carried out on each colony using a specific GDF-9 forward primer (F9) coupled with a plasmid specific reverse primer (BGHR). N stands for incorrect orientation where the product sized at around 300bp is a result of PCR reaction using a plasmid specific forward primer (T7F) and a GDF-9 specific forward primer as a reverse primer (F9). T stands for the PCR reaction using T7F and BGHR plasmid specific primers, which should amplify the entire MCS of the plasmid (1600bp). Colony 1 (C-1) is the only positive colony, the rest are mixed as they have the gene both in the correct (P) and incorrect (N) orientation. **B.** Following plasmid purification from colony C-1, the same PCR reactions were carried out as in 3.2A, but using the purified plasmid as the template, rather than the bacterial colony. As there is a 532bp band for the P reaction, no band for the N reaction, and a 1600bp band for the T reaction, this suggests that the purified plasmid contains the GDF-9 transgene in the correct orientation within the MCS of the plasmid.

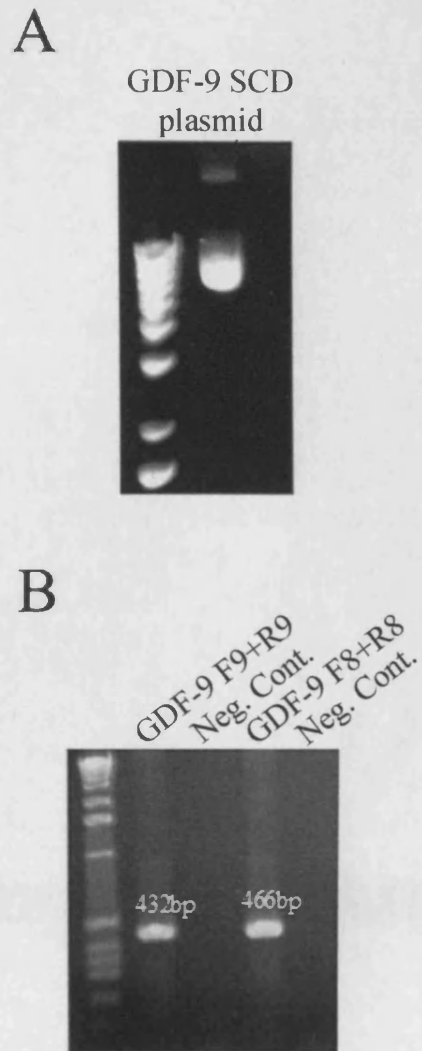


Figure 3.3: **A.** Following plasmid extraction and verification from colony C-1, the purified GDF-9 SCD S-3 plasmid was run and visualised on an agarose gel in order to demonstrate plasmid integrity. **B.** The plasmid was further used as a template for two PCR reactions using two different sets of GDF-9 specific primers; GDF-9 F9+R9 (432bp product), and GDF-9 F8+R8 (466bp product), in order to further confirm that the plasmid contained the correct sequence.

3.3.3 Generation of a GDF-9 ribozyme transgene

In order to silence the expression of GDF-9 in prostate cancer cells, ribozyme transgenes of GDF-9 were generated and cloned into a pEF6/His plasmid to allow for mammalian cell transfection. This would allow for comparison between the effects of knocking down, and over-expressing GDF-9 in prostate cancer cells. Figure 3.5 depicts the series of PCR actions carried out to construct a plasmid containing a GDF-9 ribozyme transgene. Based on the secondary structure of GDF-9, an appropriate targeting site for the ribozyme was first ascertained.

This was followed by ribozyme synthesis through touchdown PCR, and cloning into a pEF6/His plasmid. In order to verify correct orientation of the ribozyme transgene, primers RbTPF and RbBMR were paired with T7F, respectively. These primers were specific to the ribozyme transgenes.

If the transgene is correctly orientated, a PCR product of around 140bp (T7F promoter starts 90bp before insert and ribozyme sequence is around 50bp) should arise for the T7F+RbBMR reaction. However, if it is incorrectly orientated, a product of a similar size should appear for the T7F+RbTPF reaction. Following colony analysis, all those found to be positive for the transgenes underwent further amplification and finally, plasmid extraction. Colonies 2-9 and 3-10 were shown to have the highest levels of correctly orientated ribozyme transgene. The plasmids were then verified using DNA electrophoresis, in order to demonstrate successful isolation of correctly sized plasmids (Figure 3.5D).

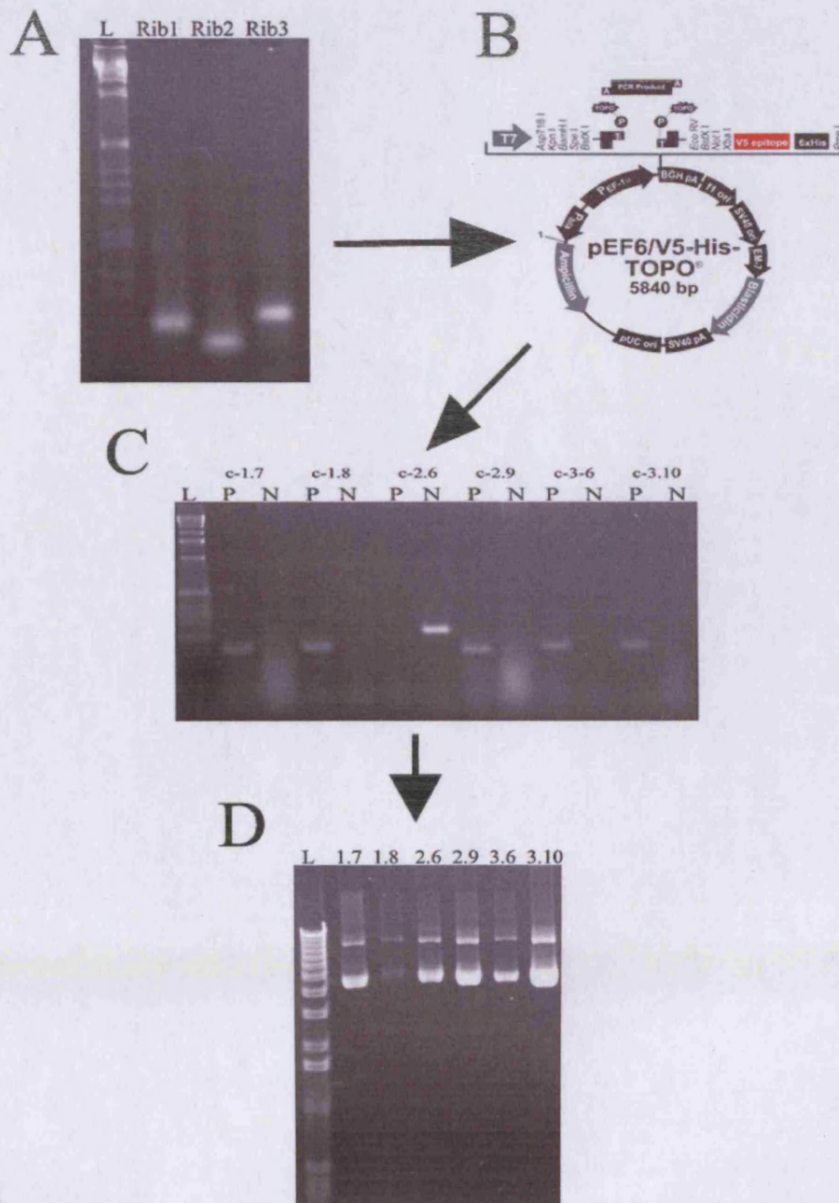


Figure 3.5: Ribozyme transgene synthesis. **A.** The ribozymes were generated using touchdown PCR and run on an agarose gel. **B.** The transgenes were cloned into a pEF6/V5-His-TOPO plasmid for mammalian cell transfection. **C.** After transformation into *E. coli* cells, the colonies were analysed using PCR in order to verify correct orientation of the transgene. L stands for ladder, P for correct orientation (140bp), which refers to a PCR reaction that uses a plasmid specific forward primer (T7F) and a ribozyme specific reverse primer (RbBMR), and N stands for incorrect orientation (140bp), where a plasmid specific forward primer (T7F) is coupled with a ribozyme forward primer as a reverse primer (RbTPF), in a PCR reaction. All of the colonies except for c-2.6 had the transgene in the correct orientation. **D.** The plasmids were extracted from the correct colonies and verified with DNA electrophoresis.

3.3.4 Expression of GDF-9 in prostate cell lines

The expression of GDF-9 was examined in seven prostate cell lines, including PC-3, DU-145, LNCaP, CAHPV-10, PZHPV7, PNT1A, and PNT2C2. The first four are prostate cancer cells. PC-3 is derived from bone metastatic lesions originating from prostate cancer, DU-145 from brain metastasis, LNCaP from lymphatic metastasis, and CAHPV-10 from a localised prostate carcinoma. The remaining three are immortalised prostatic epithelial cells. Figure 3.6A shows mRNA levels of GDF-9 in these seven prostate cell lines using RT-PCR. Relatively lower levels of GDF-9 were revealed in PC-3 cells compared to the other prostate cancer cells or epithelial cells. This was consistent with the protein expression of GDF-9 in these cells (Figure 3.6B). This not only demonstrated expression of GDF-9 in prostate cancer and epithelial cells, but also provided useful information for choosing cell lines and establishing *in vitro* cell models for subsequent experimental study.

3.3.5 Verification of GDF-9 forced expression in PC-3 cells

Following plasmid extraction, transfection into mammalian cell lines was possible. GDF-9 expression was found to be detectable in PC-3 cells, albeit at rather low levels (Figure 3.6). It was therefore chosen as the preferred cell line for GDF-9 over-expression. PC-3 cells were electroporated and hence transfected with the GDF-9 over-expression plasmid constructs (PC-3^{GDF-9 exp.}), as well as empty plasmid control, respectively (PC-3^{pEF}). The cells were transfected on two different occasions within a few hours of each other (PC-3^{GDF-9 exp.} 1 and 2), to ensure successful plasmid expression.

Following selection with blasticidin, RNA and protein were extracted from these cells as well as from PC-3^{WT} cells. Successful forced expression of GDF-9 was confirmed using PCR (Figure 3.7A), western blotting, and immunoprecipitation (Figure 3.7B). Both of these methods demonstrated considerably higher levels of GDF-9 expression in the PC-3^{GDF-9 exp.} cells, compared to both the WT and pEF controls. β -actin and GAPDH were used as loading controls

by acting to exhibit standardized levels of cDNA within the samples. ICC was also carried out to further confirm GDF-9 forced expression at the protein level. Stronger staining of GDF-9 was seen in the PC-3^{GDF-9 exp.} cells compared to both the WT and pEF controls ($p < 0.01$) (Figure 3.7D).

3.3.6 Verification of GDF-9 suppression with ribozyme transgenes in PC-3 and DU-145 cells

In order to obtain reliable results, ribozyme transgenes were used to silence the expression of GDF-9 in both PC-3 and DU-145 cells. As mentioned previously, PC-3 expresses GDF-9 at relatively low levels, but still sufficiently enough for its expression to be suppressed. DU-145 meanwhile was demonstrated to express relatively high levels of GDF-9, making it a suitable candidate for GDF-9 knock-down (Figure 3.6). Therefore, similarly to GDF-9 over-expression, both PC-3 and DU-145 cells were transfected with three separate GDF-9 targeting ribozymes, alongside an empty plasmid control, respectively.

Using PCR, expression of GDF-9 mRNA was reduced in the case of ribozyme 2 (PC-3^{GDF-9rib2}), and completely eliminated with ribozyme 3 (PC-3^{GDF-9rib3}), compared to the controls (PC-3^{WT} and PC-3^{pEF}) (Figure 3.7A). Ribozyme 1 was unsuccessful in repressing GDF-9 expression and hence is not shown. In DU-145 meanwhile, both ribozymes managed to completely eliminate GDF-9 expression (DU-145^{GDF-9rib2}, DU-145^{GDF-9rib3}) (Figure 3.7B). A similar reduction in GDF-9 protein levels was demonstrated in both PC-3 and DU-145 cells, when carrying out western blot analysis and ICC (Figure 3.8 and 3.9).

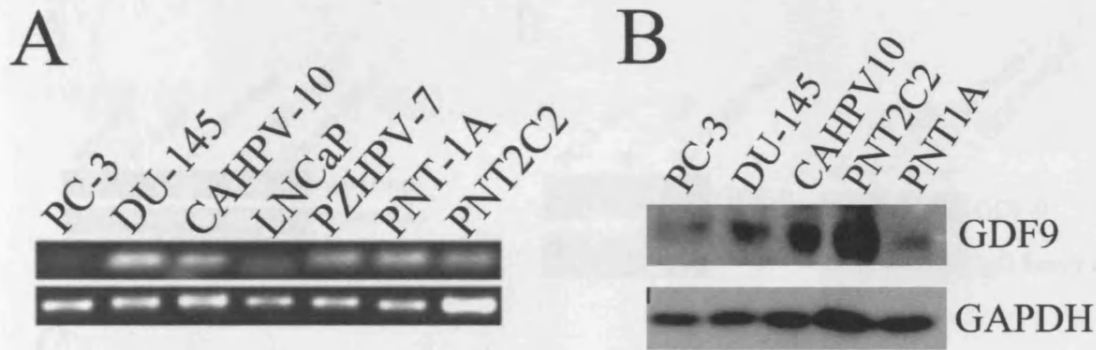


Figure 3.6: Screen of different prostate cell lines for GDF-9 expression using **A.** specific GDF-9 F9+R9 primers in a PCR to show mRNA levels and **B.** an anti-GDF-9 antibody in a western blot to show mature GDF-9 mature dimer protein levels (40kDa). Unfortunately, no protein for PZHPV-7 was available in the laboratory's stocks.

Figure 3.7: Verification of GDF-9 overexpression in PC-3 cells. **A.** PCR analysis showing consistently higher expression levels of GDF-9 in the three prostate cell lines compared to the controls. **B.** Left: Western blot (WB) analysis showing increased protein GDF-9 protein levels in PC-3^{GDF-9} cells compared to the controls. Right: Immunoprecipitation (IP) of GDF-9 (the IP results may be plausible due to the broad of the IgG heavy chain, below the band for GDF-9), with PC-3^{GDF-9} cells demonstrating significantly higher GDF-9 protein levels compared to the controls. The same anti-GDF-9 antibody used in the WB was used in IP. **C.** Immunocytochemical (ICC) analysis using 1A8 (anti-IGF1R) used the same anti-GDF-9 antibody as the WB and IP. The results were visualized with Hoechst staining before analysis with confocal microscopy. The results are similar to WB analysis, with the PC-3^{GDF-9} cells demonstrating significantly stronger staining for GDF-9 protein compared to the controls. The graph shows the quantification of the intensity of GDF-9 cytoplasmic staining in each sample.

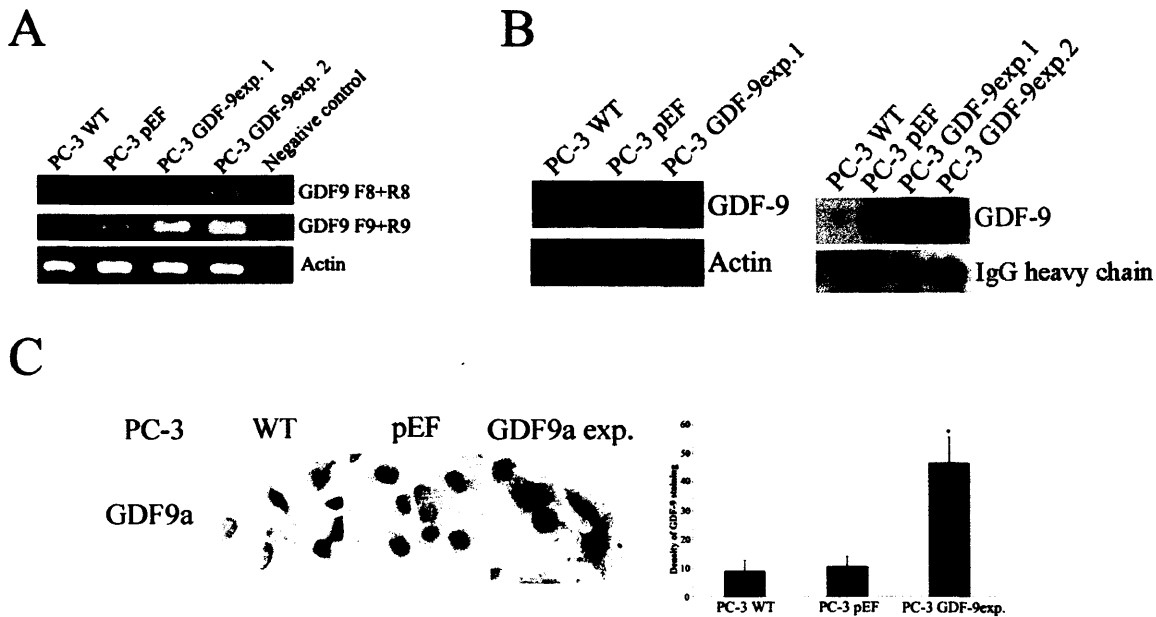


Figure 3.7: Verification of GDF-9 over-expression in PC-3 cells. **A.** PCR demonstrating considerably higher expression levels of GDF-9 in the three transfected cell lines compared to the controls. **B.** Left; Western blot (WB) analysis showing increased protein GDF-9 protein levels in PC-3^{GDF-9 exp.} cells compared to the controls. Right; Immunoprecipitation (IP) of GDF-9 (The IP results may be plausible due to the bands of the IgG heavy chain, below the band for GDF-9), with PC-3^{GDF-9exp.} cells demonstrating significantly higher GDF-9 protein levels compared to the controls. The same anti-GDF-9 antibody used in the WB was used in IP. **C.** Immunocytochemical (ICC) analysis (using DAB chromagen) uses the same anti-GDF-9 antibody as for WB and IP, and the nuclei were counterstained with Haemotoxylin, before analysis was carried out. The results are similar to WB analysis, with the PC-3^{GDF-9exp.} cells demonstrating significantly stronger staining for GDF-9 protein compared to the controls. The graph shows the quantification of the density of GDF-9 cytoplasmic staining in each sample.

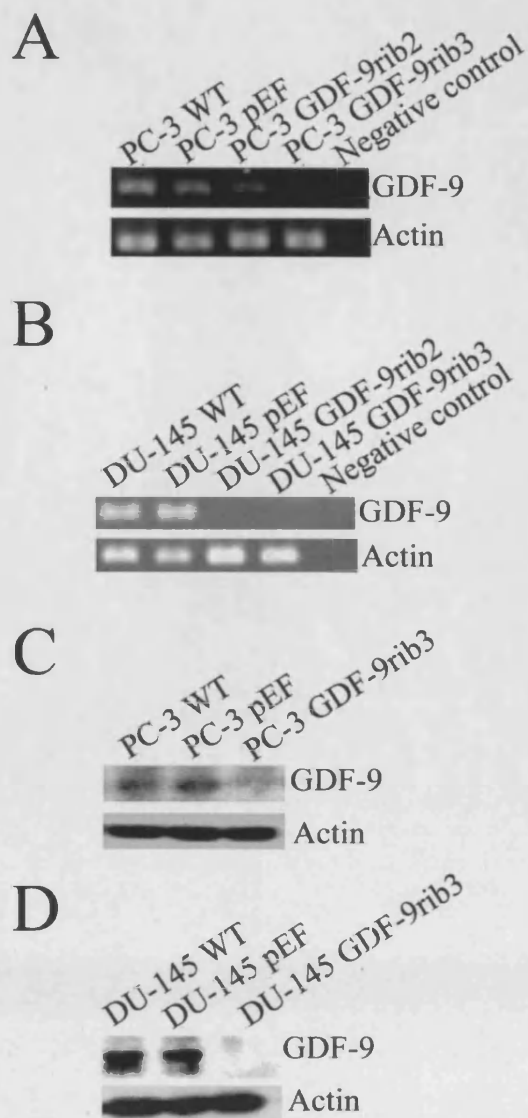
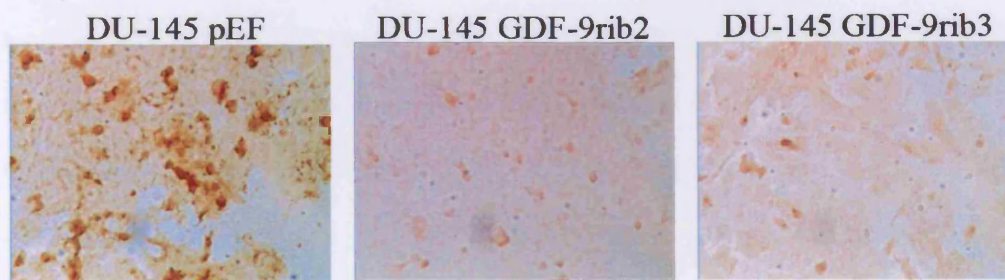


Figure 3.8: Verification of GDF-knockdown in PC-3 and DU-145 cells. **A.** PCR demonstrating considerably reduced expression levels of GDF-9 in the two transfected cell lines compared to the controls. **B.** PCR showing reduced GDF-9 levels in the two knock-down DU-145 cell lines compared to the controls. **C.** Western blot analysis demonstrating significantly reduced levels of mature GDF-9 protein in PC-3^{GDF-9rib3} cells compared to the controls. **D.** Western blot analysis demonstrating significantly reduced levels of GDF-9 protein in DU-145^{GDF-9rib3} cells compared to the controls.

A



B

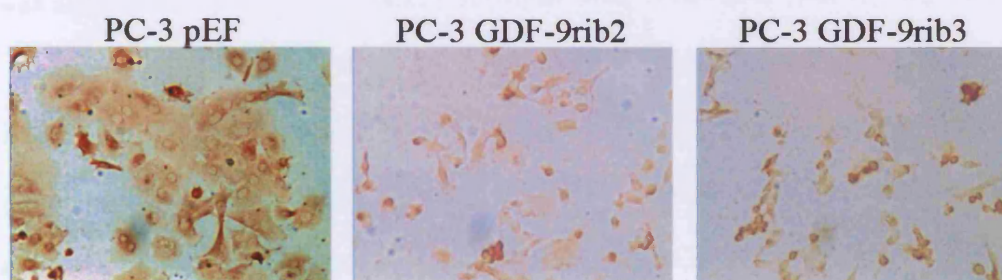


Figure 3.9: Verification of GDF-knockdown protein levels using ICC with an anti-GDF-9 antibody.

A. The PC-3^{GDF-9rib2} and PC-3^{GDF-9rib3} cells demonstrated considerably less staining for GDF-9 compared to the empty plasmid control. **B.** DU-145^{GDF-9rib2} and DU-145^{GDF-9rib3} demonstrated considerably weaker staining for GDF-9 compared to the control.

3.4 Discussion

GDF-9 is renowned for its role as an oocyte derived growth factor vital in follicular development and although its expression was initially thought to be exclusive to the ovaries, subsequent studies have shown a wider tissue distribution including breast cancer cells, and oral squamous carcinomas (Hanavadi *et al.*, 2007; Zhuang *et al.*, 2010). No previous study however, has investigated the expression levels of GDF-9 in the normal or malignant prostate, even though significant roles have been demonstrated for many of its BMP relatives in prostate cancer. The apparent importance of BMPs in prostate cancer lies in their osteoinductive properties and regulatory roles during bone development and remodelling. Bone metastasis is a common complication of many cancers, including that of the prostate with 90% of patients with advanced prostate cancer developing skeletal metastasis (Bubendorf *et al.*, 2000).

BMPs have been demonstrated to stimulate osteoblast differentiation, and if enriched in bone matrix can facilitate bone metastasis development. Prostate cancer cells that acquire genetic phenotypes that allow them to up-regulate expression of bone specific cytokines including BMPs, can then adapt to the bone microenvironment with more ease and establish bone metastases. Expression of BMP-6, BMP-7, and GDF-15, for example is highly elevated in bone metastases originating from prostate cancer suggesting they aid in the metastatic process (Thomas *et al.*, 1998; Dai *et al.*, 2004). Although the osteogenic properties of GDF-9 have not been investigated, it is possible that like its relatives it may have some function in prostate cancer progression and metastasis.

In this current study, we firstly demonstrated the presence of GDF-9 expression in seven prostatic cell lines. The cell lines used here have extensively been used as models for *in vitro* studies on prostate cancer. PC-3, DU-145, and LNCaP are aggressive prostatic carcinomas derived from metastatic sites of the bone, brain, and lymph nodes, respectively. CA-HPV-10 meanwhile represents a less aggressive prostatic adenocarcinoma cell line immortalised with

HPV-18. PZ-HPV-7, PNT-1A, and PNT2-C2 meanwhile, are immortalised prostatic epithelial cell lines. According to the mRNA levels of GDF-9, its expression appears to be higher in the less aggressive prostatic carcinoma cell lines, along with those of the prostatic epithelium. DU-145 is the only exception, as it expresses relatively high levels of GDF-9. PC-3, the main cell line used in this study meanwhile, expresses relatively low levels of GDF-9. The protein levels show a similar trend. Unfortunately, due to inappropriate freezing down of cell stocks, it was not possible to culture the prostatic epithelial cell lines in order to determine whether altering the expression of GDF-9 would have an effect on these cells.

This screening process also aided in the determination of which cell lines to use for the remainder of the study. As previously mentioned, like other BMPs, GDF-9 is secreted from cells in order for it to bind to its receptors on the cell surface. Therefore, in order to investigate the effect of GDF-9 on the biological functions of prostate cancer cells, we altered GDF-9 expression in PC-3 and DU-145 cells. Initially, a mammalian expression vector was constructed containing the entire GDF-9 coding region. This coding region contained a stop codon in order to allow for production and secretion of native GDF-9 protein, without any expression of plasmid by-products downstream from the insert.

As PC-3 cells express low levels of GDF-9, it was chosen as the cell line to transfect in order to determine the effects of GDF-9 over-expression in this cell line. GDF-9 over-expression was verified at both the mRNA and protein level using PCR and western blot analysis, amongst others. It was hypothesised that over-expression of GDF-9 would increase its secretion by PC-3 cells and hence allow it to compete for receptor binding with other BMP ligands already present in the cells, thereby promoting GDF-9 downstream signalling and its associated effects. As endogenous expression levels of GDF-9 in DU-145 cells were already high, over-expression was not attempted as it was assumed that this would have no added effect.

In addition, we generated hammerhead ribozyme transgenes in order to silence GDF-9 expression in both PC-3 and DU-145 cells which both express the protein, DU-145 at a high level. The ribozymes proved to be successful as they efficiently down-regulated expression of GDF-9 both at the mRNA and protein level. This would allow for determination of whether the effect over-expressing GDF-9 in PC-3 is genuinely due to its alteration, or whether other factors are having an influence. These tools of genetic manipulation aid in the generation of useful *in vitro* models allowing for the investigation of the impact a single molecule has in a cell line. Subsequent functional assays carried out in the rest of this study, are based on both the GDF-9 knock-out and over-expressing cells.

Chapter 4

Effects of targeting GDF-9 on the proliferative, adhesive, invasive, and motile capacity of prostate cancer cells

4.1 Introduction:

A cancer cell relies on varying vital biological processes with which to establish itself in its environment, and go on to further survive and progress. The most important of these include changes in cell growth, adhesive and invasive capacity, motility, and migration. Cancer cells can influence these processes in several ways, most significantly by altering the expression of molecules that play key roles in controlling these cellular traits. In the case of growth for example, a cancer cell might have reduced expression of cell cycle inhibitors, and up-regulated levels of growth promoters so as to allow it to continue through the cell cycle undeterred and at a greater capacity, despite having several mutations which would under normal circumstances induce growth arrest.

As previously mentioned, BMPs play an important role in the progression of prostate cancer and have been shown to influence all of these aforementioned cellular processes. Indeed, the majority of the BMPs appear to have reduced expression in prostate cancer cells, implying a tumour inhibitory role for these proteins. Expression of BMP-9 and -10 for example, is decreased or absent in prostate cancer tissues, especially in those of a higher grade. In addition, when BMP-9 and BMP-10 were force-expressed in these prostate cancer cells respectively, there was an inhibition of cell growth, adhesion, invasion, and migration, suggesting that both BMPs function as tumour suppressors in prostate cancer (Ye *et al.*, 2008). Based on this and other studies, this laboratory has recently shown that expression of GDF-9, a family member of BMP-10, has reduced expression in breast cancer cells and when force-expressed in these cells, reduces their invasive capacity, suggesting that GDF-9 has an inhibitory effect on breast cancer progression (Hanavadi *et al.*, 2007).

Chapter 3 describes how the expression of GDF-9 in prostate cancer cells was altered in two different ways; force-expression using a mammalian expression plasmid vector, and knock-down using ribozyme transgenes. This following chapter now goes on to investigate the effect, if any, that these changes in GDF-9 expression have on these cells. The stable transfected cells,

both the GDF-9 over-expressing and GDF-9 knock-down cells, were used in various *in vitro* cell function assays including; growth, adhesion, invasion, and motility. These assays are a well established and simple method of investigating the biological properties of cancer cells *in vitro*, providing a basic hypothesis with which to continue onwards in *in vivo* models. Following on from its supposed role in breast cancer, these function assays were carried out in order to determine what role, if any GDF-9 plays on these cellular processes, and in the progression of prostate cancer.

4.2 Materials and methods

4.2.1 Cell lines

PC-3 and DU-145 prostate cancer cell lines were used in this current chapter, including the wild-type control, empty plasmid control and transfected cell lines. Cells were continuously maintained in DMEM media with 10% FBS and antibiotics. The stable transfected cells were maintained in the same media but with 0.5 μ g/ml blasticidin.

4.2.2 *In vitro* growth assay

The cells were seeded into four 96 well plates, and incubated for 24 hours, 48 hours, 72 hours and 120 hours respectively, as described in section 2.9.3. Following incubation, the cells were stained with crystal violet before the absorbance was measured in order to determine cell number.

4.2.3 *In vitro* adhesion assay

The cells were seeded into a 96 well plate coated with matrigel as described in section 2.9.1. The cells were left to adhere for a period of 40 minutes, before being stained with crystal violet, and the cells counted.

4.2.4 *In vitro* invasion assay

The cells were seeded into transwell inserts with 8µm pores coated with 50 µg matrigel, in a 24 well plate and were incubated for a period of 4 days. Following incubation, the cells which had migrated through the matrigel to the other side of the insert were stained with crystal violet and counted.

4.2.5 *In vitro* motility assay

The protocol followed is described by Rosen and Jiang (Rosen *et al.*, 1990; Jiang *et al.*, 1995b). The cells were incubated with cytodex-2 beads and left over night, by which time the cells will have adhered to the surface of the beads. The beads carrying the cells were then transferred into a 24 well plate, where the cells move from the beads onto the surface of the culture plate. These cells were then stained with crystal violet, and counted.

4.2.6 ECIS

The cells were seeded into 8W10E electrical arrays and placed in an incubator with connection to ECIS™ machine (model 1600R) allowing the cells to adhere to the gold electrodes within the arrays, causing a change in resistance. The software was set up so that resistance to the current flow was measured at 400Hz.

4.3 Results

4.3.1 Effect of altering GDF-9 expression on prostate cancer cell growth

The force-expressing and knock-down transfected prostate cancer cells were used in an *in vitro* growth assay alongside their wild-type and empty plasmid controls. Cell growth was significantly promoted in the GDF-9 over-expressing cells compared to the two controls (Figure 4.1A). The cell growth at 120 hours was significantly greater in the PC-3^{GDF-9exp.} (1922.9%±79.1%) compared to both PC-3^{WT} (958.6%±90.6%) and PC-3^{pEF} (1297.5%±82.0%), $p < 0.001$ versus both controls. Meanwhile, the opposite effect was seen in the GDF-9 knock-down cells. A significant reduction in growth was seen at 120 hours in both PC-3^{GDF-9rib2} (631.1%±11.7%) and PC-3^{GDF-9rib3} (435.7%±95.1%) cells compared to the PC-3^{WT} (989.4%±35.4%) and PC-3^{pEF} (929.3%±24.9%) controls, $p < 0.001$ for both PC-3^{GDF-9rib2} and PC-3^{GDF-9rib3}, compared to both controls (Figure 4.1B).

The same effect was demonstrated with the DU-145 GDF-9 knock-down cells where both DU-145^{GDF-9rib2} (481.5%±26.7%) and DU-145^{GDF-9rib3} (380.4%±55.0%) had significantly reduced proliferative capacity compared to DU-145^{WT} (703.8%±40.1%) and DU-145^{pEF} (641.5%±55.0%), $p = 0.001$ for DU-145^{GDF-9rib2} versus DU-145^{pEF}, and $p < 0.001$ versus DU-145^{WT}, whereas $p < 0.001$ for DU-145^{GDF-9rib3} compared to both controls (Figure 4.2). In both the cell lines, GDF-9 ribozyme three seemed to have the most pronounced effect on growth, suggesting that it may have lower levels of GDF-9 expression as is demonstrated in chapter 3.

4.3.2 Effect of GDF-9 on prostate cancer cell adhesion

The cells were further analysed for their adhesive capacity in an *in vitro* matrigel adhesion assay. The GDF-9 over-expressing PC-3 cells had a significantly enhanced adhesive capacity compared to its controls. Significantly more PC-3^{GDF-9exp.} cells (70.5±12.1) had adhered to the matrigel compared to both the PC-3^{WT} (46.0±10.9) and PC-3^{pEF} (32.7±6.71) controls, $p = 0.004$ in

comparison with PC-3^{WT}, and $p < 0.001$ compared to PC-3^{pEF} (Figure 4.3A). In the case of the GDF-9 knock-down cells, the opposite effect was seen in that lower numbers of both PC-3^{GDF-9^{rib2}} (28.7±3.01) and PC-3^{GDF-9^{rib3}} (31.1±7.10) cells had adhered to the matrigel compared to PC-3^{WT} (47.4±16.1) and PC-3^{pEF} (60.3±9.85), $p = 0.001$ for PC-3^{GDF-9^{rib3}} versus PC-3^{WT}, and $p < 0.001$ versus PC-3^{pEF} (Figure 4.3B). Meanwhile, $p < 0.001$ for PC-3^{GDF-9^{rib2}} versus both controls.

This effect was less pronounced in DU-145 cells, where DU-145^{GDF-9^{rib2}} (70.4±9.74) and DU-145^{GDF-9^{rib3}} (64.3±8.70) cells demonstrated marginally reduced numbers of adherent cells compared to both DU-145^{WT} (88.44±11.0) and DU-145^{pEF} (80.2±8.30), $p = 0.013$ for DU-145^{GDF-9^{rib2}} versus DU-145^{WT}, and $p = 0.09$ versus DU-145^{pEF}, whereas $p = 0.009$ for DU-145^{GDF-9^{rib3}} versus DU-145^{WT}, and $p = 0.0018$ versus DU-145^{pEF} (Figure 4.4).

4.3.3 Effect of GDF-9 on prostate cancer cell invasiveness

The cells were further analysed for their invasive capacity with the use of an *in vitro* invasion assay. The GDF-9 over-expressing PC-3 cells demonstrated a significant promotion in their invasiveness. A greater number of PC-3^{GDF-9^{exp.}} cells (58.3±9.69) had invaded through the matrigel to the other side of the insert compared to PC-3^{WT} (21.2±4.36) and PC-3^{pEF} (32.7±4.37), $p < 0.001$ for PC-3^{GDF-9^{exp.}} compared to both controls (Figure 4.5A). However, knocking down GDF-9 in PC-3 cells; PC-3^{GDF-9^{rib2}} (30.0±4.36) and PC-3^{GDF-9^{rib3}} (27.3±5.51), no change was seen on the invasive capacity of the cells compared to the PC-3^{WT} (26.3±4.16) and PC-3^{pEF} (28.7±3.51) controls, $p = 0.70$ and $p = 0.74$ for PC-3^{GDF-9^{rib2}} and PC-3^{GDF-9^{rib3}} compared to PC-3^{pEF} and $p = 0.35$ and $p = 0.81$ compared to PC-3^{WT}, respectively (Figure 4.5B).

In the case of DU-145^{GDF-9^{rib2}} (49.0±6.08) however, a marginal reduction in the invasive capacity of the cells was demonstrated compared to the DU-145^{WT} (56.3±6.66) and DU-145^{pEF} (59.7±1.53) controls, $p = 0.23$ compared to DU-145^{WT} and $p = 0.04$ compared to DU-145^{pEF}. DU-145^{GDF-9^{rib3}} (60.3±8.50) cells however showed no difference in invasiveness, $p = 0.56$ compared to DU-145^{WT} and $p = 0.90$ compared to DU-145^{pEF} (Figure 4.6).

4.3.4 Effect of GDF-9 on prostate cancer cell motility

The cells were additionally evaluated for their motility using a cytodex-2 bead motility assay. Over-expression of GDF-9 demonstrated enhanced cell motility compared to the controls. A significantly larger proportion of PC-3^{GDF-9exp.} cells (99.2±16.1) had migrated from the beads onto the surface of the culture plate in comparison with the PC-3^{WT} (64.1±10.0) and PC-3^{pEF} (76.6±2.22) controls, p=0.049 versus PC-3^{WT} and p=0.073 versus PC-3^{pEF} (Figure 4.7A). Although the effect is only statistically significant when comparing to the WT control, the trend remains evident.

In contrast, the two GDF-9 knock-down cells demonstrated reduced cell motility compared to these two controls, with PC-3^{GDF-9rib2} (57.2±2.22) and PC-3^{GDF-9rib3} (29.7±2.00) both having smaller numbers of migrating cells compared to PC-3^{WT} and PC-3^{pEF}, p<0.001 for PC-3^{pEF} versus both knock-down cells, and p=0.320 for PC-3^{WT} versus PC-3^{GDF-9rib2}, and 0.028 versus PC-3^{GDF-9rib3} (Figure 4.7B). In the case of DU-145 cells however, although a slight reduction in the number of motile cells was observed in both the DU-145^{GDF-9rib2} (30.7±5.98) and DU-145^{GDF-9rib3} (29.3±5.73) cells compared to the DU-145^{WT} (33.7±6.10) and DU-145^{pEF} (35.8±4.88) controls, the data was not found to be significant, p=0.41 and p=0.13 for DU-145^{GDF-9rib2} and DU-145^{GDF-9rib3} compared to DU-145^{WT} and p=0.13 and p=0.06 compared to DU-145^{pEF}, respectively (Figure 4.8).

These results suggest that GDF-9 over-expression has a more significant effect on the invasiveness of prostate cancer cells. This is plausible, as when a gene is over-expressed in a cell, it competes with other ligands for receptor binding, allowing it to dominate the resulting phenotype of that cell, whereas if a gene is knocked-down the cell compensates for this loss by allowing other genes to take over, making its loss unnoticeable, unless the gene is a main player in a certain trait.

4.3.5 The effect of GDF-9 on the electrical resistance of prostate cancer cells

Electrical cellular impedance sensing (ECIS) is an electrical method used to monitor cellular processes such as cell attachment, spreading, migration, and micromotion. The process entails a monolayer of cells being grown on a small gold film electrode deposited on the bottom of an electrical array. With the culture medium acting as an electrolyte, a current is applied to the system. As the cells begin to spread on the electrode, this current is impeded resulting in changes in both the impedance and resistance, which are measurable. The greater the resistance to the current flow, the more cells there are on the electrode, allowing for cell attachment to be quantifiably analysed.

PC-3^{GDF-9exp.} cells (1.19 ± 0.035) demonstrated an increased resistance compared to both PC-3^{WT} (1.03 ± 0.033) and PC-3^{pEF} (1.01 ± 0.019), $p=0.036$ compared to PC-3^{WT}, and $p=0.0051$ compared to PC-3^{pEF}. This increase in electrical resistance correlates with increased cellular attachment. This result follows on from that demonstrated in the conventional adhesion assay as described in section 4.3.2, suggesting that GDF-9 has a promotional effect on the adhesive capacity of PC-3 cells. In the case of DU-145 cells, there was no obvious reduction in the electrical resistance of DU-145^{GDF-9rib2} (1.23 ± 0.12) and DU-145^{GDF-9rib3} (1.35 ± 0.067) compared to DU-145^{WT} (1.37 ± 0.23) and DU-145^{pEF} (1.50 ± 0.35), $p=0.510$ for DU-145^{GDF-9rib2} cells compared to DU-145^{pEF} and $p=0.606$ compared to DU-145^{WT}. For DU-145^{GDF-9rib3} $p=0.943$ versus DU-145^{WT} and $p=0.53$ versus DU-145^{pEF}.

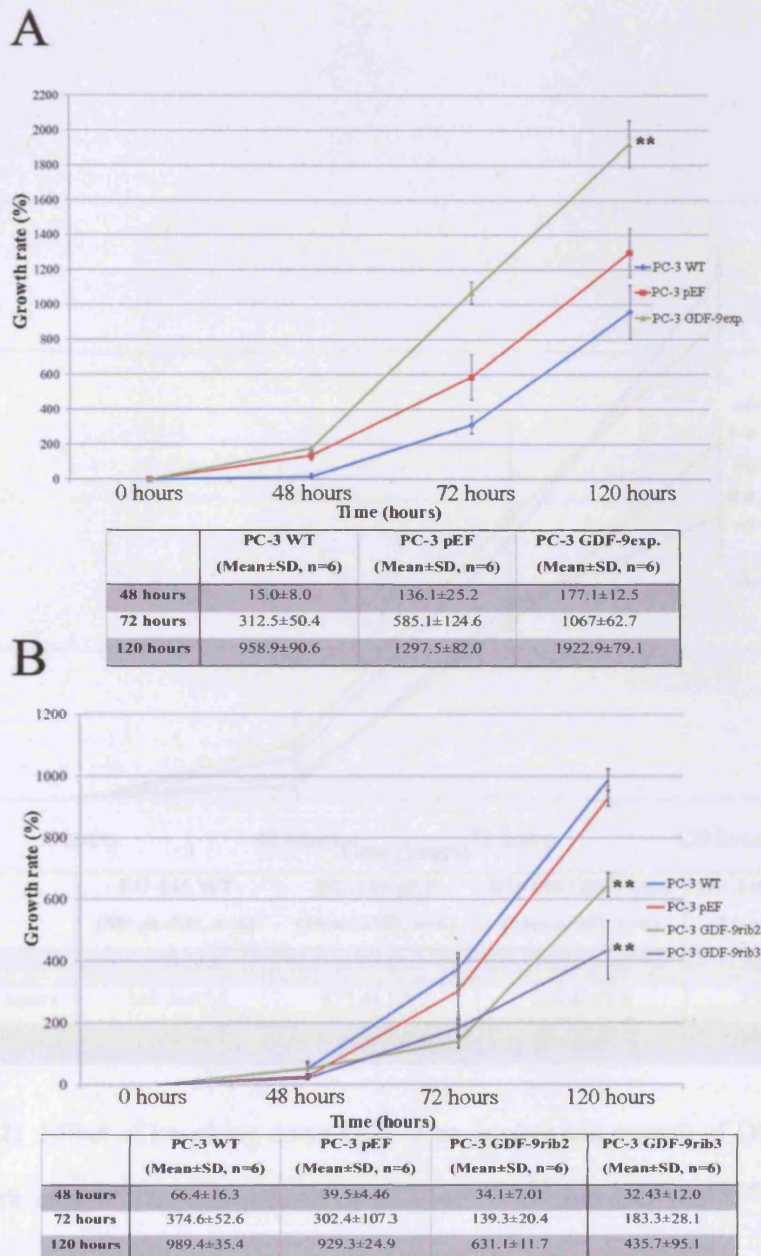
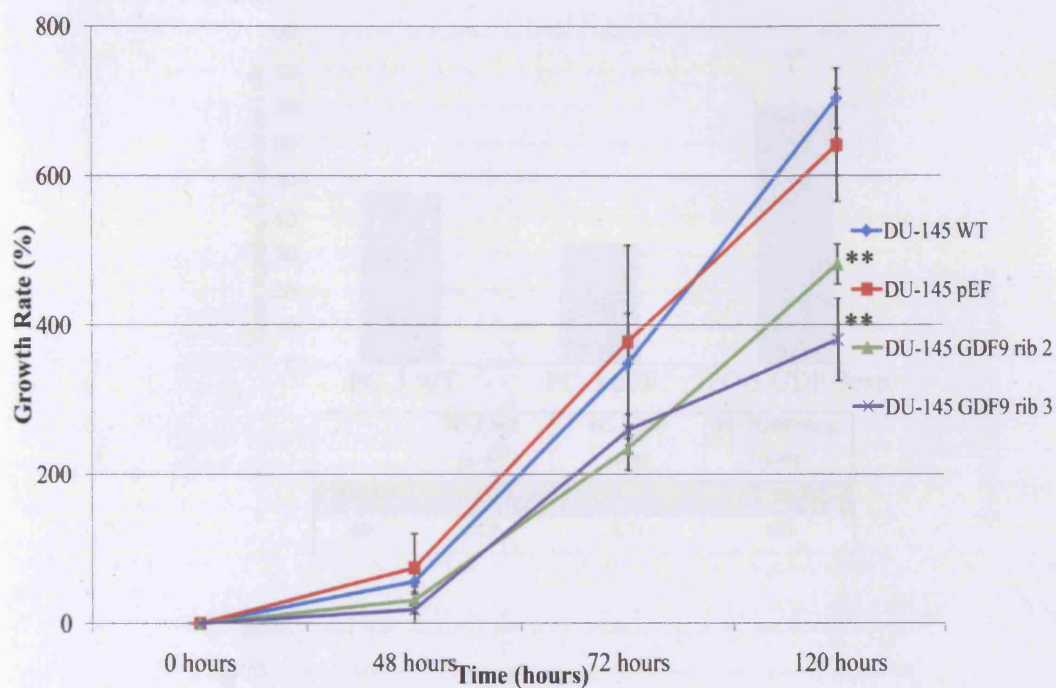


Figure 4.1: Effect of GDF-9 on *in vitro* cell growth of PC-3 cells using the cell growth assay.

A. The cell growth of PC-3^{GDF-9 exp.} cells was significantly increased in comparison to the two controls, ** $p < 0.001$ for GDF-9exp. cells compared to both controls. **B.** The cell growth of PC-3^{GDF-9rib2} and PC-3^{GDF-9rib3} was significantly reduced compared to both controls, ** $p = 0.001$ for PC-3^{GDF-9rib3} versus PC-3^{WT}, and ** $p < 0.001$ versus PC-3^{pEF}. Meanwhile, ** $p < 0.001$ for PC-3^{GDF-9rib2} versus both controls. Data shown is representative of at least 3 independent repeats. Error bars represent standard deviation. The 0 hour time point refers to an over night incubation before the cells were stained, and the absorbance used as a baseline in order to normalise the data.



	DU-145 WT (Mean±SD, n=6)	DU-145 pEF (Mean±SD, n=6)	DU-145 GDF-9rib2 (Mean±SD, n=6)	DU-145 GDF-9rib2 (Mean±SD, n=6)
48 hours	55.9±14.0	74.1±45.8	31.03±18.0	18.4±20.8
72 hours	348.3±67.5	377.4±129.2	234.4±28.8	259.5±20.7
120 hours	703.8±40.1	641.5±75.4	481.5±26.7	380.4±55.0

Figure 4.2: Effect of knocking down GDF-9 on *in vitro* cell growth of DU-145 cells using the cell growth assay. The cell growth of DU-145^{GDF-9rib2} and DU-145^{GDF-9rib3} was significantly reduced compared to both controls, **p=0.001 for DU-145^{GDF-9rib2} versus DU-145^{pEF}, and **p<0.001 versus DU-145^{WT}, whereas **p<0.001 for DU-145^{GDF-9rib3} compared to both the controls. Data shown is representative of at least 3 independent repeats. Error bars represent standard deviation. The 0 hour time point refers to an over night incubation before the cells were stained, and the absorbance used as a baseline in order to normalise the data. Due to the high endogenous levels of DU-145, no over-expression studies were attempted in this cell line, and hence only functional assays on DU-145 knock-down cells were carried out.

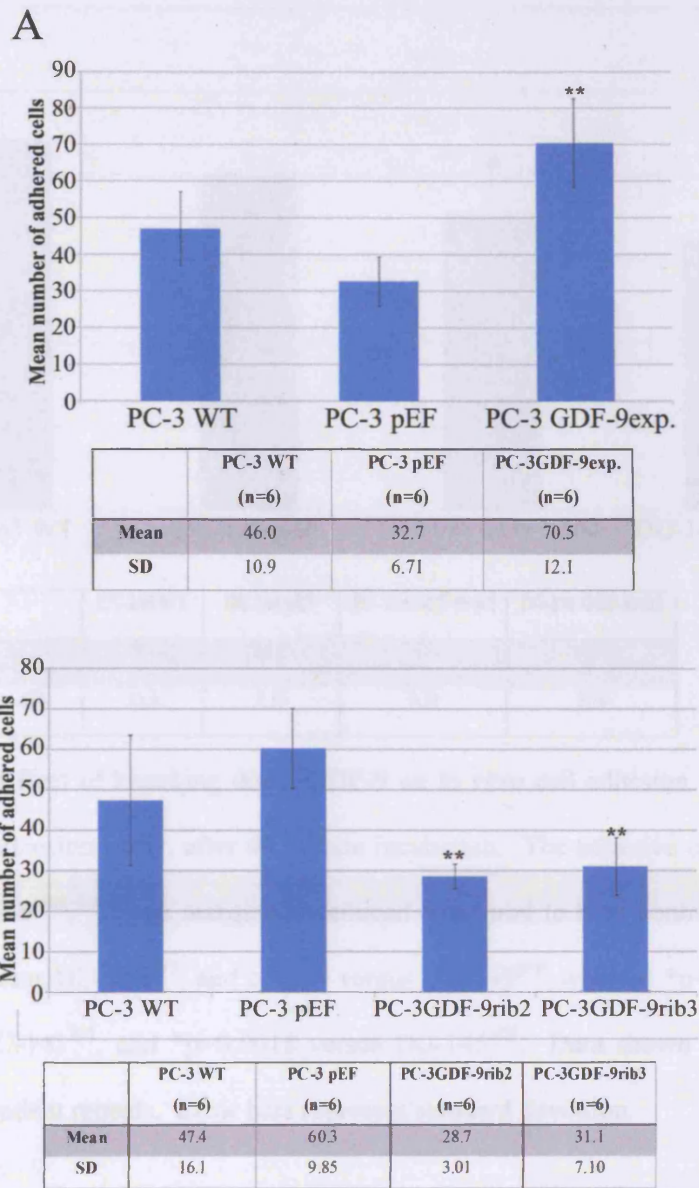
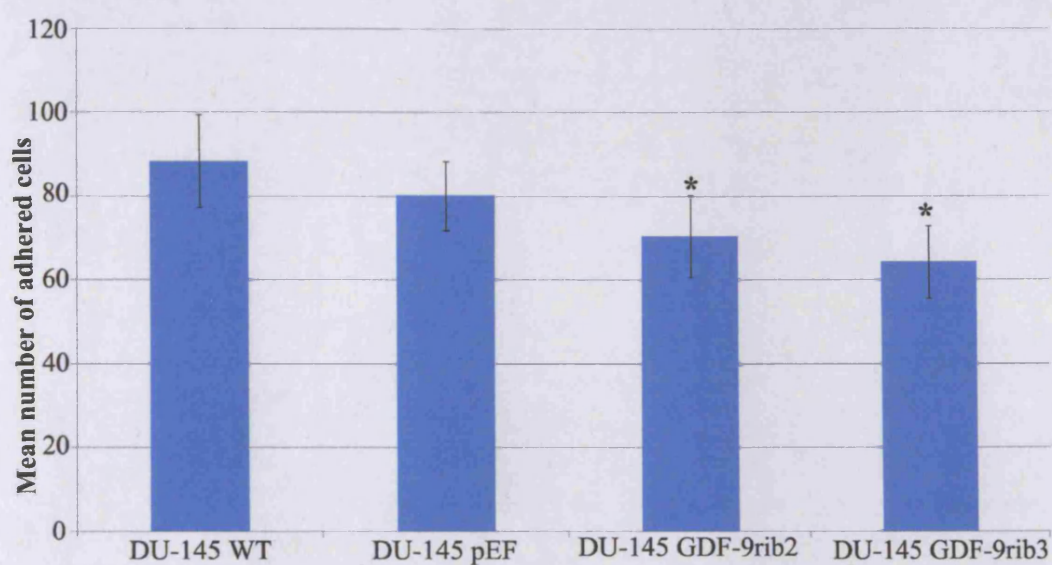


Figure 4.3: Effect of GDF-9 on *in vitro* cell adhesion of PC-3 cells after 40 minute incubation. **A.** The adhesive capacity of PC-3^{GDF-9 exp.} cells was significantly increased in comparison to the two controls, ** $p < 0.001$ for GDF-9exp. cells compared to both controls. **B.** Adhesive capacity of PC-3^{GDF-9rib2} and PC-3^{GDF-9rib3} was significantly reduced compared to both controls, ** $p = 0.001$ for PC-3^{GDF-9rib3} versus PC-3^{WT}, and $p < 0.001$ versus PC-3^{pEF}. Meanwhile, ** $p < 0.001$ for PC-3^{GDF-9rib2} versus both controls. Data shown is representative of at least 3 independent repeats. Error bars represent standard deviation.



	DU-145 WT	DU-145 pEF	DU-145 GDF-9rib2	DU-145 GDF-9rib3
Mean	88.44	80.17	70.44	64.33
SD	11.0	8.30	9.74	8.70

Figure 4.4: Effect of knocking down GDF-9 on *in vitro* cell adhesion of DU-145 cells using the matrigel adhesion assay, after 40 minute incubation. The adhesive capacity of DU-145^{GDF-9rib2} and DU-145^{GDF-9rib3} was marginally reduced compared to both controls, *p=0.013 for DU-145^{GDF-9rib2} versus DU-145^{WT}, and p=0.09 versus DU-145^{pEF}, whereas *p=0.009 for DU-145^{GDF-9rib3} versus DU-145^{WT}, and *p=0.0018 versus DU-145^{pEF}. Data shown is representative of at least 3 independent repeats. Error bars represent standard deviation.

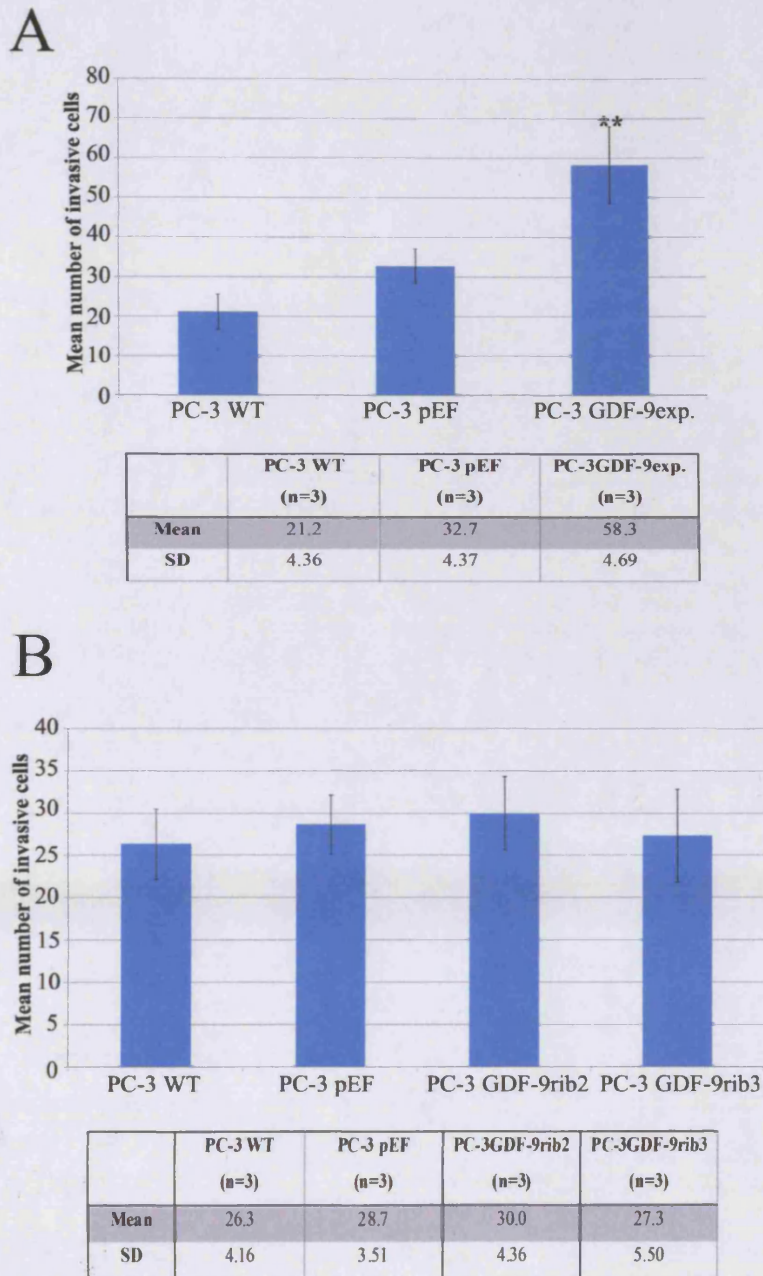
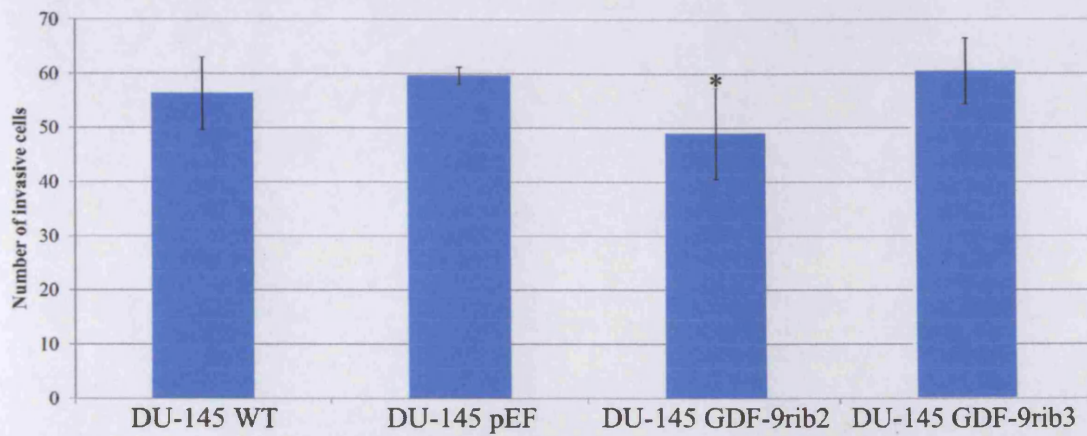


Figure 4.5: Effect of GDF-9 on *in vitro* cell invasiveness of PC-3 cells using the *in vitro* transwell invasion assay, following 4 days incubation. **A.** The invasive capacity of PC-3^{GDF-9 exp.} cells was significantly increased in comparison to the two controls, ** $p < 0.001$ for GDF-9exp cells compared to both controls. **B.** There was no significant difference in the invasive capacity of PC-3^{GDF-9rib2} and PC-3^{GDF-9rib3} cells compared to the controls, $p = 0.70$ and $p = 0.74$ for PC-3^{GDF-9rib2} and PC-3^{GDF-9rib3} cells compared to PC-3^{pEF}, meanwhile $p = 0.35$ and $p = 0.81$ compared to PC-3^{WT}, respectively. Data shown is representative of at least 3 independent repeats. Error bars represent standard deviation.



	DU-145 WT (n=3)	DU-145 pEF (n=3)	DU-145 GDF-9rib2 (n=3)	DU-145 GDF-9rib3 (n=3)
Mean	56.3	59.7	49.0	60.3
SD	6.66	1.53	6.08	8.50

Figure 4.6: Effect of GDF-9 on *in vitro* cell invasiveness of DU-145 cells using the transwell invasion assay, following 4 days incubation. There was a slight decrease in the invasive capacity of DU-145^{GDF-9rib2} compared to the controls, *p=0.04 compared to DU-145^{pEF} and p=0.23 compared to DU-145^{WT}. In the case of DU-145^{GDF-9rib3} however, no difference was seen in the invasive capacity compared to the controls, p=0.56 compared to DU-145^{WT} and p=0.90 compared DU-145^{pEF}. Data shown is representative of at least 3 independent repeats. Error bars represent standard deviation.

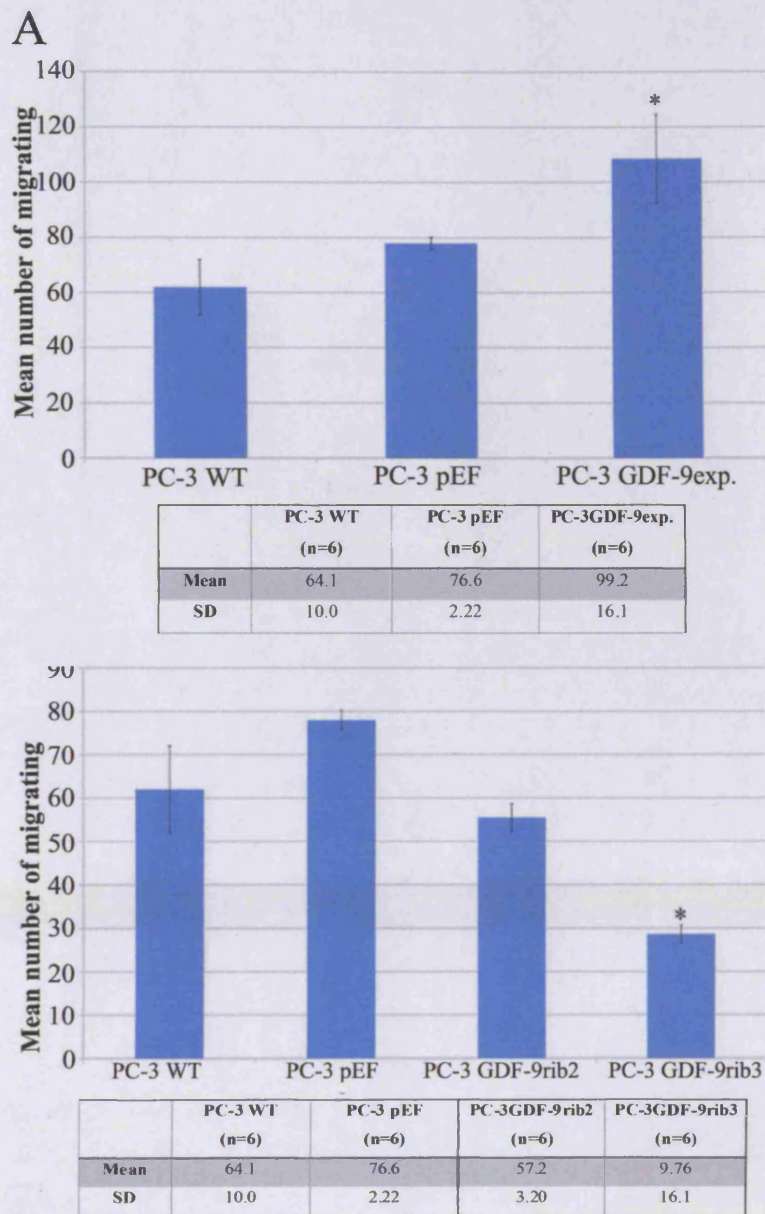


Figure 4.7: Effect of GDF-9 on *in vitro* cell motility of PC-3 cells using the cytodex-2 bead motility assay. **A.** The motility of PC-3^{GDF-9 exp.} cells was significantly increased in comparison to the two controls, * $p=0.049$ versus PC-3^{WT} and * $p=0.073$ versus PC-3^{pEF}. **B.** Both GDF-9 knock-down cells showed reduced motility compared to the controls, ** $p<0.001$ for PC-3^{pEF} versus both knock-down cells, and $p=0.320$ for PC-3^{WT} versus PC-3^{GDF-9rib2}, and * $p=0.028$ versus PC-3^{GDF-9rib3}. Data shown is representative of at least 3 independent repeats. Error bars represent standard deviation.

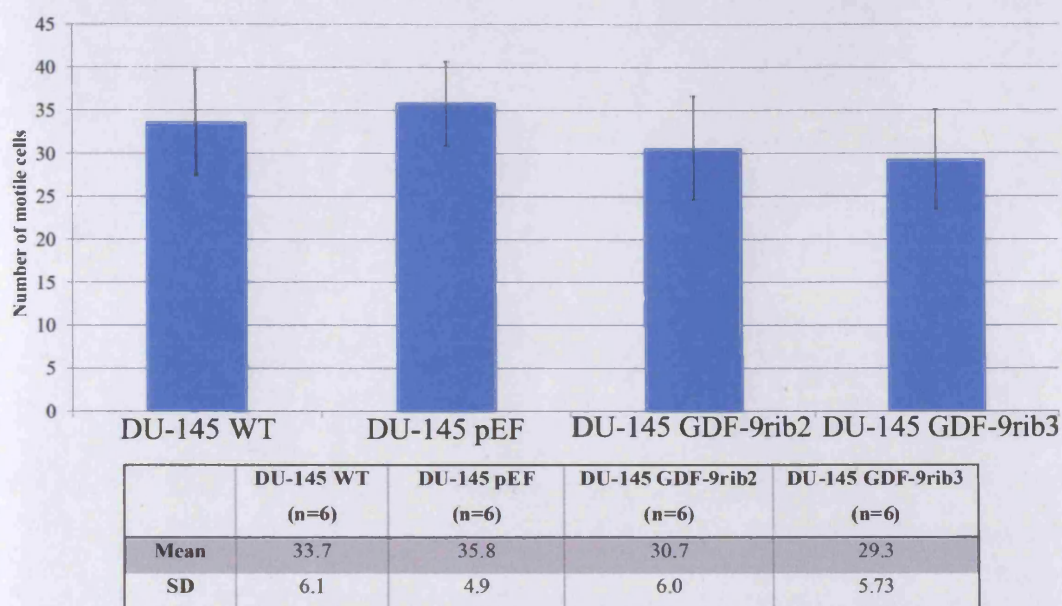
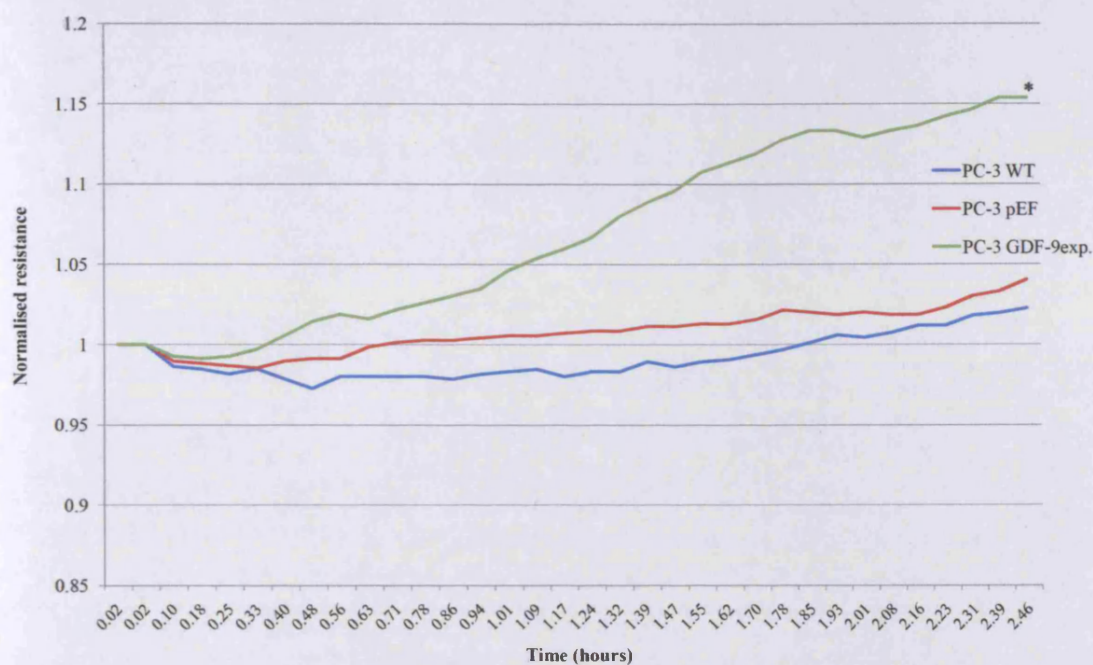
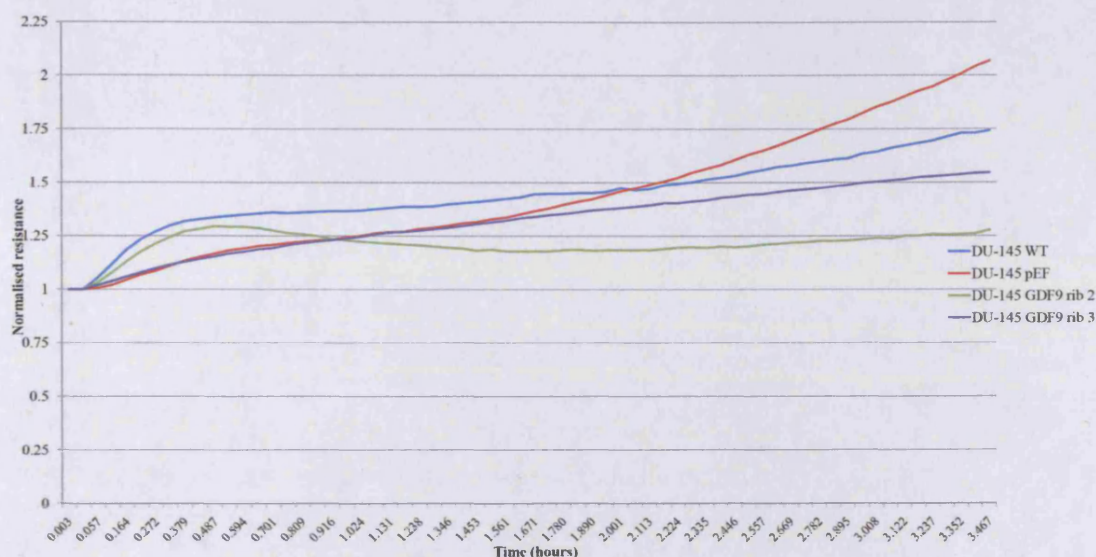


Figure 4.8: Effect of GDF-9 on the cell motility of DU-145 cells using the cytodex-2 bead motility assay. The motility of DU-145^{GDF-9rib2} and DU-145^{GDF-9rib3} cells was slightly decreased in comparison to the two controls, $p=0.510$ for DU-145^{GDF-9rib2} compared to DU-145^{pEF}, and $p=0.606$ compared to DU-145^{WT}. For DU-145^{GDF-9rib3}, $p=0.943$ versus DU-145^{WT} and $p=0.53$ versus DU-145^{pEF}. Data shown is representative of at least 3 independent repeats. Error bars represent standard deviation.



	PC-3 WT (n=6)	PC-3 pEF (n=6)	PC-3 GDF-9exp. (n=6)
Mean	1.03	1.01	1.19
SD	0.03	0.02	0.04

Figure 4.9: A. Effect of GDF-9 on electrical resistance of PC-3 cells using ECIS analysis, at a 2 hour time point. The electrical resistance of PC-3^{GDF-9 exp.} cells was significantly increased in comparison to the two controls, * $p=0.036$ for GDF-9exp. cells compared to PC-3^{WT}, and $p=0.0051$ compared to PC-3^{pEF}. Graph shown is representative of at least 3 independent repeats. Table shows the means and standard error of means of the normalised resistance values obtained from these independent repeats.



	DU-145 WT (n=6)	DU-145 pEF (n=6)	DU-145 GDF-9rib2 (n=6)	DU-145 GDF-9rib3 (n=6)
Mean	1.37	1.50	1.23	1.35
SD	0.23	0.35	0.12	0.07

Figure 4.10: A. Effect of GDF-9 on electrical resistance of DU-145 using ECIS analysis, at 2 hour time point. The electrical resistance of DU-145^{GDF-9rib2} and DU-145^{GDF-9rib3} cells was marginally decreased in comparison to the two controls, $p=0.510$ for DU-145^{GDF-9rib2} cells compared to DU-145^{pEF}, and $p=0.606$ compared to DU-145^{WT}. For DU-145^{GDF-9rib3} $p=0.943$ versus DU-145^{WT} and $p=0.53$ versus DU-145^{pEF}. Graph shown is representative of at least 3 independent repeats. Table shows the means and standard error of means of the normalised resistance values obtained from these independent repeats

4.4 Discussion

GDF-9 is a well established follicular growth factor that has been shown to be vital during early follicular development. More specifically, GDF-9 is expressed throughout follicular development, and in the mammalian oocyte induces granulosa cell proliferation, pre-antral follicle growth, and cumulus cell expansion, partly by the inhibition of FSH-induced cAMP production and steroidogenesis. In addition, when human follicles are treated with GDF-9, it results in a greater percentage of viable cells in organ culture, suggesting it also plays a role in follicular survival (Vitt *et al.*, 2000).

The role of GDF-9 in cancer however, remains more elusive. The laboratory has previously shown that GDF-9 has an inhibitory effect on the invasiveness of breast cancer cells (Hanavadi *et al.*, 2007). A similar tumour suppressing role was observed in a human lung adenocarcinoma cell line with silenced mutant P53, where GDF-9 was upregulated (Ma *et al.*, 2006). In contrast, another study demonstrated that GDF-9 expression is up-regulated in an oral squamous carcinoma cell line, suggesting that it may act as a pro-tumourogenic factor in oral cancers (Zhuang *et al.*, 2010).

Much research has been carried out on BMPs and their function in cancer, which has made it clear that they play important roles during cancer progression and metastasis. In addition, due to their key role as regulators in the bone, it's not a far stretch to suggest that they may be vital in bone metastasis, especially that of prostate cancer. This current study now shows that by altering the expression of endogenous GDF-9 in prostate cancer cells, that it is capable of promoting cell growth, adhesion, and motility, suggesting a pro-tumourogenic role for GDF-9 in prostate cancer.

When GDF-9 was over-expressed in PC-3 cells, they demonstrated an increase in cell growth adhesion, motility, and invasion *in vitro*, compared to the two controls. This effect was inhibited when GDF-9 was knocked-down in these cells using ribozyme transgenes, which showed a

reduction in all of the previously mentioned cellular properties. Although to a lesser extent, DU-145 cells transfected with GDF-9 ribozymes exhibited with a reduction in their proliferative and adhesive capacity, but no change in their motile and invasive capacity. The disparity seen between the DU-145 and PC-3 cell lines in response to GDF-9 may be due to variability in their expression profiles. For example, DU-145 has lower expression levels of BMPR-II, the type-II receptor for GDF-9, and lower levels of BMP antagonists Noggin and Follistatin, which may hinder GDF-9 signalling. Furthermore, unlike PC-3 cells that grow in a scattered fashion as independent cells, DU-145 cells grow in tight epithelial colonies, which may explain why GDF-9 was incapable of promoting their motility and invasion (Wells *et al.*, 2005).

The promotion of cell growth in PC-3 and DU-145 cells by GDF-9 is in line with its role during folliculogenesis where it greatly promotes the proliferation and survival of granulosa cells (Vitt *et al.*, 2000). In addition, GDF-9 was shown to up-regulate levels of cyclooxygenase-2 (COX-2), an enzyme that's been implicated in carcinogenesis due to its association with VEGF (Elvin *et al.*, 1999). This, along with its expression being shown to be up-regulated in an oral cancer cell line, GDF-9 may also act as a survival factor in oral squamous cell carcinomas (Zhuang *et al.*, 2010).

In addition, the increase in the motile and invasive capacity of PC-3^{GDF-9exp.} cells has also been demonstrated in keloids, a type of scar caused by excessive fibrous tissue, that unlike hypertrophic scars extends beyond the margins of the scar. GDF-9 expression was significantly higher in fibroblasts of the peripheral invasive area of the scar, compared to the central area. Furthermore, its expression was also higher in keloid rather than hypertrophic scars and normal skin, suggesting that GDF-9 aids in the invasive phenotype of this condition (Gao *et al.*, 2010).

In the case of other BMPs in prostate cancer, their roles seem to greatly vary, and depend on a large range of different factors. For example, it has previously been shown that BMP-9 and -10 can inhibit the growth, adhesion, invasion, and migration of prostate cancer cells (Ye *et al.*,

2008; Ye *et al.*, 2009). In contrast, BMP-2 and -7 have been demonstrated to promote the migration and invasion of osteoblastic prostate cancer cells LAPC-4 and LAPC-9, while both BMP-2 and -6 had a similar effect on the invasive capacity of C4-2B and LNCaP prostate cancer cell lines (Dai *et al.*, 2005; Feeley *et al.*, 2005).

However, it is often difficult to confirm the effects that BMPs have on cells as the same BMP can have contrasting effects in different cell types and environments due to factors including the supplement of FBS, presence or absence of androgen, receptor type, and source of BMPs and their antagonists. BMP-2 for example, signals via BMPR-IA to promote the growth of LNCaP cells but can also signal via BMPR-IB to inhibit growth of these cells (Ide *et al.*, 1997). Meanwhile, BMP-7 has been shown to induce epithelial-mesenchymal transition and thereby invasiveness of PC-3 cells, despite a different study claiming that BMP-7 had no effect on the migration and invasion of these cells (Yang *et al.*, 2005; Feeley *et al.*, 2006).

This study suggests that GDF-9 is an important regulator of the biological properties of prostate cancer cells, one which has a positive effect on the progression of prostate cancer. In order to further determine the role of GDF-9 in these processes, the following chapters analyse the effect of exogenous GDF-9 on these cells, and also investigate and highlight mechanisms to explain how GDF-9 goes about exerting its effects.

Chapter 5
Generating recombinant human
GDF-9

5.1 Introduction:

In the previous chapter, the effects of altering the expression of GDF-9 on the biological properties of prostate cancer cells was investigated, and showed a pronounced effect on cell growth and adhesive capacity. These methods however, only act as a means of investigating the effects of endogenous GDF-9 in these cells, and in addition may inadvertently affect other genes within the cell. One other alternative therefore, is to treat the cells with exogenous protein, allowing it to bind to their cell surface receptors and induce downstream signalling. As this protein is made in the laboratory, its structure and quality are known, and as it is not incorporated into the genome of the cell, it theoretically should not have an effect on other genes. Therefore, in order to determine whether treating the cells with exogenous GDF-9 protein would provide similar results to those seen when altering endogenous levels of GDF-9, a strategy for production of recombinant human GDF-9 (rh-GDF-9) protein was considered.

In recent years, the use of recombinant proteins in the laboratory has increased greatly, due to the simplicity and convenience of their use. Initially, the GDF-9 coding sequence was cloned into a pEF/V5-His-TOPO plasmid vector, similarly to GDF-9 forced-expression, except that in this case, the primers used to generate the coding sequence did not contain a stop codon. As the pEF/V5-His-TOPO plasmid vector has a six histidine tag downstream of the cloning site, this allowed for the recombinant protein to be expressed with a histidine tag on one end of it, which would eventually allow for easier and more effective protein purification. The plasmid was then transfected into 3T3 cells, a popular cell line for recombinant protein production, and grown to large numbers in order to allow for protein purification.

As recombinant GDF-9 was not commercially available and the downstream signalling pathway of the protein unclear, recombinant GDF-9 was produced in order to further elucidate its functions and signalling in prostate cancer cells. This chapter therefore focuses on the procedure of recombinant protein production, and its use in cell function assays and time course

treatments, necessary for finally determining a possible role for GDF-9 in prostate cancer progression.

5.2 Materials and methods

5.2.1 Materials

The same antibodies as were used in chapter 3 were used to carry out studies in this current chapter. 3T3 cells were regularly maintained in DMEM-F12 medium supplemented with 10% foetal bovine serum, antibiotics, and 0.5µg/ml blasticidin for those in maintenance.

5.2.2 Amplifying GDF-9 coding sequence

Using primers which amplify the human GDF-9 coding sequence without a stop codon (Table 2.3), a high-fidelity PCR was carried out following the same procedure as described in section 3.2.3, before the corresponding band was excised from the gel following DNA electrophoresis, and purified.

5.2.3 Cloning of GDF-9 coding sequence into pEF/His TOPO plasmid vector

The GDF-9 coding sequence was cloned into the pEF/His TOPO plasmid vector in the same way as was described in sections 3.2.5 and 2.7, using the same primers for verification. The resulting plasmids were then purified as previously described.

5.2.4 Transfection

3T3 cells were then transfected with the GDF-9 and empty plasmid respectively, using electroporation at 290V. The electroporated cells were then put under blasticidin selection as described in section 2.7.

5.2.5 Verification of GDF-9 over-expression in 3T3 cells using RT-PCR and western blotting

Both RNA and protein were extracted from the stable transfectant cells and were used in either western blot analysis or RT-PCR in order to confirm GDF-9 over-expression at both the mRNA and protein level. These methods were carried out as previously described in sections 2.4 and 2.5.

5.2.6 Purifying recombinant human GDF-9 (rh-GDF-9)

Following verification, the transfected 3T3 cells were grown to large quantities and both conditioned media and cell lysate were used for recombinant protein purification using affinity chromatography as described in section 2.8.

5.2.7 Desaltification of purified rh-GDF-9

Following purification, the imidazole used during protein elution was removed using Vivaspin centrifugal concentrators as described in section 2.8.4.

5.2.8 Rh-GDF-9 quantification

The purified recombinant protein was run alongside a serial dilution of BSA standard on a 10% SDS-PAGE gel and stained using Coomassie blue. The bands were then photographed and the concentration of the recombinant protein quantified as described in section 2.8.5.

5.2.9 *In vitro* cell growth assay

The cells were seeded into a single 96 well plate as described in section 2.9.3. Triplicates of each cell line were incubated with 10% FBS containing DMEM media either with or without 20ng/ml of rh-GDF-9. Due to the high value and small volume of the rh-GDF-9 available, instead of analysing growth at days 1, 3, and 5, which would require multiple treatments with rh-GDF-9, growth was instead examined at day 4 alone. The cells were therefore fixed

following 4 days incubation, and stained with crystal violet before the absorbance was measured in order to determine the effect of rh-GDF-9 on cell growth.

5.2.10 *In vitro* adhesion assay

The cells were seeded into a 96 well plate coated with matrigel as described in section 2.9.1. Triplicates of each cell line were incubated either with or without 20ng/ml of rh-GDF-9, for a period of 40 minutes, before being stained with crystal violet, and the cells counted.

5.2.11 *In vitro* invasion assay

The cells were seeded into a 24 well plate containing transwell inserts with 8µm pores coated with 50 µg matrigel, and were incubated with or without 20ng/ml rh-GDF-9 in serum free media for a period of 4 days. Following incubation, the cells which had migrated through the matrigel to the other side of the insert were stained with crystal violet and counted.

5.2.12 *In vitro* motility assay

The cells were incubated with cytodex-2 beads and left over night with or without 20ng/ml rh-GDF-9 in serum free media, by which time the cells will have adhered to the surface of the beads. The beads carrying the cells were then transferred into a 24 well plate, where the cells move from the beads onto the surface of the culture plate. These cells were then stained with crystal violet, and counted.

5.3 Results

5.3.1 Amplification of GDF-9 NSCD coding sequence

In contrast to the construction of a GDF-9 expression plasmid as was done in chapter 3, in order to generate rh-GDF-9, the primers used to amplify the GDF-9 coding sequence were designed to lack a stop codon (GDF-9 NSCD). Once cloned into the pEF/V5-His-TOPO plasmid, the

deleted stop codon enables the recombinant protein to be expressed with a histidine tag, which allows for more effective protein purification during affinity chromatography. The resulting products of the LA-PCR and the subsequently purified coding sequence are shown in Figure 5.1.

5.3.2 Cloning GDF-9 NSCD into pEF/V5-His-TOPO plasmid vector

Following purification and verification of the GDF-9 coding sequence, it was cloned into a pEF/V5-His-TOPO plasmid vector and transformed into *E.coli*. The resulting colonies were then analysed for GDF-9 using PCR with T7F and BGHR primers, as described in section 3.3.2. Figure 5.2 shows colony analysis for GDF-9 using these primers. The colonies found to be positive for GDF-9 expression were then selected and used for plasmid extraction. The resulting purified plasmids were run on a gel, and then used as a template for an RT-PCR using GDF-9 specific primers (Figure 5.3A and B).

5.3.3 Verification of GDF-9 over-expression in 3T3 cells

The constructed GDF-9 plasmid vectors were then transfected into 3T3 cells alongside the empty plasmid control. Following several weeks of selection with blasticidin, the expression levels of GDF-9 both at the mRNA and protein level were assessed in the transfected cells. Figure 5.4A is a PCR demonstrating increased mRNA levels of GDF-9 in 3T3^{GDF-9exp.} cells compared to the 3T3^{WT} and 3T3^{pEF} controls. Figure 5.4B meanwhile, is a western blot demonstrating increased levels of the histidine protein (corresponding to recombinant GDF-9 protein with the histidine tag) and GDF-9, in both 3T3^{GDF-9N4exp.} and 3T3^{GDF-9N8 exp.} compared to the empty plasmid control. These successfully confirmed GDF-9 over-expressing 3T3 cells were then used for further experiments.

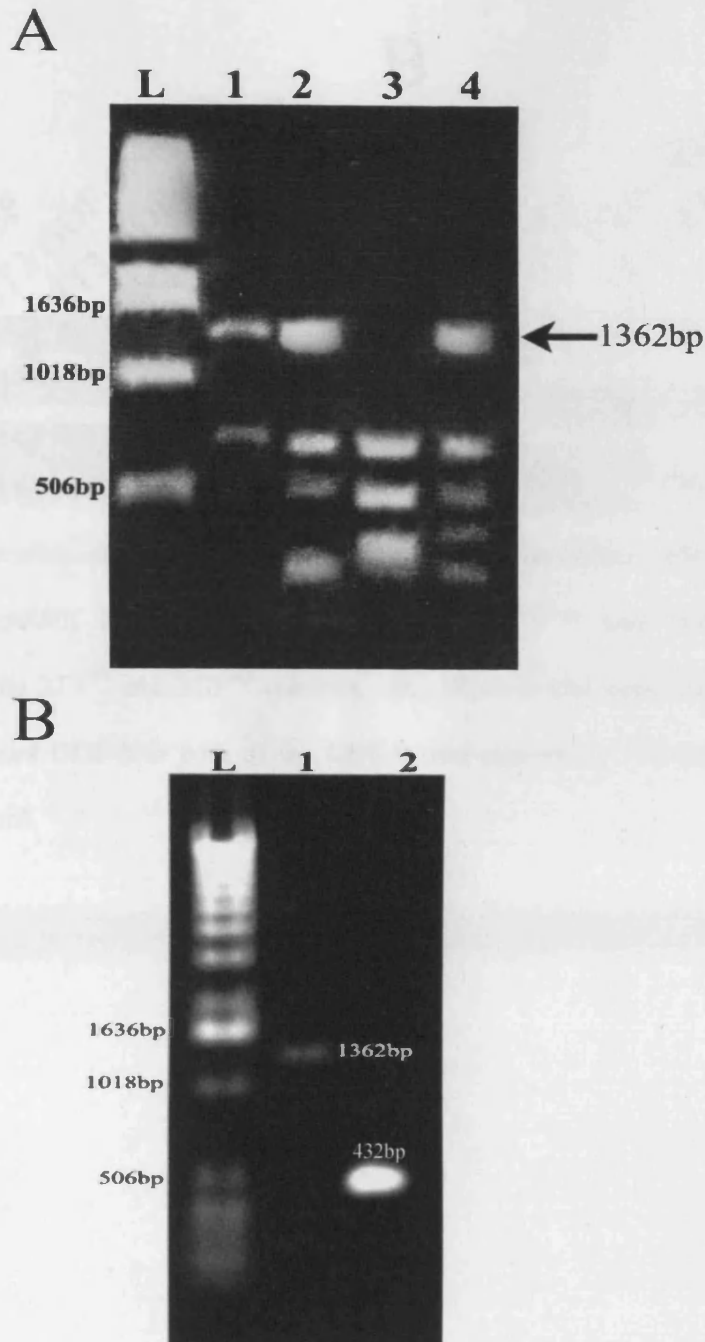


Figure 5.1: **A.** An LA-PCR was carried out in order to amplify the GDF-9 NSCD coding sequence, the products of which were run on an agarose gel. L is the DNA ladder, and the annealing temperatures used during the LA-PCR in lanes 1, 2, 3, and 4 are; 58°C, 60°C, 62°C, and 64°C, respectively. The correct size of the GDF-9 NSCD product is 1362bp as indicated by the arrow. **B.** This 1362bp band was then excised from the gel above, and run in lane 1 of the agarose gel below it. Lane 2 shows a PCR carried out using this gel extract as a template with GDF-9 specific primers GDF-9 F9+R9 (432bp product), in order to ensure that excised band contained the GDF-9 sequence.

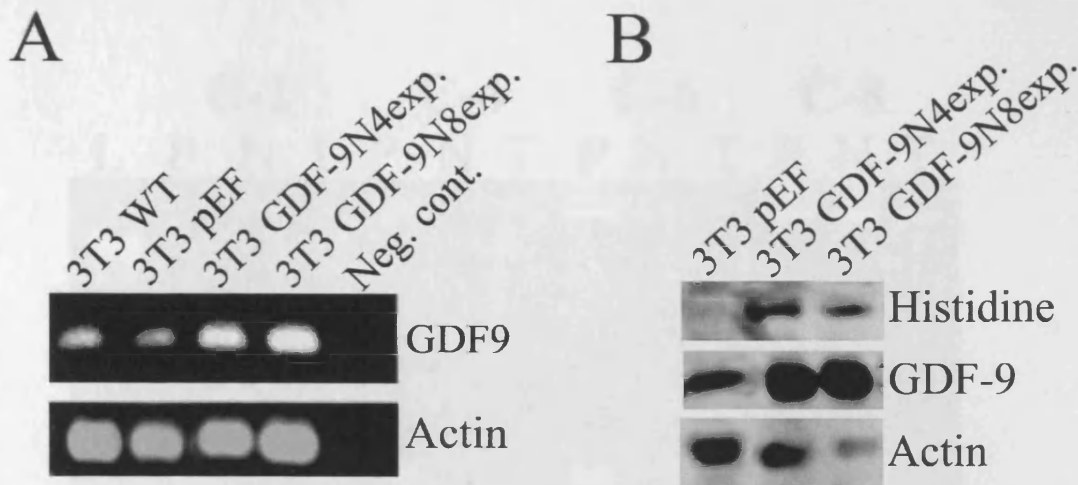


Figure 5.4: Verification of GDF-9 over-expression in 3T3 transfected cells. **A.** RT-PCR showing elevated mRNA levels of GDF-9 in both 3T3^{GDF-9N4exp.} and 3T3^{GDF-9N8exp.} cells, compared to both the 3T3^{WT} and 3T3^{pEF} controls. **B.** Western blot demonstrating increased levels of histidine and GDF-9 in both of the GDF-9 over-expressing 3T3 cells compared to empty plasmid control.

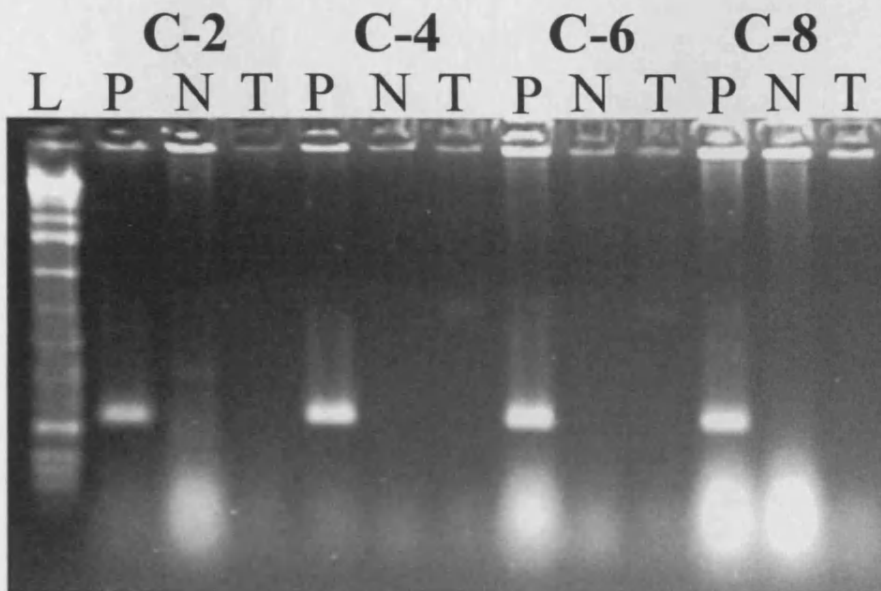


Figure 5.2: Agarose gel showing PCR of *E.coli* colony analysis. L is the ladder, P stands for correct orientation of GDF-9 (F9+BGHR-532bp), N for incorrect orientation (F9+T7F-300bp), and T for T7F+BGHR (1600bp). Colony 2 (C-2) is mixed and has the insert both in the incorrect, and correct orientation, whereas colonies C-4, C-6, and C-8 have the correctly orientated insert, and were selected for plasmid extraction.

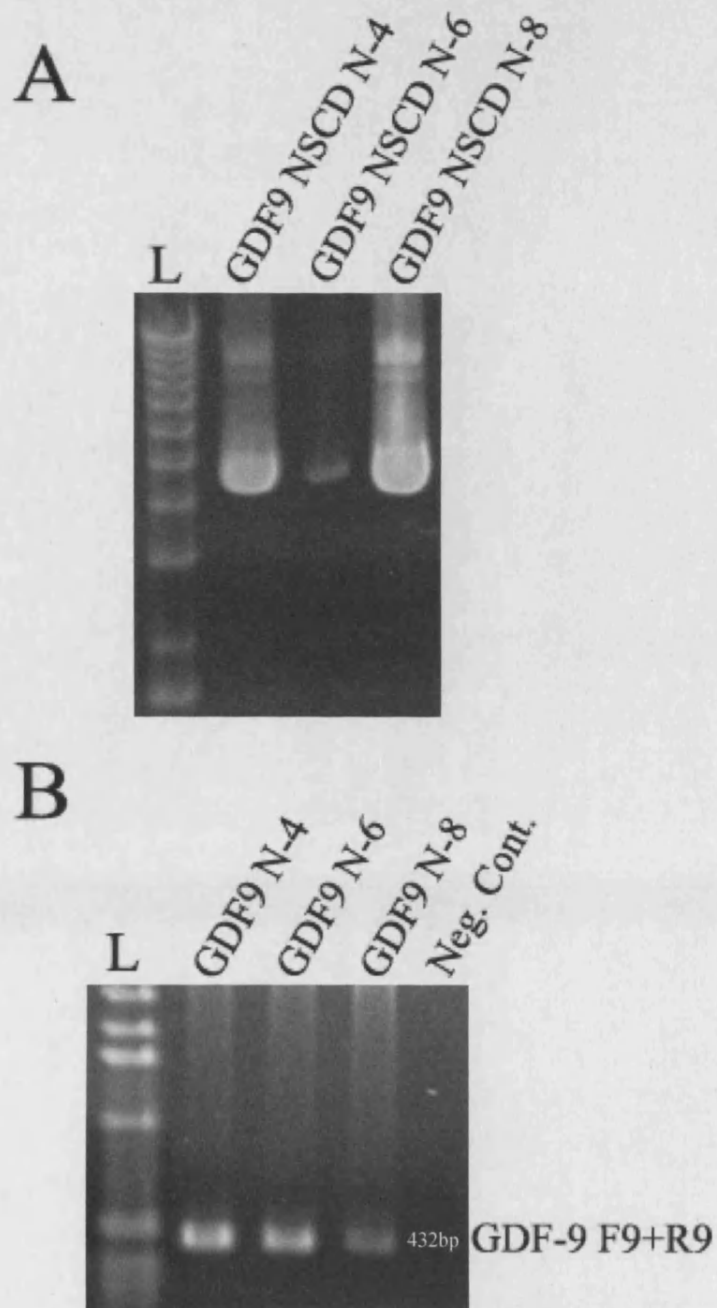


Figure 5.3: A. The GDF-9 NSCD plasmids were extracted from the selected colonies, and run on an agarose gel in order to confirm integrity. B. A diluted sample of each plasmid was then used as a template for a PCR GDF-9 specific primers; GDF-9 F9+R9 (432bp) in order to ensure they contained the GDF-9 NSCD sequence.

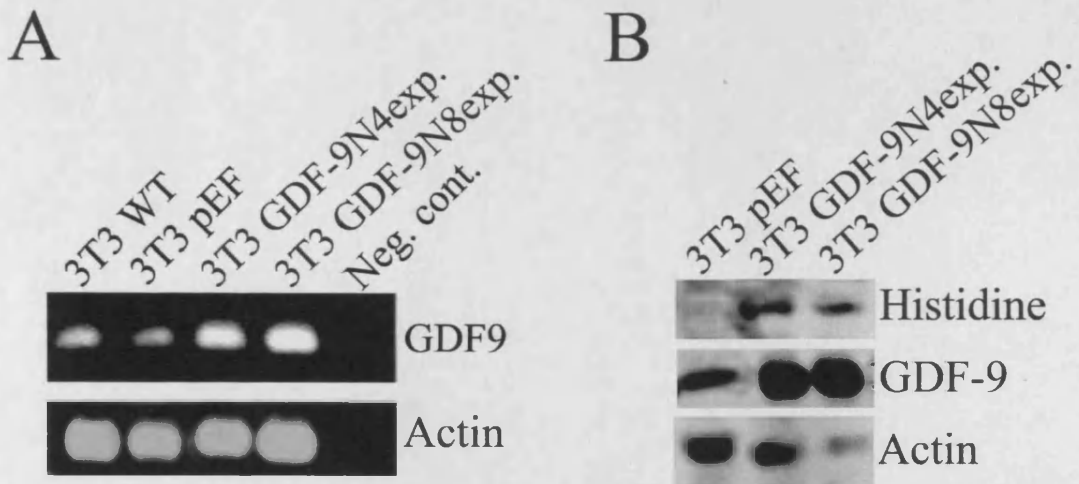


Figure 5.4: Verification of GDF-9 over-expression in 3T3 transfected cells. **A.** RT-PCR showing elevated mRNA levels of GDF-9 in both 3T3^{GDF-9N4exp.} and 3T3^{GDF-9N8exp.} cells, compared to both the 3T3^{WT} and 3T3^{pEF} controls. **B.** Western blot demonstrating increased levels of histidine and GDF-9 in both of the GDF-9 over-expressing 3T3 cells compared to empty plasmid control.

5.3.4 Purification of rh-GDF-9

Following verification of the transfectants for GDF-9, the 3T3^{GDF-9 N4 exp.} cells were grown to large quantities and both conditioned media and cell lysate were used to purify the recombinant protein through the use of metal (nickel) chelating affinity chromatography. The successfully purified rh-GDF-9 protein is demonstrated using western blot analysis with GDF-9 and anti-histidine antibodies in order to verify that the protein purified was the required one (Figure 5.5). Following desalting using Vivaspin centrifugal concentrators, the two eluates containing rh-GDF-9 were analysed once more for GDF-9 by western blotting analysis (Figure 5.6).

5.3.5 Quantification of rh-GDF-9

Following verification of rh-GDF-9, the recombinant protein was then quantified by running an SDS-PAGE with a serial dilution of known BSA concentrations (Figure 5.7). The gel was then stained in Coomassie blue, and photographed in order to allow the volume of the recombinant protein bands to be quantified by comparing it to the standard BSA curve. This then allowed for calculation of the concentration of the recombinant protein. Two of the eluates appeared to have the recombinant protein termed; Rh-GDF-9 1 and Rh-GDF-9 2, and were shown to have a concentration of 2.61µg/ml and 16.8µg/ml, respectively (Figure 5.8). The more concentrated recombinant protein was then used to carry out further experiments.

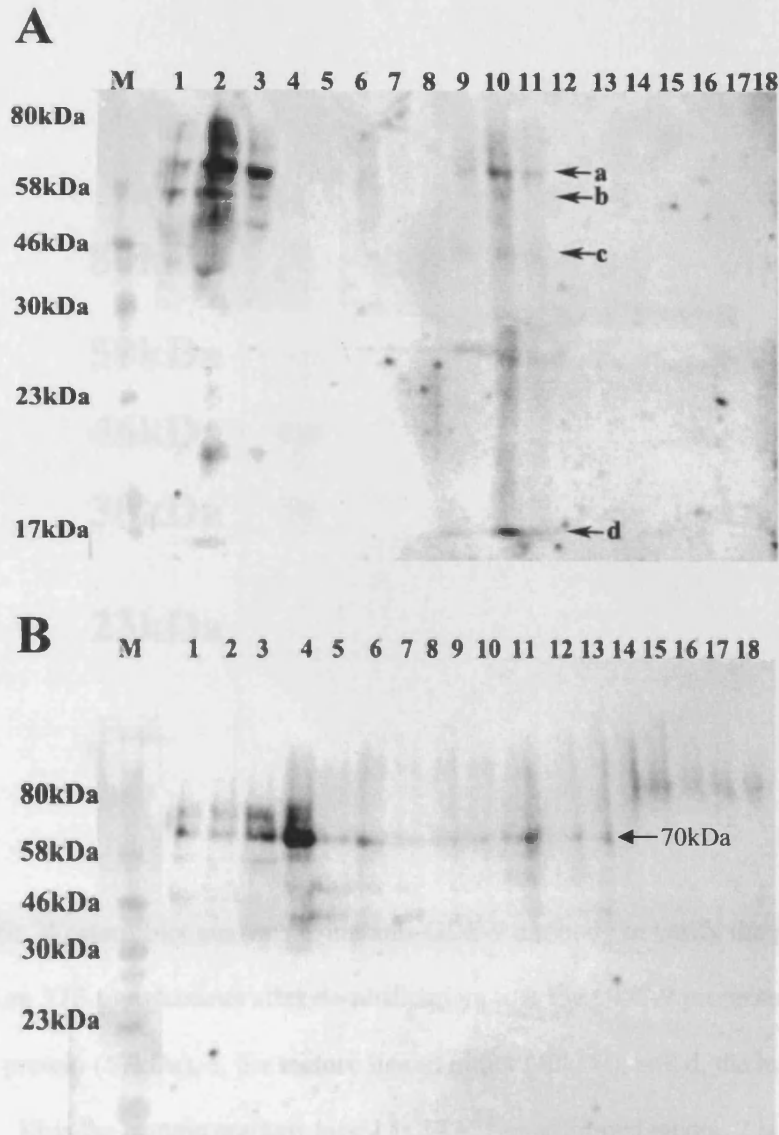


Figure 5.5: Western blot analysis verifying purification of rh-GDF-9 from 3T3 transfectants using **A.** Anti-GDF-9 antibody; a, is the GDF-9 proprotein (70kDa), b, the precursor protein (57kDa), c, the mature ligand dimer (40kDa), and d, the mature monomer (18kDa). **B.** Anti-Histidine antibody, resulting in a product sized just over 70kDa, corresponding to the GDF-9 proprotein and its histidine tag. M is the protein marker, lane 1 is 3T3^{PEF} conditioned media, 2 is 3T3^{GDF-9N4 exp.} conditioned media, 3 is the media flow-through, 4 is the binding buffer flow-through, 5 is elution 1 (PBS), 6 is elution 2 (1mM imidazole), 7 is elution 3 (5mM imidazole), 8 is elution 4 (10mM imidazole), 9 is elution 5 (20mM imidazole), 10 is 3T3^{GDF-9N4 exp.} cell lysate, 11 is cell lysate flow through, 12 is cell lysate binding buffer flow through, and 13-18 are elutions 1-5 at same concentration as previous elutions.

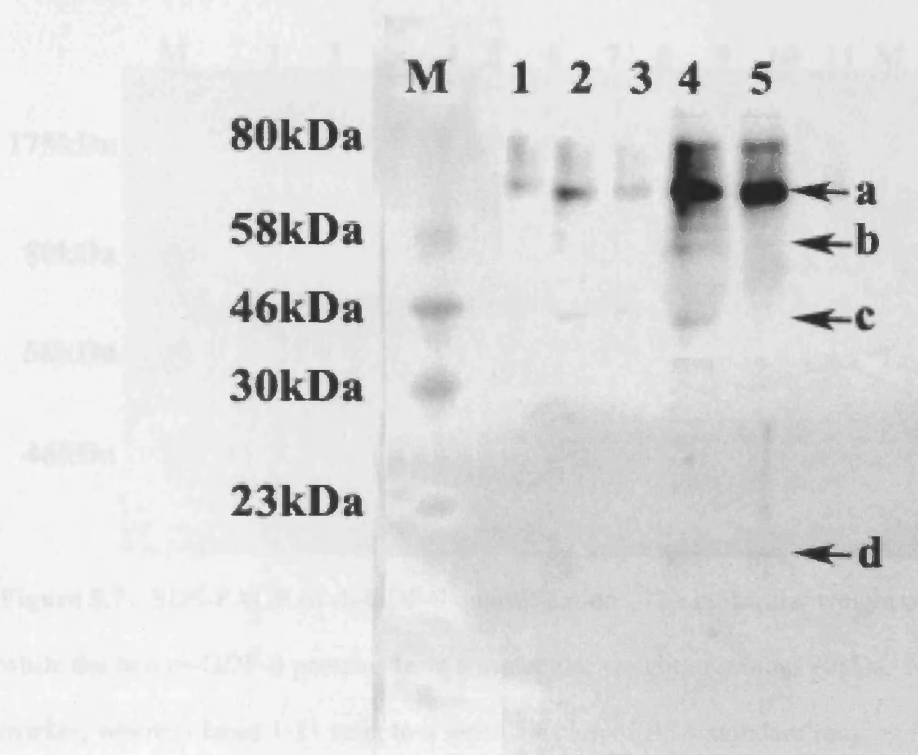


Figure 5.6: Western blot analysis using anti-GDF-9 antibody to verify the purification of rh-GDF-9 from 3T3 transfectants after desaltification; a, is the GDF-9 proprotein (70kDa), b, the precursor protein (57kDa), c, the mature ligand dimer (40kDa), and d, the mature monomer (18kDa). M is the protein marker; lane 1 is 3T3^{pEF} conditioned media, 2 is 3T3^{GDF-9N4 exp.} conditioned media, 3 is 1 μm imidazole, 4 is rh-GDF-9 elution 1, and 5 is rh-GDF-9 elution 2.

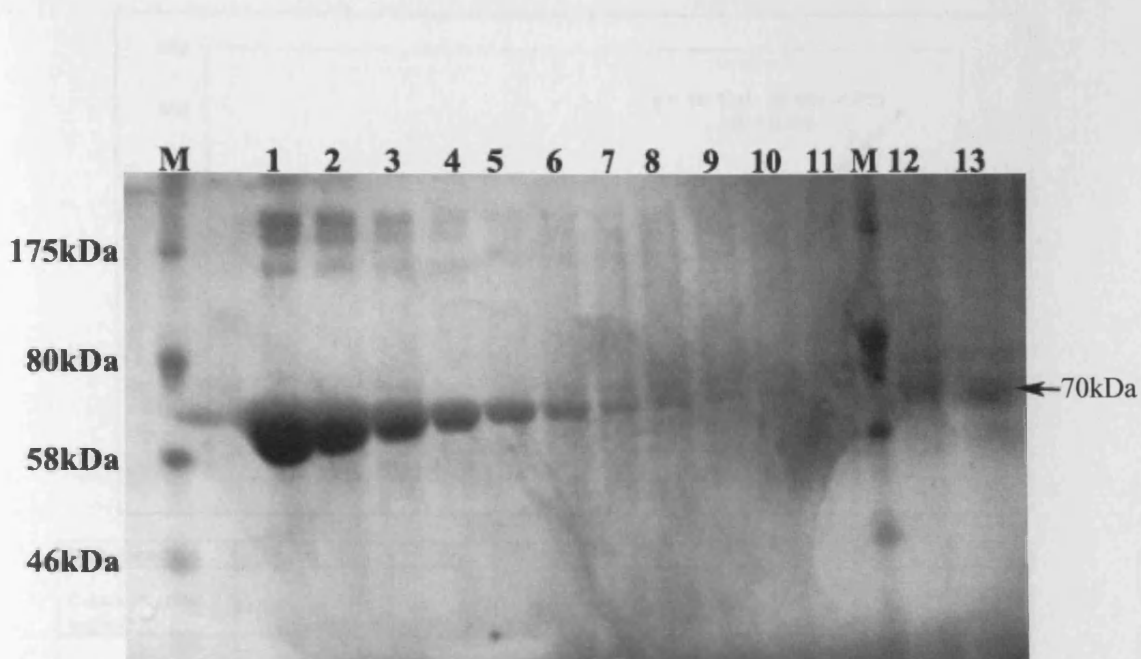
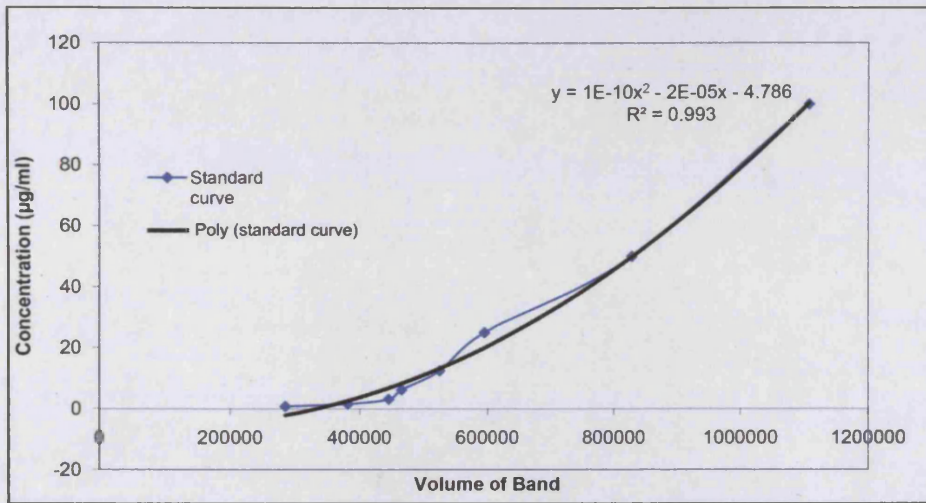


Figure 5.7: SDS-PAGE of rh-GDF-9 quantification. The molecular weight of BSA is 66.4kDa, while the two rh-GDF-9 proteins have a molecular weight of around 70kDa. M is the protein marker, whereas lanes 1-11 refer to a serial dilution of BSA standard ranging from 100 μ g/ml down to a concentration of 0.049 μ g/ml. Lanes 12 and 13 contain the two recombinant protein eluates.



BSA Standard	1	2	3	4	5	6	7
Concentration (µg/ml)	95.74069	47.31168	18.72412	12.29947	7.592855	6.15792	2.1433
Volume of Band	1107607	828685	595082	525276	465778	445607	381599

	RhGDF9 1	RhGDF9 2
Volume of Band	15.98515	39.75938
Concentration (µg/ml)	2.61	16.8

Figure 5.8: Graph showing quantification of rh-GDF-9 using a standard curve of BSA standards of a known concentration. The resulting equation of the line was then used to calculate the concentration of rh-GDF-9 compared to the BSA standards.

5.3.6 Effect of rh-GDF-9 on the *in vitro* cell growth of prostate cancer cells

In order to determine whether treating prostate cancer cells with exogenous GDF-9 had similar effects on their biological properties as altering its endogenous expression, PC-3 WT cells were treated with 20ng/ml of rh-GDF-9 for a period of 4 days, and analysed for differences in cell growth, with the use of an *in vitro* cell growth assay. The PC-3 WT cells treated with rh-GDF-9 (1.35 ± 0.28) had a significantly increased absorbance (and hence proliferation) compared to the untreated PC-3 cells (0.79 ± 0.05), $p=0.026$ (Figure 5.9). This implies that rh-GDF-9 promotes the growth of PC-3 cells. Six independent repeats were carried out, all showing the same trend.

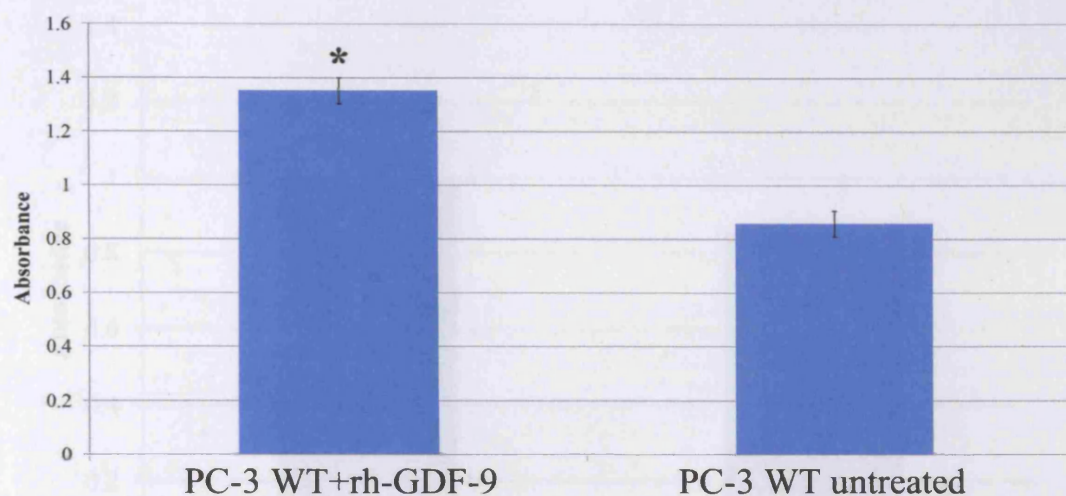
A similar trend was seen in the DU-145 WT cells, in that the rh-GDF-9 treated cells (1.00 ± 0.18) demonstrated an increased growth compared to the non-treated cells (0.85 ± 0.02), $p=0.292$. Despite the clear trend however, the difference between treated and non-treated cell growth rate was not found to be statistically significant (Figure 5.10). The concentration of rh-GDF-9 (20ng/ml) was chosen, as it was the lowest concentration at which an effect on the growth of PC-3 cells was observed, and is the concentration commonly used for other rh-BMPs (See appendix, figure A1).

5.3.7 Effect of rh-GDF-9 on the *in vitro* adhesive capacity of PC-3 cells

In order to determine the effect of rh-GDF-9 on the *in vitro* adhesive capacity of PC-3 cells, PC-3 WT cells were treated with 20ng/ml of rh-GDF-9 for 40 minutes, before the cells were stained with crystal violet, and counted. The PC-3 WT cells treated with rh-GDF-9 (50.1 ± 4.89) demonstrated a significant increase in adhesion in comparison to the untreated PC-3 WT cells (37.3 ± 2.09), $p=0.05$ (Figure 5.11). At least three independent repeats were carried out for accuracy.

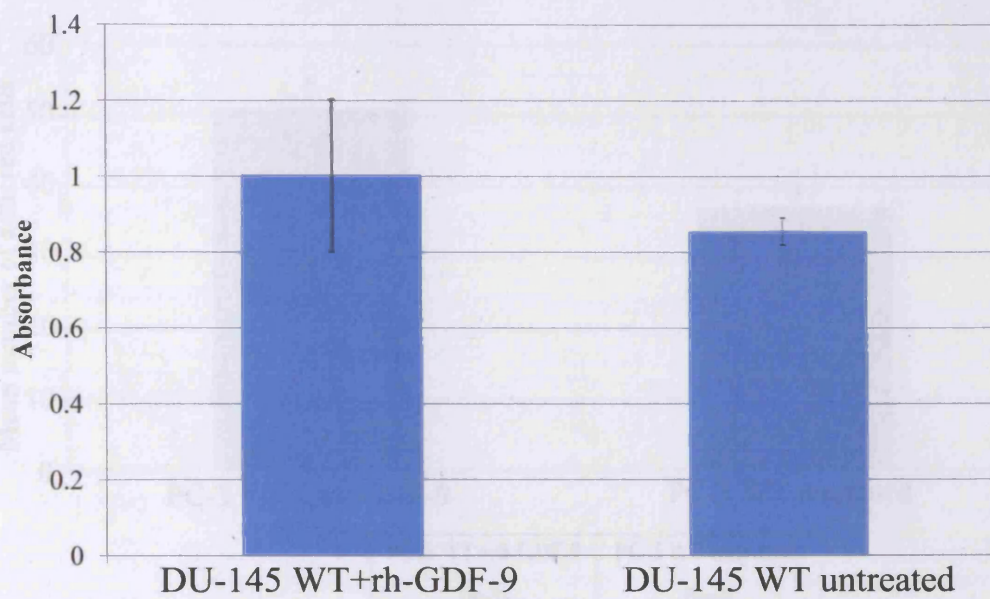
5.3.8 The effect of rh-GDF-9 on the invasive and motile capacity of PC-3 cells

As shown in chapter 4, over-expression of GDF-9 in PC-3 cells led to an enhancement in both their invasive and motile capacity. In order to determine that this effect was due to GDF-9, the PC-3 cells were treated with 20ng/ml rh-GDF-9 and assessed for their motility and invasion. The rh-GDF-9 treated cells (36.3 ± 5.13) demonstrated a slight increase in their invasive capacity compared to the untreated control (25.7 ± 3.06), $p=0.036$ (Figure 5.12). In the case of motility meanwhile, rh-GDF-9 had a more significant enhancing effect on the motile capacity of the PC-3 cells (56.2 ± 7.0), compared to the untreated control (30.0 ± 5.6), $p < 0.01$ (Figure 5.13). Three independent runs were carried out for accuracy.



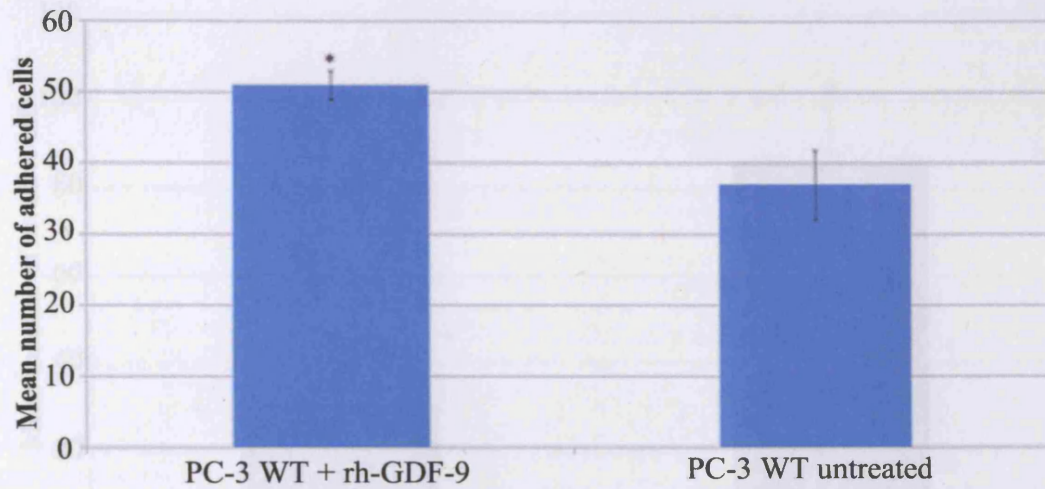
	PC-3 WT+rh-GDF-9 (n=3)	PC-3 WT untreated (n=3)
Mean	1.35	0.79
SD	0.28	0.05

Figure 5.9: Effect of rh-GDF-9 on *in vitro* cell growth of PC-3 cells after 4 days incubation. Due to the value and small volume of rh-GDF-9, growth was only examined on day 4, as opposed to days 0, 1, 3, and 5, as demonstrated in chapter 4. After being stained with crystal violet, acetic acid was added in order to dissolve the stain allowing the absorbance to be measured. The absorbance and hence cell number of PC-3 cells was significantly increased when treated with 20ng/ml of rh-GDF-9 compared to untreated PC-3^{WT}, *p=0.026. Data shown is representative of 6 independent repeats. Error bars represent standard deviation.



	DU-145 WT +rh-GDF-9 (n=3)	DU-145 WT untreated (n=3)
Mean	1.0	0.85
SD	0.18	0.02

Figure 5.10: Effect of rh-GDF-9 on *in vitro* cell growth of DU-145 cells, following 4 days incubation as mentioned above. The cell growth of DU-145 cells was marginally increased when treated with 20ng/ml of rh-GDF-9, $p=0.292$. Data shown is representative of at least 3 independent repeats. Error bars represent standard deviation.



	PC-3 WT+rh-GDF-9 (n=3)	PC-3 WT untreated (n=3)
Mean	50.1	37.3
SD	4.89	2.09

Figure 5.11: Effect of rh-GDF-9 on the *in vitro* adhesive capacity of PC-3 cells using the adhesion matrigel assay, following 40 minutes incubation. The adhesive capacity of PC-3 cells was significantly increased when treated with 20ng/ml of rh-GDF-9, compared to the untreated PC-3^{WT} cells, *p=0.05. Data shown is representative of at least 3 independent repeats. Error bars represent standard deviation.

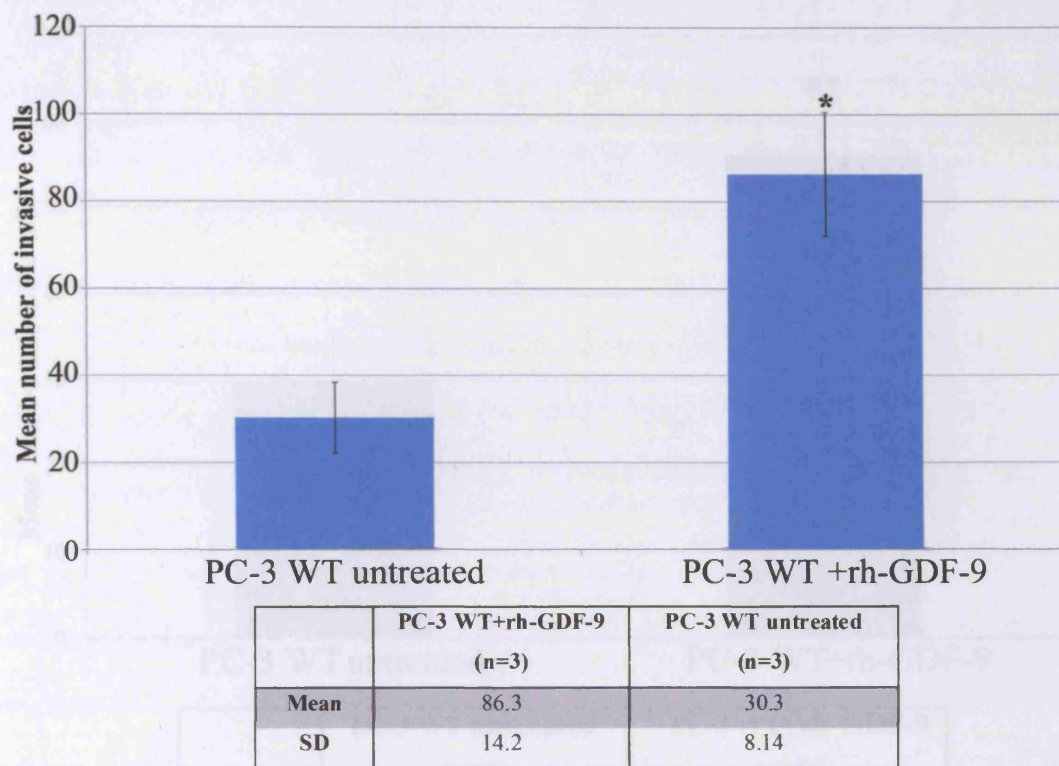
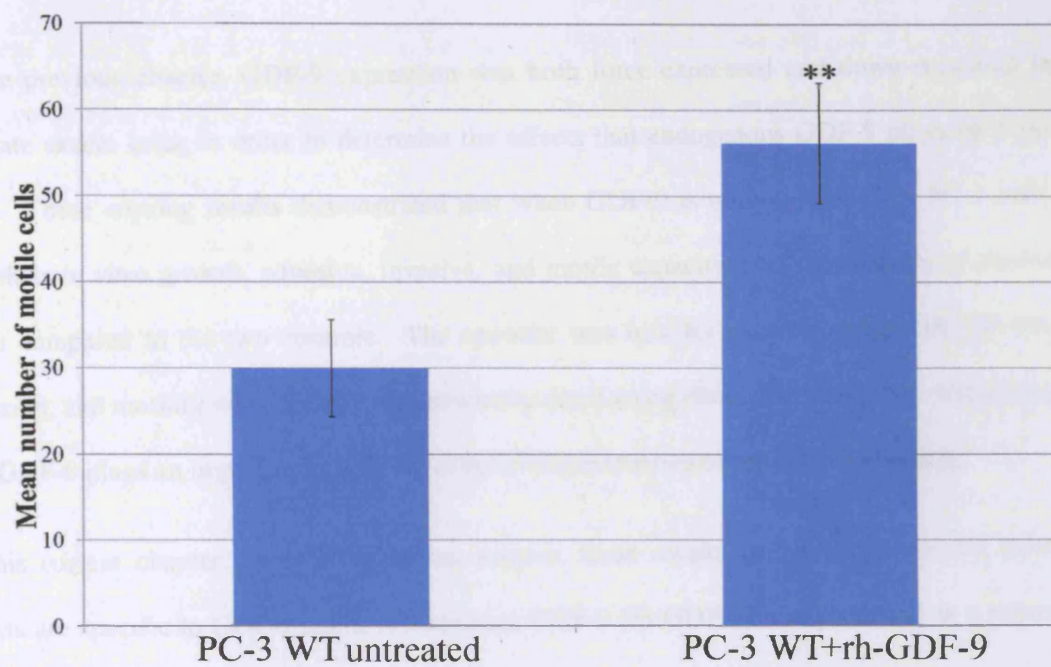


Figure 5.12: Effect of rh-GDF-9 on the invasive capacity of PC-3 cells, following 4 days incubation. The PC-3 cells treated with 20ng/ml rh-GDF-9 demonstrated a slightly increased invasive capacity compared to the untreated control cells, *p=0.036. Data shown is representative of at least 3 independent repeats. Error bars represent standard deviation.



	PC-3 WT untreated (n=6)	PC-3 WT+rh-GDF-9 (n=6)
Mean	30.0	56.2
SD	5.6	7.0

Figure 5.13: Effect of rh-GDF-9 on the *in vitro* motile capacity of PC-3 cell using the cytodex-2 bead motility assay. The PC-3 cells treated with 20ng/ml rh-GDF-9 demonstrated a marked promotion in their motile capacity compared to the untreated control cells, ** $p < 0.001$. Data shown is representative of at least 3 independent repeats. Error bars represent standard deviation.

5.4 Discussion

In the previous chapter, GDF-9 expression was both force-expressed and down-regulated in prostate cancer cells, in order to determine the effects that endogenous GDF-9 plays on these cells. These ensuing results demonstrated that when GDF-9 is over-expressed in PC-3 cells, that their *in vitro* growth, adhesive, invasive, and motile capacity was significantly promoted when compared to the two controls. The opposite was true for prostate cancer cell growth, adhesion, and motility when GDF-9 was down-regulated using ribozyme transgenes, suggesting that GDF-9 plays an important role in the cellular characteristics of prostate cancer cells.

In this current chapter, in order to further support these results and demonstrate that these effects are specific to GDF-9 itself, recombinant GDF-9 (rh-GDF-9) was produced as a source of exogenous GDF-9 protein with which to treat the cells. This was carried out using a mammalian expression factor to transfect 3T3 cells, a mouse fibroblast cell line, well established in the production of rh-proteins, with which previous rh-proteins had successfully been purified in the laboratory.

In order to simplify recombinant protein purification, the expression plasmid used adds a histidine tag to the C-terminal of the protein, thereby allowing for protein purification by metal chelating affinity chromatography. This is a very effective and reliable method in which to ensure purity of the resulting recombinant protein, with maximum exclusion of irrelevant molecules. This was verified with the use of western blot analysis with several antibodies to ensure that it was indeed GDF-9.

Once purified and quantified, rh-GDF-9 was then used in various *in vitro* assays to treat wild-type PC-3 and DU-145 prostate cancer cells in order to determine whether this would demonstrate with similar results to those seen in the previous chapter, and prove that these functional changes were specific to GDF-9. Indeed, when the PC-3 cells were treated with rh-GDF-9, an increase in the cell growth, adhesive, invasive, and motile capacity of these cells was

evident when comparing to the untreated cells. In rh-GDF-9 treated DU-145 cells however, the increase in cell growth was found to be statistically insignificant. As DU-145 expresses high endogenous levels of GDF-9, it is possible that further addition of exogenous rh-GDF-9 would have little effect compared to that seen in the PC-3 cells, which express low levels of the protein. For this reason, no more functional assays were carried out on DU-145 cells.

These experiments along with those in the previous chapter, further imply that GDF-9 has an important role in the proliferative, adhesive, and motile capacity of prostate cancer cells, and that the use of recombinant protein is a simple and effective method which can be utilised in further experiments, including investigation of a protein's signal transduction pathway.

Chapter 6

GDF-9 promotes growth of prostate cancer cells by protecting them from apoptosis

6.1 Introduction

The previous chapters have shown that GDF-9 can promote the growth rate of prostate cancer cells, in both its endogenous and exogenous form. An increase in cell growth is vital for the progression of cancer cells as it allows for tumours to grow and establish themselves quicker.

Most oncogenic factors can affect cell proliferation in two different ways; by disrupting the cell cycle, and/or by inhibiting the process of apoptosis.

TGF- β is known for its growth-inhibitory effects in a variety of cell types. Additionally, BMP-6 and BMP-2 have been shown to inhibit the growth of prostate cancer cells including LNCaP and DU-145 (Brubaker *et al.*, 2004). The laboratory has recently shown that BMP-9 and -10 can inhibit the growth, adhesion, invasion, and migration of prostate cancer cells by inducing apoptosis via Smad 1, 5, and 8 mediated up-regulation of pro-apoptotic factor Par-4, and the Smad independent pathway, respectively (Ye *et al.*, 2008; Ye *et al.*, 2009).

GDF-9 meanwhile, has been shown to promote the proliferation and survival of granulosa cells (Vitt *et al.*, 2000). In addition, its expression is up-regulated in an oral cancer cell line less apoptotic in nature, suggesting that GDF-9 acts as a survival factor in this cell type (Zhuang *et al.*, 2010). The previous chapters have now shown that it has the same effect in prostate cancer cells. Therefore, in order to determine the mechanism behind this growth induction, the cells underwent apoptosis and cell cycle analysis using flow cytometry in order to investigate the effects of GDF-9 on prostate cancer cell growth in more depth.

6.2 Materials and methods

6.2.1 Materials

The antibodies used in this chapter are shown in Table 2.1 and include anti-caspase 3, P38, JNK, ERK, ALK-5, pSmad1, Smad3, pSmad3, and phospho-serine/threonine.

6.2.2 Investigating expression of apoptotic and cell cycle molecules using PCR and western blotting

Both RNA and protein were extracted from the stable transfectant cells treated with or without rh-GDF-9, and were used in either western blot analysis or RT-PCR, in order to investigate expression levels of apoptotic and cell cycle molecules at both the mRNA and protein level. These methods were carried out as previously described in sections 2.4 and 2.5.

6.2.3 Immunoprecipitation of serine/threonine phosphorylated ERK, JNK, and ALK-5

Protein extracted from PC-3 WT cells treated either with nothing, 3ng/ml Smad3 inhibitor alone, or 20ng/ml rh-GDF-9 alone, or in conjunction with 3ng/ml Smad3 inhibitor, was immuno-precipitated with anti-phosphorylated serine/threonine antibody in order to be able to detect levels of phosphorylated proteins. These immuno-precipitated protein samples were then run on an SDS-PAGE and blotted with anti-ERK, anti-JNK, and anti-ALK-5 antibody. Refer to section 2.5.3 for further details on immunoprecipitation method.

6.2.4 Immuno-flourescent staining of pSmad3 and pSmad1 in GDF-9 transfected cells

The cells were lysed before being incubated with primary anti-pSmad3 or pSmad1 antibody for an hour. The primary antibody was then washed off and replaced with the corresponding FITC labelled secondary antibody, before the cells were viewed using a fluorescent microscope.

6.2.5 *In vitro* cell growth assay

The cells were seeded into a 96 well plate as described in sections 2.9.3. Triplicates of each cell line were incubated with 10% FBS containing DMEM media either with or without 20ng/ml of rh-GDF-9, and/or 3ng/ml Smad3 inhibitor. The cells were fixed following 4 days incubation and stained with crystal violet, before the absorbance was measured in order to determine cell number.

6.2.6 Hoechst staining for apoptosis

The cells were incubated either with DMEM with 10% FBS or serum free, for a period of 48 hours, before both the adherent cells and those floating in the culture medium were harvested and washed in PBS. The cells were then stained with Hoechst 33342 DNA stain for 20 minutes, before the apoptotic cells were counted, and using the total number of cells, a percentage for the amount of apoptotic cells was calculated.

6.2.7 Apoptosis and cell cycle analysis using flow cytometry

Both the transfected PC-3 cells and PC-3^{WT} cells treated with either 20ng/ml rh-GDF-9 alone or in conjunction with 3ng/ml Smad3 inhibitor, or 3ng/ml Smad3 inhibitor alone, underwent serum starvation for 48 hours before undergoing apoptosis analysis by flow cytometry. In order to detect apoptotic cells, this current study uses the Vybrant® Apoptosis Assay Kit (Invitrogen, Inc., Paisley, UK) which contains recombinant fluorescein conjugated annexin V (FITC annexin V) and propidium iodide (PI) solution. The cells were stained with both FITC annexin V and PI solution, before the stained cells were analysed using the flow cytometer and FlowMax software package, by measuring any fluorescence emission at 530nm (FL1) and >575nm (FL3).

For cell cycle analysis, following harvestation of both the adherent and floating cells, the cells were centrifuged and counted. 1×10^6 cells were then fixed with ethanol, and subsequently stained with PI solution including TritonX100 for cell permeabilisation and RNAase A to digest any dsRNA. After an incubation period of 30 minutes, the fluorescence emitted by PI was detected using cell cycle analysis with the FlowMax software.

6.3 Results

6.3.1 Analysing role of GDF-9 on the cell cycle using flow cytometry

As demonstrated in the previous chapters, GDF-9 can promote the growth of prostate cancer cell lines PC-3 and DU-145. In order to determine the mechanism by which GDF-9 promotes cell growth, the effect of GDF-9 on the cell cycle was analysed. This demonstrated that PC-

PC-3^{GDF-9exp.} had a slightly lower percentage of cells in the G1 phase (44.6%±2.57) and higher percentage in the G2/M phase (43.2%±9.77), compared to the PC-3^{pEF} control which had the majority of its cells in the G1 phase (59.8%±7.77) as opposed to the G2/M phase (30.2%±5.02), p=0.03 when comparing the G1 phase and p=0.10 for the G2/M phase. Furthermore, the PC-3^{GDF-9rib3} cells like the control, had the majority of its cells in the G1 phase (56.6±4.13) compared to the G2/M phase (26.9±4.56), p=0.71 for G1 phase and p=0.34 for G2/M phase compared to PC-3^{pEF} (Figure 6.1).

6.3.2 The role of Cyclin D1 in GDF-9 associated growth promotion

The cyclins are responsible for regulating the Cyclin Dependant Kinases (CDKs) and for committing cells to the cell cycle. Cyclin D1 in particular, is responsible for regulating transition from G1 to S phase and thereby allowing cells to pass through the G1 check point and prepare for cell division (Harbour and Dean, 2000). As GDF-9 was shown to promote the progression of cells through the cell cycle, the expression of Cyclin D1 in response to GDF-9 was analysed. An up-regulation in the expression of Cyclin D1 was demonstrated after 2 hours of treatment with rh-GDF-9 at both the mRNA and protein level (Figure 6.2).

6.3.2 Analysing the role of GDF-9 in apoptosis using flow cytometry

However, as the effect on the cell cycle was insufficient to explain the marked effect that GDF-9 had on the growth of prostate cancer cells, the effect of GDF-9 on the proportion of apoptotic cells was analysed using flow cytometry. GDF-9 appeared to reduce the level of apoptosis in PC-3 cells under starvation from serum. As shown in figure 6.3, there was a smaller proportion of apoptotic cells (both early and late) in PC-3^{GDF-9exp.} cells (7.46%±1.54) compared to the PC-3^{pEF} (12.9%±2.86) control, p=0.04. In addition, PC-3^{GDF-9rib3} cells had a far greater proportion of apoptotic cells (27.0%±8.12) compared to the control, p=0.046. Meanwhile, PC-3 WT cells treated with rh-GDF-9 for 48 hours under serum starvation, also demonstrated a significant

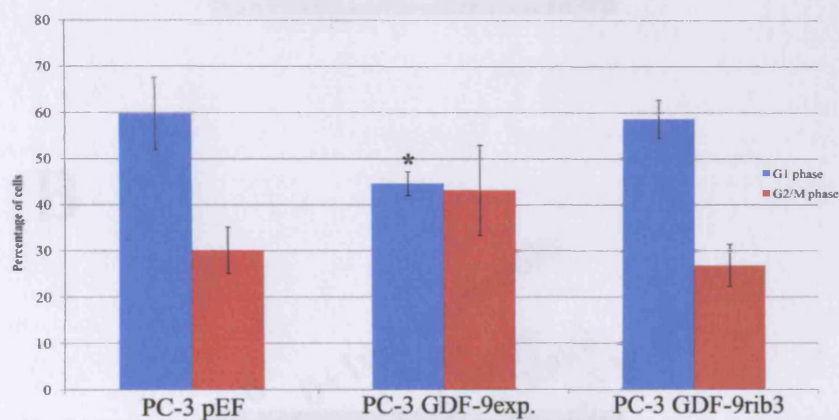
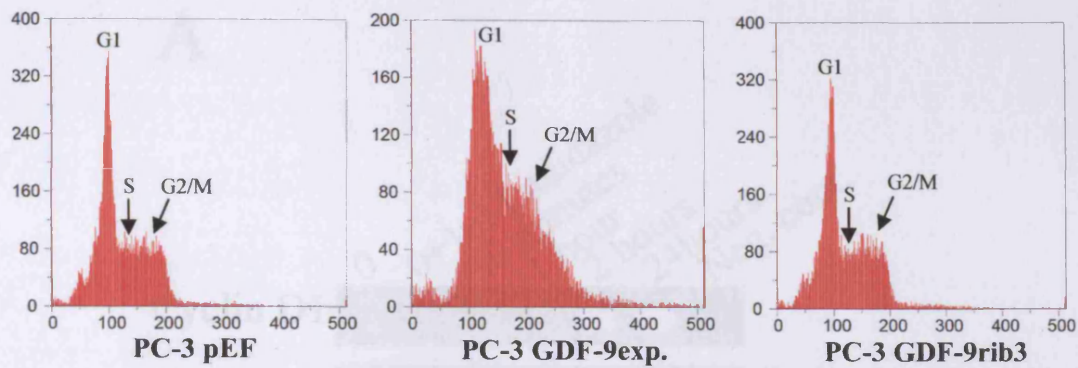
reduction in the number of apoptotic cells ($3.69\% \pm 1.33$) compared to the untreated control ($13.2\% \pm 1.34$), $p < 0.001$ (Figure 6.4).

6.3.4 Analysing role of GDF-9 in apoptosis using Hoechst DNA stain

In order to further determine whether GDF-9 has an effect on apoptosis, another method of analysing apoptosis was carried out. The cells were stained with Hoechst 33342 DNA stain, which when viewed under fluorescent light can help distinguish apoptotic cells with condensed chromatin, a hallmark of apoptosis. Figure 6C shows that PC-3^{GDF-9exp.} ($6.06\% \pm 0.61$) cells have a significantly lower percentage of apoptotic cells compared to PC-3^{pEF} ($12.9\% \pm 1.57$), $p = 0.004$. In addition, the PC-3^{GDF-9rib3} ($29.7\% \pm 4.66$) cells demonstrated a significantly higher percentage of apoptotic cells compared to the control, $p = 0.006$ (Figure 6.5).

6.3.5 Analysing expression of apoptosis effector molecules

Caspase 3, an executioner caspase is indicative of end-stage apoptosis. Therefore, in order to further determine whether GDF-9 has an effect on prostate cancer cell apoptosis, levels of caspase 3 were examined in the transfected PC-3 cells using western blot analysis. Caspase-3 is expressed as an inactive precursor, which is cleaved into p11 and p17 mature caspase-3 subunits during apoptosis. The caspase-3 precursor is first cleaved to form a p20 peptide and the p11 subunit, and then the p20 peptide is further cleaved to form the mature p17 subunit. PC-3^{GDF-9exp.} demonstrated significantly lower expression levels of caspase-3 mature subunits, compared to both the controls and the PC-3^{GDF-9rib3} cells, shown with the use of western blotting (Figure 6.6A). In addition, down-regulation in caspase-3 protein levels was also seen in PC-3 WT cells exposed to 20ng/ml of rh-GDF-9 over a time period of up to 24 hours (Figure 6.6B). The levels of caspase-3 expression begin to show down-regulation after around 4 hours, and at 24 hours its expression is only marginally visible.



	PC-3 pEF (n=3)	PC-3 GDF-9exp. (n=3)	PC-3 GDF-9rib3 (n=3)
G1 phase (Mean%±SD)	59.8±7.77	44.6±2.57	58.6±4.13
G2/M phase (Mean%±SD)	30.2±5.02	43.2±9.77	26.9±4.56

Figure 6.1: Analysis of cell cycle in PC-3 cells using flow cytometry. PC-3^{GDF-9exp.} cells had similar numbers of cells in both the G1 and G2/M phases, compared to the PC-3^{pEF} control and PC-3^{GDF-9rib3} cells, which had the majority of their cells in the G1 phase as opposed to the G2/M phase, *p=0.03 when comparing the G1 phase, and p=0.10 for the G2/M phase of PC-3^{GDF-9exp.} cells compared to PC-3^{pEF}, p=0.71 for the G1 phase and p=0.34 for G2/M phase of PC-3^{GDF-9rib3} compared to PC-3^{pEF}.

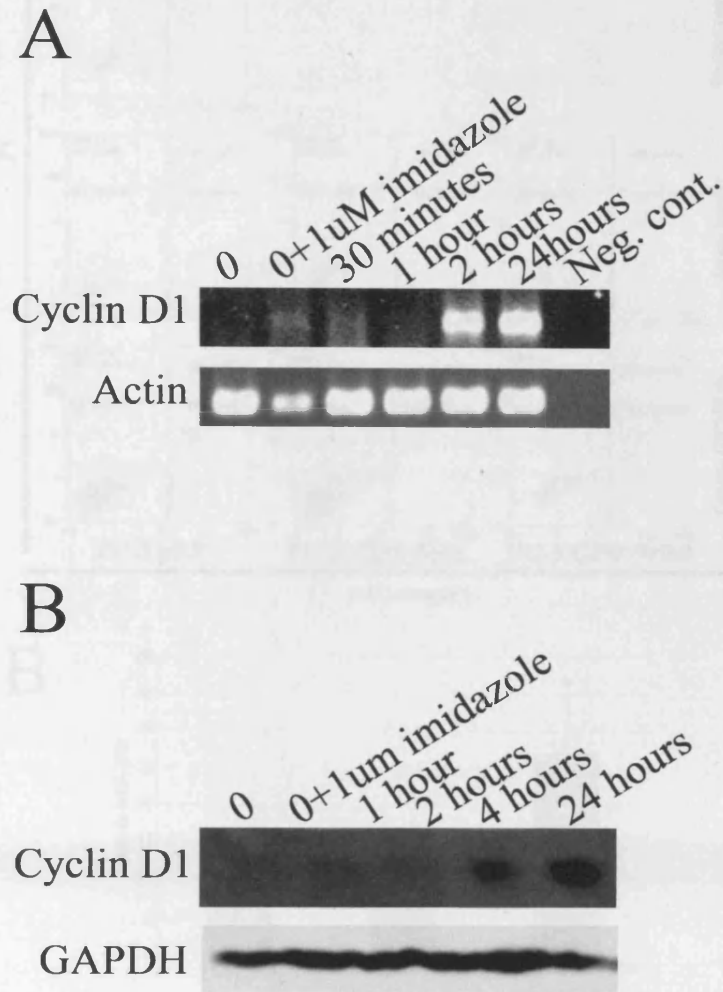
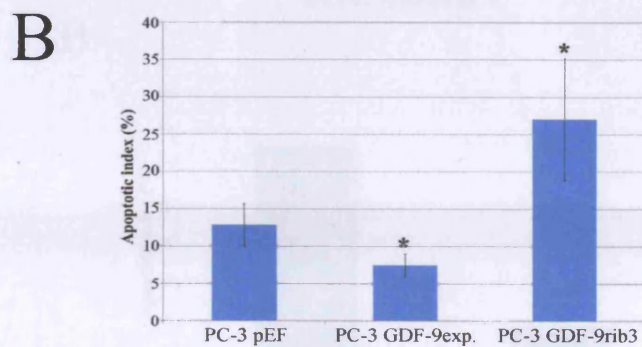
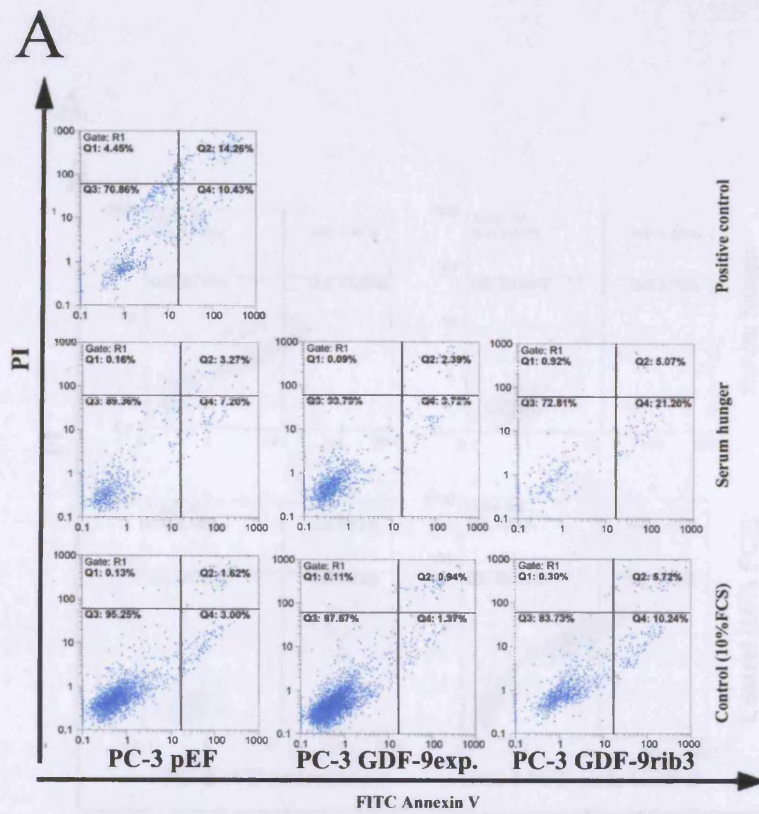


Figure 6.2: The effect of GDF-9 on Cyclin D1 expression was analysed by treating PC-3 cells with 20ng/ml rh-GDF-9 for varying amounts of time at the **A.** mRNA level using PCR with Cyclin D1 specific primers, demonstrating an up-regulation in Cyclin D1 expression and at **B.** the protein level using western blotting with an anti-Cyclin D1 antibody, which showed a similar effect.



	PC-3 pEF (n=3)	PC-3 GDF-9exp. (n=3)	PC-3 GDF-9rib3 (n=3)
Apoptotic index (Q2+Q4)	12.9	7.56	27.0
SD	2.86	1.54	8.12

Figure 6.3: The apoptotic population in PC-3 cells was analysed using flow cytometry following serum hunger for 48 hours, in order to induce apoptosis. The positive control indicated PC-3 cells treated with H₂O₂ to show induction of apoptosis. The percentage of apoptotic cells in the PC-3^{GDF-9exp} cells was significantly reduced compared to the control, *p=0.045. In addition there was a significant increase in the numbers of apoptotic cells in PC-3^{GDF-9rib3} cells compared to the control, *p=0.046. **A.** Data shown demonstrates representative data of three independent repeats. Segment Q1 of the quadrants refers to necrotic cells stained with high levels of PI, Q2 to late apoptotic cells with high staining of both annexinV and PI, Q3 to healthy live cells with low staining of both PI and annexinV, and Q4 to early apoptotic cells with high annexinV but low PI staining. **B.** Bar graph demonstrates the mean apoptotic percentage of three independent repeats. Error bars represent standard error of mean. Apoptotic index refers to total apoptotic population including both late apoptotic cells (Q2) and early apoptotic cells (Q4).

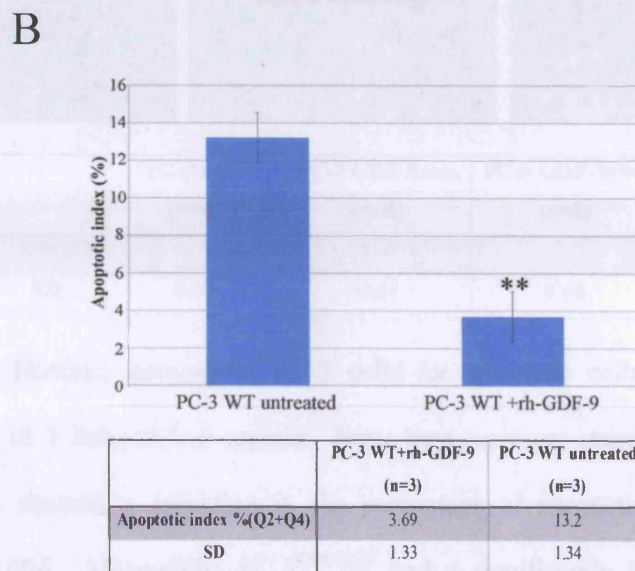
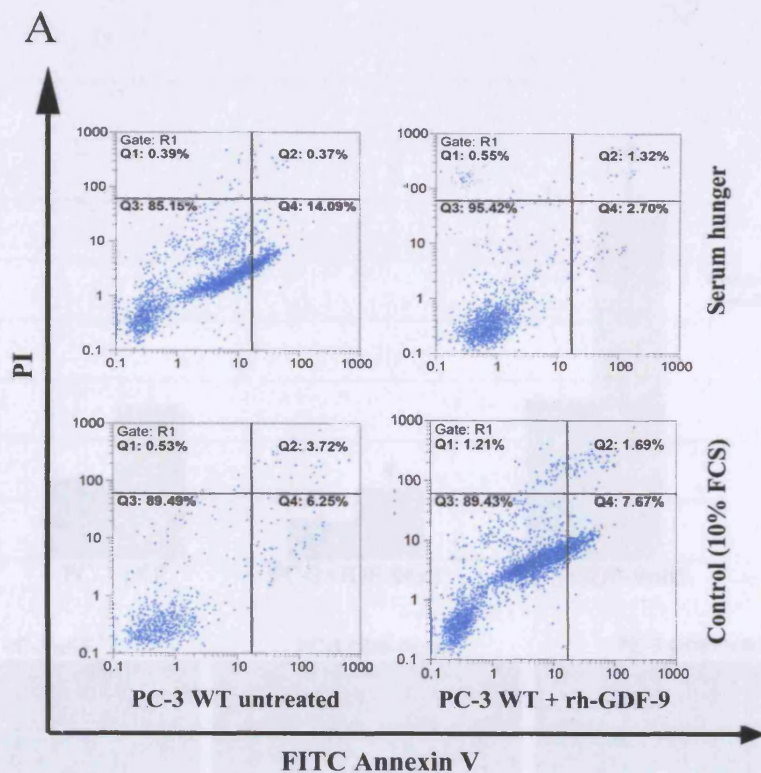
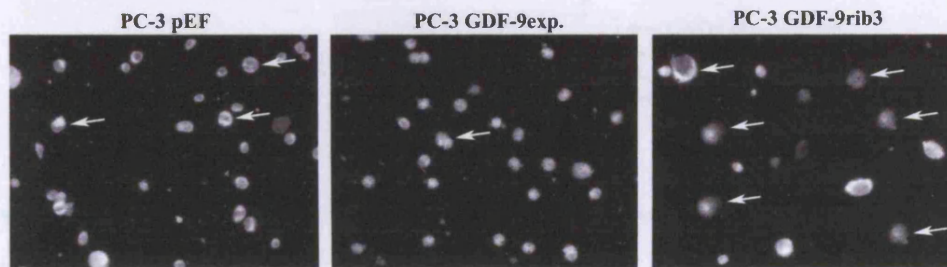
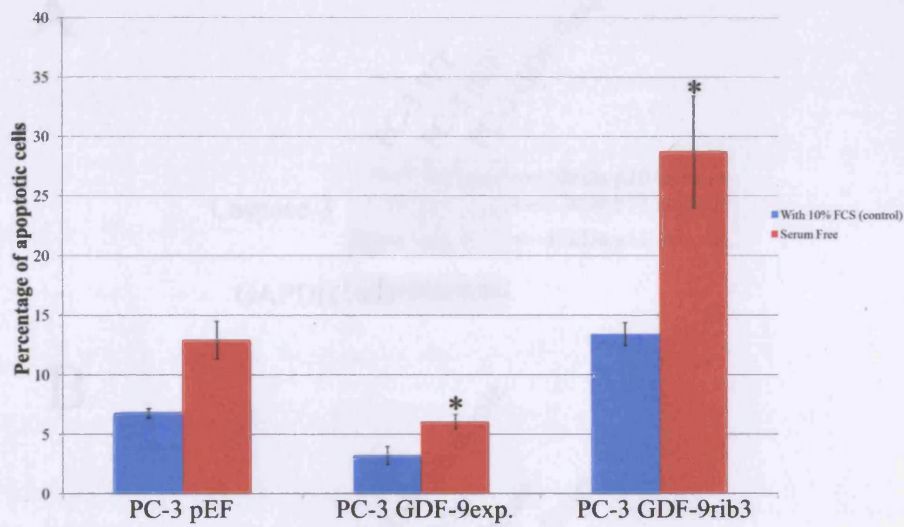


Figure 6.4: PC-3 cells were treated with serum free media with or without 20ng/ml rh-GDF-9 for 48 hours, and analysed for apoptosis using flow cytometry. The percentage of apoptotic cells in the PC-3 cells treated with rh-GDF-9 was significantly reduced compared to the untreated control, $**p < 0.001$. **A.** Data shown demonstrates representative data of three independent repeats. **B.** Bar graph demonstrates the mean apoptotic percentage of three independent repeats. Error bars represent standard error of mean. Apoptotic index refers to total apoptotic population including both early apoptotic cells (Q4) and late apoptotic cells (Q2).



	PC-3 pEF (n=6)	PC-3 GDF-9exp. (n=6)	PC-3 GDF-9rib3 (n=6)
Mean	12.9	6.06	29.7
SD	1.57	0.61	4.66

Figure 6.5: Hoechst staining of PC-3 cells for apoptotic cells. Graph shown is representative of 3 independent repeats. Error bars represent standard deviation. PC-3^{GDF-9exp.} cells showed a reduction in the percentage of apoptotic cells compared to control, *p=0.004. Meanwhile, PC-3^{GDF-9rib3} had a significantly higher percentage of apoptotic cells compared to PC-3^{pEF}, *p=0.006.

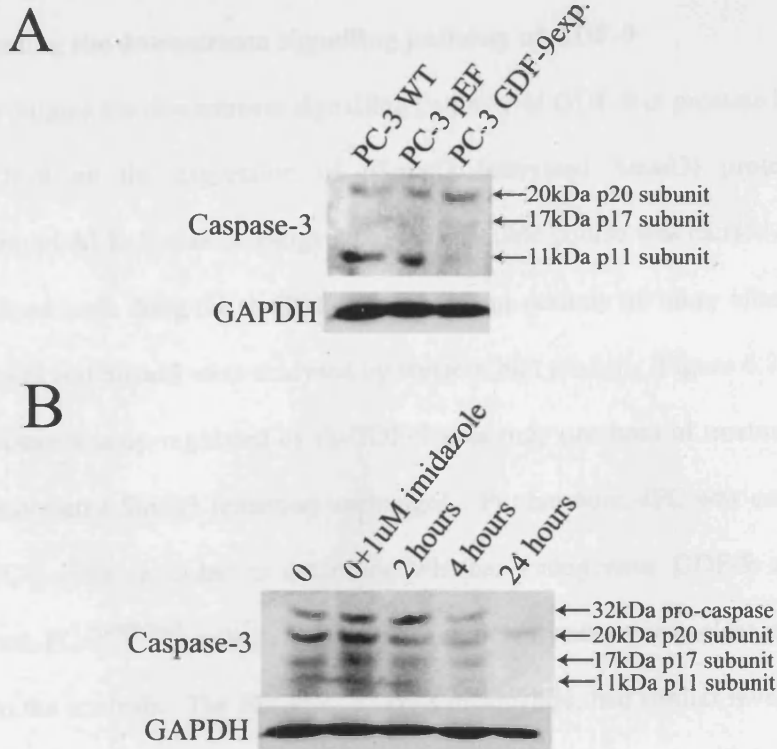


Figure 6.6: The effect of GDF-9 on caspase-3 protein levels using western blot analysis. **A.** PC-3^{GDF-9exp} cells show a reduction in protein levels of mature caspase-3 subunits compared to the two controls. **B.** Expression levels of mature caspase-3 subunits were gradually reduced over time when treated with 20ng/ml rh-GDF-9.

6.3.5 Investigating the downstream signalling pathway of GDF-9

In order to investigate the downstream signalling pathway of GDF-9 in prostate cancer cells, the effect of GDF-9 on the expression of pSmad3 (activated Smad3) protein levels, and phosphorylation of ALK-5, was investigated. Firstly, a time course was carried out where PC-3 cells were treated with 20ng/ml rh-GDF-9 for different periods of time, after which protein levels of pSmad3 and Smad3 were analysed by western blot analysis (Figure 6.7A). Expression of pSmad3 protein was up-regulated by rh-GDF-9 after only one hour of treatment while levels of non-phosphorylated Smad3 remained unchanged. Furthermore, IFC was carried out on the transfected PC-3 cells in order to determine whether endogenous GDF-9 also signals via Smad3. Indeed, PC-3^{GDF-9exp.} cells demonstrated significantly stronger nuclear staining of GDF-9 compared to the controls. The PC-3^{GDF-9rib3} cells meanwhile, had similar levels of pSmad3 as the controls. Meanwhile, no nuclear staining of pSmad1 was found in the PC-3^{GDF-9exp.} cells or the controls, suggesting that GDF-9 does not signal via Smad1 to exert its effects (Figure 6.7B).

The Smad3 inhibitor (Calbiochem, Gibbstown, USA) prevents phosphorylation and hence activation of Smad3, and so is an effective way of investigating its involvement. In order to demonstrate the actions of the Smad3 inhibitor, PC-3 cells were treated either with 20ng/ml rh-GDF-9, 3ng/ml Smad3 inhibitor alone, or 20ng/ml rh-GDF-9 along with 3ng/ml Smad3 inhibitor. The cells treated with rh-GDF-9 alone demonstrated an up-regulation of pSmad3 expression, whereas this was inhibited when the cells were treated with the Smad3 inhibitor, further suggesting that GDF-9 signals via this Smad (Figure 6.7C).

Furthermore, treatment with rh-GDF-9 alone or in conjunction with Smad3 inhibitor, resulted in an upregulation in levels of phosphorylated ALK-5 implying that GDF-9 signals via this receptor as has been previously reported. The addition of Smad3 inhibitor alone resulted in a reduction of p-ALK-5 levels. Although the reason for this remains unclear, the literature suggests that Smads may be involved in receptor up-regulation via a positive feedback loop (Figure 6.7D) (Miyazono, 2000).

6.3.6 GDF-9 and Smad-independent signalling

Apart from the Smad-dependent pathway, BMPs are known to signal independently of the Smads via the mitogen-activated protein kinase (MAPK) pathway, a major signalling pathway involved in cellular proliferation affecting both apoptosis and the cell cycle (Nohe *et al.*, 2002). As GDF-9 has been shown to affect both of these processes, its effect on the expression of two key players of the MAPK pathway, ERK and JNK in PC-3 cells was analysed in response to rh-GDF-9. The cells treated with rh-GDF-9 demonstrated an up-regulation in the levels of both ERK and JNK. However, while this up-regulation in JNK levels was inhibited when treating the cells with Smad3 inhibitor, apparently being Smad3 dependent, in the case of ERK, treating cells with the Smad3 inhibitor either alone or alongside rh-GDF-9 did not affect the levels of ERK.

Furthermore, carrying out immunoprecipitation with a serine threonine phosphorylated antibody, and carrying out a western blot using ERK and JNK antibodies, levels of phosphorylated and thereby active ERK and JNK could be analysed. This demonstrated that rh-GDF-9 treatment could lead to an increase in the levels of active p-ERK and p-JNK both of which were shown to be Smad3 independent, suggesting that while JNK itself may be a target gene of GDF-9, that GDF-9 may signal Smad independently via both ERK and JNK (Figure 6.8).

6.3.7 The role of Smad3 in GDF-9 associated growth promotion

As previously shown, rh-GDF-9 can promote the growth of PC-3 cells. In order to determine whether this effect is due to GDF-9 signalling via Smad3, the PC-3 cells were treated with Smad3 inhibitor and a growth assay was carried out. The PC-3 cells treated with rh-GDF-9 alone (0.93 ± 0.03) showed the usual increase in growth compared to the untreated (0.72 ± 0.07) control, $p=0.042$. Meanwhile, those treated with the Smad3 inhibitor alone (0.78 ± 0.005) and along with rh-GDF-9 (0.72 ± 0.05), showed similar growth rates to the untreated controls suggesting that the Smad3 inhibitor results in an inhibition of GDF-9 growth promotion, $p < 0.05$ for both the Smad3 inhibitor treated cells compared to the rh-GDF-9 treated cells (Figure 6.9).

However, when these cells were analysed for apoptosis using flow cytometry, the addition of Smad3 inhibitor alongside GDF-9 did not inhibit its anti-apoptotic effect suggesting that GDF-9 doesn't signal through Smad3 to induce its anti-apoptotic effects. The PC-3 cells treated with Smad3 inhibitor alone ($10.8\% \pm 1.99$) exhibited similar apoptotic levels to the untreated cells ($11.5\% \pm 2.54$), whereas those treated with Smad3 inhibitor and rh-GDF-9 ($4.72\% \pm 1.06$) had reduced apoptotic levels, similar to those seen in cells treated with rh-GDF-9 alone ($3.53\% \pm 1.00$), $p=0.722$ for untreated cells compared to Smad3 inhibitor treated cells, and $p=0.05$ compared to Smad3 inhibitor and rh-GDF-9 treated cells (Figure 6.10). This suggests that GDF-9 may signal via Smad3 to affect the cell cycle and thereby promote cell growth.

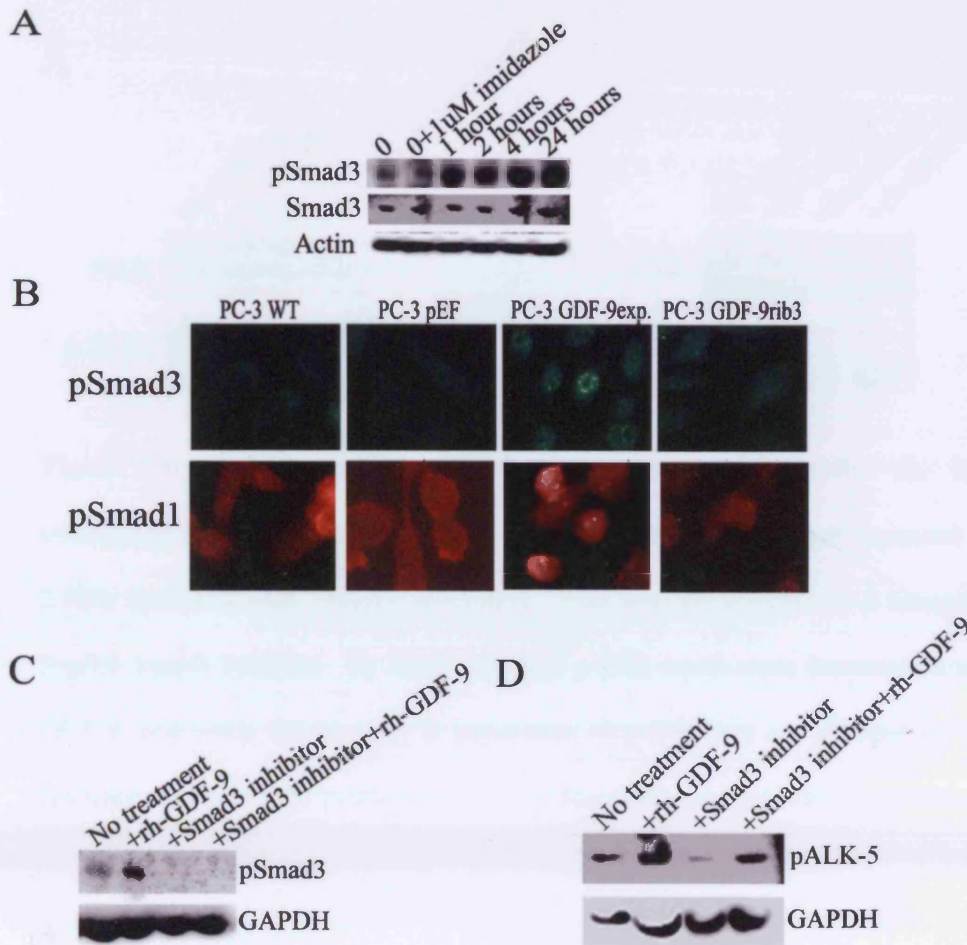


Figure 6.7: Downstream signalling of GDF-9. **A.** PC-3 cells treated with rh-GDF-9 demonstrated increased pSmad3 protein levels compared to untreated control. Levels of total Smad3 remained unchanged. **B.** IFC staining demonstrating increased levels of nuclear pSmad3 staining in the PC-3^{GDF-9exp.} cells compared to controls and knock-down cells. Levels of pSmad1 meanwhile, remained unchanged in the PC-3^{GDF-9exp.} cells compared to the controls. **C.** Western blot analysis showing that treatment of PC-3 with Smad3 inhibitor resulted in an inhibition of GDF-9 associated pSmad3 up-regulation. **D.** Treating PC-3 cells with 20ng/ml rh-GDF-9 for a period of 2 hours, resulted in increased phosphorylation of type I receptor ALK-5 compared to control, an effect that was downregulated by the Smad3 inhibitor.

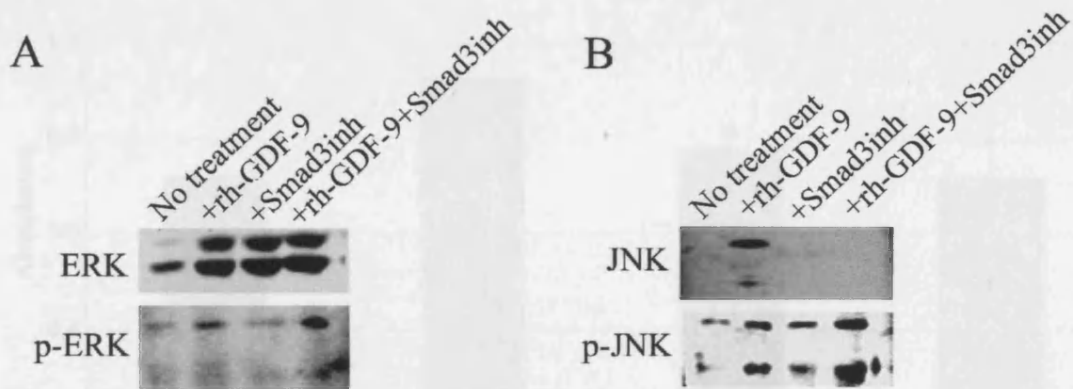
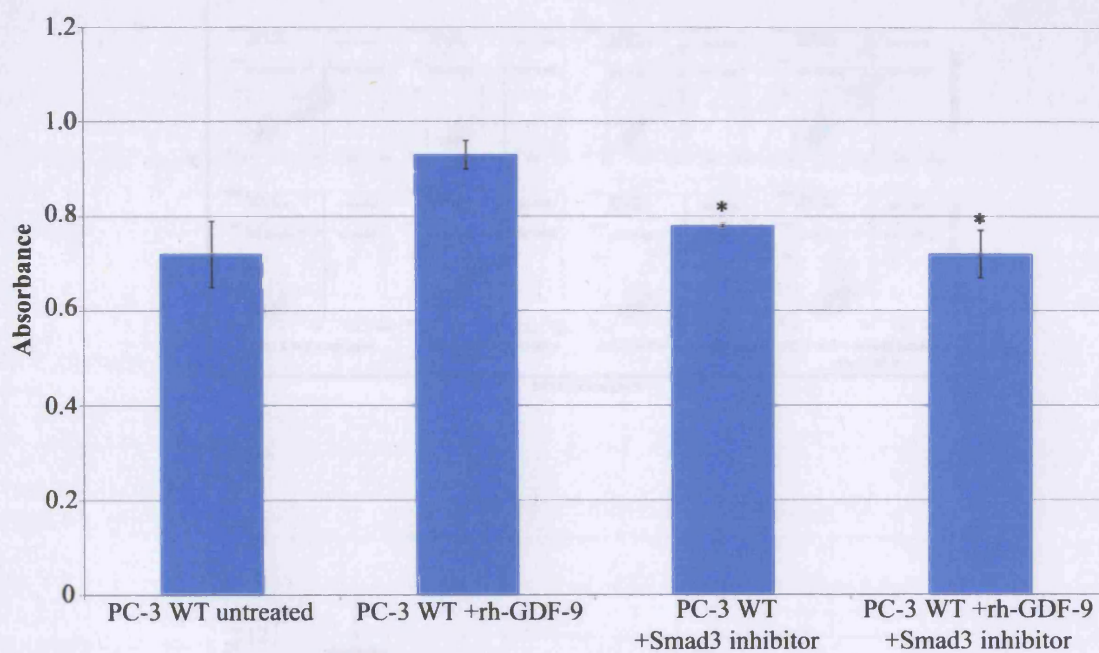


Figure 6.8: GDF-9 signalling via MAPK pathway in PC-3 cells. **A.** Levels of both unactivated ERK1/2 (particularly ERK1) and activated p-ERK were increased in response to 2 hour treatment with 20ng/ml rh-GDF-9. This was not affected by 2 hours treatment with 3ng/ml Smad3 inhibitor. **B.** Both JNK and p-JNK levels were increased in response to rh-GDF-9, and while the increase in expression of p-JNK was not affected by 3ng/ml Smad3 inhibitor, levels of JNK expression were inhibited when treated with this inhibitor.



	PC-3 WT untreated (n=3)	PC-3 +rh-GDF-9 (n=3)	PC-3 +Smad3 inhibitor (n=3)	PC-3+rh-GDF-9 +Smad3 inhibitor (n=3)
Mean	0.72	0.93	0.78	0.69
SD	0.07	0.03	0.005	0.04

Figure 6.9: Growth assay showing that treatment of PC-3 cells with 3ng/ml Smad3 inhibitor alone, or in conjunction with 20ng/ml rh-GDF-9, results in an inhibition of the GDF-9 associated increased growth rate, *p<0.05 for both the Smad3 inhibitor treated cells, compared to the rh-GDF-9 treated cells. Data is representative of three independent repeats. Error bars represent standard deviation.

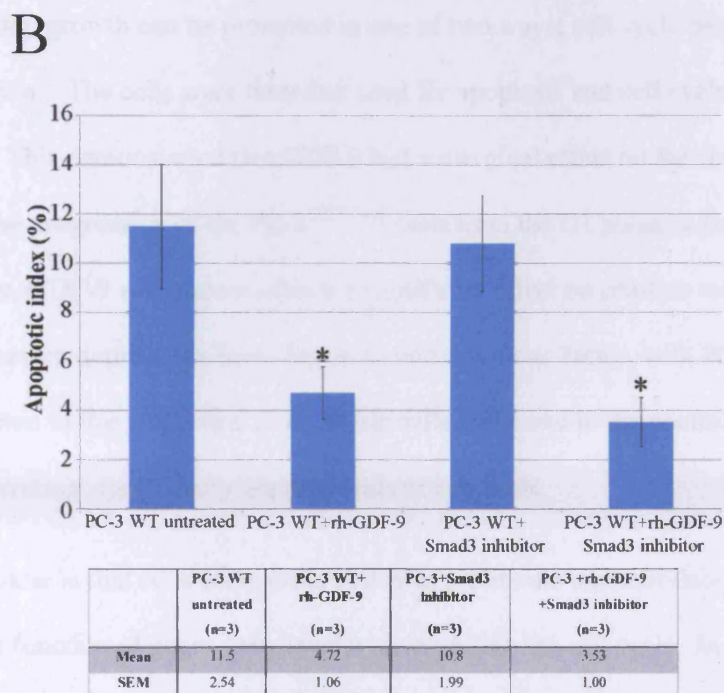
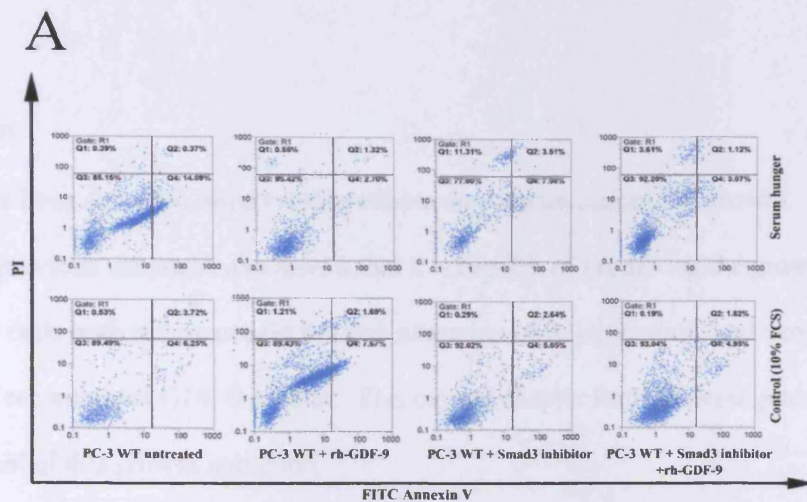


Figure 6.10: Role of Smad3 in GDF-9 associated apoptosis. The cells treated with both 3ng/ml Smad3 inhibitor and 20ng/ml rh-GDF-9 demonstrated similar apoptotic levels to those cells treated with rh-GDF-9 alone suggesting that the anti-apoptotic effect of GDF-9 is Smad3 independent, $p=0.722$ for untreated cells compared to Smad3 inhibitor treated cells, and $*p=0.005$ compared to Smad3 inhibitor and rh-GDF-9 treated cells. Meanwhile, $*p=0.01$ for Smad3 inhibitor treated cells compared to the dual treated cells and $*p=0.037$ for untreated cells compared to rh-GDF-9 treatment alone. **A.** Data shown demonstrates representative data of three independent repeats. **B.** Bar graph demonstrates the mean apoptotic percentage of three independent repeats. Error bars represent standard error of mean. Apoptotic index refers to total apoptotic population including both early apoptotic cells (Q4) and late apoptotic cells (Q2).

6.4 Discussion

The BMPs have been shown to have varying effects on prostate cancer cell growth. In the case of GDF-9, the previous chapters have shown that it is capable of promoting the growth of prostate cancer cells both endogenously through alteration of its expression, and exogenously with the use of recombinant GDF-9 protein. This current chapter further investigates the mechanisms behind this growth induction.

Generally speaking, growth can be promoted in one of two ways; cell cycle progression or apoptosis inhibition. The cells were therefore used for apoptosis and cell cycle analysis by flow cytometry. This demonstrated that GDF-9 had a marginal effect on the cell cycle by acting to aid in the progression of the PC-3^{GDF-9exp.} cells from the G1 phase to the G2/M phase. More importantly, GDF-9 was shown to have a significant effect on prostate cancer cell apoptosis under serum deprivation by acting as an anti-apoptotic factor, with PC-3^{GDF-9exp.} cells showing a reduction in the proportion of apoptotic cells compared to the controls, and PC-3^{GDF-9rib3} cells demonstrating significantly greater levels of apoptosis.

A hallmark of cancer is that cells acquire the ability to proliferate uncontrollably and thereby typically lose the function of genes associated with inhibiting the cell cycle. In order for cells to progress from the G1 phase and commit to the G2/M phase, they rely on the actions of cyclins which act as sensors to growth factor signals and lead to Rb phosphorylation and hence cell cycle progression (Sherr, 1996). As GDF-9 was demonstrated to have an effect on the progression into the G2/M phase, the expression of Cyclin D1 in response to GDF-9 was analysed. Carrying out a time course of rh-GDF-9 treatment on PC-3 cells led to an up-regulation of Cyclin D1 expression, both at the mRNA and protein level. However, the effect of GDF-9 on the cell cycle was only found to be marginal, insufficient to explain the significant effect that GDF-9 has on prostate cancer cell growth.

Apoptosis meanwhile, is orchestrated by a variety of molecules, including a family of cysteine proteases known as the caspases. Caspase 3 is known as an executioner caspase essential for Cytochrome C action and DNA fragmentation (Slee *et al.*, 2001). Levels of mature caspase-3 protein subunits were shown to be reduced in the PC-3^{GDF-9exp.} cells compared to the controls. In addition, protein levels of caspase-3 were gradually reduced over time when treated with rh-GDF-9, further showing a reduction in the levels of apoptosis in cells over-expressing GDF-9. This effect on apoptosis was further demonstrated using Hoechst 33342 DNA stain, where the PC-3^{GDF-9exp.} cells demonstrated significantly lower percentages of apoptotic cells compared to the control, and knock-down cells which had a much higher percentage of apoptotic cells.

In the ovary, GDF-9 has been shown to signal via ALK-5 and BMPR-II to activate Smads2 and 3 and trigger expression of its target genes (Mazerbourg *et al.*, 2004). In order to establish if this was also the case in prostate cancer cells, PC-3 cells were treated with rh-GDF-9 and analysed for pSmad3 and p-ALK-5 expression levels using both immunoprecipitation and western blot analysis. The results demonstrated an increase in the phosphorylation of both Smad3 and ALK-5 suggesting that GDF-9 uses a similar pathway in prostate cancer cells as it does in the ovary. Furthermore, p-ALK-5 levels were shown to be downregulated in response to the Smad3 inhibitor, suggesting that perhaps ALK-5 activation is dependent on Smad3. This positive form of regulation has been previously shown in TGF- β signalling (Miyazono, 2000). Unfortunately due to the lack of specificity of the anti-BMPR-II antibody, the type-II receptor for GDF-9 was not able to be determined in this study.

Apart from Smad-dependent signalling, BMPs are known to signal via a Smad-independent MAPK pathway. GDF-9 was found to be no exception as cells treated with rh-GDF-9 demonstrated increased levels of un-phosphorylated ERK and JNK, as well as p-ERK and p-JNK. Whereas JNK up-regulation was found to possibly be Smad3 dependent (needs further investigation), ERK, p-ERK, and p-JNK were not affected by the Smad3 inhibitor suggesting that while JNK and ERK may be GDF-9 target genes one Smad dependent and the other not,

GDF-9 may also signal via these molecules in a Smad independent manner. Other studies have previously shown that cross talk between the JNK and the Smad dependent pathway is interdependent. For example, primary rapid activation of JNK by TGF- β 1 was demonstrated to be Smad independent, but the secondary more sustained JNK response was Smad dependent. Both of these pathways were shown to require Rho GTPase (Engel *et al.*, 1999). This suggests that it is possible for Smad3 to up-regulate levels of JNK, as shown in this study.

Furthermore, treating PC-3 WT cells with Smad3 inhibitor not only prevented pSmad3 up-regulation, it also led to an inhibition of GDF-9 associated promoted cell growth suggesting that GDF-9 signals via Smad3 to induce cell growth of prostate cancer cells. However, when the cells were analysed for apoptosis using flow cytometry, the Smad3 inhibitor had no effect suggesting that GDF-9 protects cells from apoptosis in a Smad3 independent manner, but that it may signal via Smad3 to promote the cell cycle via Cyclin D1 up-regulation. All in all, these results suggest that GDF-9 may act as an anti-apoptotic factor to promote the growth and survival of prostate cancer via the ERK and JNK pathway in a Smad-independent pathway, while acting to promote the proliferation through regulation of cell cycle via Cyclin D1 in a Smad-dependent manner.

Chapter 7

**GDF-9 promotes cell-matrix
adhesion, invasion, and motility of
prostate cancer cells by regulating
adhesion and EMT molecules**

7.1 Introduction

As previously demonstrated in chapter 4, GDF-9 can promote the adhesive, invasive, and motile capacity of prostate cancer cells. These cellular properties are all vital for tumour growth and aid in their progression and metastasis. As cells become more invasive, the tumour cells lose cell-cell adhesiveness while gaining mobility, allowing them to leave the primary tumour site and invade into adjacent tissues.

Following intravasation and survival in the blood stream, the cells extravasate at distant sites, leaving the blood stream. Here they undergo a process known as epithelial-mesenchymal transition (EMT), an important mechanism in the early stages of metastasis where epithelial cells become more fibroblastic in nature and exhibit reduced intercellular adhesion and increased motility (Thiery, 2002).

Several BMPs, including BMP-2 and BMP-7 have been shown to control motility and invasiveness of prostate cancer cells (Ye *et al.*, 2007; Lai *et al.*, 2008). BMP-4 meanwhile has been reported to induce EMT and hence motility of ovarian cancer cells (Theriault *et al.*, 2007). There are several molecules that have been implicated in the control of these processes including known BMP target genes which may help explain their effects on these processes. This chapter therefore focuses on the mechanisms behind the capability of GDF-9 to promote prostate cancer cell motility and invasiveness by investigating expression levels of genes associated with both motility and EMT. These results will help clarify the role of GDF-9 in prostate cancer progression and motility.

7.2 Materials and methods

7.2.1 Analysing expression levels of target molecules using RT and Q-PCR

PC-3 WT cells were treated with 20ng/ml rh-GDF-9 for varying amounts of time, alone or along with 3ng/ml Smad3 inhibitor, for 0, 30 minutes, and 1, 2, and 24 hours, respectively. RNA was isolated from both of these cells and the stable transfectants, before being used as a

template for both Q-PCR and RT-PCR using specific primers for FAK, paxillin, RhoC, SNAI1, N-cadherin, E-cadherin, and ROCK-1. Refer to section 2.4 for further details.

7.2.2 Analysing protein levels of focal adhesion and EMT associated molecules using western blotting

PC-3 WT cells were treated with a time course of 20ng/ml rh-GDF-9 for 0, 1, 2, 4, and 24 hours, respectively, before protein was extracted. In addition, protein was extracted from PC-3 WT cells treated with 20ng/ml rh-GDF-9 alone or in conjunction with 3ng/ml Smad3 inhibitor for a period of 2 hours. Equal concentrations of the protein samples were then run on an SDS-PAGE and blotted using anti-FAK, anti-Paxillin, anti-p-FAK, anti-p-paxillin, anti-E-Cadherin, anti-SNAI1, and anti-RhoC antibodies.

7.2.3 Immuno-cytochemical staining of FAK and paxillin

Immuno-cytochemical staining of FAK and paxillin in PC-3 cells was carried out using specific primary antibody for the proteins, followed by HRP conjugated secondary antibody, ABC complex, and DAB. The cells were counterstained with Haematoxylin. For detailed ICC procedure refer to section 2.5.9.

7.2.4 Immuno-flourescent staining for RhoC and SNAI1 in GDF-9 transfected cells

The cells were incubated for an hour with anti-RhoC and anti-SNAI1 primary antibody, before the primary antibody was washed off and replaced with FITC labelled secondary antibody. The cells were then viewed using a fluorescent microscope. Refer to section 2.5.10 for further details.

7.2.5 Adhesion assay using Smad3 inhibitor and rh-GDF-9

PC-3 WT cells were treated with 20ng/ml rh-GDF-9 either alone, or in conjunction with 3ng/ml Smad3 inhibitor for 40 minutes, while allowing them to adhere to matrigel before they were stained with crystal violet, and counted.

7.3 Results

7.3.1 The effect of endogenous GDF-9 on FAK and paxillin expression

As shown in the previous chapters, GDF-9 can promote the adhesive, motile, and invasive capacity of prostate cancer cells. Therefore, with the intention of determining a mechanism by which GDF-9 can exert these effects, the expression levels of well-established adhesion molecules FAK and paxillin were analysed at both the mRNA and protein level. PC-3^{GDF-9exp.} cells demonstrated increased expression of FAK and paxillin compared to the two controls, both at the mRNA level using PCR, and at the protein level where enhanced staining for both FAK and paxillin was demonstrated using ICC staining (Figure 7.1 and 7.2). In addition, PC-3^{GDF-9rib3} cells had similar mRNA levels of both molecules to the controls, suggesting that GDF-9 is capable of up-regulating expression of these molecules. Furthermore, DU-145^{GDF-9rib3} cells demonstrated decreased expression of FAK and paxillin compared to the controls (Figure 7.1B and D). Due to the large amount of molecules that were screened, only DU-145^{GDF-9rib3} and PC-3^{GDF-9rib3} were used as they were found to express the lowest levels of GDF-9.

7.3.2 Effect of rh-GDF-9 on expression of FAK and paxillin

To further confirm this hypothesis, PC-3 WT cells were treated with rh-GDF-9 for varying amounts of time to see if exogenous GDF-9 would have a similar effect on FAK and paxillin expression. Protein and mRNA was extracted from these cells, and using PCR and western blot analysis, expression levels of FAK and paxillin were analysed. Levels of FAK and paxillin mRNA were increased after only half an hour of treatment with rh-GDF-9 compared to the untreated controls (Figure 7.3A). This was further confirmed using Q-PCR where the mRNA levels of both molecules were quantified. The transcript levels of FAK were increased after 24 hours ($2.60 \times 10^{11} \pm 1.09 \times 10^{11}$) of treatment with rh-GDF-9 compared to the untreated control ($1.38 \times 10^{10} \pm 2.76 \times 10^{11}$), $p=0.07$. The same effect was seen on paxillin mRNA levels where

the levels at 24 hours ($5.30 \times 10^{11} \pm 2.10 \times 10^{11}$) were higher compared to the untreated control ($9.51 \times 10^{11} \pm 2.82 \times 10^{11}$), $p=0.26$.

In the case of protein levels, expression of paxillin was only increased after 4 hours treatment, and that of FAK only after 24 hours (Figure 7.3B). Furthermore, protein levels of phosphorylated and hence activated FAK and paxillin (p-FAK and p-paxillin), were analysed in order to determine whether GDF-9 not only up-regulates but also activates these molecules. Indeed, levels of p-FAK and p-paxillin were up-regulated at earlier time points than their non-phosphorylated counterparts, compared to the untreated controls.

7.3.3 Smad3 and its role in GDF-9 associated adhesion

As the previous results demonstrate, GDF-9 downstream signalling involves the Smad-dependent pathway via Smad3, which it uses in order to exert its effects. The Smad3 inhibitor used in the previous chapter was used to treat PC-3 WT cells that were to be used in an adhesion assay, in order to determine whether GDF-9 signals via Smad3 to induce cell adhesion. The cells treated with Smad3 inhibitor along with rh-GDF-9 (33.1 ± 7.18) resulted in inhibition of the previously seen GDF-9 associated increase in cellular adhesion (86.9 ± 4.76), suggesting that GDF-9 signals via Smad3 to exert its effects on prostate cancer cell adhesion, $p=0.002$ compared to PC-3 WT treated with rh-GDF-9, and $p=0.027$ compared to untreated control (Figure 7.5).

7.3.4 Smad3 and GDF-9 target gene expression

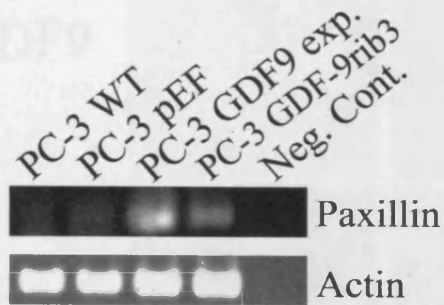
Furthermore, in order to establish whether GDF-9 up-regulation of adhesion molecules FAK and paxillin is due to Smad3 signalling, and thereby associated with prostate cancer cell adhesion, PC-3 cells were treated with either 20ng/ml rh-GDF-9, 3ng/ml Smad3 inhibitor, or both 20ng/ml rh-GDF-9 and 3ng/ml Smad3 inhibitor, respectively, for a time period of 2 hours.

FAK and paxillin mRNA levels were analysed using both normal and Q-PCR, and protein levels were analysed using western blotting. The results of the RT-PCR and western blot showed that rh-GDF-9 mediated upregulation of FAK and paxillin mRNA and protein levels, that were inhibited in the presence of Smad3 inhibitor, suggesting that they are both Smad3 gene targets (Figure 7.6).

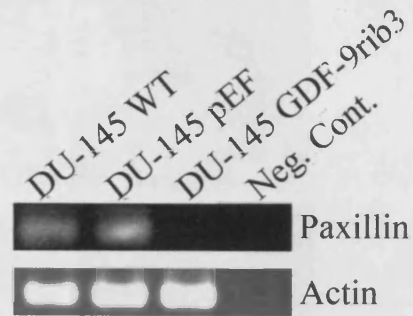
Furthermore, the Q-PCR results demonstrated that when the PC-3 cells were treated with rh-GDF-9 alone, transcript levels of FAK ($7.7 \times 10^4 \pm 1.04 \times 10^4$) and paxillin ($1.60 \times 10^7 \pm 2.15 \times 10^6$) were increased when compared to the untreated controls. However, this up-regulation in FAK and paxillin transcript levels, was inhibited when PC-3 cells were treated with the Smad3 inhibitor, $p=0.18$ for FAK transcripts ($4.40 \times 10^3 \pm 5.30 \times 10^2$) and $p=0.43$ for paxillin transcripts ($5.63 \times 10^5 \pm 1.40 \times 10^5$) compared to the rh-GDF-9 treated cells.

These levels were similar to those seen in the untreated control for FAK ($2.72 \times 10^3 \pm 0.45$) and paxillin ($1.75 \times 10^6 \pm 5.86 \times 10^6$). In addition, when these cells were treated with both the Smad3 inhibitor and rh-GDF-9, FAK ($4.52 \times 10^3 \pm 3.66 \times 10^3$) and paxillin ($2.62 \times 10^5 \pm 2.95 \times 10^4$) levels remained low, $p=0.08$ for FAK and $p=0.43$ for paxillin compared to cells treated with rh-GDF-9 alone (figure 7.7). This suggests that GDF-9 signals via Smad3 to up-regulate expression of these adhesion molecules.

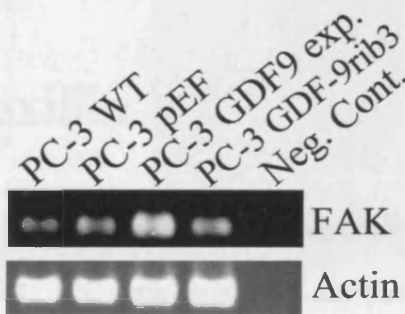
A



B



C



D

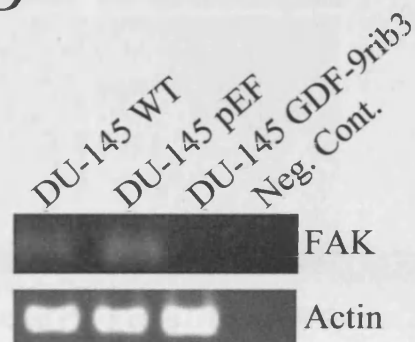


Figure 7.1: Expression of FAK and paxillin in transfected prostate cancer cells using PCR. The expression of **A.** paxillin and **C.** FAK was increased in the PC-3^{GDF-9exp.} cells compared to the controls and PC-3^{GDF-9rib3} cells. The mRNA levels of **B.** paxillin and **D.** FAK were reduced in the DU-145^{GDF-9rib3} cells compared to the controls. Only DU-145^{GDF-9rib3} and PC-3^{GDF-9rib3} are analysed for their expression of FAK and paxillin as they were shown to have the lowest expression levels of GDF-9.

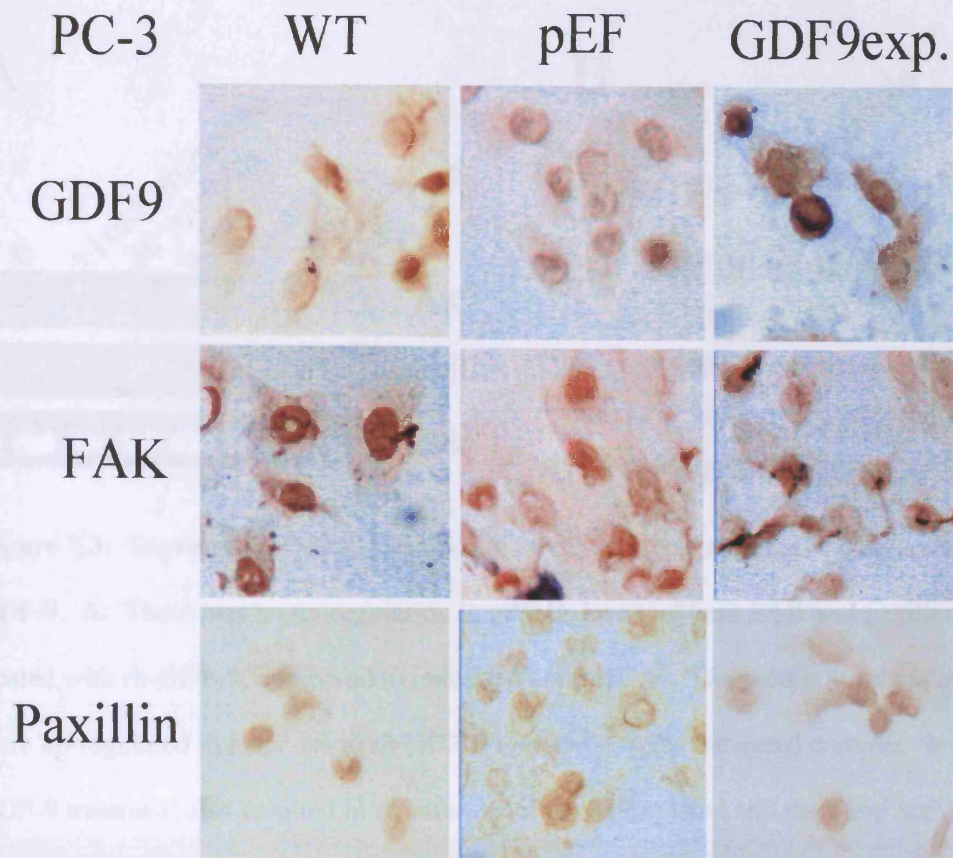


Figure 7.2: ICC staining of FAK and paxillin in transfected PC-3 cells. The GDF-9 overexpressing PC-3 cells were treated with anti-FAK and anti-paxillin primary antibodies, followed by treatment with the corresponding HRP-conjugated secondary antibodies, ABC complex, and DAB chromagen. The cell nuclei were then counterstained with Haematoxylin. The cytoplasmic staining for FAK and paxillin was enhanced in the PC-3^{GDF-9exp.} cells compared to the controls which showed weak staining for both proteins.

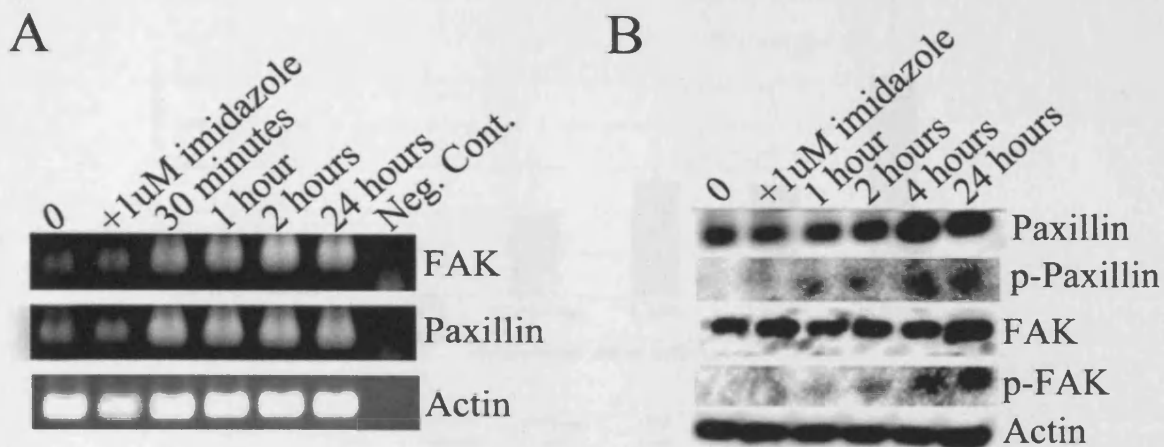
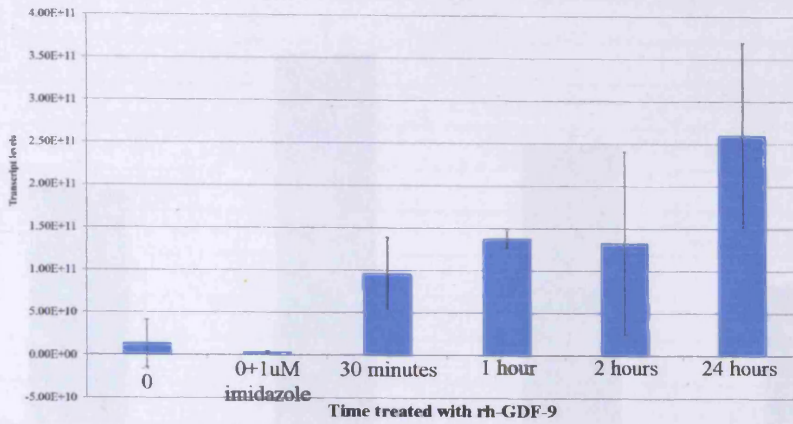


Figure 7.3: Expression of FAK and paxillin in PC-3 cells in response to 2 hours treatment with rh-GDF-9. **A.** There was an up-regulation in mRNA levels of both FAK and paxillin in PC-3 cells treated with rh-GDF-9, compared to untreated controls. **B.** The protein levels of paxillin and FAK were up-regulated in response to rh-GDF-9 compared to the untreated controls. In addition, rh-GDF-9 treatment also resulted in an increase of phosphorylated and therefore active levels of FAK and paxillin (p-FAK and p-paxillin).

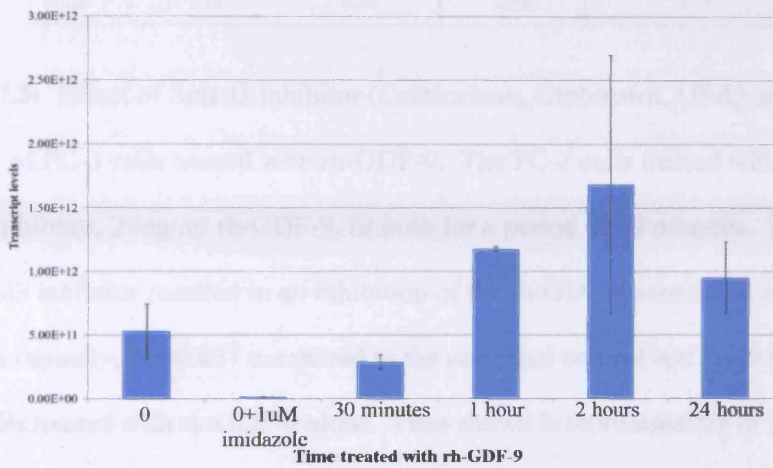
Figure 7.4. Q-PCR quantifying mRNA levels of FAK and paxillin in response to treatment with 20 ng/ml rh-GDF-9. **A.** An increase in the transcript levels of FAK was seen in the PC-3 cells treated with rh-GDF-9 compared to the untreated controls, $p < 0.07$ for the cells treated with rh-GDF-9 for 24 hours compared to untreated control. **B.** The transcript levels of paxillin were increased in PC-3 cells treated with rh-GDF-9 compared to the untreated controls, $p < 0.26$ for the cells treated with rh-GDF-9 for 24 hours compared to untreated control. Data shown is representative of 3 independent repeats. Error bars represent standard deviation.

A



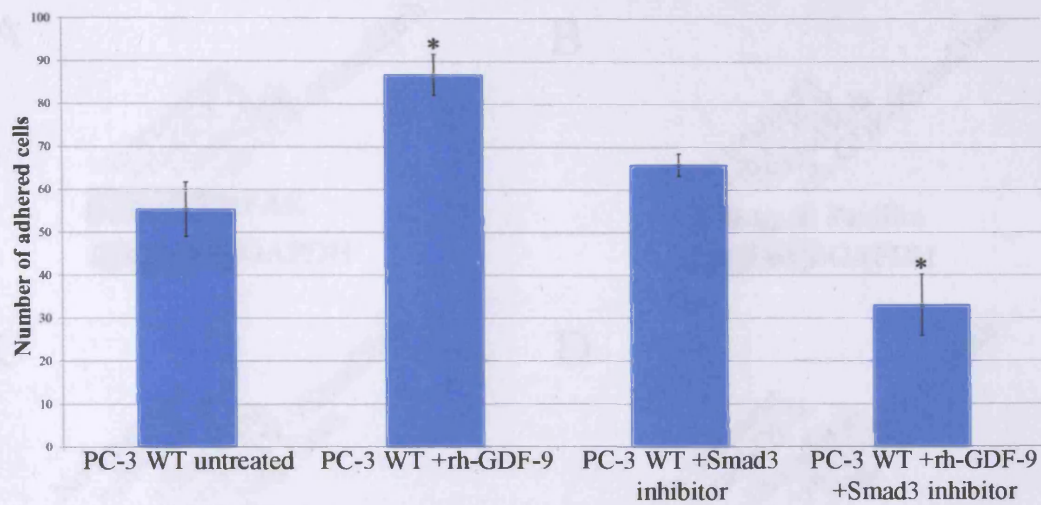
	0 (n=3)	0+1uM imidazole (n=3)	30 minutes (n=3)	1 hour (n=3)	2 hours (n=3)	24 hours (n=3)
Mean	1.38x10 ¹⁰	3.65x10 ⁹	9.60x10 ¹⁰	1.38x10 ¹¹	1.35x10 ¹¹	2.60x10 ¹¹
SD	2.76x10 ¹⁰	8.89x10 ⁹	4.24x10 ¹⁰	1.06x10 ¹¹	1.06x10 ¹⁰	1.09x10 ¹¹

B



	0 (n=3)	0+1uM imidazole (n=3)	30 minutes (n=3)	1 hour (n=3)	2 hours (n=3)	24 hours (n=3)
Mean	5.31x10 ¹¹	1.48x10 ⁹	2.88x10 ¹⁰	1.18x10 ¹²	1.68x10 ¹²	9.31x10 ¹¹
SD	2.76x10 ¹⁰	8.89x10 ⁹	4.24x10 ¹⁰	1.06x10 ¹⁰	1.01x10 ¹²	2.92x10 ¹¹

Figure 7.4: Q-PCR quantifying mRNA levels of FAK and paxillin in response to treatment with 20ng/ml rh-GDF-9. **A.** An increase in the transcript levels of FAK was seen in the PC-3 cells treated with rh-GDF-9 compared to the untreated controls, $p=0.07$ for the cells treated with rh-GDF-9 for 24 hours compared to untreated control. **B.** Transcript levels of paxillin were increased in PC-3 cells treated with rh-GDF-9 compared to the untreated controls, $p=0.26$ for the cells treated with rh-GDF-9 for 24 hours compared to untreated control. Data shown is representative of 3 independent repeats. Error bars represent standard deviation.



	PC-3 WT untreated (n=3)	PC-3 +rh-GDF-9 (n=3)	PC-3 +Smad3 inhibitor (n=3)	PC-3+rh-GDF-9 +Smad3 inhibitor (n=3)
Mean	55.4	86.9	65.9	33.1
SD	6.35	4.76	2.59	7.18

Figure 7.5: Effect of Smad3 inhibitor (Calbiochem, Gibbstown, USA) on the adhesive capacity of PC-3 cells treated with rh-GDF-9. The PC-3 cells treated with either 3ng/ml Smad3 inhibitor, 20ng/ml rh-GDF-9, or both for a period of 40 minutes. Treatment with the Smad3 inhibitor resulted in an inhibition of the rh-GDF-9 associated enhanced adhesive capacity, *p=0.027 compared to the untreated control and *p=0.002 compared to PC-3 cells treated with rh-GDF-9 alone. Data shown is representative of 3 independent repeats. Error bars represent standard deviation.

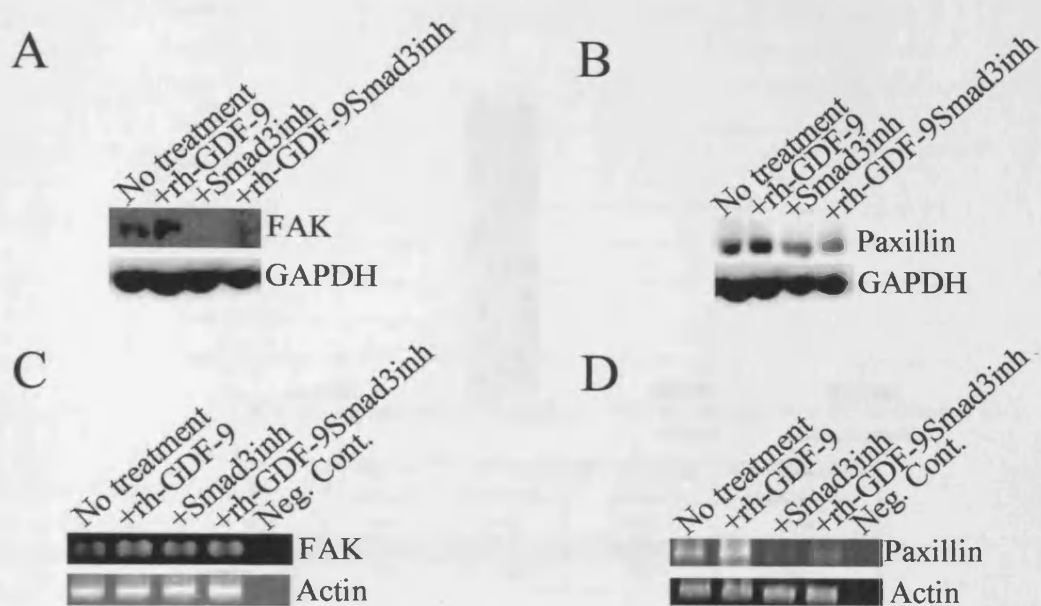


Figure 7.6: PC-3^{WT} cells were treated either with 3ng/ml Smad3 inhibitor (Calbiochem, Gibbstown, USA), 20ng/ml rh-GDF-9, or both for a period of two hours before carrying out PCR and western blotting using FAK and paxillin specific primers and antibodies. Treatment of PC-3 cells with 3ng/ml Smad3 inhibitor resulted in an inhibition in expression levels of rh-GDF-9 associated up-regulation of **A.** FAK and **B.** paxillin expression using western blot analysis. **C.** and **D.** demonstrate the same effect but in FAK and paxillin mRNA levels, using PCR.

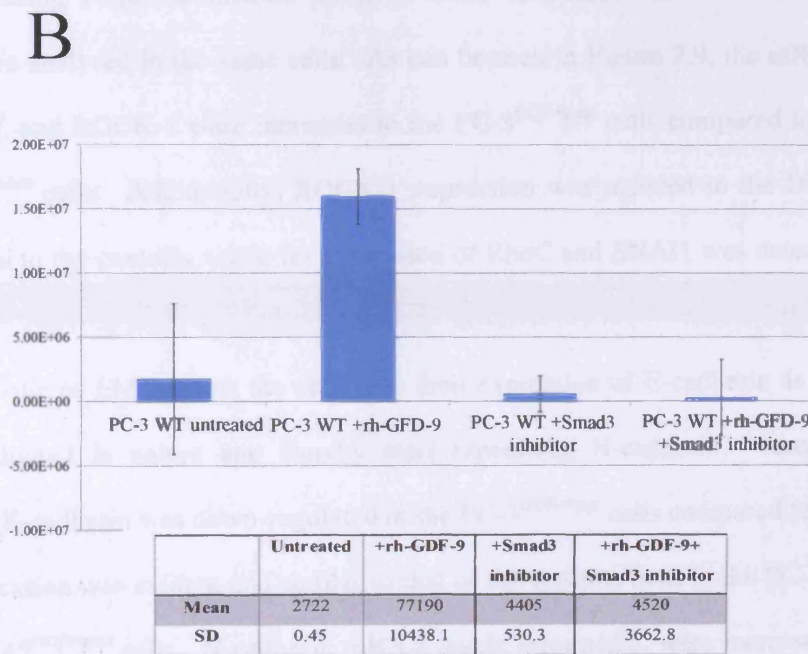
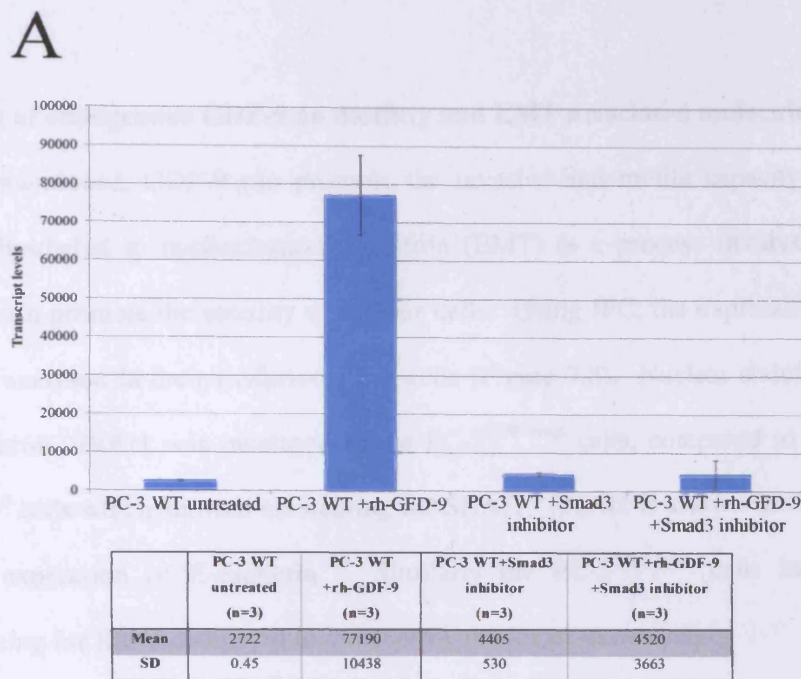


Figure 7.7: Q-PCR demonstrating quantification of FAK and paxillin mRNA levels in response to 2 hour treatment with Smad3 inhibitor. The cells treated with 3ng/ml Smad3 inhibitor alone and along with 20ng/ml rh-GDF-9 demonstrated reduced levels of **A.** FAK, $p=0.18$ for cells treated with Smad3 inhibitor alone, and $p=0.08$ for cells treated with Smad3 inhibitor and rh-GDF-9 compared to those treated with rh-GDF-9 alone. **B.** The same was true for the expression of paxillin, $p=0.43$ for cells treated with Smad3 inhibitor alone and along with rh-GDF-9, compared to those treated with rh-GDF-9 alone. Data shown is representative of 3 independent repeats. Error bars represent standard deviation.

7.3.4 The effect of endogenous GDF-9 on motility and EMT associated molecules

As previously mentioned, GDF-9 can promote the invasive and motile capacity of prostate cancer cells. Epithelial to mesenchymal transition (EMT) is a process involved in cancer metastasis that can promote the motility of tumour cells. Using IFC, the expression of SNAI1 and RhoC was analysed in the transfected PC-3 cells (Figure 7.8). Nuclear staining for EMT associated molecule SNAI1 was increased in the PC-3^{GDF-9exp.} cells, compared to the controls and PC-3^{GDF-9rib3} cells which showed no staining for SNAI1. SNAI1 is known for its inhibitory effect on the expression of E-cadherin. Similarly the PC-3^{GDF-9exp.} cells had increased membrane staining for RhoC compared to the control and knock-down cells.

Furthermore, using PCR, the mRNA levels of these molecules and other EMT associated molecules were analysed in the same cells. As can be seen in Figure 7.9, the mRNA levels of RhoC, SNAI1, and ROCK-1 were increased in the PC-3^{GDF-9exp.} cells compared to the controls and PC-3^{GDF-9rib3} cells. Additionally, ROCK-1 expression was reduced in the DU-145^{GDF-9rib3} cells compared to the controls, while no expression of RhoC and SNAI1 was detectable in DU-145 cells.

One characteristic of EMT is that the cells lose their expression of E-cadherin as they become more mesenchymal in nature and thereby start expressing N-cadherin. Accordingly, the expression of E-cadherin was down-regulated in the PC-3^{GDF-9exp.} cells compared to the controls, while its expression was evident and similar to that of the controls both in the PC-3^{GDF-9rib3} cells and the DU-145^{GDF-9rib3} cells. N-cadherin mRNA levels meanwhile, were increased in the PC-3^{GDF-9exp.} cells compared to the controls which had low levels of N-cadherin, and the knock-down cells which showed no expression. Meanwhile, no expression of N-cadherin was detected in the DU-145 cells (Figure 7.10).

7.3.5 The effect of rh-GDF-9 on motility and EMT associated molecules

In order to further confirm the role of GDF-9 on these molecules, PC-3 WT cells were treated with 20ng/ml rh-GDF-9 for varying amounts of time, and both normal and Q-PCR were used to

analyse their expression levels. Treating the cells with rh-GDF-9 resulted in an up-regulation of the mRNA levels of N-Cadherin, SNAI1, TWIST, ROCK-1, and RhoC compared to the untreated controls, while levels of E-cadherin and SLUG remained relatively unchanged in response to rh-GDF-9 treatment (Figure 7.11). Protein levels of RhoC and SNAI1 meanwhile, were also shown to be up-regulated in response to rh-GDF-9, while E-cadherin levels were reduced compared to the untreated controls (Figure 7.16).

Q-PCR analysis meanwhile, allowed for these mRNA levels to be quantified. Both ROCK-1 and RhoC are molecules associated with cellular migration and motility and are frequently over-expressed in cancers. In the case of PC-3 cells treated with rh-GDF-9, levels of ROCK-1 were up-regulated after about 24 hours ($1.42 \times 10^9 \pm 1.82 \times 10^8$), compared to the untreated control ($2.97 \times 10^7 \pm 7.78 \times 10^6$), $p=0.40$. The same was true for RhoC whose expression was also up-regulated in response to rh-GDF-9, except after just 30 minutes of exposure. Transcript levels of RhoC in the untreated cells were at $3.02 \times 10^6 \pm 1.81 \times 10^6$, and after 24 hours treatment with rh-GDF-9 had increased to $4.45 \times 10^6 \pm 2.86 \times 10^6$, $p=0.19$.

Furthermore, the rh-GDF-9 associated up-regulation of ROCK-1 mRNA levels ($1.19 \times 10^5 \pm 1.02 \times 10^5$) was demonstrated to be Smad3 dependent as treating these cells with Smad3 inhibitor ($1.83 \times 10^4 \pm 1.66 \times 10^4$), either alone or with rh-GDF-9 ($6.5 \times 10^3 \pm 3.56 \times 10^3$), resulted in an inhibition of ROCK-1 up-regulation, $p=0.28$ for cells treated with Smad3 inhibitor alone, and $p=0.33$ for cells treated with both Smad3 inhibitor and rh-GDF-9 compared to cells treated with rh-GDF-9 alone (Figure 7.13).

As previously mentioned, transcript levels of E-Cadherin in PC-3 cells were decreased in response to rh-GDF-9 after just 30 minutes of treatment. Levels of E-cadherin were $9.31 \times 10^9 \pm 3.78 \times 10^8$ in the untreated PC-3 cells and after 24 hours had reduced to $2.43 \times 10^9 \pm 2.98 \times 10^8$, $p=0.34$. Levels of N-Cadherin meanwhile began to increase after an hour of treatment with rh-GDF-9 and had reached levels of $6.57 \times 10^5 \pm 6.25 \times 10^5$ compared to the untreated control ($1.08 \times 10^4 \pm 1.69 \times 10^3$), $p=0.72$ (Figure 7.14). Finally, transcript levels of SLUG remained relatively unchanged while those of TWIST demonstrated a marginal increase

in response to rh-GDF-9, with levels after 24 hours ($6.58 \times 10^6 \pm 9.52 \times 10^5$ and $3.64 \times 10^6 \pm 5.03 \times 10^5$, respectively) being similar to those seen in the untreated cells ($6.70 \times 10^6 \pm 7.06 \times 10^5$ for SLUG and $3.44 \times 10^6 \pm 7.56 \times 10^5$ for TWIST), $p=0.78$ for SLUG and $p=0.19$ for TWIST (Figure 7.15).

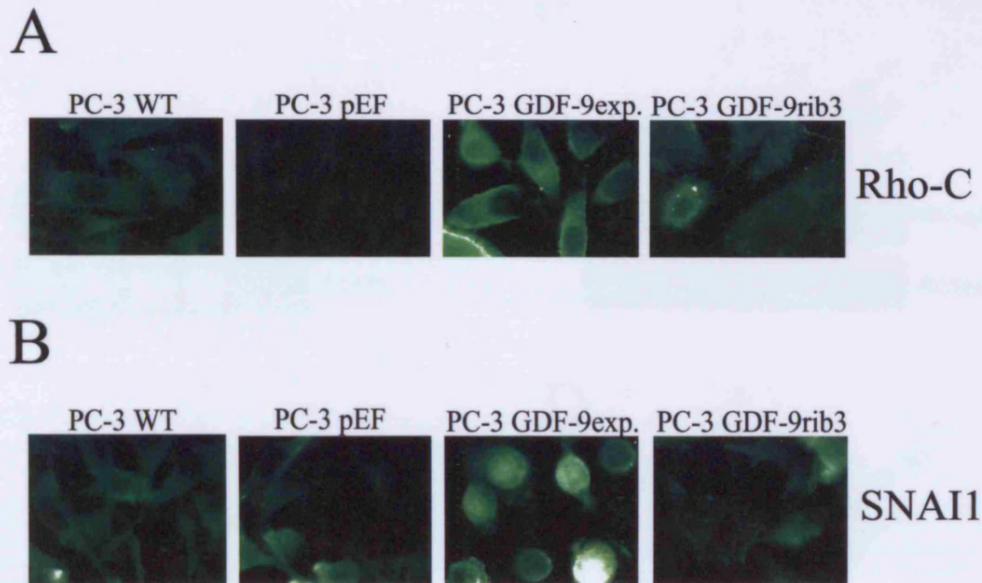


Figure 7.8: Immunofluorescent staining of EMT molecules in GDF-9 over-expressing and knock-down PC-3 cells using anti-RhoC and anti-SNAI1 antibodies. **A.** The PC-3^{GDF-9exp.} cells demonstrated enhanced peripheral staining for RhoC compared to the controls and PC-3^{GDF-9rib3} cells. **B.** The PC-3^{GDF-9exp.} cells demonstrated increased nuclear staining for SNAI1 compared to the controls and PC-3^{GDF-9rib3} cells.

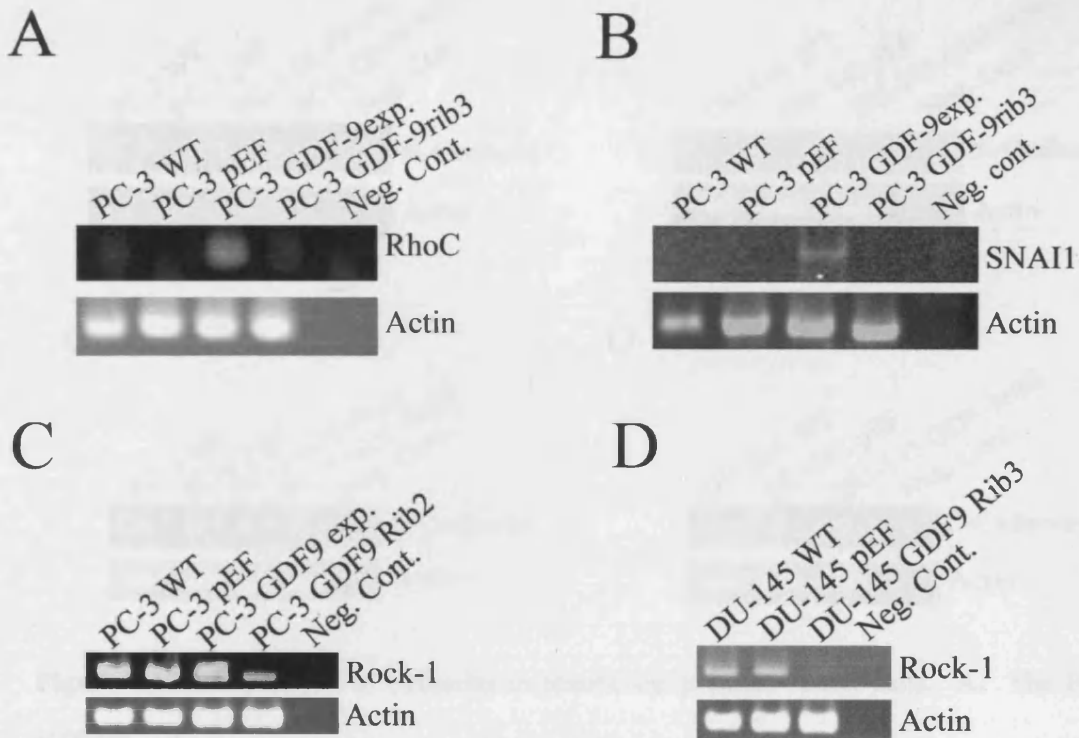


Figure 7.9: Expression of EMT molecules in transfected prostate cancer cells using PCR. The PC-3^{GDF-9exp.} cells demonstrated increased expression of **A.** RhoC and **B.** SNAI1 compared to the controls and the PC-3^{GDF-9rib3} cells. No expression of SNAI1 or RhoC was found in the DU-145 cells. **C.** The PC-3^{GDF-9exp.} cells had increased mRNA levels of ROCK-1 compared to the controls and PC-3^{GDF-9rib3} cells. **D.** The DU-145^{GDF-9rib3} cells demonstrated decreased expression of ROCK-1 compared to controls.

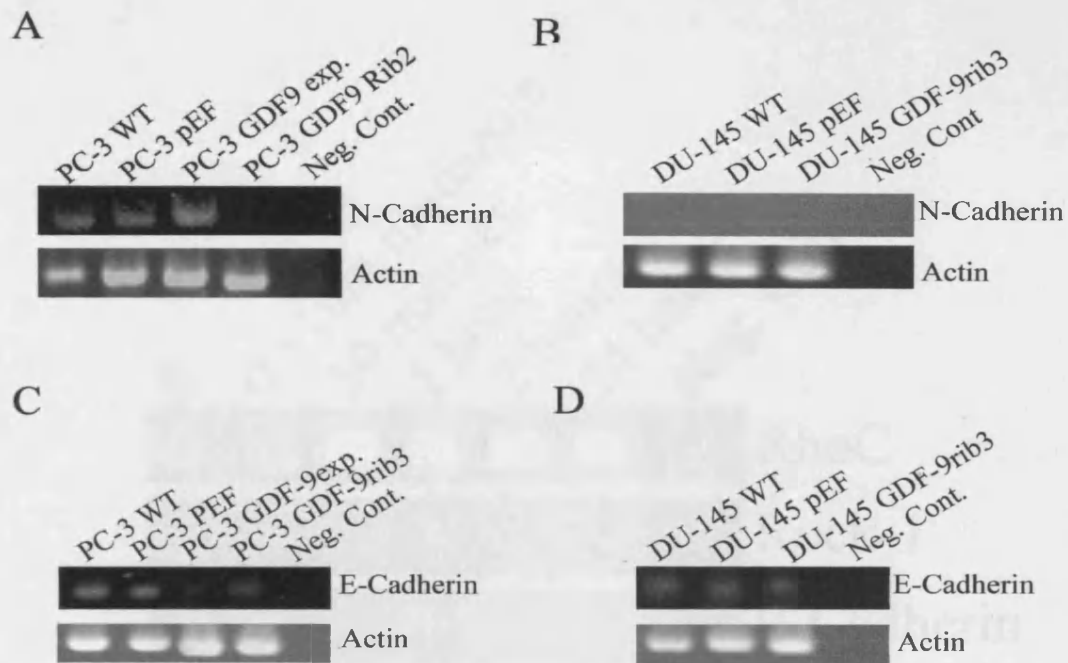


Figure 7.10: Expression of cadherins in transfected prostate cancer cells. **A.** The PC-3^{GDF-9exp.} cells demonstrated increased levels of N-cadherin compared to the controls and the PC-3^{GDF-9rib3} cells. **B.** No expression of N-cadherin was found in DU-145 cells. **C.** The PC-3^{GDF-9exp.} cells demonstrated decreased levels of E-cadherin compared to the controls and PC-3^{GDF-9rib3} cells. **D.** Decreased levels of E-cadherin were seen in the DU-145^{GDF-9rib3} cells compared to the controls.

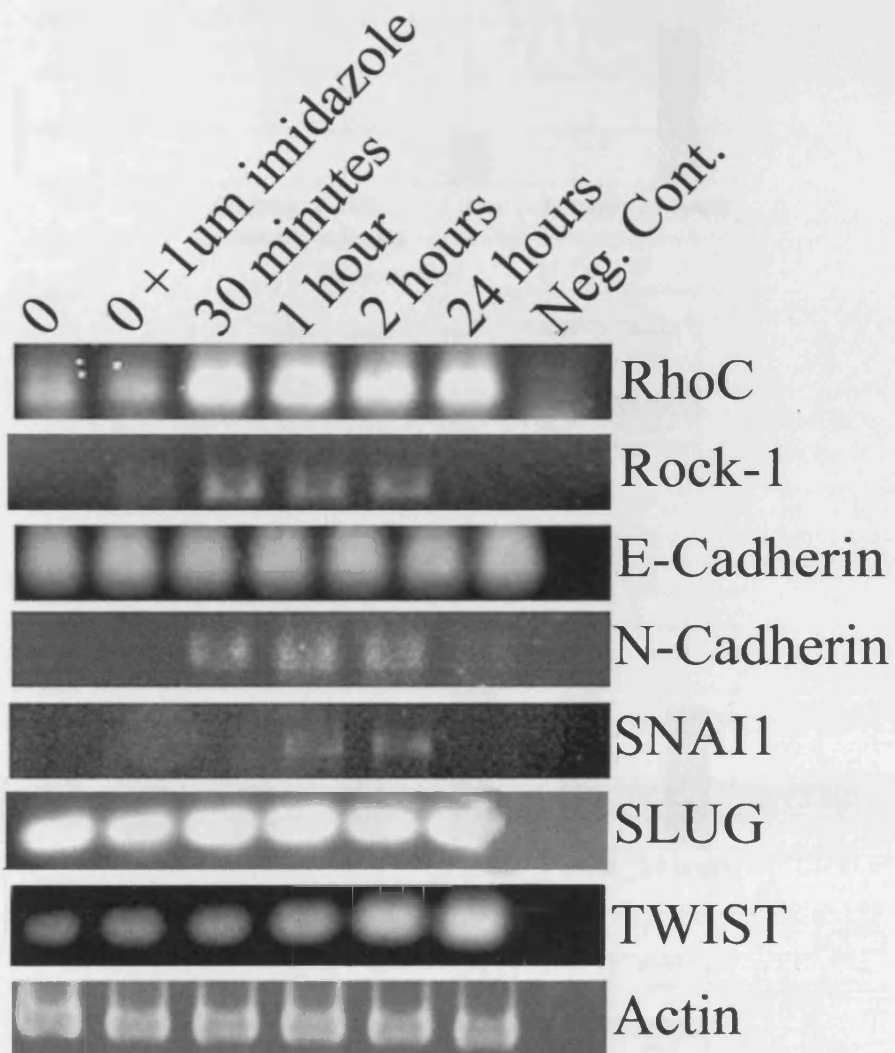
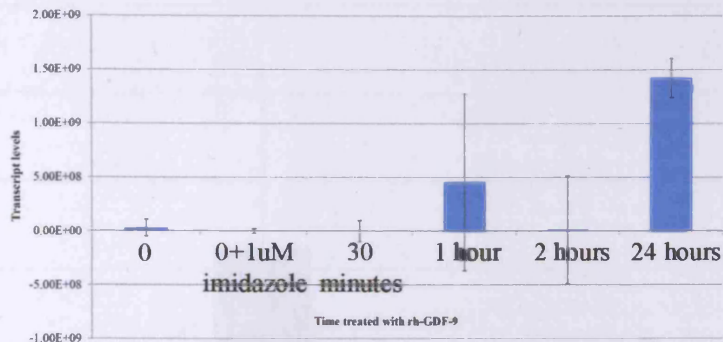


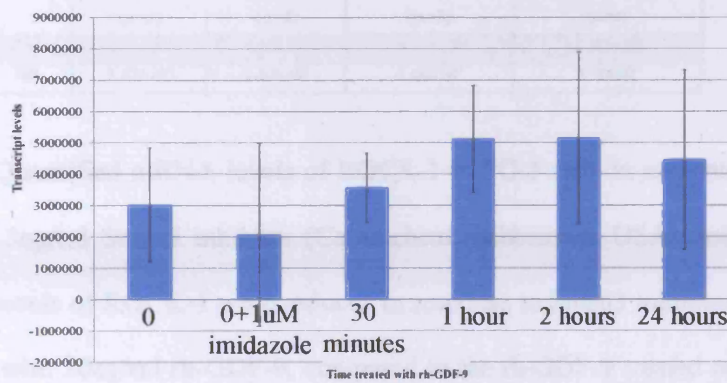
Figure 7.11: Expression of EMT associated molecules in PC-3 cells treated with a time course of 20ng/ml rh-GDF-9 using PCR. The levels of RhoC, ROCK-1, N-cadherin, SNAI1, and TWIST were increased in response to rh-GDF-9, while those of E-Cadherin and appeared to SLUG remain unchanged throughout the time course.

A



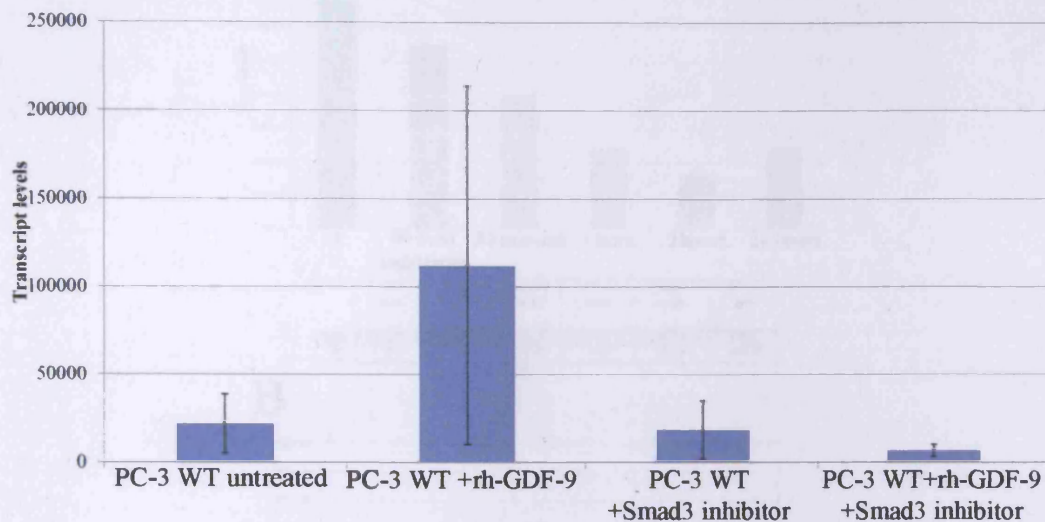
	0 (n=3)	0+1uM imidazole (n=3)	30 minutes (n=3)	1 hour (n=3)	2 hours (n=3)	24 hours (n=3)
Mean	2.97x10 ⁸	4.88x10 ⁸	7.74x10 ⁸	4.58x10 ⁸	1.18x10 ⁹	1.42x10 ⁹
SD	7.78x10 ⁸	9.79x10 ⁸	9.79x10 ⁸	8.21x10 ⁸	5.00x10 ⁸	1.82x10 ⁹

B



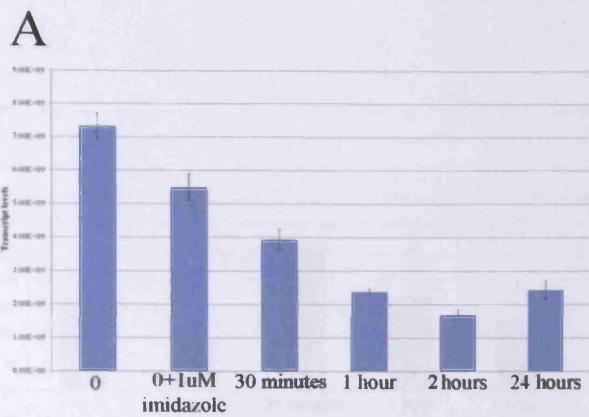
	0 (n=3)	0+1uM imidazole (n=3)	30 minutes (n=3)	1 hour (n=3)	2 hours (n=3)	24 hours (n=3)
Mean	3.02x10 ⁶	2.07x10 ⁶	3.57x10 ⁶	5.12x10 ⁶	5.18x10 ⁶	4.45x10 ⁶
SD	1.81x10 ⁶	2.92x10 ⁶	1.09x10 ⁶	1.71x10 ⁶	2.74x10 ⁶	2.86x10 ⁶

Figure 7.12: Quantified mRNA levels of ROCK-1 and RhoC in PC-3 cells treated with 20ng/ml rh-GDF-9. **A.** ROCK-1 mRNA levels were increased in response to rh-GDF-9 compared to the untreated controls, $p=0.40$ for cells treated with rh-GDF-9 for 24 hours compared to the untreated control. **B.** Expression levels of RhoC were increased in response to rh-GDF-9, $p=0.19$ for 24 hours of rh-GDF-9 treatment, compared to untreated control. Data shown is representative of 3 independent repeats. Error bars represent standard deviation.

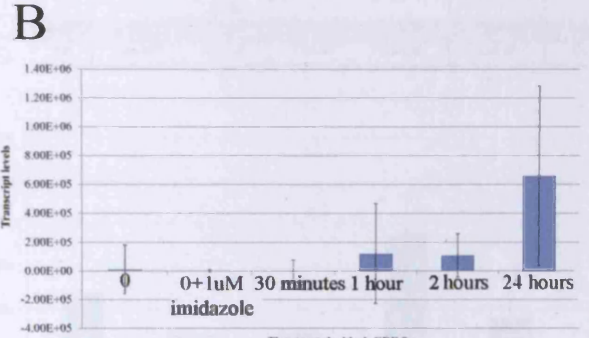


	PC-3 WT untreated (n=3)	PC-3 WT +rh-GDF-9 (n=3)	PC-3 WT+Smad3 inhibitor (n=3)	PC-3 WT+rh-GDF-9 +Smad3 inhibitor (n=3)
Mean	2.17×10^4	1.19×10^5	1.83×10^4	6.50×10^3
SD	1.67×10^4	1.02×10^5	1.66×10^4	3.50×10^3

Figure 7.13: Quantified mRNA levels of ROCK-1 in PC-3 cells in response to 2 hour treatment with 3ng/ml Smad3 inhibitor (Calbiochem, Gibbstown, USA), using Q-PCR. The transcript levels of ROCK-1 were reduced in response to Smad3 inhibitor alone, and in conjunction with 20ng/ml rh-GDF-9, compared to the rh-GDF-9 treated cells, $p=0.28$ for cells treated with Smad3 inhibitor alone, and $p=0.33$ for dual treated cells compared to rh-GDF-9 treated cells. Data shown is representative of 3 independent repeats. Error bars represent standard deviation.



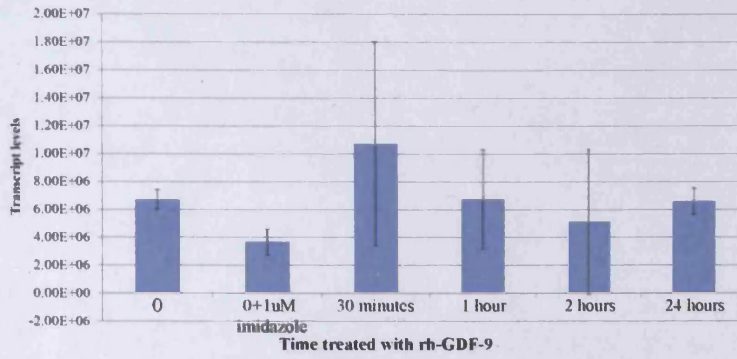
	0 (n=3)	0+1uM imidazole (n=3)	30 minutes (n=3)	1 hour (n=3)	2 hours (n=3)	24 hours (n=3)
Mean	7.51x10 ⁵	5.41x10 ⁵	3.93x10 ⁵	2.38x10 ⁵	1.69x10 ⁵	2.43x10 ⁵
SD	1.78x10 ⁴	3.91x10 ⁴	1.06x10 ⁴	7.64x10 ⁴	1.60x10 ⁴	2.98x10 ⁴



	0 (n=3)	0+1uM imidazole (n=3)	30 minutes (n=3)	1 hour (n=3)	2 hours (n=3)	24 hours (n=3)
Mean	1.08x10 ⁵	1.26x10 ⁵	1.13x10 ⁵	1.56x10 ⁵	1.08x10 ⁵	6.57x10 ⁵
SD	1.09x10 ⁴	7.53x10 ⁴	7.48x10 ⁴	3.89x10 ⁴	1.52x10 ⁴	6.25x10 ⁴

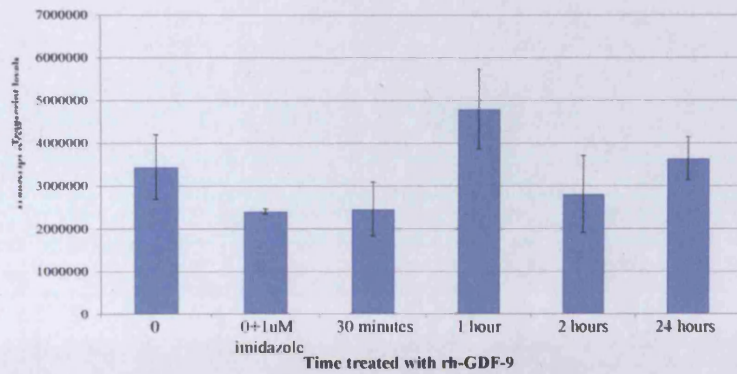
Figure 7.14: Quantified mRNA levels of E-cadherin and N-cadherin in PC-3 cells treated with a time course of 20ng/ml rh-GDF-9, using Q-PCR. **A.** E-cadherin mRNA levels were decreased in response to rh-GDF-9 compared to the untreated controls, $p=0.34$ for cells treated with rh-GDF-9 for 24 hours compared to the untreated control. **B.** Expression levels of N-Cadherin were increased in response to rh-GDF-9, $p=0.72$ for 24 hours of rh-GDF-9 treatment compared to untreated control. Data shown is representative of 3 independent repeats. Error bars represent standard deviation.

A



	0 (n=3)	0+1uM imidazole (n=3)	30 minutes (n=3)	1 hour (n=3)	2 hours (n=3)	24 hours (n=3)
Mean	6.70x10 ⁶	3.67x10 ⁶	1.07x10 ⁷	6.75x10 ⁶	5.12x10 ⁶	6.45x10 ⁶
SD	7.06x10 ⁵	9.50x10 ⁵	7.29x10 ⁵	3.56x10 ⁵	5.20x10 ⁵	9.52x10 ⁵

B



	0 (n=3)	0+1uM imidazole (n=3)	30 minutes (n=3)	1 hour (n=3)	2 hours (n=3)	24 hours (n=3)
Mean	3.44x10 ⁶	2.40x10 ⁶	2.46x10 ⁶	4.79x10 ⁶	2.80x10 ⁶	3.64x10 ⁶
SD	7.56x10 ⁵	6.09x10 ⁵	6.29x10 ⁵	9.33x10 ⁵	8.97x10 ⁵	5.03x10 ⁵

Figure 7.15: Quantified mRNA levels of SLUG and TWIST in PC-3 cells treated with a time course of 20ng/ml rh-GDF-9, using Q-PCR. **A.** SLUG mRNA levels remained relatively unchanged in response to rh-GDF-9, $p=0.78$ for cells treated with rh-GDF-9 for 24 hours compared to the untreated control. **B.** Expression levels of TWIST were relatively increased in response to rh-GDF-9, $p=0.19$ for 24 hours of rh-GDF-9 treatment compared to untreated control. Data shown is representative of 3 independent repeats. Error bars represent standard deviation.

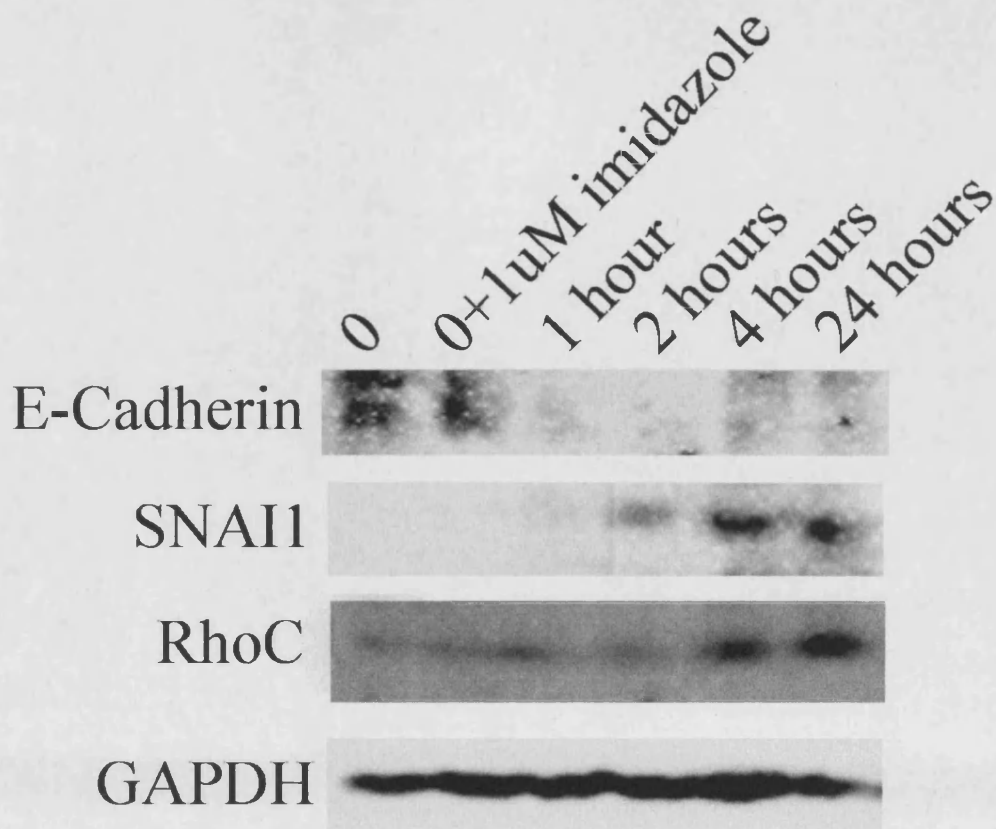


Figure 7.16: Western blot demonstrating levels of EMT associated molecules in response to a time course of 20ng/ml rh-GDF-9 in PC-3 WT cells. Protein levels of E-cadherin were reduced in response to rh-GDF-9, while SNAI1 and RhoC levels were up-regulated.

7.4 Discussion

In chapter 4, GDF-9 was demonstrated to be capable of promoting the adhesive, invasive, and motile capacity of prostate cancer cells, both endogenously and exogenously. These cellular properties are all required in order for a cancer cell to progress and thereby metastasise, and so cells either acquire mutations or over-express genes that will aid them in these processes. Several BMPs have been shown to influence cell motility and migration. Unlike GDF-9, over-expression of BMP-9 and BMP-10 in PC-3 prostate cancer cells resulted in a decrease in cell matrix adhesion, invasion, and migration (Ye *et al.*, 2008; Ye *et al.*, 2009). BMP-2 and BMP-7 meanwhile were shown to have an opposite effect on osteoblastic prostate cancer cell lines LAPC-4 and LAPC-9, where they were demonstrated to promote cell migration and invasion (Feeley *et al.*, 2005).

FAK and paxillin are focal adhesion-associated proteins that transmit signals downstream of the integrins. These downstream integrin signals are important in regulating processes such as cell adhesion, migration, and survival. Cell motility is a process involving changes in actin filament dynamics and cell adhesion sites that lead to the formation of membrane protrusions and traction forces (Brakebusch and Fassler, 2003). FAK has been shown to influence the cytoskeleton, cell adhesion structure sites, and membrane protrusions to regulate cell movement (Mitra *et al.*, 2005). Paxillin meanwhile interacts with FAK to recruit signal cascade molecules into close proximity in order to allow for efficient signal transduction (Turner, 1998).

Over-expressing GDF-9 in PC-3 cells as well as treating them with rh-GDF-9, resulted in an up-regulation of both FAK and paxillin mRNA and protein levels in a Smad3 dependent manner. Furthermore, treating the PC-3 cells with Smad3 inhibitor resulted in an inhibition of the GDF-9 associated increase in cell matrix adhesion, suggesting that GDF-9 signals via Smad3 to promote the adhesive capacity of prostate cancer cells via up-regulation of adhesion molecules FAK and paxillin, both of which appear to be GDF-9 target genes.

In addition to up-regulating FAK and paxillin, GDF-9 also appeared to increase their phosphorylation and activation. Phosphorylation of these molecules normally occurs in response to integrin mediated cell adhesion and growth factor stimulation (Turner, 1998). This suggests that GDF-9 may act as a growth factor to stimulate up-regulation and activation of FAK and paxillin, resulting in increased prostate cancer cell adhesion and motility. Another BMP that has been reported to have an effect on these molecules is BMP-7. Primary cultures of chondrocytes treated with rh-BMP-7, demonstrated up-regulated levels of FAK and paxillin expression (Vinall *et al.*, 2002). In PC-3 prostate cancer cells however, knocking out BMP-7 resulted in enhanced immuno-fluorescent staining of paxillin and FAK, and a promotion in cell matrix adhesion, invasion, and motility (Ye *et al.*, 2007).

Epithelial to mesenchymal transition (EMT) is a process involving a sequence of changes in gene-expression patterns, during which epithelial cells dissipate their epithelial features and acquire characteristics typical of mesenchymal cells. EMT has been shown to play an important role during tumour progression where the cells acquire mesenchymal cell properties in order to acquire enhanced motile and adhesive capacities, allowing them to spread and metastasise. The key changes during EMT include a loss of E-cadherin expression and an increase in expression of N-cadherin, SNAI1, SLUG (SNAI2), TWIST, vimentin, and fibronectin. Accordingly, many of these molecules have been shown to be deregulated in cancer (Thiery and Sleeman, 2006).

TGF- β 1, 2, and 3 are renowned for regulating EMT of renal tubular cells, ventricular canal cells, and mammary ductal epithelial cells, respectively (Zavadil and Bottinger, 2005). More recently, BMPs have also been associated with EMT. BMP-4 for example, was demonstrated to induce EMT in ovarian cancer cells by up-regulating SNAI1 and SLUG, and down-regulating E-cadherin, while BMP-7 was shown to reverse TGF- β 1 induced EMT by up-regulating E-cadherin in renal cells (Zeisberg *et al.*, 2003; Theriault *et al.*, 2007). These

results now show that both endogenous and exogenous GDF-9 is capable of aiding in the process of EMT by up-regulating molecules including SNAIL1, TWIST, and N-cadherin, and down-regulating E-cadherin expression. This may also help explain the positive effect of GDF-9 on prostate cancer cell adhesion, invasion, and motility.

Rho GTPases are molecular switches involved in cell motility, invasion, and survival, and their over-expression has also been associated with enhanced metastasis of several cancer types. RhoC for example has been shown to up-regulate the expression of angiogenic factors, promote cellular motility, and be vital for PC-3 cell invasion (Yao *et al.*, 2006). Rho GTPases exert their effects via their effectors Rho kinases or ROCKs, whose actions are required for assembling integrins into focal adhesions which subsequently lead to ERK and FAK activation (Hauck *et al.*, 2002).

Furthermore, both Rho GTPases and ROCKs have been associated with the onset of EMT, acting as molecular switches for EMT morphology. BMP-4 induced EMT in ovarian cancer cells for example, was shown to be Rho dependent, while ROCK1 was up-regulated at the onset of EMT in early heart development, a process dependent on TGF- β 3 and BMP-2 (Theriault *et al.*, 2007; Sakabe *et al.*, 2008). This study now shows an up-regulation of both RhoC and ROCK1 expression in PC-3 cells treated with rh-GDF-9, with ROCK-1 upregulation being Smad3 dependent. This suggests that GDF-9 may act as a growth factor to induce expression of these molecules which are in turn involved in the GDF-9 associated invasion and motility by inducing the onset of EMT leading to an up-regulation in the expression of EMT associated molecules.

However, as these results refer to only total protein levels and not phosphorylated and therefore active levels, these results are limited. It would therefore be of use to analyse levels of Rho regulators; Rho GTPase activating proteins (GAPs) and guanine nucleotide exchange factors (GEFs) in response to rh-GDF-9, as this would help determine if GDF-9 not only up-regulates Rho/ROCK levels but also results in their activation. Furthermore, LIMK1, a downstream

effector of Rho GTPases that is responsible for phosphorylating and deactivating cofilin, an actin severing and depolymerisation factor, has been shown to associate with the tail region of BMPR-II. This suggests that BMPs may work with Rho GTPases to regulate actin dynamics and the thereby associated cellular motility and migration (Foletta *et al.*,2003). It would therefore also be of interest to investigate the effect of GDF-9 on LIMK1, cofilin, and myosin light chain kinase (MLCK), an enzyme involved in actin contraction, which could help explain GDF-9 associated increased motility and invasion seen in PC-3 cells.

In conclusion, these results suggest that in prostate cancer cells, GDF-9 induced adhesion, invasion, and motility is due to a complex network of signalling molecules working together to induce the onset of EMT in a Smad-dependent manner, allowing the cancer cells to become more aggressive. However, more work is required on the role of Rhos in this process, and the associated changes in the actin cytoskeleton.

Chapter 8

General discussion

GDF-9, a member of the BMP family, is known for its role as an oocyte derived growth factor vital in early ovarian folliculogenesis and female fertility. Here its actions include regulating interactions between oocytes and their surrounding granulosa cells, follicular development, granulosa cell proliferation, and cumulus cell expansion. As its expression was initially thought to be exclusive to the ovary, it has mainly been studied in the context of female fertility (Dong *et al.*, 1996). One of these studies demonstrated that mice with the GDF-9 gene knocked-out were not only infertile, but also developed ovarian tumours (Wu *et al.*, 2004). Apart from this observation, there has been little research carried out on the role of GDF-9 in human cancers.

This laboratory recently demonstrated that highly aggressive breast cancer samples from patients with poor prognosis lacked expression of GDF-9. This was in comparison to primary breast cancer samples from patients with good predicted prognosis including those who remained disease free after a 10 year follow up, which expressed significantly higher levels. Furthermore, when GDF-9 was over-expressed in a breast cancer cell line it reduced their invasive capacity suggesting that GDF-9 acts as a tumour suppressor in breast cancer (Hanavadi *et al.*, 2007). In contrast, another group reported GDF-9 up-regulation in oral squamous carcinoma cell lines more proliferative and less apoptotic in nature, suggesting a pro-tumourigenic for GDF-9 in this cancer type (Zhuang *et al.*, 2010). Finally, human lung adenocarcinoma cells with silenced mutant P53 demonstrated with an up-regulation of GDF-9 expression suggesting that mutant P53 normally inhibits expression of GDF-9 due to its tumour suppressing role (Ma *et al.*, 2006).

Despite the abundance of literature on the role of BMPs in prostate cancer, no studies have investigated the role of GDF-9 in this prevalent cancer. Therefore, due to the well-established role of BMPs in carcinogenesis, as well as the previous success and experience of studying other BMPs in prostate cancer in this laboratory, this study aimed to determine a role for GDF-9 in prostate cancer progression and metastasis. In addition, as previous studies have suggested possible roles for GDF-9 in cancer, as well as demonstrating its anti-apoptotic and pro-

proliferative role in the ovary, suggested that GDF-9 could be an interesting candidate for prostate cancer progression.

The way we went about doing this firstly involved cloning of the coding sequence of human GDF-9 and over-expressing it in the prostate cancer cell line PC-3. This was followed by construction of ribozyme transgenes in order to knock-down its expression in both PC-3 and DU-145 cells. As GDF-9 is an oocyte growth-factor that is processed and secreted in a similar fashion to its BMP relatives, and the laboratory had previously shown GDF-9 expression in both normal and malignant prostate epithelial cells (unpublished data), it was hypothesised that prostate epithelial cells would be capable of secreting GDF-9. Therefore, by altering the endogenous expression of GDF-9 in prostate cancer cells, it was anticipated that the secretion of GDF-9 would be modified accordingly, allowing the stable transfectants to be used in functional assays in order to investigate the effect that altering GDF-9 expression would have on the biological properties of prostate cancer cells.

8.1 Effect of altering expression of GDF-9 on prostate cancer cell properties

The over-expression of GDF-9 in PC-3 cells resulted in a promotion in their growth, cell matrix adhesion, invasion, and motility compared to the controls. The opposite was observed in the GDF-9 knock-down cells, which displayed a decrease in all the aforementioned processes apart from invasion, which remained unchanged. The reason for this may be either that GDF-9 plays a less important role in prostate cancer cell invasion than it does on the other processes, or that when a gene is over-expressed in a cell it can dominate its resulting phenotype, whereas when it is silenced, other genes can take over in order to rectify the effect that its absence may have on the cell.

In order to ensure that it is actually GDF-9 exerting these effects and not some other factor that may have been altered during the incorporation of the GDF-9 plasmid into the cell genome, recombinant GDF-9 was generated using metal affinity chromatography, and used to treat the

cells before carrying out further functional assays. Treating PC-3 WT cells with rh-GDF-9 resulted in a promotion of their proliferative, adhesive, invasive, and motile capacity, further strengthening the evidence that GDF-9 itself does actually influence these processes.

8.2 Effect of GDF-9 on the cell cycle

One of the hallmarks of cancer cell progression is limitless replicative potential by being self sufficient in growth signals and insensitive to growth inhibitory signals, thereby allowing the tumour to grow and establish itself in its site of origin (Hanahan and Weinberg, 2000). Cancer cells mainly achieve this potential in one of two ways; by regulating genes involved either in the cell cycle, or those involved in apoptosis. Therefore, in order to establish a mechanism by which GDF-9 can promote prostate cancer cell growth, both the transfected cells and those treated with rh-GDF-9 underwent cell cycle and apoptotic analysis with the use of flow cytometry. In the case of the cell cycle, the PC-3^{GDF-9exp.} cells demonstrated a significant increase in the fraction of cells present in the G2/M phase compared to the controls and PC-3^{GDF-9rib3} cells suggesting that GDF-9 may promote cells into the replicative stages of mitosis, only partially explaining its positive role on prostate cancer cell growth.

During the G1 phase of the cell cycle, cells respond to growth factor stimulation, mitogens, and cyclins to either commit to further division and thereby progress to the G2/M phase, or exiting the cycle into a resting state known as the G0 phase. Cyclin D1 peaks during mid G1 phase where it binds to CDK4/6 resulting in phosphorylation and inhibition of Rb, thereby releasing the transcription factor E2F to activate the transcription of genes required for G1 to S phase transition, and hence cell cycle progression (Tashiro *et al.*, 2007). Furthermore, Cyclin D1 has been shown to have oncogenic potential and is often over-expressed in lymphomas and thyroid cancers. Tumour cells that overexpress Cyclin D1 overcome the G1/S checkpoint as it competes with CDK inhibitor P16 for CDK4 binding, resulting in cell cycle progression despite DNA damage. Its oncogenic effects include VEGF production, promotion of anchorage-

independent growth, and resistance to chemotherapeutic agents by protecting cells from Fas induced apoptosis (Shintani *et al.*, 2002).

As GDF-9 was shown to promote cells into the G2/M phase of the cell cycle, PC-3 cells were treated with rh-GDF-9 in order to determine its effect on Cyclin D1 expression. This resulted in an increase of both the mRNA and protein levels of Cyclin D1, compared to the untreated control, suggesting that GDF-9 may promote cell cycle progression by up-regulation of Cyclin D1, which may further aid in prostate cancer cell progression. These results are in line with previous reports which demonstrated that GDF-9 promotes the proliferation of human granulosa cells by enhancing cell transition from G1 to S and G2/M phases, by up-regulating expression of cyclins D1 and E, decreasing expression of CDK inhibitors P15 and P16, and activating Rb, via both Smad-dependent and Smad-independent pathways (Huang *et al.*, 2009). In contrast, most other BMPs have been shown to have inhibitory effects on the cell cycle, with BMP-2 stimulating levels of CDK inhibitor P21 and its association with cyclins D1 and E, to induce inhibition of MDA-MB-231 breast cancer cell proliferation, and BMPs -6 and -7 inducing cell cycle arrest via induction of CDK inhibitors in keratinocytes and thyroid carcinoma cells, respectively (Ghosh-Choudhury *et al.*, 2000; Franzen and Heldin, 2001; Gosselet *et al.*, 2007).

8.3 Effect of GDF-9 on apoptosis

As the effect of GDF-9 on the cell cycle of prostate cancer cells was insufficient to explain the considerable induction of cell growth, the cells underwent apoptotic analysis with flow cytometry and Hoechst DNA staining. Both the PC-3^{GDF-9exp.} cells and PC-3 cells treated with rh-GDF-9 showed a significant reduction in the percentage of apoptotic cells under serum starvation, compared to the controls. Furthermore, PC-3^{GDF-9rib3} cells had around 15% more apoptotic cells than the controls, suggesting that GDF-9 may act as an anti-apoptotic factor protecting PC-3 cells from undergoing apoptosis.

Apoptosis is orchestrated by a variety of molecules, including a family of cysteine proteases known as the caspases. Caspase 3 is known as an executioner caspase essential for cytochrome C action and DNA fragmentation. Caspase-3 is expressed as an inactive precursor, which is cleaved into mature caspase-3 subunits during apoptosis (Slee *et al.*, 2001). Due to the anti-apoptotic nature of GDF-9, PC-3^{GDF-9exp.} demonstrated significantly lower expression levels of caspase-3 mature subunits compared to both the controls and the knock-down cells. In addition, protein levels of caspase-3 were gradually reduced over time when treated with rh-GDF-9, suggesting that GDF-9 may act as an anti-apoptotic factor in prostate cancer cells, protecting them from caspase-3 mediated apoptosis.

This anti-apoptotic effect of GDF-9 has also been demonstrated in granulosa cells where the cells are protected from undergoing ceramide induced apoptosis due to GDF-9 associated activation of the PI3K/AKT pathway promoting follicular cell growth and survival. Furthermore, GDF-9 antisense resulted in caspase-3 activation and induced apoptosis in granulosa cells of early antral follicles, suggesting that similarly to in prostate cancer cells, GDF-9 acts as an anti-apoptotic factor in preantral follicles (Orisaka *et al.*, 2006). In addition, its family member, BMP-2 was demonstrated to prevent an up-regulation of caspase-3 levels in MCF-7 breast cancer cells grown in serum free media (Clement *et al.*, 2000)

Other BMPs have been shown to regulate apoptosis through several signalling pathways. BMP-2 for example has been shown to induce apoptosis in medulloblastoma cells by activating the P38 mitogen-activated protein kinase (MAPK) pathway, while protecting MCF-7 cells from hypoxic cell death by activating the MAPK extracellular-signal-regulated kinases 1/2 (ERK1/2) pathways (Hallahan *et al.*, 2003; Raida *et al.*, 2005). BMP-9 meanwhile was previously shown to signal via BMPRII and BMPRII to induce prostate cancer cell apoptosis in a Smad1/5/8 dependent manner via Par-4, while BMP-4, -5, -6, and -7 can induce apoptosis of myeloma cells through ALK3/6, ALK3, and ALK2, respectively (Ro *et al.*, 2004; Ye *et al.*, 2008).

In order to determine which pathway GDF-9 uses to inhibit apoptosis, the PC-3 cells were treated with Smad3 inhibitor and analysed for proliferation, and then apoptosis. While the Smad3 inhibitor prevented GDF-9 associated increased growth, unexpectedly, it had no effect on the anti-apoptotic role of GDF-9, suggesting that while GDF-9 induced growth promotion is Smad3 dependent, its effects on apoptosis are not. This implies that GDF-9 may only signal via Smad3 to induce cell cycle progression to promote cell growth, and that a Smad-independent pathway may be responsible for its anti-apoptotic effects.

8.4 Signalling pathway of GDF-9 in prostate cancer cells

As previously mentioned, BMPs signal via two main pathways; the Smad-dependent, activated when the ligands bind to a preformed receptor complex, and Smad-independent, triggered when the ligand first binds the type I receptor, and then recruits the type-II receptor. In the ovary, GDF-9 has been shown to signal via ALK-5 and BMPR-II to activate Smads2 and 3 (Mazerbourg *et al.*, 2004). This study now shows that in prostate cancer, GDF-9 signals via ALK-5 to activate Smad3. Both the PC-3^{GDF-9exp.} cells and those treated with rh-GDF-9 demonstrated increased protein levels of pSmad3, an effect that was inhibited by the Smad3 inhibitor. In addition, levels of phosphorylated ALK-5 were also up-regulated in response to rh-GDF-9 suggesting that GDF-9 binds to ALK-5, and an as of yet unconfirmed type-II receptor, to phosphorylate and activate Smad3 in order to induce expression of its target genes.

Surprisingly, ALK-5 phosphorylation was inhibited by treatment with the Smad3 inhibitor. Smad7 is known to associate with Smurf following TGF- β stimulation, and ubiquitinates TGF- β receptors, resulting in their degradation. As Smad7 is a TGF- β target gene, this mechanism acts as a form of negative regulation, and while this form of regulation is more established, positive forms also exist (Moustakas and Heldin, 2009). For example, it has been shown that in some cell types, Smads are also capable of up-regulating BMP receptor expression in a positive

feedback loop (Engel *et al.*, 1999). Therefore, it is possible that GDF-9 acting via Smad3, can lead to up-regulation of its type-I receptor as a way of amplifying its downstream signalling.

The Smad-independent pathway involves ERK-1 and 2, P38, and JNK MAPKs, as well as RAS signalling (Nohe *et al.*, 2002). Treating PC-3 cells with rh-GDF-9 resulted in increased levels of ERK and JNK, an effect that was Smad3 dependent in the case of JNK only. Furthermore, immunoprecipitating the cells with a serine/threonine phosphorylated antibody, resulted in elevated levels of active p-ERK and p-JNK, both of which were unaffected by the Smad3 inhibitor. This suggests that while JNK itself may be a GDF-9 target gene, that GDF-9 activates and signals via ERK and JNK independently of the Smads, thereby exerting MAPK associated effects on the PC-3 cells.

Although BMPs normally activate the MAPK pathway independently of the Smads, there has been proof of cross talk between the JNK and Smad dependent pathways. For example, JNK was shown to promote Smad signalling by phosphorylating Smad3 and inducing its nuclear translocation. Furthermore, this relationship was shown to be interdependent in that although the initial rapid induction of JNK is independent of the Smads, the sustained secondary JNK response is Smad dependent, and both require Rho GTPase (Engel *et al.*, 1999). Therefore, it is possible that GDF-9 can not only signal via the MAPK pathway (shown by its induction of p-JNK and p-ERK), but that it can also up-regulate and activate JNK signalling via Smad3, and possibly RhoC.

The MAPK pathway is a major signalling pathway involved in cellular proliferation, affecting both apoptosis and the cell cycle. JNKs are a sub-family of the MAPK superfamily and have been shown to phosphorylate and regulate transcription factors including P53 and c-Myc, as well as members of the Bcl-2 family, in response to extracellular stimuli (Liu and Lin, 2005). The role of JNK in apoptosis is two-fold, as it has been demonstrated to exert both pro-, and anti-apoptotic functions, depending on cell type, the nature of the death stimulus, the extent of

its activation, and cross talk with other signalling pathways. Its anti-apoptotic effects are induced by its capability of phosphorylating pro-apoptotic molecule BAD, and thereby triggering its sequestration, and preventing inactivation of anti-apoptotic Bcl-2 (Liu and Lin, 2005). Furthermore, BMP-7 was shown to protect LNCaP and C4-2B prostate cancer cells by stabilising survivin levels and restoring JNK activity (Yang *et al.*, 2006). Apart from its anti-apoptotic roles, treating KB-3 carcinoma cells with JNK inhibitor resulted in an inhibition of cell growth with an increase of cells in the G2/M phase and apoptotic fractions, suggesting that JNK is involved in cellular proliferation as well as apoptosis (Du *et al.*, 2004).

Similarly, ERK1 and 2 are members of the MAPK superfamily that can mediate cell proliferation and apoptosis in response to different growth signals. Accordingly, this pathway is frequently deregulated in several types of cancers. Like JNK, ERK can exert both pro-apoptotic and anti-apoptotic effects, depending on the cell and signal type (Mebratu and Tesfaigzi, 2009). For example, as previously mentioned, MCF-7 cells can be rescued from hypoxic cell death via BMP-2 induced ERK1/2 activation, while senescent cells treated with BMP-4, demonstrated reduced levels of ERK activation, VEGF, and Bcl-2, consistent with the less proliferative and more apoptotic nature of senescent cells (Buckley *et al.*, 2004; Raida *et al.*, 2005). This evidence makes it plausible that GDF-9 activation of ERK and JNK may be one of the ways in which it can promote prostate cancer cell growth via cell cycle progression and protection from apoptosis.

8.5 Effect of GDF-9 on FAK and paxillin mediated cell movement

As previously shown, GDF-9 can promote the adhesive, invasive, and motile capacity of prostate cancer cells, both endogenously and exogenously. In order to determine a mechanism by which GDF-9 exerts these effects, several motility associated molecules were screened as potential GDF-9 target genes. FAK and paxillin are focal adhesion-associated proteins that mediate integrin cellular properties, including; cell adhesion, migration, motility, and survival.

Cell motility involves changes in the cytoskeleton as well as focal adhesion turnover, and FAK along with paxillin have been demonstrated to regulate cell movement via influences on the cytoskeleton and cell adhesion sites (Brakebusch and Fassler, 2003). Fibroblasts from FAK or paxillin knock-out mice exhibit reduced rates of migration and cell spreading, proving how vital FAK and paxillin are in these processes (Ilic *et al.*, 1995). This therefore makes them worthy candidates as GDF-9 target genes. Indeed, both PC-3^{GDF-9exp.} cells and PC-3 WT cells treated with rh-GDF-9, resulted in an up-regulation of both inactive and active FAK and paxillin. As FAK and paxillin phosphorylation normally occurs in response to growth factor stimulation, this suggests that GDF-9 may act as a growth factor to induce their activation and up-regulation, in order to promote prostate cancer cell adhesion and motility.

Furthermore, the MAPK/ ERK pathway is a well known target of FAK-Src signalling whose activation is assisted by interaction with paxillin. A recent study showed that FAK, paxillin, and Src, along with ERK, are critical for adhesion turnover, a process that is central to cell migration (Webb *et al.*, 2004). This implies that GDF-9 may up-regulate levels of active FAK, paxillin, and ERK, in order for them to interact and promote prostate cancer cell migration. This is not the first BMP found to affect FAK and paxillin levels. BMP-2 can act to enhance cell migration of osteosarcoma cells via focal adhesion formation induced by FAK phosphorylation, whereas BMP-7 was shown to up-regulate levels of paxillin and FAK in both bovine chondrocytes and prostate cancer cells, an effect that enhanced their adhesive, invasive, and motile capacity (Vinall *et al.*, 2002; Sotobori *et al.*, 2006; Ye *et al.*, 2007).

8.6 Effect of GDF-9 on Rho GTPase and ROCK

Rho GTPases, and their most common effectors ROCKs, are important regulators of cellular processes including cell motility, proliferation, and apoptosis. They play a central role in cell adhesion and motility, by reorganising the actin cytoskeleton and regulating actomyosin contractility. Furthermore, Rho-ROCK interactions have been demonstrated to be involved in

tumour invasion and metastasis by increasing cell motility through regulation of actomyosin driven amoeboid movement, disrupting epithelial sheet organisation, and promoting extracellular matrix (ECM) degradation through secretion of matrix-metalloproteinases (MMPS) (Itoh *et al.*, 1999). Accordingly, RhoC has been associated with the invasive phenotype of cancers and was shown to be over-expressed in more aggressive and metastatic pancreatic ductal adenocarcinomas (Suwa *et al.*, 1998). Furthermore, in melanomas it has been implicated as a metastasis gene, and in breast cancer by interacting with ROCK, RhoC been shown to induce expression of angiogenic factors (van Golen *et al.*, 2000; Collisson *et al.*, 2003). Consequently, ROCK has been implicated in increased breast cancer cell migration during tumour cell invasion and metastasis (Bourguignon *et al.*, 1999).

These findings are of interest because this current study shows that GDF-9 can induce expression of both RhoC and ROCK-1. And while without measuring levels of their phosphorylated forms, or levels of their activators Rho GEFs or GAPs, these preliminary results suggest that GDF-9 may promote prostate cancer cell invasion and motility by induction and up-regulation of the Rho-ROCK pathway.

Furthermore, Rho and ROCK can induce changes in the expression, activation, and distribution of focal adhesion proteins, and are required for the assembly of integrins into focal adhesions resulting in activation of ERK1/2 and FAK (Sahai and Marshall, 2002). More specifically, high levels of RhoC in PC-3 cells can induce paxillin/PKL interaction resulting in increased cell motility, and knocking-out RhoC in these cells resulted in decreased levels of FAK and p-paxillin suggesting that RhoC can induce expression of these molecules to promote prostate cancer cell invasion and motility (Yao *et al.*, 2006). Therefore, as GDF-9 has been shown to activate FAK and paxillin, these observations add to the claim that GDF-9 may be able to promote prostate cancer cell motility and adhesion via RhoC, possibly via activation of FAK and paxillin.

Rho GTPases have also been implicated in cell proliferation, by affecting both the cell cycle and apoptosis. For example, RhoA along with RhoC has been shown to promote the proliferation of human gastric carcinoma cells by protecting them from apoptosis via activation of the PI3K/AKT pathway (Sun *et al.*, 2007). Meanwhile, caspase-3 mediated cleavage and activation of ROCK1, is vital for the formation of membrane blebbing during apoptosis (Coleman *et al.*, 2001). However, despite this pro-apoptotic role, ROCK mediated survival effects have been shown in cancer cells, epithelial cells, and endothelial cells. Inhibition of Rho and ROCK for example, triggered apoptosis of anaplastic thyroid cancer and glioma cells, by inducing the release of cytochrome C and activating caspases 3 and 9, whereas sole inhibition of ROCK by Y27632, reduced cardiomyocyte apoptosis by preventing down-regulation of Bcl-2 (Zhong *et al.*, 2003; Bao *et al.*, 2004; Rattan *et al.*, 2006).

As this current study shows that GDF-9 results in down-regulation of caspase-3, these findings suggest that GDF-9 may exert its anti-apoptotic effects either by preventing caspase-3 mediated ROCK cleavage and thereby apoptosis, and/or by up-regulating and activating the Rho-ROCK pathway which thereby induce survival signals and reduce levels of caspase-3. Furthermore, another link exists between GDF-9 associated increased growth and the Rho-ROCK pathway. Rho signalling is vital for sustaining the ERK signal required for mid G1-phase, Cyclin D1 up-regulation, and thereby promotion of cell cycle progression (Welsh *et al.*, 2001). As PC-3 cells treated with rh-GDF-9 demonstrated increased levels of activated ERK and Cyclin D1, it adds to the idea that GDF-9 may signal via RhoC and ROCK to promote prostate cancer cell adhesion, motility, and growth. However, more work is required in order to make this claim conclusive.

8.7 Effect of GDF-9 on EMT associated molecules

Epithelial to mesenchymal transition is positively correlated with increased cell motility and invasion, and so it makes sense that cancer cells often manipulate this process in order to

progress and metastasise. Adenocarcinoma invasion for example, involves the release of single cancer cells that have undergone EMT (Thiery, 2002).

One hallmark of EMT is the loss of E-cadherin expression, an epithelial cell marker involved in cell-cell adhesion and formation of adherens junctions, and the up-regulation in levels of N-cadherin which is a mesenchymal cell marker. Loss of E-cadherin expression is often observed in sites of EMT that occur during embryonic development and cancer progression (Cowin *et al.*, 2005). Several transcription factors have been implicated as repressors of E-cadherin expression, including; SNAI1, SLUG (SNAI2), and TWIST. They also act as molecular triggers of EMT, by acting to both repress epithelial cell markers, and induce expression of known promoters of EMT, including growth factors such as epidermal growth factor (EGF), hepatocyte growth factor (HGF), and TGF- β . As the loss of E-cadherin is associated with tumour progression and hence poor clinical outcome, these E-cadherin repressors are considered as markers of malignancy (Gavert and Ben-Ze'ev, 2008).

This change in expression profile was also demonstrated in PC-3 cells in the presence of GDF-9, where GDF-9 induced expression of SNAI1, TWIST, and N-cadherin. E-Cadherin levels meanwhile were reduced compared to the untreated controls, while no changes were seen in the expression of SLUG. As the literature suggests that SNAI1 and TWIST are capable of repressing E-cadherin expression, it implies that GDF-9 induces up-regulation of these transcription factors, resulting in E-cadherin repression and increased cell aggressiveness. However, in order to confirm this hypothesis, levels of the phosphorylated and thereby active forms of these transcription factors need to be assessed. Despite this, these observations along with the more mesenchymal like nature of the PC-3^{GDF-9exp.} cells, were all in line with the onset of EMT, suggesting that GDF-9 can induce EMT in PC-3 cells by up-regulating levels of EMT inducing molecules, resulting in a promotion of cell invasion and motility.

Furthermore, SNAI1 has also been demonstrated to act as a survival factor independently of its EMT inducing actions, by protecting cells from undergoing apoptosis, induced either by a deficit of survival factors or by direct apoptotic stimuli, and can also control cell adhesion and migration (Kajita *et al.*, 2004). These characteristics of SNAI1 match with the observations of GDF-9 made in this study, signifying that GDF-9 induced SNAI1 up-regulation may, as well as aiding in induction of EMT, affect cell adhesion and migration, and protect the cells from undergoing apoptosis.

TGF- β is a powerful inducer of EMT not only during embryonic development but also during tumour progression. For example, Smad2 and 3 over-expression induces EMT in a mammary epithelial model, where they can down-regulate levels of epithelial cell markers including E-Cadherin and ZO-1, while up-regulating levels of mesenchymal proteins such as fibronectin and vimentin, amongst others. In addition, several BMPs have also been implicated as inducers of EMT. BMP-2 signalling in gastric cancer cells for example, can promote EMT associated morphological changes including repression of E-cadherin, and induction of SNAI1 and vimentin expression (Kang *et al.*). BMP-4 meanwhile, induces EMT in primary epithelial ovarian cancer cells by up-regulating SNAI1 and SLUG, and repressing E-cadherin expression while increasing cell adhesion, invasion, and motility (Theriault *et al.*, 2007).

Ras, MAPK, and Rho/ROCK signalling pathways have been demonstrated to cooperate with TGF- β and BMPs to promote EMT. TGF- β 1 for example, activates Rho-ROCK signalling via ALK-5 to induce EMT in NMuMG breast cancer cells, while ROCK-1 was upregulated at the onset of TGF- β and BMP-2 induced EMT in early heart development (Bhowmick *et al.*, 2001; Sakabe *et al.*, 2008; Xu *et al.*, 2009). In addition, Rho GTPases were highly expressed in the ovarian cancer cells that underwent BMP-4 induced EMT, suggesting that the process was mediated by Rho GTPase signalling (Theriault *et al.*, 2007). Meanwhile, RhoA can mediate JNK and p38 activation in order to induce Smad mediated signalling and EMT associated characteristics, including delocalisation of E-cadherin from cell junctions, and elevation of N-

cadherin levels, suggesting that both TGF- β Smad-dependent and independent signalling is required for EMT induction (Xu *et al.*, 2009). These observations speculate that GDF-9 induced EMT seen in PC-3 cells, may be partially dependent on Rho-ROCK signalling and that this pathway may interact with the Smad-dependent pathway in order to control the EMT process.

8.8 Main findings/significance of this study

This study is the first to reveal a role for GDF-9 in the progression of prostate cancer cells. This was initially achieved by altering the endogenous expression of GDF-9 via both over-expression using cloning in PC-3 cells, and for reliability, gene silencing using ribozyme transgenes, in both PC-3 and DU-145 cells. These cells were then examined for any changes in their biological properties by carrying out functional assays that analyse the proliferative, adhesive, invasive, and motile capacity of these cells. Furthermore, recombinant GDF-9 was generated, in order to treat the cells and confirm the effect it has on prostate cancer cell biological properties, as well as any target genes and downstream signalling which would act as mechanisms for these effects.

Both endogenous and exogenous GDF-9 was capable of promoting prostate cancer cell adhesion, invasion, motility, and growth, an effect that was reversed in the GDF-9 knock-down cells. GDF-9 mediated growth promotion was shown to be associated both with an increase in cell cycle progression via up-regulation of Cyclin D1, and protection from apoptosis in a Smad-independent manner, possibly via a combination of SNAI1, Rho-ROCK, and/or ERK/JNK signalling all of which were activated by GDF-9. However, this requires further research into the activated forms of SNAI1 and Rho/ROCK. Furthermore, GDF-9 associated cell adhesion, motility, and invasion appeared to be due to the interactions of FAK, paxillin, Rho-ROCK signalling, and the induction of EMT via its associated inducers, in a Smad-dependent and

Smad-independent manner. All of these effects result in an increase in the aggressiveness of PC-3 cells, aiding in their progression and possibly metastasis.

Additionally, with the use of recombinant rh-GDF-9, GDF-9 was shown to signal via ALK-5 to activate Smad3 signalling in order to exert some of its effects on prostate cancer cells. FAK, paxillin, and ROCK-1 were shown to be Smad3 target genes, while GDF-9 associated growth and adhesion were also shown to be Smad-dependent. A type II BMP receptor was not able to be identified however, due to the lack of a specific anti-BMPR-II antibody, and hence needs further investigation. Apart from Smad dependent signalling, GDF-9 was capable of activating MAPK pathways including ERK and JNK, which contributed to some of the GDF-9 associated effects observed.

These results suggest that GDF-9 may play an important role in prostate cancer aggressiveness via activation of a complex network of signalling pathways and molecules. It provides researchers in the field of prostate cancer with further proof of the importance of BMP signalling, and suggests that perhaps novel treatments based on BMPs should be investigated. Manufacturing of drugs capable of blocking or altering BMP signalling may prove beneficial to the treatment of prostate cancer. In addition, some BMPs could perhaps be used as prognostic indicators of disease, aiding in diagnosis and treatment. Whether or not this would include GDF-9 requires further investigation.

8.9 Future work

Although this study gives an idea of the role of GDF-9 in prostate cancer, there are many loose ends that still need to be tied up in order to fully understand its importance in the field. For example, although we have demonstrated an anti-apoptotic role for GDF-9 in prostate cancer, the mechanisms still remain unclear. The literature suggests that in the ovary GDF-9 protects from cells from apoptosis by activating the PI3K/AKT pathway (Orisaka *et al.*, 2006).

In addition, Rho/ROCK signalling has been demonstrated to regulate both Bad and Bcl-2, and as GDF-9 can up-regulate RhoC and ROCK-1, the expression levels of these molecules should be investigated (Rattan *et al.*, 2006). Furthermore, signalling molecules of the Smad-independent pathway with anti-apoptotic effects such as TAK-1 and XIAP, should also be analysed. Although Cyclin D1 appears to be one of the mechanisms behind the role of GDF-9 in the cell cycle, a more precise mechanism needs to be determined. We found that oncogene C-myc, a known activator of Cyclin D1 was up-regulated by rh-GDF-9. However, this data was inconclusive and requires further study (Mateyak *et al.*, 1999).

Meanwhile, while this study has proposed that GDF-9 may play a role in prostate cancer motility and has suggested several key players such as Rho/ROCK, EMT transcription factors, and MAPK signalling, little work was carried out on the phosphorylated, and hence activated levels of these proteins. It would therefore be of interest to analyse levels of Rho GTPase regulators Rho GAPs and GEFs, as well as their downstream regulators Wiskott-Aldrich syndrome proteins (WASPs) and WAVES, in order to confirm the role that these proteins play in GDF-9 associated prostate cancer progression.

As previously mentioned, LIMK1 has been shown to bind to the tail region of BMPR-II to regulate cofilin, a regulator of actin dynamics, and therefore cell migration (Folleta *et al.*, 2003). As this has been shown to involve Rho GTPases, and GDF-9 signals via BMPR-II, analysis of activated levels of LIMK1, cofilin, Arp2/3, formin, and MLCK, would also be of use. In addition, as all these molecules are involved in actin dynamics, and relatively little microscopy work was carried out during this study due to several restrictions in equipment, it would be necessary to carry out some confocal microscopy to visualise the actin filaments and stress fibres via phalloidin and the proteins mentioned above, and focal adhesion complexes via FAK, paxillin, integrins, and Src, to further establish the role of GDF-9 in motility.

Furthermore, although we have shown that GDF-9 can signal via ALK-5 to activate Smad3, immunoprecipitation and western blotting effects on determining a type-II receptor for GDF-9 mediated signalling were unsuccessful. The literature suggests that the type-II receptor for GDF-9 is BMPR-II and so further attempts are required in order to confirm if this is also the case in prostate cancer cells. Although some of the target genes were found to be Smad3 dependent, there was not enough time to determine the signalling pathway of the other target genes.

As this study portrays an interesting role for GDF-9 in prostate cancer, its role in prostate cancer metastasis and angiogenesis, as well as in the bone was not investigated. As several other BMPs have been implicated in aiding in bone metastasis from prostate cancer, it would be of interest to perhaps carry out some tubule formation assays, as well as analyse levels of VEGF. On the other side of the spectrum, it might also be appealing to see the effect of GDF-9 on normal prostate epithelial cell lines such as PNT2C2 and PNT1A, and see if it would make them more aggressive. Unfortunately, there were problems in growing and transfecting these cell lines and hence this could not be done.

All of the experiments carried out in this study have been *in vitro*, therefore, in order to get a clearer role for GDF-9 in prostate cancer progression, the role of GDF-9 *in vivo* should also be studied, possibly in the form of GDF-9 knock-out mice. In addition, analysing GDF-9 expression in clinical samples from patients with prostate cancer would also help in determining if any therapeutic or diagnostic value for GDF-9 in prostate cancer exists.

Bibliography:

- Adjei, A. A. (2001). Blocking oncogenic Ras signaling for cancer therapy. *J Natl Cancer Inst* **93**(14): 1062-74.
- Ahmed, N., J. Sammons, R. J. Carson, M. A. Khokher and H. T. Hassan (2001). Effect of bone morphogenetic protein-6 on haemopoietic stem cells and cytokine production in normal human bone marrow stroma. *Cell Biol Int* **25**(5): 429-35.
- Alarmo, E. L., T. Kuukasjarvi, R. Karhu and A. Kallioniemi (2007). A comprehensive expression survey of bone morphogenetic proteins in breast cancer highlights the importance of BMP4 and BMP7. *Breast Cancer Res Treat* **103**(2): 239-46.
- Alarmo, E. L., J. Parssinen, J. M. Ketolainen, K. Savinainen, R. Karhu, and A. Kallioniemi (2009). BMP7 influences proliferation, migration, and invasion of breast cancer cells. *Cancer Lett* **275**(1): 35-43.
- Allendorph, G. P., W. W. Vale, and S. Choe (2006). Structure of the ternary signaling complex of a TGF-beta superfamily member. *Proc Natl Acad Sci U S A* **103**(20): 7643-8.
- Andersson, O., P. Bertolino, and C. F. Ibanez (2007). Distinct and cooperative roles of mammalian Vg1 homologs GDF1 and GDF3 during early embryonic development. *Dev Biol* **311**(2): 500-11.
- Andersson, O., M. Korach-Andre, E. Reissmann, C. F. Ibanez, and P. Bertolino (2008). Growth/differentiation factor 3 signals through ALK7 and regulates accumulation of adipose tissue and diet-induced obesity. *Proc Natl Acad Sci U S A* **105**(20): 7252-6.
- Andersson, O., E. Reissmann, and C. F. Ibanez (2006). Growth differentiation factor 11 signals through the transforming growth factor-beta receptor ALK5 to regionalize the anterior-posterior axis. *EMBO Rep* **7**(8): 831-7.
- Aoki, H., M. Fujii, T. Imamura, K. Yagi, K. Takehara, M. Kato, and K. Miyazono (2001). Synergistic effects of different bone morphogenetic protein type I receptors on alkaline phosphatase induction. *J Cell Sci* **114**(Pt 8): 1483-9.

- Ash, P., J. F. Loutit, and K. M. Townsend (1980). Osteoclasts derived from haematopoietic stem cells. *Nature* **283**: 669-70.
- Athanasou, N. A. (1996). Cellular biology of bone-resorbing cells. *J Bone Joint Surg Am* **78**(7): 1096-112.
- Attisano, L. and S. T. Lee-Hoeflich (2001). The Smads. *Genome Biol* **2**(8): REVIEWS 3010.
- Attisano, L., J. L. Wrana, F. Lopez-Casillas, and J. Massague (1994). TGF-beta receptors and actions. *Biochim Biophys Acta* **1222**(1): 71-80.
- Bagshaw, M. A. (1969). Definitive radiotherapy in carcinoma of the prostate. *JAMA* **210**(2): 326-7.
- Bagshaw, M. A., D. A. Pistenma, G. R. Ray, F. S. Freiha, and R. L. Kempson (1977). Evaluation of extended-field radiotherapy for prostatic neoplasm: 1976 progress report. *Cancer Treat Rep* **61**(2): 297-306.
- Bandyopadhyay, S., R. Zhan, A. Chaudhuri, M. Watabe, S. K. Pai, S. Hirota, S. Hosobe, T. Tsukada, K. Miura, Y. Takano, K. Saito, M. E. Pauza, S. Hayashi, Y. Wang, S. Mohinta, T. Mashimo, M. Iizumi, E. Furuta, and K. Watabe (2006). Interaction of KAI1 on tumor cells with DARC on vascular endothelium leads to metastasis suppression. *Nat Med* **12**(8): 933-8.
- Bao, W., E. Hu, L. Tao, R. Boyce, R. Mirabile, D. T. Thudium, X. L. Ma, R. N. Willette, and T. L. Yue (2004). Inhibition of Rho-kinase protects the heart against ischemia/reperfusion injury. *Cardiovasc Res* **61**(3): 548-58.
- Baron, R., L. Neff, D. Louvard, and P. J. Courtoy (1985). Cell-mediated extracellular acidification and bone resorption: evidence for a low pH in resorbing lacunae and localization of a 100-kD lysosomal membrane protein at the osteoclast ruffled border. *J Cell Biol* **101**(6): 2210-22.
- Batson, O. V. (1995). The function of the vertebral veins and their role in the spread of metastases. 1940. *Clin Orthop Relat Res* (312): 4-9.

- Beck, H. N., K. Drahushuk, D. B. Jacoby, D. Higgins and P. J. Lein (2001). Bone morphogenetic protein-5 (BMP-5) promotes dendritic growth in cultured sympathetic neurons. *BMC Neurosci* 2: 12.
- Bendre, M. S., A. G. Margulies, B. Walser, N. S. Akel, S. Bhattacharrya, R. A. Skinner, F. Swain, V. Ramani, K. S. Mohammad, L. L. Wessner, A. Martinez, T. A. Guise, J. M. Chirgwin, D. Gaddy, and L. J. Suva (2005). Tumor-derived interleukin-8 stimulates osteolysis independent of the receptor activator of nuclear factor-kappaB ligand pathway. *Cancer Res* 65(23): 11001-9.
- Bhowmick, N. A., M. Ghiassi, A. Bakin, M. Aakre, C. A. Lundquist, M. E. Engel, C. L. Arteaga, and H. L. Moses (2001). Transforming growth factor-beta1 mediates epithelial to mesenchymal transdifferentiation through a RhoA-dependent mechanism. *Mol Biol Cell* 12(1): 27-36.
- Bill-Axelson, A., L. Holmberg, M. Ruutu, M. Haggman, S. O. Andersson, S. Bratell, A. Spangberg, C. Busch, S. Nordling, H. Garmo, J. Palmgren, H. O. Adami, B. J. Norlen, and J. E. Johansson (2005). Radical prostatectomy versus watchful waiting in early prostate cancer. *N Engl J Med* 352(19): 1977-84.
- Bobinac, D., I. Maric, S. Zoricic, J. Spanjol, G. Dordevic, E. Mustac, and Z. Fuckar (2005). Expression of bone morphogenetic proteins in human metastatic prostate and breast cancer. *Croat Med J* 46(3): 389-96.
- Borley, N. and M. R. Feneley (2009). Prostate cancer: diagnosis and staging. *Asian J Androl* 11(1): 74-80.
- Bostwick, D. G. (1999). Prostatic intraepithelial neoplasia is a risk factor for cancer. *Semin Urol Oncol* 17(4): 187-98.
- Bourguignon, L. Y., H. Zhu, L. Shao, D. Zhu, and Y. W. Chen (1999). Rho-kinase (ROK) promotes CD44v(3,8-10)-ankyrin interaction and tumor cell migration in metastatic breast cancer cells. *Cell Motil Cytoskeleton* 43(4): 269-87.

- Brakebusch, C. and R. Fassler (2003). The integrin-actin connection, an eternal love affair. *EMBO J* **22**(10): 2324-33.
- Brodin, G., P. ten Dijke, K. Funahashi, C. H. Heldin, and M. Landstrom (1999). Increased smad expression and activation are associated with apoptosis in normal and malignant prostate after castration. *Cancer Res* **59**(11): 2731-8.
- Brodsky, B. and A. V. Persikov (2005). Molecular structure of the collagen triple helix. *Adv Protein Chem* **70**: 301-39.
- Brown, M. A., Q. Zhao, K. A. Baker, C. Naik, C. Chen, L. Pukac, M. Singh, T. Tsareva, Y. Parice, A. Mahoney, V. Roschke, I. Sanyal, and S. Choe (2005). Crystal structure of BMP-9 and functional interactions with pro-region and receptors. *J Biol Chem* **280**(26): 25111-8.
- Brown, M. D., C. A. Hart, E. Gazi, S. Bagley, and N. W. Clarke (2006). Promotion of prostatic metastatic migration towards human bone marrow stroma by Omega 6 and its inhibition by Omega 3 PUFAs. *Br J Cancer* **94**(6): 842-53.
- Brubaker, K. D., E. Corey, L. G. Brown, and R. L. Vessella (2004). Bone morphogenetic protein signaling in prostate cancer cell lines. *J Cell Biochem* **91**(1): 151-60.
- Bryden, A. A., A. J. Freemont, N. W. Clarke, and N. J. George (1999). Paradoxical expression of E-cadherin in prostatic bone metastases. *BJU Int* **84**(9): 1032-4.
- Bubendorf, L., A. Schopfer, U. Wagner, G. Sauter, H. Moch, N. Willi, T. C. Gasser, and M. J. Mihatsch (2000). Metastatic patterns of prostate cancer: an autopsy study of 1,589 patients. *Hum Pathol* **31**(5): 578-83.
- Buckley, S., W. Shi, B. Driscoll, A. Ferrario, K. Anderson, and D. Warburton (2004). BMP4 signaling induces senescence and modulates the oncogenic phenotype of A549 lung adenocarcinoma cells. *Am J Physiol Lung Cell Mol Physiol* **286**(1): L81-6.
- Bussemakers, M. J., A. van Bokhoven, G. W. Verhaegh, F. P. Smit, H. F. Karthaus, J. A. Schalken, F. M. Debruyne, N. Ru, and W. B. Isaacs (1999). DD3: a new prostate-specific gene, highly overexpressed in prostate cancer. *Cancer Res* **59**(23): 5975-9.

- Camps, J. L., S. M. Chang, T. C. Hsu, M. R. Freeman, S. J. Hong, H. E. Zhau, A. C. von Eschenbach, and L. W. Chung (1990). Fibroblast-mediated acceleration of human epithelial tumor growth in vivo. *Proc Natl Acad Sci U S A* **87**(1): 75-9.
- Canalis, E., A. N. Economides, and E. Gazzo (2003). Bone morphogenetic proteins, their antagonists, and the skeleton. *Endocr Rev* **24**(2): 218-35.
- Candia, A. F., T. Watabe, S. H. Hawley, D. Onichtchouk, Y. Zhang, R. Derynck, C. Niehrs, and K. W. Cho (1997). Cellular interpretation of multiple TGF-beta signals: intracellular antagonism between activin/BVg1 and BMP-2/4 signaling mediated by Smads. *Development* **124**(22): 4467-80.
- Carducci, M. A., R. J. Padley, J. Breul, N. J. Vogelzang, B. A. Zonnenberg, D. D. Daliani, C. C. Schulman, A. A. Nabulsi, R. A. Humerickhouse, M. A. Weinberg, J. L. Schmitt and, J. B. Nelson (2003). Effect of endothelin-A receptor blockade with atrasentan on tumor progression in men with hormone-refractory prostate cancer: a randomized, phase II, placebo-controlled trial. *J Clin Oncol* **21**(4): 679-89.
- Carter, H. B., C. H. Morrell, J. D. Pearson, L. J. Brant, C. C. Plato, E. J. Metter, D. W. Chan, J. L. Fozard, and P. C. Walsh (1992). Estimation of prostatic growth using serial prostate-specific antigen measurements in men with and without prostate disease. *Cancer Res* **52**(12): 3323-8.
- Catalona, W. J., A. W. Partin, J. A. Finlay, D. W. Chan, H. G. Rittenhouse, R. L. Wolfert, and D. L. Woodrum (1999). Use of percentage of free prostate-specific antigen to identify men at high risk of prostate cancer when PSA levels are 2.51 to 4 ng/mL and digital rectal examination is not suspicious for prostate cancer: an alternative model. *Urology* **54**(2): 220-4.
- Catalona, W. J., A. W. Partin, K. M. Slawin, M. K. Brawer, R. C. Flanigan, A. Patel, J. P. Richie, J. B. deKernion, P. C. Walsh, P. T. Scardino, P. H. Lange, E. N. Subong, R. E. Parson, G. H. Gasior, K. G. Loveland, and P. C. Southwick (1998). Use of the percentage of free prostate-specific antigen to enhance differentiation of prostate cancer

- from benign prostatic disease: a prospective multicenter clinical trial. *JAMA* **279**(19): 1542-7.
- Catalona, W. J., D. S. Smith, T. L. Ratliff, K. M. Dodds, D. E. Coplen, J. J. Yuan, J. A. Petros, and G. L. Andriole (1991). Measurement of prostate-specific antigen in serum as a screening test for prostate cancer. *N Engl J Med* **324**(17): 1156-61.
- Cellini, N., S. Luzi, G. Mantini, G. C. Mattiucci, A. G. Morganti, C. Digesu, A. Bavasso, F. Deodato, D. Smaniotto, and V. Valentini (2003). Lymphatic drainage and CTV in carcinoma of the prostate. *Rays* **28**(3): 337-41.
- Chambers, T. J., P. M. McSheehy, B. M. Thomson, and K. Fuller (1985). The effect of calcium-regulating hormones and prostaglandins on bone resorption by osteoclasts disaggregated from neonatal rabbit bones. *Endocrinology* **116**(1): 234-9.
- Chan, J. M., M. J. Stampfer, E. Giovannucci, P. H. Gann, J. Ma, P. Wilkinson, C. H. Hennekens, and M. Pollak (1998). Plasma insulin-like growth factor-I and prostate cancer risk: a prospective study. *Science* **279**: 563-6.
- Chang, B., S. L. Zheng, S. D. Isaacs, K. E. Wiley, J. D. Carpten, G. A. Hawkins, E. R. Bleecker, P. C. Walsh, J. M. Trent, D. A. Meyers, W. B. Isaacs, and J. Xu (2001). Linkage and association of CYP17 gene in hereditary and sporadic prostate cancer. *Int J Cancer* **95**(6): 354-9.
- Chang, B. L., S. L. Zheng, G. A. Hawkins, S. D. Isaacs, K. E. Wiley, A. Turner, J. D. Carpten, E. R. Bleecker, P. C. Walsh, J. M. Trent, D. A. Meyers, W. B. Isaacs, and J. Xu (2002). Polymorphic GGC repeats in the androgen receptor gene are associated with hereditary and sporadic prostate cancer risk. *Hum Genet* **110**(2): 122-9.
- Chang, B. L., S. L. Zheng, S. D. Isaacs, K. E. Wiley, A. Turner, G. Li, P. C. Walsh, D. A. Meyers, W. B. Isaacs and J. Xu (2004). A polymorphism in the CDKN1B gene is associated with increased risk of hereditary prostate cancer. *Cancer Res* **64**(6): 1997-9.
- Chang, C. F., R. Westbrook, J. Ma, and D. Cao (2007). Transforming growth factor-beta signaling in breast cancer. *Front Biosci* **12**: 4393-401.

- Chang, J. J., K. Shinohara, V. Bhargava and J. C. Presti, Jr. (1998). Prospective evaluation of lateral biopsies of the peripheral zone for prostate cancer detection. *J Urol* 160(6 Pt 1): 2111-4.
- Chen, W., X. Fu, and Z. Sheng (2002). Review of current progress in the structure and function of Smad proteins. *Chin Med J (Engl)* 115(3): 446-50.
- Chen, X., A. Zankl, F. Niroomand, Z. Liu, H. A. Katus, L. Jahn, and C. Tiefenbacher (2006). Upregulation of ID protein by growth and differentiation factor 5 (GDF5) through a smad-dependent and MAPK-independent pathway in HUVSMC. *J Mol Cell Cardiol* 41(1): 26-33.
- Chen, Y. C., J. H. Page, R. Chen, and E. Giovannucci (2008). Family history of prostate and breast cancer and the risk of prostate cancer in the PSA era. *Prostate* 68(14): 1582-91.
- Chen, Y.G., A. Hata, R.S. Lo, D. Wotton, Y. Shi, N. Pavletich N., and J. Massague (1998) Determinants of specificity in TGF-beta signal transduction. *Genes dev* 12(14): 2144-52.
- Cheng, L., M. Nagabhushan, T. P. Pretlow, S. B. Amini, and T. G. Pretlow (1996). Expression of E-cadherin in primary and metastatic prostate cancer. *Am J Pathol* 148(5): 1375-80.
- Cheng, S. K., F. Olale, J. T. Bennett, A. H. Brivanlou and A. F. Schier (2003). EGF-CFC proteins are essential coreceptors for the TGF-beta signals Vg1 and GDF1. *Genes Dev* 17(1): 31-6.
- Chodak, G., R. Sharifi, B. Kasimis, N. L. Block, E. Macramalla, and G. T. Kennealey (1995). Single-agent therapy with bicalutamide: a comparison with medical or surgical castration in the treatment of advanced prostate carcinoma. *Urology* 46(6): 849-55.
- Chodak, G. W., R. A. Thisted, G. S. Gerber, J. E. Johansson, J. Adolfsson, G. W. Jones, G. D. Chisholm, B. Moskovitz, P. M. Livne, and J. Warner (1994). Results of conservative management of clinically localized prostate cancer. *N Engl J Med* 330(4): 242-8.

- Clark, P. E. and F. M. Torti (2003). Prostate cancer and bone metastases: medical treatment. *Clin Orthop Relat Res* (415 Suppl): S148-57.
- Clarke, B. (2008). Normal bone anatomy and physiology. *Clin J Am Soc Nephrol* 3 Suppl 3: S131-9.
- Clarke, N. W., C. A. Hart, and M. D. Brown (2009). Molecular mechanisms of metastasis in prostate cancer. *Asian J Androl* 11(1): 57-67.
- Clement, J. H., N. Marr, A. Meissner, M. Schwalbe, W. Sebald, K. O. Kliche, K. Hoffken, and S. Wolfli (2000). Bone morphogenetic protein 2 (BMP-2) induces sequential changes of Id gene expression in the breast cancer cell line MCF-7. *J Cancer Res Clin Oncol* 126(5): 271-9.
- Cohen, M. M., Jr. (2006). The new bone biology: pathologic, molecular, and clinical correlates. *Am J Med Genet A* 140(23): 2646-706.
- Cohen, P., D. M. Peehl, H. C. Graves, and R. G. Rosenfeld (1994). Biological effects of prostate specific antigen as an insulin-like growth factor binding protein-3 protease. *J Endocrinol* 142(3): 407-15.
- Coleman, M. L., E. A. Sahai, M. Yeo, M. Bosch, A. Dewar, and M. F. Olson (2001). Membrane blebbing during apoptosis results from caspase-mediated activation of ROCK I. *Nat Cell Biol* 3(4): 339-45.
- Collisson, E. A., C. Kleer, M. Wu, A. De, S. S. Gambhir, S. D. Merajver, and M. S. Kolodney (2003). Atorvastatin prevents RhoC isoprenylation, invasion, and metastasis in human melanoma cells. *Mol Cancer Ther* 2(10): 941-8.
- Conery, A. R., Y. Cao, E. A. Thompson, C. M. Townsend, Jr., T. C. Ko, and K. Luo (2004). Akt interacts directly with Smad3 to regulate the sensitivity to TGF-beta induced apoptosis. *Nat Cell Biol* 6(4): 366-72.
- Cordenonsi, M., M. Montagner, M. Adorno, L. Zacchigna, G. Martello, A. Mamidi, S. Soligo, S. Dupont, and S. Piccolo (2007). Integration of TGF-beta and Ras/MAPK signaling through p53 phosphorylation. *Science* 315: 840-3.

- Coussens, L. M. and Z. Werb (2002). Inflammation and cancer. *Nature* **420**: 860-7.
- Cowin, P., T. M. Rowlands, and S. J. Hatsell (2005). Cadherins and catenins in breast cancer. *Curr Opin Cell Biol* **17**(5): 499-508.
- Crawford, E. D., M. A. Eisenberger, D. G. McLeod, J. T. Spaulding, R. Benson, F. A. Dorr, B. A. Blumenstein, M. A. Davis, and P. J. Goodman (1989). A controlled trial of leuprolide with and without flutamide in prostatic carcinoma. *N Engl J Med* **321**(7): 419-24.
- Cress, A. E., I. Rabinovitz, W. Zhu, and R. B. Nagle (1995). The alpha 6 beta 1 and alpha 6 beta 4 integrins in human prostate cancer progression. *Cancer Metastasis Rev* **14**(3): 219-28.
- D'Amico, A. V., J. Manola, M. Loffredo, A. A. Renshaw, A. DellaCroce, and P. W. Kantoff (2004). 6-month androgen suppression plus radiation therapy vs radiation therapy alone for patients with clinically localized prostate cancer: a randomized controlled trial. *JAMA* **292**(7): 821-7.
- Dagnelie, P. C., A. G. Schuurman, R. A. Goldbohm, and P. A. Van den Brandt (2004). Diet, anthropometric measures and prostate cancer risk: a review of prospective cohort and intervention studies. *BJU Int* **93**(8): 1139-50.
- Dai, J., J. Keller, J. Zhang, Y. Lu, Z. Yao, and E. T. Keller (2005). Bone morphogenetic protein-6 promotes osteoblastic prostate cancer bone metastases through a dual mechanism. *Cancer Res* **65**(18): 8274-85.
- Dai, J., Y. Kitagawa, J. Zhang, Z. Yao, A. Mizokami, S. Cheng, J. Nor, L. K. McCauley, R. S. Taichman, and E. T. Keller (2004). Vascular endothelial growth factor contributes to the prostate cancer-induced osteoblast differentiation mediated by bone morphogenetic protein. *Cancer Res* **64**(3): 994-9.
- Dalkin, B. L., F. R. Ahmann, and J. B. Kopp (1993). Prostate specific antigen levels in men older than 50 years without clinical evidence of prostatic carcinoma. *J Urol* **150**(6): 1837-9.

- Daluiski, A., T. Engstrand, M. E. Bahamonde, L. W. Gamer, E. Agius, S. L. Stevenson, K. Cox, V. Rosen, and K. M. Lyons (2001). Bone morphogenetic protein-3 is a negative regulator of bone density. *Nat Genet* **27**(1): 84-8.
- Datta, H. K., W. F. Ng, J. A. Walker, S. P. Tuck, and S. S. Varanasi (2008). The cell biology of bone metabolism. *J Clin Pathol* **61**(5): 577-87.
- Datto, M. B., Y. Yu, and X. F. Wang (1995). Functional analysis of the transforming growth factor beta responsive elements in the WAF1/Cip1/p21 promoter. *J Biol Chem* **270**(48): 28623-8.
- De Angelis, G., H. G. Rittenhouse, S. D. Mikolajczyk, L. Blair Shamel, and A. Semjonow (2007). Twenty Years of PSA: From Prostate Antigen to Tumor Marker. *Rev Urol* **9**(3): 113-23.
- DeChello, L. M., D. I. Gregorio, and H. Samociuk (2006). Race-specific geography of prostate cancer incidence. *Int J Health Geogr* **5**: 59.
- Denmeade, S. R. and J. T. Isaacs (2002). A history of prostate cancer treatment. *Nat Rev Cancer* **2**(5): 389-96.
- Dermer, G. B. (1978). Basal cell proliferation in benign prostatic hyperplasia. *Cancer* **41**(5): 1857-62.
- Derynck, R., R. J. Akhurst, and A. Balmain (2001). TGF-beta signaling in tumor suppression and cancer progression. *Nat Genet* **29**(2): 117-29.
- di Sant'Agnes, P. A. (1998). Neuroendocrine cells of the prostate and neuroendocrine differentiation in prostatic carcinoma: a review of morphologic aspects. *Urology* **51**(5A Suppl): 121-4.
- Dong, J., D. F. Albertini, K. Nishimori, T. R. Kumar, N. Lu and M. M. Matzuk (1996). Growth differentiation factor-9 is required during early ovarian folliculogenesis. *Nature* **383**: 531-5.
- Du, L., C. S. Lyle, T. B. Obey, W. A. Gaarde, J. A. Muir, B. L. Bennett and T. C. Chambers (2004). Inhibition of cell proliferation and cell cycle progression by specific inhibition

- of basal JNK activity: evidence that mitotic Bcl-2 phosphorylation is JNK-independent. *J Biol Chem* **279**(12): 11957-66.
- Ducy, P., M. Starbuck, M. Priemel, J. Shen, G. Pinero, V. Geoffroy, M. Amling and G. Karsenty (1999). A Cbfa1-dependent genetic pathway controls bone formation beyond embryonic development. *Genes Dev* **13**(8): 1025-36.
- Ebisawa, T., M. Fukuchi, G. Murakami, T. Chiba, K. Tanaka, T. Imamura and K. Miyazono (2001). Smurf1 interacts with transforming growth factor-beta type I receptor through Smad7 and induces receptor degradation. *J Biol Chem* **276**(16): 12477-80.
- Ebisawa, T., K. Tada, I. Kitajima, K. Tojo, T. K. Sampath, M. Kawabata, K. Miyazono and T. Imamura (1999). Characterization of bone morphogenetic protein-6 signaling pathways in osteoblast differentiation. *J Cell Sci* **112** (Pt 20): 3519-27.
- Edwards, S. J., K. L. Reader, S. Lun, A. Western, S. Lawrence, K. P. McNatty and J. L. Juengel (2008). The cooperative effect of growth and differentiation factor-9 and bone morphogenetic protein (BMP)-15 on granulosa cell function is modulated primarily through BMP receptor II. *Endocrinology* **149**(3): 1026-30.
- Elvin, J.A., A.T. Clark, P. Wang, N.M. Wolfman, and M.M. Matzuk (1999). Paracrine Actions Of Growth Differentiation Factor-9 in the Mammalian Ovary. *Mol Endocrinol* **13**(6): 1035-48.
- Engel, M., M.A. McDonnell, B.K. Law, and H.L. Moses (1999). Interdependent SMAD and JNK Signaling in Transforming Growth Factor- β -mediated Transcription. *J Biol Chem* **274**(52): 37413-20.
- Feeley, B.T., S.C. Gamradt, W.K. Hsu, N. Liu, L. Krenek, P. Robbins, J. Huard, and J.R. Lieberman (2005). Influence of BMPs on the formation of osteoblastic lesions in metastatic prostate cancer. *J Bone Miner Res* **20**(12): 2189-99.
- Feeley, B. T., L. Krenek, N. Liu, W. K. Hsu, S. C. Gamradt, E. M. Schwarz, J. Huard and J. R. Lieberman (2006). Overexpression of noggin inhibits BMP-mediated growth of osteolytic prostate cancer lesions. *Bone* **38**(2): 154-66.

- Feng, X. H., X. Lin and R. Derynck (2000). Smad2, Smad3 and Smad4 cooperate with Sp1 to induce p15 (Ink4B) transcription in response to TGF-beta. *EMBO J* **19**(19): 5178-93.
- Fidler, I. J. (2001). Seed and soil revisited: contribution of the organ microenvironment to cancer metastasis. *Surg Oncol Clin N Am* **10**(2): 257-69, vii-viii.
- Fili, S., M. Karalaki and B. Schaller (2009). Mechanism of bone metastasis: the role of osteoprotegerin and of the host-tissue microenvironment-related survival factors. *Cancer Lett* **283**(1): 10-9.
- Foletta, V.C., M.A. Lim, J. Soosairajah, A.P. Kelly, E.G. Stanley, M. Shannon, W. He, S. Das, J. Massague, and O. Bernard (2003). Direct signaling by the BMP type II receptor via the cytoskeletal regulator LIMK1. *JCB* **162**(6): 1089-98.
- Foronda, D., L. F. de Navas, D. L. Garaulet and E. Sanchez-Herrero (2009). Function and specificity of Hox genes. *Int J Dev Biol* **53**(8-10): 1404-19.
- Foster, C. S. (1990). Predictive factors in prostatic hyperplasia and neoplasia. *Hum Pathol* **21**(6): 575-7.
- Foster, C. S. and P. D. Abel (1992). Clinical and molecular techniques for diagnosis and monitoring of prostatic cancer. *Hum Pathol* **23**(4): 395-401.
- Franz-Odendaal, T. A., B. K. Hall and P. E. Witten (2006). Buried alive: how osteoblasts become osteocytes. *Dev Dyn* **235**(1): 176-90.
- Franzen, A. and N. E. Heldin (2001). BMP-7-induced cell cycle arrest of anaplastic thyroid carcinoma cells via p21(CIP1) and p27(KIP1). *Biochem Biophys Res Commun* **285**(3): 773-81.
- Gann, P. H., C. H. Hennekens and M. J. Stampfer (1995). A prospective evaluation of plasma prostate-specific antigen for detection of prostatic cancer. *JAMA* **273**(4): 289-94.
- Gao, Z., X. Wu, N. Song, L. Zhang, and W. Liu (2010). Differential expression of growth differentiation factor-9 in keloids. *Burns* [Epub ahead of print].
- Garnick, M. B. (1993). Prostate cancer: screening, diagnosis, and management. *Ann Intern Med* **118**(10): 804-18.

- Gatza, C.E., S.Y. Oh, and G.C. Blobe (2010). Roles for the type III TGF-beta receptor in human cancer. *Cellular signalling* **22**(8): 1163-74.
- Gavert, N. and A. Ben-Ze'ev (2008). Epithelial-mesenchymal transition and the invasive potential of tumors. *Trends Mol Med* **14**(5): 199-209.
- Germain, S., M. Howell, G. M. Esslemont and C. S. Hill (2000). Homeodomain and winged-helix transcription factors recruit activated Smads to distinct promoter elements via a common Smad interaction motif. *Genes Dev* **14**(4): 435-51.
- Getzenberg, R. H., K. J. Pienta, E. Y. Huang and D. S. Coffey (1991). Identification of nuclear matrix proteins in the cancer and normal rat prostate. *Cancer Res* **51**(24): 6514-20.
- Ghosh-Choudhury, N., K. Woodruff, W. Qi, A. Celeste, S. L. Abboud and G. Ghosh Choudhury (2000). Bone morphogenetic protein-2 blocks MDA MB 231 human breast cancer cell proliferation by inhibiting cyclin-dependent kinase-mediated retinoblastoma protein phosphorylation. *Biochem Biophys Res Commun* **272**(3): 705-11.
- Gillooly, D.J., A. Simonsen, and H. Stenmarki (2001). Cellular functions of phosphatidylinositol 3-phosphate and FYVE domain proteins. *Biochem J* **355**(Pt 2): 249-58.
- Gleason, D. F. and G. T. Mellinger (1974). Prediction of prognosis for prostatic adenocarcinoma by combined histological grading and clinical staging. *J Urol* **111**(1): 58-64.
- Gordon, K. J. and G. C. Blobe (2008). Role of transforming growth factor-beta superfamily signaling pathways in human disease. *Biochim Biophys Acta* **1782**(4): 197-228.
- Gosselet, F. P., T. Magnaldo, R. M. Culerrier, A. Sarasin and J. C. Ehrhart (2007). BMP2 and BMP6 control p57(Kip2) expression and cell growth arrest/terminal differentiation in normal primary human epidermal keratinocytes. *Cell Signal* **19**(4): 731-9.

- Granjeiro, J. M., R. C. Oliveira, J. C. Bustos-Valenzuela, M. C. Sogayar and R. Taga (2005). Bone morphogenetic proteins: from structure to clinical use. *Braz J Med Biol Res* **38**(10): 1463-73.
- Greene, F. L. and L. H. Sobin (2002). The TNM system: our language for cancer care. *J Surg Oncol* **80**(3): 119-20.
- Greene, F. L., A. K. Stewart and H. J. Norton (2002). A new TNM staging strategy for node-positive (stage III) colon cancer: an analysis of 50,042 patients. *Ann Surg* **236**(4): 416-21.
- Greenwald, J., W. H. Fischer, W. W. Vale and S. Choe (1999). Three-finger toxin fold for the extracellular ligand-binding domain of the type II activin receptor serine kinase. *Nat Struct Biol* **6**(1): 18-22.
- Guise, T. A., J. J. Yin and K. S. Mohammad (2003). Role of endothelin-1 in osteoblastic bone metastases. *Cancer* **97**(3 Suppl): 779-84.
- Habara, T., H. Morioka and N. Akiyama (1966). Variations in the activity of specific protein antigen of preserved fetal blood serum. *Nihon Hoigaku Zasshi* **20**(5): 458-65.
- Haggman, M. J., J. A. Macoska, K. J. Wojno and J. E. Oesterling (1997). The relationship between prostatic intraepithelial neoplasia and prostate cancer: critical issues. *J Urol* **158**(1): 12-22.
- Hallahan, A. R., J. I. Pritchard, R. A. Chandraratna, R. G. Ellenbogen, J. R. Geyer, R. P. Overland, A. D. Strand, S. J. Tapscott and J. M. Olson (2003). BMP-2 mediates retinoid-induced apoptosis in medulloblastoma cells through a paracrine effect. *Nat Med* **9**(8): 1033-8.
- Hallstrom, T. M. and M. Laiho (2008). Genetic changes and DNA damage responses in the prostate. *Prostate* **68**(8): 902-18.
- Hanahan, D. and R. A. Weinberg (2000). The hallmarks of cancer. *Cell* **100**(1): 57-70.

- Hanavadi, S., T. A. Martin, G. Watkins, R. E. Mansel and W. G. Jiang (2007). The role of growth differentiation factor-9 (GDF-9) and its analog, GDF-9b/BMP-15, in human breast cancer. *Ann Surg Oncol* **14**(7): 2159-66.
- Hanks, G. E., A. L. Hanlon, T. E. Schultheiss, G. M. Freedman, M. Hunt, W. H. Pinover and B. Movsas (1997). Conformal external beam treatment of prostate cancer. *Urology* **50**(1): 87-92.
- Harbour, J. W. and D. C. Dean (2000). The Rb/E2F pathway: expanding roles and emerging paradigms. *Genes Dev* **14**(19): 2393-409.
- Hart, C. A., L. J. Scott, S. Bagley, A. A. Bryden, N. W. Clarke and S. H. Lang (2002). Role of proteolytic enzymes in human prostate bone metastasis formation: in vivo and in vitro studies. *Br J Cancer* **86**(7): 1136-42.
- Haseloff, J., and W. L. Gerlach (1988). Simple RNA enzymes with new and highly specific endoribonuclease activities. *Nature* **334**:585-591.
- Hata, A., G. Lagna, J. Massague, and A. Hemmati-Brivanlou (1998). Smad6 inhibits BMP/Smad1 signaling by specifically competing with the Smad4 tumor suppressor. *Genes Dev* **12**(2): 186-97.
- Hauck, C. R., D. A. Hsia and D. D. Schlaepfer (2002). The focal adhesion kinase--a regulator of cell migration and invasion. *IUBMB Life* **53**(2): 115-9.
- Haudenschild, D. R., S. M. Palmer, T. A. Moseley, Z. You and A. H. Reddi (2004). Bone morphogenetic protein (BMP)-6 signaling and BMP antagonist noggin in prostate cancer. *Cancer Res* **64**(22): 8276-84.
- Hayashi, H., S. Abdollah, Y. Qiu, J. Cai, Y. Y. Xu, B. W. Grinnell, M. A. Richardson, J. N. Topper, M. A. Gimbrone, Jr., J. L. Wrana and D. Falb (1997). The MAD-related protein Smad7 associates with the TGFbeta receptor and functions as an antagonist of TGFbeta signaling. *Cell* **89**(7): 1165-73.
- Heldin, C. H., K. Miyazono and P. ten Dijke (1997). TGF-beta signalling from cell membrane to nucleus through SMAD proteins. *Nature* **390**: 465-71.

- Helms, M. W., J. Packeisen, C. August, B. Schittek, W. Boecker, B. H. Brandt and H. Buerger (2005). First evidence supporting a potential role for the BMP/SMAD pathway in the progression of oestrogen receptor-positive breast cancer. *J Pathol* **206**(3): 366-76.
- Hofbauer, L. C., D. L. Lacey, C. R. Dunstan, T. C. Spelsberg, B. L. Riggs and S. Khosla (1999). Interleukin-1beta and tumor necrosis factor-alpha, but not interleukin-6, stimulate osteoprotegerin ligand gene expression in human osteoblastic cells. *Bone* **25**(3): 255-9.
- Holen, I., P. I. Croucher, F. C. Hamdy and C. L. Eaton (2002). Osteoprotegerin (OPG) is a survival factor for human prostate cancer cells. *Cancer Res* **62**(6): 1619-23.
- Holmbeck, K., P. Bianco, I. Pidoux, S. Inoue, R. C. Billingham, W. Wu, K. Chrysovergis, S. Yamada, H. Birkedal-Hansen and A. R. Poole (2005). The metalloproteinase MT1-MMP is required for normal development and maintenance of osteocyte processes in bone. *J Cell Sci* **118**(Pt 1): 147-56.
- Huang, Q., A. P. Cheung, Y. Zhang, H. F. Huang, N. Auersperg and P. C. Leung (2009). Effects of growth differentiation factor 9 on cell cycle regulators and ERK42/44 in human granulosa cell proliferation. *Am J Physiol Endocrinol Metab* **296**(6): E1344-53.
- Hudes, G. R., F. Nathan, C. Khater, N. Haas, M. Cornfield, B. Giantonio, R. Greenberg, L. Gomella, S. Litwin, E. Ross, S. Roethke and C. McAleer (1997). Phase II trial of 96-hour paclitaxel plus oral estramustine phosphate in metastatic hormone-refractory prostate cancer. *J Clin Oncol* **15**(9): 3156-63.
- Humphrey, P. A. (2004). Gleason grading and prognostic factors in carcinoma of the prostate. *Mod Pathol* **17**(3): 292-306.
- Ide, H., T. Yoshida, N. Matsumoto, K. Aoki, Y. Osada, T. Sugimura and M. Terada (1997). Growth regulation of human prostate cancer cells by bone morphogenetic protein-2. *Cancer Res* **57**(22): 5022-7.

- Ilic, D., Y. Furuta, S. Kanazawa, N. Takeda, K. Sobue, N. Nakatsuji, S. Nomura, J. Fujimoto, M. Okada and T. Yamamoto (1995). Reduced cell motility and enhanced focal adhesion contact formation in cells from FAK-deficient mice. *Nature* **377**: 539-44.
- Im, J. H., W. Fu, H. Wang, S. K. Bhatia, D. A. Hammer, M. A. Kowalska and R. J. Muschel (2004). Coagulation facilitates tumor cell spreading in the pulmonary vasculature during early metastatic colony formation. *Cancer Res* **64**(23): 8613-9.
- Ishitani, T., J. Ninomiya-Tsuji, S. Nagai, M. Nishita, M. Meneghini, N. Barker, M. Waterman, B. Bowerman, H. Clevers, H. Shibuya and K. Matsumoto (1999). The TAK1-NLK-MAPK-related pathway antagonizes signalling between beta-catenin and transcription factor TCF. *Nature* **399**: 798-802.
- Itoh, F., S. Itoh, M. J. Goumans, G. Valdimarsdottir, T. Iso, G. P. Dotto, Y. Hamamori, L. Kedes, M. Kato and P. ten Dijke Pt (2004). Synergy and antagonism between Notch and BMP receptor signaling pathways in endothelial cells. *EMBO J* **23**(3): 541-51.
- Itoh, K., K. Yoshioka, H. Akedo, M. Uehata, T. Ishizaki and S. Narumiya (1999). An essential part for Rho-associated kinase in the transcellular invasion of tumor cells. *Nat Med* **5**(2): 221-5.
- Iwamura, M., P. A. Abrahamsson, K. A. Foss, G. Wu, A. T. Cockett and L. J. Deftos (1994). Parathyroid hormone-related protein: a potential autocrine growth regulator in human prostate cancer cell lines. *Urology* **43**(5): 675-9.
- Jaworski, Z. F., B. Duck and G. Sekaly (1981). Kinetics of osteoclasts and their nuclei in evolving secondary Haversian systems. *J Anat* **133**(Pt 3): 397-405.
- Jemal, A., R. Siegel, E. Ward, Y. Hao, J. Xu and M. J. Thun (2009). Cancer statistics, 2009. *CA Cancer J Clin* **59**(4): 225-49.
- Jiang, W. G., G. Davies, T. A. Martin, C. Parr, G. Watkins, M. D. Mason, K. Mokbel and R. E. Mansel (2005). Targeting matrilysin and its impact on tumor growth in vivo: the potential implications in breast cancer therapy. *Clin Cancer Res* **11**(16): 6012-9.

- Jiang, W. G., T. A. Martin, K. Matsumoto, T. Nakamura and R. E. Mansel (1999). Hepatocyte growth factor/scatter factor decreases the expression of occludin and transendothelial resistance (TER) and increases paracellular permeability in human vascular endothelial cells. *J Cell Physiol* **181**(2): 319-29.
- Jiang, W. G., S. Hiscox, S. K. Singhrao, T. Nakamura, M. C. Puntis and M. B. Hallett (1995). Inhibition of HGF/SF-induced membrane ruffling and cell motility by transient elevation of cytosolic free Ca²⁺. *Exp Cell Res*. **220**(2):424-433.
- Jinnin, M., H. Inn, and K. Tamaki (2006). Characterization of SIS3, a Novel Specific Inhibitor of Smad3, and Its Effect on Transforming Growth Factor- β -Induced Extracellular Matrix Expression. *Mol Pharmacol* **69**(2): 597-607.
- Johnen, H., S. Lin, T. Kuffner, D. A. Brown, V. W. Tsai, A. R. Bauskin, L. Wu, G. Pankhurst, L. Jiang, S. Junankar, M. Hunter, W. D. Fairlie, N. J. Lee, R. F. Enriquez, P. A. Baldock, E. Corey, F. S. Apple, M. M. Murakami, E. J. Lin, C. Wang, M. J. During, A. Sainsbury, H. Herzog and S. N. Breit (2007). Tumor-induced anorexia and weight loss are mediated by the TGF-beta superfamily cytokine MIC-1. *Nat Med* **13**(11): 1333-40.
- Jonsson, B. A., H. O. Adami, M. Hagglund, A. Bergh, I. Goransson, P. Stattin, F. Wiklund and H. Gronberg (2004). -160C/A polymorphism in the E-cadherin gene promoter and risk of hereditary, familial and sporadic prostate cancer. *Int J Cancer* **109**(3): 348-52.
- Kaarbo, M., T. I. Klok and F. Saatcioglu (2007). Androgen signaling and its interactions with other signaling pathways in prostate cancer. *Bioessays* **29**(12): 1227-38.
- Kajita, M., K. N. McClinic and P. A. Wade (2004). Aberrant expression of the transcription factors snail and slug alters the response to genotoxic stress. *Mol Cell Biol* **24**(17): 7559-66.
- Takechi, Y., T. Segawa, X. X. Wu, P. Kulkarni, R. Dhir and R. H. Getzenberg (2004). Down-regulation of macrophage inhibitory cytokine-1/prostate derived factor in benign prostatic hyperplasia. *Prostate* **59**(4): 351-6.

- Kang, H. Y., K. E. Huang, S. Y. Chang, W. L. Ma, W. J. Lin and C. Chang (2002). Differential modulation of androgen receptor-mediated transactivation by Smad3 and tumor suppressor Smad4. *J Biol Chem* **277**(46): 43749-56.
- Kang, M. H., J. S. Kim, J. E. Seo, S. C. Oh and Y. A. Yoo BMP2 accelerates the motility and invasiveness of gastric cancer cells via activation of the phosphatidylinositol 3-kinase (PI3K)/Akt pathway. *Exp Cell Res* **316**(1): 24-37.
- Keeton, M. R., S. A. Curriden, A. J. van Zonneveld and D. J. Loskutoff (1991). Identification of regulatory sequences in the type 1 plasminogen activator inhibitor gene responsive to transforming growth factor beta. *J Biol Chem* **266**(34): 23048-52.
- Khanna, C., X. Wan, S. Bose, R. Cassaday, O. Olomu, A. Mendoza, C. Yeung, R. Gorlick, S. M. Hewitt and L. J. Helman (2004). The membrane-cytoskeleton linker ezrin is necessary for osteosarcoma metastasis. *Nat Med* **10**(2): 182-6.
- Khosla, S. (2001). Minireview: the OPG/RANKL/RANK system. *Endocrinology* **142**(12): 5050-5.
- Kim, I. Y., D. H. Lee, H. J. Ahn, H. Tokunaga, W. Song, L. M. Devereaux, D. Jin, T. K. Sampath and R. A. Morton (2000). Expression of bone morphogenetic protein receptors type-IA, -IB and -II correlates with tumor grade in human prostate cancer tissues. *Cancer Res* **60**(11): 2840-4.
- Kim, I. Y., D. H. Lee, D. K. Lee, H. J. Ahn, M. M. Kim, S. J. Kim and R. A. Morton (2004). Loss of expression of bone morphogenetic protein receptor type II in human prostate cancer cells. *Oncogene* **23**(46): 7651-9.
- Kim, M. S., C. J. Day, C. I. Selinger, C. L. Magno, S. R. Stephens and N. A. Morrison (2006). MCP-1-induced human osteoclast-like cells are tartrate-resistant acid phosphatase, NFATc1, and calcitonin receptor-positive but require receptor activator of NFkappaB ligand for bone resorption. *J Biol Chem* **281**(2): 1274-85.

- Kimura, N., R. Matsuo, H. Shibuya, K. Nakashima and T. Taga (2000). BMP2-induced apoptosis is mediated by activation of the TAK1-p38 kinase pathway that is negatively regulated by Smad6. *J Biol Chem* 275(23): 17647-52.
- Kingsley, D. M. (1994). The TGF-beta superfamily: new members, new receptors, and new genetic tests of function in different organisms. *Genes Dev* 8(2): 133-46.
- Kirby R.S., J.M. Fitzpatrick., and J Irani (2009). Prostate cancer diagnosis in the new millennium: strengths and weaknesses of prostate-specific antigen and the discovery and clinical evaluation of prostate cancer gene 3 (PCA3). *BJU Int* 103(4): 441-5.
- Kirsch, T., W. Sebald and M. K. Dreyer (2000). Crystal structure of the BMP-2-BRIA ectodomain complex. *Nat Struct Biol* 7(6): 492-6.
- Koenig, B. B., J. S. Cook, D. H. Wolsing, J. Ting, J. P. Tiesman, P. E. Correa, C. A. Olson, A. L. Pecquet, F. Ventura, R. A. Grant and et al. (1994). Characterization and cloning of a receptor for BMP-2 and BMP-4 from NIH 3T3 cells. *Mol Cell Biol* 14(9): 5961-74.
- Koinuma, D., M. Shinozaki, A. Komuro, K. Goto, M. Saitoh, A. Hanyu, M. Ebina, T. Nukiwa, K. Miyazawa, T. Imamura and K. Miyazono (2003). Arkadia amplifies TGF-beta superfamily signalling through degradation of Smad7. *EMBO J* 22(24): 6458-70.
- Koutsilieris, M. and C. Polychronakos (1992). Proteinolytic activity against IGF-binding proteins involved in the paracrine interactions between prostate adenocarcinoma cells and osteoblasts. *Anticancer Res* 12(3): 905-10.
- Kretschmar, M., J. Doody and J. Massague (1997). Opposing BMP and EGF signalling pathways converge on the TGF-beta family mediator Smad1. *Nature* 389: 618-22.
- Kretschmar, M., J. Doody, I. Timokhina and J. Massague (1999). A mechanism of repression of TGFbeta/ Smad signaling by oncogenic Ras. *Genes Dev* 13(7): 804-16.
- Kurisaki, K., A. Kurisaki, U. Valcourt, A. A. Terentiev, K. Pardali, P. Ten Dijke, C. H. Heldin, J. Ericsson and A. Moustakas (2003). Nuclear factor YY1 inhibits transforming growth

- factor beta- and bone morphogenetic protein-induced cell differentiation. *Mol Cell Biol* **23**(13): 4494-510.
- Kusanagi, K., H. Inoue, Y. Ishidou, H. K. Mishima, M. Kawabata and K. Miyazono (2000). Characterization of a bone morphogenetic protein-responsive Smad-binding element. *Mol Biol Cell* **11**(2): 555-65.
- Kyprianou, N., H. F. English and J. T. Isaacs (1990). Programmed cell death during regression of PC-82 human prostate cancer following androgen ablation. *Cancer Res* **50**(12): 3748-53.
- Labrie, F., A. Dupont, A. Belanger, L. Cusan, Y. Lacourciere, G. Monfette, J. G. Laberge, J. P. Emond, A. T. Fazekas, J. P. Raynaud and J. M. Husson (1982). New hormonal therapy in prostatic carcinoma: combined treatment with an LHRH agonist and an antiandrogen. *Clin Invest Med* **5**(4): 267-75.
- Lacey, D. L., E. Timms, H. L. Tan, M. J. Kelley, C. R. Dunstan, T. Burgess, R. Elliott, A. Colombero, G. Elliott, S. Scully, H. Hsu, J. Sullivan, N. Hawkins, E. Davy, C. Capparelli, A. Eli, Y. X. Qian, S. Kaufman, I. Sarosi, V. Shalhoub, G. Senaldi, J. Guo, J. Delaney and W. J. Boyle (1998). Osteoprotegerin ligand is a cytokine that regulates osteoclast differentiation and activation. *Cell* **93**(2): 165-76.
- Lai, T. H., Y. C. Fong, W. M. Fu, R. S. Yang and C. H. Tang (2008). Osteoblasts-derived BMP-2 enhances the motility of prostate cancer cells via activation of integrins. *Prostate* **68**(12): 1341-53.
- Lee, S. K. and J. A. Lorenzo (1999). Parathyroid hormone stimulates TRANCE and inhibits osteoprotegerin messenger ribonucleic acid expression in murine bone marrow cultures: correlation with osteoclast-like cell formation. *Endocrinology* **140**(8): 3552-61.
- Lee, S. W., S. I. Han, H. H. Kim and Z. H. Lee (2002). TAK1-dependent activation of AP-1 and c-Jun N-terminal kinase by receptor activator of NF-kappaB. *J Biochem Mol Biol* **35**(4): 371-6.

- Lee, Y., E. Schwarz, M. Davies, M. Jo, J. Gates, J. Wu, X. Zhang and J. R. Lieberman (2003). Differences in the cytokine profiles associated with prostate cancer cell induced osteoblastic and osteolytic lesions in bone. *J Orthop Res* **21**(1): 62-72.
- Lee-Hoeflich. S.T., C.G. Causing, M. Podkowa, X. Zhao, J.L. Wrana, and L. Attisano (2004). Activation of LIMK1 by binding to the BMP receptor, BMPRII, regulates BMP-dependent dendritogenesis. *EMBO J* **23**(24): 4792-801.
- Liao, W. X., R. K. Moore, F. Otsuka and S. Shimasaki (2003). Effect of intracellular interactions on the processing and secretion of bone morphogenetic protein-15 (BMP-15) and growth and differentiation factor-9. Implication of the aberrant ovarian phenotype of BMP-15 mutant sheep. *J Biol Chem* **278**(6): 3713-9.
- Lin, D. W. (2009). Beyond PSA: utility of novel tumor markers in the setting of elevated PSA. *Urol Oncol* **27**(3): 315-21.
- Ling, M. T., X. Wang, X. Zhang and Y. C. Wong (2006). The multiple roles of Id-1 in cancer progression. *Differentiation* **74**(9-10): 481-7.
- Littrup, P. J. and A. C. Goodman (1994). Costs and benefits of prostate cancer screening. Investigators of the American Cancer Society--National Prostate Cancer Detection Project. *In Vivo* **8**(3): 423-7.
- Liu, F., F. Ventura, J. Doody and J. Massague (1995). Human type II receptor for bone morphogenic proteins (BMPs): extension of the two-kinase receptor model to the BMPs. *Mol Cell Biol* **15**(7): 3479-86.
- Liu, J. and A. Lin (2005). Role of JNK activation in apoptosis: a double-edged sword. *Cell Res* **15**(1): 36-42.
- Lo, R.S., Y.G. Chen. Y. Shi, N.P. Pavletich, and J. Massague (1998). The L3 loop: a structural motif determining specific interactions between SMAD proteins and TGF- β receptors. *The Embo Journal* **17**(4): 996-1005.

- Loeb, S. and W. J. Catalona (2008). What to do with an abnormal PSA test. *Oncologist* **13**(3): 299-305.
- Lokeshwar, B. L., M. G. Selzer, N. L. Block and Z. Gunja-Smith (1993). Secretion of matrix metalloproteinases and their inhibitors (tissue inhibitor of metalloproteinases) by human prostate in explant cultures: reduced tissue inhibitor of metalloproteinase secretion by malignant tissues. *Cancer Res* **53**(19): 4493-8.
- Long, R. M., C. Morrissey, J. M. Fitzpatrick and R. W. Watson (2005). Prostate epithelial cell differentiation and its relevance to the understanding of prostate cancer therapies. *Clin Sci (Lond)* **108**(1): 1-11.
- Lopez-Coviella, I., T. M. Mellott, V. P. Kovacheva, B. Berse, B. E. Slack, V. Zemelko, A. Schnitzler and J. K. Blusztajn (2006). Developmental pattern of expression of BMP receptors and Smads and activation of Smad1 and Smad5 by BMP9 in mouse basal forebrain. *Brain Res* **1088**(1): 49-56.
- Ma, L. L., W. J. Sun, Z. Wang, G. Y. Zh, P. Li and S. B. Fu (2006). Effects of silencing of mutant p53 gene in human lung adenocarcinoma cell line Anip973. *J Exp Clin Cancer Res* **25**(4): 585-92.
- Mace, P. D., J. F. Cutfield and S. M. Cutfield (2006). High resolution structures of the bone morphogenetic protein type II receptor in two crystal forms: implications for ligand binding. *Biochem Biophys Res Commun* **351**(4): 831-8.
- Mailhot, G., M. Yang, A. Mason-Savas, C. A. Mackay, I. Leav and P. R. Odgren (2008). BMP-5 expression increases during chondrocyte differentiation in vivo and in vitro and promotes proliferation and cartilage matrix synthesis in primary chondrocyte cultures. *J Cell Physiol* **214**(1): 56-64.
- Manolagas, S. C. and R. L. Jilka (1995). Bone marrow, cytokines, and bone remodeling. Emerging insights into the pathophysiology of osteoporosis. *N Engl J Med* **332**(5): 305-11.

- Massague, J., L. Attisano and J. L. Wrana (1994). The TGF-beta family and its composite receptors. *Trends Cell Biol* **4**(5): 172-8.
- Massague, J., S. W. Blain and R. S. Lo (2000). TGFbeta signaling in growth control, cancer, and heritable disorders. *Cell* **103**(2): 295-309.
- Massague, J. and Y. G. Chen (2000). Controlling TGF-beta signaling. *Genes Dev* **14**(6): 627-44.
- Masuda, H., Y. Fukabori, K. Nakano, Y. Takezawa, C. S. T and H. Yamanaka (2003). Increased expression of bone morphogenetic protein-7 in bone metastatic prostate cancer. *Prostate* **54**(4): 268-74.
- Mateyak, M. K., A. J. Obaya and J. M. Sedivy (1999). c-Myc regulates cyclin D-Cdk4 and -Cdk6 activity but affects cell cycle progression at multiple independent points. *Mol Cell Biol* **19**(7): 4672-83.
- Mazerbourg, S. and A. J. Hsueh (2006). Genomic analyses facilitate identification of receptors and signalling pathways for growth differentiation factor 9 and related orphan bone morphogenetic protein/growth differentiation factor ligands. *Hum Reprod Update* **12**(4): 373-83.
- Mazerbourg, S., C. Klein, J. Roh, N. Kaivo-Oja, D. G. Mottershead, O. Korchynskiy, O. Ritvos and A. J. Hsueh (2004). Growth differentiation factor-9 signaling is mediated by the type I receptor, activin receptor-like kinase 5. *Mol Endocrinol* **18**(3): 653-65.
- Mazerbourg, S., K. Sangkuhl, C. W. Luo, S. Sudo, C. Klein and A. J. Hsueh (2005). Identification of receptors and signaling pathways for orphan bone morphogenetic protein/growth differentiation factor ligands based on genomic analyses. *J Biol Chem* **280**(37): 32122-32.
- McIntosh, C.J., S. Lun, S. Lawrence, K.P. McNatty, and J.L. Juengel (2008). The Proregion of mBMP15 Regulates the Cooperative Interactions of BMP15 and GDF9. *Biol Reprod* **79**(5): 889-96.

- McNeal, J. E. (1981). The zonal anatomy of the prostate. *Prostate* **2**(1): 35-49.
- McNeal, J. E. (1984). Anatomy of the prostate and morphogenesis of BPH. *Prog Clin Biol Res* **145**: 27-53.
- McNeal, J. E. (1988). Normal histology of the prostate. *Am J Surg Pathol* **12**(8): 619-33.
- McNeal, J. E. (1997). Prostate cancer volume. *Am J Surg Pathol* **21**(11): 1392-3.
- McNeal, J. E., D. G. Bostwick, R. A. Kindrachuk, E. A. Redwine, F. S. Freiha and T. A. Stamey (1986). Patterns of progression in prostate cancer. *Lancet* **1**: 60-3.
- McPherron, A. C. and S. J. Lee (1993). GDF-3 and GDF-9: two new members of the transforming growth factor-beta superfamily containing a novel pattern of cysteines. *J Biol Chem* **268**(5): 3444-9.
- McWilliam, L. J., C. Manson and N. J. George (1997). Neuroendocrine differentiation and prognosis in prostatic adenocarcinoma. *Br J Urol* **80**(2): 287-90.
- Mebratu, Y. and Y. Tesfaigzi (2009). How ERK1/2 activation controls cell proliferation and cell death: Is subcellular localization the answer? *Cell Cycle* **8**(8): 1168-75.
- Millin, T., C. L. Macalister and P. M. Kelly (1949). Retropubic prostatectomy; experiences based on 757 cases. *Lancet* **1**: 381-5.
- Mitra A., C. Fisher, C.S. Foster, C. Jameson, Y. Barbachanno, J. Bartlett, E. Bancroft, R. Doherty, Z. Kote-Zarai, S. Peock, D. Easton; IMPACT and EMBRACE Collaborators, and R. Eeles (2008). Prostate cancer in male BRCA1 and BRCA2 mutation carriers has a more aggressive phenotype. *Br J Cancer* **98**(2): 502-7.
- Mitra, S. K., D. A. Hanson and D. D. Schlaepfer (2005). Focal adhesion kinase: in command and control of cell motility. *Nat Rev Mol Cell Biol* **6**(1): 56-68.
- Miyazaki, H., T. Watabe, T. Kitamura and K. Miyazono (2004). BMP signals inhibit proliferation and in vivo tumor growth of androgen-insensitive prostate carcinoma cells. *Oncogene* **23**(58): 9326-35.
- Miyazawa, K., M. Shinozaki, T. Hara, T. Furuya and K. Miyazono (2002). Two major Smad pathways in TGF-beta superfamily signalling. *Genes Cells* **7**(12): 1191-204.

- Miyazono, K., S. Maeda and T. Imamura (2004). Coordinate regulation of cell growth and differentiation by TGF-beta superfamily and Runx proteins. *Oncogene* **23**(24): 4232-7.
- Miyazono, K., P. ten Dijke and C. H. Heldin (2000). TGF-beta signaling by Smad proteins. *Adv Immunol* **75**: 115-57.
- Miyazono, K.P. (2000). Positive and negative regulation of TGF- β signaling. *J Cell Sci* **113**(Pt 7): 1101-9.
- Moore, R. K., F. Otsuka and S. Shimasaki (2003). Molecular basis of bone morphogenetic protein-15 signaling in granulosa cells. *J Biol Chem* **278**(1): 304-10.
- Mori, S., K. Matsuzaki, K. Yoshida, F. Furukawa, Y. Tahashi, H. Yamagata, G. Sekimoto, T. Seki, H. Matsui, M. Nishizawa, J. Fujisawa and K. Okazaki (2004). TGF-beta and HGF transmit the signals through JNK-dependent Smad2/3 phosphorylation at the linker regions. *Oncogene* **23**(44): 7416-29.
- Moustakas, A., S. Souchelnytskyi and C. H. Heldin (2001). Smad regulation in TGF-beta signal transduction. *J Cell Sci* **114**(Pt 24): 4359-69.
- Moustakas, A., and C.H. Heldin (2009). The regulation of TGF- β signal transduction. *Development* **136**(22): 3699-714.
- Mundy, G. R. (1997). Mechanisms of bone metastasis. *Cancer* **80**(8 Suppl): 1546-56.
- Mundy, G. R. (2002). Metastasis to bone: causes, consequences and therapeutic opportunities. *Nat Rev Cancer* **2**(8): 584-93.
- Nagle, R. B., J. D. Knox, C. Wolf, G. T. Bowden and A. E. Cress (1994). Adhesion molecules, extracellular matrix, and proteases in prostate carcinoma. *J Cell Biochem Suppl* **19**: 232-7.
- Nakagawa, T., J. H. Li, G. Garcia, W. Mu, E. Piek, E. P. Bottinger, Y. Chen, H. J. Zhu, D. H. Kang, G. F. Schreiner, H. Y. Lan and R. J. Johnson (2004). TGF-beta induces proangiogenic and antiangiogenic factors via parallel but distinct Smad pathways. *Kidney Int* **66**(2): 605-13.

- Nakashima, K., M. Yanagisawa, H. Arakawa, N. Kimura, T. Hisatsune, M. Kawabata, K. Miyazono and T. Taga (1999). Synergistic signaling in fetal brain by STAT3-Smad1 complex bridged by p300. *Science* **284**: 479-82.
- Narain, V., M. L. Cher and D. P. Wood, Jr. (2002). Prostate cancer diagnosis, staging and survival. *Cancer Metastasis Rev* **21**(1): 17-27.
- Nguyen, D. X., P. D. Bos and J. Massague (2009). Metastasis: from dissemination to organ-specific colonization. *Nat Rev Cancer* **9**(4): 274-84.
- Nicholls, A., K. A. Sharp and B. Honig (1991). Protein folding and association: insights from the interfacial and thermodynamic properties of hydrocarbons. *Proteins* **11**(4): 281-96.
- Nishita, M., M. K. Hashimoto, S. Ogata, M. N. Laurent, N. Ueno, H. Shibuya and K. W. Cho (2000). Interaction between Wnt and TGF-beta signalling pathways during formation of Spemann's organizer. *Nature* **403**: 781-5.
- Nohe, A., S. Hassel, M. Ehrlich, F. Neubauer, W. Sebald, Y. I. Henis and P. Knaus (2002). The mode of bone morphogenetic protein (BMP) receptor oligomerization determines different BMP-2 signaling pathways. *J Biol Chem* **277**(7): 5330-8.
- Nohe, A., E. Keating, P. Knaus and N. O. Petersen (2004). Signal transduction of bone morphogenetic protein receptors. *Cell Signal* **16**(3): 291-9.
- Oh, S. P., C. Y. Yeo, Y. Lee, H. Schrewe, M. Whitman and E. Li (2002). Activin type IIA and IIB receptors mediate Gdf11 signaling in axial vertebral patterning. *Genes Dev* **16**(21): 2749-54.
- Olson, W. C., W. D. Heston and A. K. Rajasekaran (2007). Clinical trials of cancer therapies targeting prostate-specific membrane antigen. *Rev Recent Clin Trials* **2**(3): 182-90.
- Onichtchouk, D., Y. G. Chen, R. Dosch, V. Gawantka, H. Delius, J. Massague and C. Niehrs (1999). Silencing of TGF-beta signalling by the pseudoreceptor BAMBI. *Nature* **401**: 480-5.

- Orisaka, M., S. Orisaka, J. Y. Jiang, J. Craig, Y. Wang, F. Kotsuji and B. K. Tsang (2006). Growth differentiation factor 9 is antiapoptotic during follicular development from preantral to early antral stage. *Mol Endocrinol* **20**(10): 2456-68.
- Orr, F. W., O. H. Sanchez-Sweetman, P. Kostenuik and G. Singh (1995). Tumor-bone interactions in skeletal metastasis. *Clin Orthop Relat Res* (312): 19-33.
- Oxford, G., and D. Theodorescu (2003). Ras superfamily monomeric G proteins in carcinoma cell motility. *Cancer Lett* **189**(2): 117-28.
- Paget, S. (1989). The distribution of secondary growths in cancer of the breast. 1889. *Cancer Metastasis Rev* **8**(2): 98-101.
- Paku, S., B. Dome, R. Toth and J. Timar (2000). Organ-specificity of the extravasation process: an ultrastructural study. *Clin Exp Metastasis* **18**(6): 481-92.
- Palapattu, G. S., S. Sutcliffe, P. J. Bastian, E. A. Platz, A. M. De Marzo, W. B. Isaacs and W. G. Nelson (2005). Prostate carcinogenesis and inflammation: emerging insights. *Carcinogenesis* **26**(7): 1170-81.
- Pardali, K., and A. Moustakas (2007). Actions of TGF-beta as tumor suppressor and pro-metastatic factor in human cancer. *Biochim Biophys Acta* **1775**(1): 21-62.
- Pera, E. M., A. Ikeda, E. Eivers and E. M. De Robertis (2003). Integration of IGF, FGF, and anti-BMP signals via Smad1 phosphorylation in neural induction. *Genes Dev* **17**(24): 3023-8.
- Perez, C. A., G. E. Hanks, S. A. Leibel, A. L. Zietman, Z. Fuks and W. R. Lee (1993). Localized carcinoma of the prostate (stages T1B, T1C, T2, and T3). Review of management with external beam radiation therapy. *Cancer* **72**(11): 3156-73.
- Raida, M., J. H. Clement, K. Ameri, C. Han, R. D. Leek and A. L. Harris (2005). Expression of bone morphogenetic protein 2 in breast cancer cells inhibits hypoxic cell death. *Int J Oncol* **26**(6): 1465-70.
- Rattan, R., S. Giri, A. K. Singh and I. Singh (2006). Rho/ROCK pathway as a target of tumor therapy. *J Neurosci Res* **83**(2): 243-55.

- Rebbapragada, A., H. Benchabane, J. L. Wrana, A. J. Celeste and L. Attisano (2003). Myostatin signals through a transforming growth factor beta-like signaling pathway to block adipogenesis. *Mol Cell Biol* **23**(20): 7230-42.
- Regazzoni, C., K. H. Winterhalter and L. Rohrer (2001). Type I collagen induces expression of bone morphogenetic protein receptor type II. *Biochem Biophys Res Commun* **283**(2): 316-22.
- Richie, J. P., W. J. Catalona, F. R. Ahmann, M. A. Hudson, P. T. Scardino, R. C. Flanigan, J. B. deKernion, T. L. Ratliff, L. R. Kavoussi, B. L. Dalkin and et al. (1993). Effect of patient age on early detection of prostate cancer with serum prostate-specific antigen and digital rectal examination. *Urology* **42**(4): 365-74.
- Rifkin, D.B. (2005). Latent transforming growth factor- β (TGF- β) binding proteins: orchestrators of TGF- β availability. *J Biol Chem* **280**(9): 7409-412.
- Fro, T. B., R. U. Holt, A. T. Brenne, H. Hjorth-Hansen, A. Waage, O. Hjertner, A. Sundan, and M. Borset (2004). Bone morphogenetic protein-5, -6 and -7 inhibit growth and induce apoptosis in human myeloma cells. *Oncogene* **23**(17): 3024-32.
- Robson, M. and N. Dawson (1996). How is androgen-dependent metastatic prostate cancer best treated? *Hematol Oncol Clin North Am* **10**(3): 727-47.
- Rosen, E. M., L. Meromsky, E. Setter, D. W. Vinter and I. D. Goldberg (1990). Smooth muscle-derived factor stimulates mobility of human tumor cells. *Invasion Metastasis*. **10**(1):49-64.
- Sahai, E., and C. J. Marshall (2002). RHO-GTPases and cancer. *Nat Rev Cancer* **2**(2): 133-42.
- Sakabe, M., H. Sakata, H. Matsui, K. Ikeda, T. Yamagishi and Y. Nakajima (2008). ROCK1 expression is regulated by TGFbeta3 and ALK2 during valvuloseptal endocardial cushion formation. *Anat Rec (Hoboken)* **291**(7): 845-57.
- Sano, Y., J. Harada, S. Tashiro, R. Gotoh-Mandeville, T. Maekawa and S. Ishii (1999). ATF-2 is a common nuclear target of Smad and TAK1 pathways in transforming growth factor-beta signaling. *J Biol Chem* **274**(13): 8949-57.

- Schally, A. V., A. M. Comaru-Schally, A. Plonowski, A. Nagy, G. Halmos and Z. Rekasi (2000). Peptide analogs in the therapy of prostate cancer. *Prostate* **45**(2): 158-66.
- Scharpfenecker, M., M. van Dinther, Z. Liu, R. L. van Bezooijen, Q. Zhao, L. Pukac, C. W. Lowik and P. ten Dijke (2007). BMP-9 signals via ALK1 and inhibits bFGF-induced endothelial cell proliferation and VEGF-stimulated angiogenesis. *J Cell Sci* **120**(Pt 6): 964-72.
- Scher, H. I., W. M. Kelly, Z. F. Zhang, P. Ouyang, M. Sun, M. Schwartz, C. Ding, W. Wang, I. D. Horak and A. B. Kremer (1999). Post-therapy serum prostate-specific antigen level and survival in patients with androgen-independent prostate cancer. *J Natl Cancer Inst* **91**(3): 244-51.
- Scher, H. I., A. Sarkis, V. Reuter, D. Cohen, G. Netto, D. Petrylak, P. Lianes, Z. Fuks, J. Mendelsohn and C. Cordon-Cardo (1995). Changing pattern of expression of the epidermal growth factor receptor and transforming growth factor alpha in the progression of prostatic neoplasms. *Clin Cancer Res* **1**(5): 545-50.
- Schmierer, B. and C. S. Hill (2007). TGFbeta-SMAD signal transduction: molecular specificity and functional flexibility. *Nat Rev Mol Cell Biol* **8**(12): 970-82.
- Sequeira, L., C. W. Dubyk, T. A. Riesenberger, C. R. Cooper and K. L. van Golen (2008). Rho GTPases in PC-3 prostate cancer cell morphology, invasion and tumor cell diapedesis. *Clin Exp Metastasis* **25**(5): 569-79.
- Sherr, C. J. (1996). Cancer cell cycles. *Science* **274**: 1672-7.
- Shi, Y., Y. F. Wang, L. Jayaraman, H. Yang, J. Massague and N. P. Pavletich (1998). Crystal structure of a Smad MH1 domain bound to DNA: insights on DNA binding in TGF-beta signaling. *Cell* **94**(5): 585-94.
- Shibuya, H., K. Yamaguchi, K. Shirakabe, A. Tonegawa, Y. Gotoh, N. Ueno, K. Irie, E. Nishida and K. Matsumoto (1996). TAB1: an activator of the TAK1-MAPKKK in TGF-beta signal transduction. *Science* **272**: 1179-82.

- Shintani, M., A. Okazaki, T. Masuda, M. Kawada, M. Ishizuka, Y. Doki, I. B. Weinstein and M. Imoto (2002). Overexpression of cyclin D1 contributes to malignant properties of esophageal tumor cells by increasing VEGF production and decreasing Fas expression. *Anticancer Res* **22**(2A): 639-47.
- Shirakabe, K., K. Yamaguchi, H. Shibuya, K. Irie, S. Matsuda, T. Moriguchi, Y. Gotoh, K. Matsumoto and E. Nishida (1997). TAK1 mediates the ceramide signaling to stress-activated protein kinase/c-Jun N-terminal kinase. *J Biol Chem* **272**(13): 8141-4.
- Shweiki, D., A. Itin, D. Soffer and E. Keshet (1992). Vascular endothelial growth factor induced by hypoxia may mediate hypoxia-initiated angiogenesis. *Nature* **359**: 843-5.
- Sims, N. A. and J. H. Gooi (2008). Bone remodeling: Multiple cellular interactions required for coupling of bone formation and resorption. *Semin Cell Dev Biol* **19**(5): 444-51.
- Slee, E. A., C. Adrain and S. J. Martin (2001). Executioner caspase-3, -6, and -7 perform distinct, non-redundant roles during the demolition phase of apoptosis. *J Biol Chem* **276**(10): 7320-6.
- Smith, J. A., Jr., R. C. Chan, S. S. Chang, S. D. Herrell, P. E. Clark, R. Baumgartner and M. S. Cookson (2007). A comparison of the incidence and location of positive surgical margins in robotic assisted laparoscopic radical prostatectomy and open retropubic radical prostatectomy. *J Urol* **178**(6): 2385-9; discussion 2389-90.
- Sotobori, T., T. Ueda, A. Myoui, K. Yoshioka, M. Nakasaki, H. Yoshikawa and K. Itoh (2006). Bone morphogenetic protein-2 promotes the haptotactic migration of murine osteoblastic and osteosarcoma cells by enhancing incorporation of integrin beta1 into lipid rafts. *Exp Cell Res* **312**(19): 3927-38.
- Stover, D.G., B. Bierie, and H.L. Moses (2007) A delicate balance: TGF-beta and the tumor microenvironment. *J Cell Biochem* **101**(4): 851-61.
- Su, Y. Q., K. Sugiura, K. Wigglesworth, M. J. O'Brien, J. P. Affourtit, S. A. Pangas, M. M. Matzuk and J. J. Eppig (2008). Oocyte regulation of metabolic cooperativity between

mouse cumulus cells and oocytes: BMP15 and GDF-9 control cholesterol biosynthesis in cumulus cells. *Development* **135**(1): 111-21.

Sun, H. W., S. L. Tong, J. He, Q. Wang, L. Zou, S. J. Ma, H. Y. Tan, J. F. Luo and H. X. Wu (2007). RhoA and RhoC -siRNA inhibit the proliferation and invasiveness activity of human gastric carcinoma by Rho/PI3K/Akt pathway. *World J Gastroenterol* **13**(25): 3517-22.

Sung, S.Y., and L.W. Chung (2002). Prostate tumor-stroma interaction: molecular mechanisms and opportunities for therapeutic targeting. *Differentiation* **70**(9-10): 506-21.

Suwa, H., G. Ohshio, T. Imamura, G. Watanabe, S. Arii, M. Imamura, S. Narumiya, H. Hiai and M. Fukumoto (1998). Overexpression of the rhoC gene correlates with progression of ductal adenocarcinoma of the pancreas. *Br J Cancer* **77**(1): 147-52.

Suzawa, M., Y. Tamura, S. Fukumoto, K. Miyazono, T. Fujita, S. Kato and Y. Takeuchi (2002). Stimulation of Smad1 transcriptional activity by Ras-extracellular signal-regulated kinase pathway: a possible mechanism for collagen-dependent osteoblastic differentiation. *J Bone Miner Res* **17**(2): 240-8.

Taichman, R. S., C. Cooper, E. T. Keller, K. J. Pienta, N. S. Taichman and L. K. McCauley (2002). Use of the stromal cell-derived factor-1/CXCR4 pathway in prostate cancer metastasis to bone. *Cancer Res* **62**(6): 1832-7.

Takai, H., M. Kanematsu, K. Yano, E. Tsuda, K. Higashio, K. Ikeda, K. Watanabe and Y. Yamada (1998). Transforming growth factor-beta stimulates the production of osteoprotegerin/osteoclastogenesis inhibitory factor by bone marrow stromal cells. *J Biol Chem* **273**(42): 27091-6.

Tannock, I. F., D. Osoba, M. R. Stockler, D. S. Ernst, A. J. Neville, M. J. Moore, G. R. Armitage, J. J. Wilson, P. M. Venner, C. M. Coppin and K. C. Murphy (1996). Chemotherapy with mitoxantrone plus prednisone or prednisone alone for symptomatic

- hormone-resistant prostate cancer: a Canadian randomized trial with palliative end points. *J Clin Oncol* **14**(6): 1756-64.
- Tashiro, E., A. Tsuchiya and M. Imoto (2007). Functions of cyclin D1 as an oncogene and regulation of cyclin D1 expression. *Cancer Sci* **98**(5): 629-35.
- ten Dijke, P., H. Yamashita, H. Ichijo, P. Franzen, M. Laiho, K. Miyazono and C. H. Heldin (1994). Characterization of type I receptors for transforming growth factor-beta and activin. *Science* **264**: 101-4.
- Theriault, B. L., T. G. Shepherd, M. L. Mujoomdar and M. W. Nachtigal (2007). BMP4 induces EMT and Rho GTPase activation in human ovarian cancer cells. *Carcinogenesis* **28**(6): 1153-62.
- Thiery, J. P. (2002). Epithelial-mesenchymal transitions in tumour progression. *Nat Rev Cancer* **2**(6): 442-54.
- Thiery, J. P. and J. P. Sleeman (2006). Complex networks orchestrate epithelial-mesenchymal transitions. *Nat Rev Mol Cell Biol* **7**(2): 131-42.
- Thomas, R., W. A. Anderson, V. Raman and A. H. Reddi (1998). Androgen-dependent gene expression of bone morphogenetic protein 7 in mouse prostate. *Prostate* **37**(4): 236-45.
- Thompson, I. M., D. P. Ankerst, C. Chi, M. S. Lucia, P. J. Goodman, J. J. Crowley, H. L. Parnes and C. A. Coltman, Jr. (2005). Operating characteristics of prostate-specific antigen in men with an initial PSA level of 3.0 ng/ml or lower. *JAMA* **294**(1): 66-70.
- Tibaldi, E., G. Arrigoni, H.M. Martinez, K. Inagaki, S. Shimasaki and L.A. Pinna (2010). Golgi apparatus casein kinase phosphorylates bioactive Ser-6 of bone morphogenetic protein 15 and growth and differentiation factor 9. *FEBS letters* **584**(4): 801-5.
- Tolis, G., D. Ackman, A. Stellos, A. Mehta, F. Labrie, A. T. Fazekas, A. M. Comaru-Schally and A. V. Schally (1982). Tumor growth inhibition in patients with prostatic carcinoma treated with luteinizing hormone-releasing hormone agonists. *Proc Natl Acad Sci U S A* **79**(5): 1658-62.

- Tondravi, M. M., S. R. McKercher, K. Anderson, J. M. Erdmann, M. Quiroz, R. Maki and S. L. Teitelbaum (1997). Osteopetrosis in mice lacking haematopoietic transcription factor PU.1. *Nature* **386**: 81-4.
- Tsukazaki, T., T. A. Chiang, A. F. Davison, L. Attisano and J. L. Wrana (1998). SARA, a FYVE domain protein that recruits Smad2 to the TGFbeta receptor. *Cell* **95**(6): 779-91.
- Turner, C. E. (1998). Paxillin. *Int J Biochem Cell Biol* **30**(9): 955-9.
- Uhlenbeck, O. C. (1987). A small catalytic oligoribonucleotide. *Nature*. **328**:596-600.
- Ulloa, L., J. Doody and J. Massague (1999). Inhibition of transforming growth factor-beta/SMAD signalling by the interferon-gamma/STAT pathway. *Nature* **397**: 710-3.
- Valta, M. P., T. Hentunen, Q. Qu, E. M. Valve, A. Harjula, J. A. Seppanen, H. K. Vaananen and P. L. Harkonen (2006). Regulation of osteoblast differentiation: a novel function for fibroblast growth factor 8. *Endocrinology* **147**(5): 2171-82.
- van Golen, K. L., Z. F. Wu, X. T. Qiao, L. Bao and S. D. Merajver (2000). RhoC GTPase overexpression modulates induction of angiogenic factors in breast cells. *Neoplasia* **2**(5): 418-25.
- Varenhorst, E., L. Wallentin and K. Carlstrom (1982). The effects of orchidectomy, estrogens, and cyproterone acetate on plasma testosterone, LH, and FSH concentrations in patients with carcinoma of the prostate. *Scand J Urol Nephrol* **16**(1): 31-6.
- Vilchez-Martinez, J. A., E. Pedroza, A. Arimura and A. V. Schally (1979). Paradoxical effects of D-Trp6-luteinizing hormone-releasing hormone on the hypothalamic-pituitary-gonadal axis in immature female rats. *Fertil Steril* **31**(6): 677-82.
- Vinall, R. L., S. H. Lo and A. H. Reddi (2002). Regulation of articular chondrocyte phenotype by bone morphogenetic protein 7, interleukin 1, and cellular context is dependent on the cytoskeleton. *Exp Cell Res* **272**(1): 32-44.

- Vishnu, P. and W.W. Tan (2010). Update on options for treatment of metastatic castration-resistant prostate cancer. *Onco targets ther* **24**(3): 39-51.
- Vitt, U. A., M. Hayashi, C. Klein and A. J. Hsueh (2000). Growth differentiation factor-9 stimulates proliferation but suppresses the follicle-stimulating hormone-induced differentiation of cultured granulosa cells from small antral and preovulatory rat follicles. *Biol Reprod* **62**(2): 370-7.
- Voura, E. B., M. Sandig and C. H. Siu (1998). Cell-cell interactions during transendothelial migration of tumor cells. *Microsc Res Tech* **43**(3): 265-75.
- Ware, J. L. (1993). Growth factors and their receptors as determinants in the proliferation and metastasis of human prostate cancer. *Cancer Metastasis Rev* **12**(3-4): 287-301.
- Webb, D. J., K. Donais, L. A. Whitmore, S. M. Thomas, C. E. Turner, J. T. Parsons and A. F. Horwitz (2004). FAK-Src signalling through paxillin, ERK and MLCK regulates adhesion disassembly. *Nat Cell Biol* **6**(2): 154-61.
- Wells, C.M., T. Ahmed, J.R. Masters, and G.E. Jones (2005). Rho family GTPases are activated during HGF-stimulated prostate cancer-cell scattering. *Cell Motil Cytoskeleton* **62**(3): 180-94.
- Welsh, C. F., K. Roovers, J. Villanueva, Y. Liu, M. A. Schwartz and R. K. Assoian (2001). Timing of cyclin D1 expression within G1 phase is controlled by Rho. *Nat Cell Biol* **3**(11): 950-7.
- Whittemore, A. S., L. N. Kolonel, A. H. Wu, E. M. John, R. P. Gallagher, G. R. Howe, J. D. Burch, J. Hankin, D. M. Dreon, D. W. West and et al. (1995). Prostate cancer in relation to diet, physical activity, and body size in blacks, whites, and Asians in the United States and Canada. *J Natl Cancer Inst* **87**(9): 652-61.
- Wrana, J. L., L. Attisano, R. Wieser, F. Ventura and J. Massague (1994). Mechanism of activation of the TGF-beta receptor. *Nature* **370**: 341-7.

- Wrana, J. L., H. Tran, L. Attisano, K. Arora, S. R. Childs, J. Massague and M. B. O'Connor (1994). Two distinct transmembrane serine/threonine kinases from *Drosophila melanogaster* form an activin receptor complex. *Mol Cell Biol* **14**(2): 944-50.
- Wu, H., L. Sun, J. W. Moul, H. Y. Wu, D. G. McLeod, C. Amling, R. Lance, L. Kusuda, T. Donahue, J. Foley, A. Chung, W. Sexton and D. Soderdahl (2004). Watchful waiting and factors predictive of secondary treatment of localized prostate cancer. *J Urol* **171**(3): 1111-6.
- Wu, X., L. Chen, C. A. Brown, C. Yan and M. M. Matzuk (2004). Interrelationship of growth differentiation factor 9 and inhibin in early folliculogenesis and ovarian tumorigenesis in mice. *Mol Endocrinol* **18**(6): 1509-19.
- Wynder, E. L., K. Mabuchi and W. F. Whitmore, Jr. (1971). Epidemiology of cancer of the prostate. *Cancer* **28**(2): 344-60.
- Xu, J., T. R. Kimball, J. N. Lorenz, D. A. Brown, A. R. Bauskin, R. Klevitsky, T. E. Hewett, S. N. Breit and J. D. Molkentin (2006). GDF15/MIC-1 functions as a protective and antihypertrophic factor released from the myocardium in association with SMAD protein activation. *Circ Res* **98**(3): 342-50.
- Xu, J., S. Lamouille and R. Derynck (2009). TGF-beta-induced epithelial to mesenchymal transition. *Cell Res* **19**(2): 156-72.
- Yamaguchi, K., S. Nagai, J. Ninomiya-Tsuji, M. Nishita, K. Tamai, K. Irie, N. Ueno, E. Nishida, H. Shibuya and K. Matsumoto (1999). XIAP, a cellular member of the inhibitor of apoptosis protein family, links the receptors to TAB1-TAK1 in the BMP signaling pathway. *EMBO J* **18**(1): 179-87.
- Yamaguchi, K., K. Shirakabe, H. Shibuya, K. Irie, I. Oishi, N. Ueno, T. Taniguchi, E. Nishida and K. Matsumoto (1995). Identification of a member of the MAPKKK family as a potential mediator of TGF-beta signal transduction. *Science* **270**: 2008-11.
- Yamaji, N., A. J. Celeste, R. S. Thies, J. J. Song, S. M. Bernier, D. Goltzman, K. M. Lyons, J. Nove, V. Rosen and J. M. Wozney (1994). A mammalian serine/threonine kinase

- receptor specifically binds BMP-2 and BMP-4. *Biochem Biophys Res Commun* **205**(3): 1944-51.
- Yang, L., M. Butcher, R. R. Simon, S. L. Osip and S. G. Shaughnessy (2005). The effect of heparin on osteoblast differentiation and activity in primary cultures of bovine aortic smooth muscle cells. *Atherosclerosis* **179**(1): 79-86.
- Yang, S., M. Lim, L. K. Pham, S. E. Kendall, A. H. Reddi, D. C. Altieri and P. Roy-Burman (2006). Bone morphogenetic protein 7 protects prostate cancer cells from stress-induced apoptosis via both Smad and c-Jun NH2-terminal kinase pathways. *Cancer Res* **66**(8): 4285-90.
- Yang, S., C. Zhong, B. Frenkel, A. H. Reddi and P. Roy-Burman (2005). Diverse biological effect and Smad signaling of bone morphogenetic protein 7 in prostate tumor cells. *Cancer Res* **65**(13): 5769-77.
- Yang, X. B., H. I. Roach, N. M. Clarke, S. M. Howdle, R. Quirk, K. M. Shakesheff and R. O. Oreffo (2001). Human osteoprogenitor growth and differentiation on synthetic biodegradable structures after surface modification. *Bone* **29**(6): 523-31.
- Yao, H., E. J. Dashner, C. M. van Golen and K. L. van Golen (2006). RhoC GTPase is required for PC-3 prostate cancer cell invasion but not motility. *Oncogene* **25**(16): 2285-96.
- Ye, L., H. Kynaston and W. G. Jiang (2008). Bone morphogenetic protein-9 induces apoptosis in prostate cancer cells, the role of prostate apoptosis response-4. *Mol Cancer Res* **6**(10): 1594-606.
- Ye, L., H. Kynaston and W. G. Jiang (2009). Bone morphogenetic protein-10 suppresses the growth and aggressiveness of prostate cancer cells through a Smad independent pathway. *J Urol* **181**(6): 2749-59.
- Ye, L., J. M. Lewis-Russell, G. Davies, A. J. Sanders, H. Kynaston and W. G. Jiang (2007). Hepatocyte growth factor up-regulates the expression of the bone morphogenetic protein (BMP) receptors, BMPR-IB and BMPR-II, in human prostate cancer cells. *Int J Oncol* **30**(2): 521-9.

- Ye, L., J. M. Lewis-Russell, H. G. Kyanaston and W. G. Jiang (2007). Bone morphogenetic proteins and their receptor signaling in prostate cancer. *Histol Histopathol* **22**(10): 1129-47.
- Ye, L., J. M. Lewis-Russell, H. Kynaston and W. G. Jiang (2007). Endogenous bone morphogenetic protein-7 controls the motility of prostate cancer cells through regulation of bone morphogenetic protein antagonists. *J Urol* **178**(3 Pt 1): 1086-91.
- Ye, L., J. M. Lewis-Russell, A. J. Sanders, H. Kynaston and W. G. Jiang (2008). HGF/SF up-regulates the expression of bone morphogenetic protein 7 in prostate cancer cells. *Urol Oncol* **26**(2): 190-7.
- Yi, B., P. J. Williams, M. Niewolna, Y. Wang and T. Yoneda (2002). Tumor-derived platelet-derived growth factor-BB plays a critical role in osteosclerotic bone metastasis in an animal model of human breast cancer. *Cancer Res* **62**(3): 917-23.
- Yoshida, Y., S. Tanaka, H. Umemori, O. Minowa, M. Usui, N. Ikematsu, E. Hosoda, T. Imamura, J. Kuno, T. Yamashita, K. Miyazono, M. Noda, T. Noda and T. Yamamoto (2000). Negative regulation of BMP/Smad signaling by Tob in osteoblasts. *Cell* **103**(7): 1085-97.
- Zavadil, J. and E. P. Bottinger (2005). TGF-beta and epithelial-to-mesenchymal transitions. *Oncogene* **24**(37): 5764-74.
- Zeisberg, M., J. Hanai, H. Sugimoto, T. Mammoto, D. Charytan, F. Strutz and R. Kalluri (2003). BMP-7 counteracts TGF-beta1-induced epithelial-to-mesenchymal transition and reverses chronic renal injury. *Nat Med* **9**(7): 964-8.
- Zelefsky, M. J., H. Chan, M. Hunt, Y. Yamada, A. M. Shippy and H. Amols (2006). Long-term outcome of high dose intensity modulated radiation therapy for patients with clinically localized prostate cancer. *J Urol* **176**(4 Pt 1): 1415-9.
- Zeng, L., R. G. Rowland, S. M. Lele and N. Kyprianou (2004). Apoptosis incidence and protein expression of p53, TGF-beta receptor II, p27Kip1, and Smad4 in benign, premalignant, and malignant human prostate. *Hum Pathol* **35**(3): 290-7.

- Zhang, Y., C. Chang, D. J. Gehling, A. Hemmati-Brivanlou and R. Derynck (2001). Regulation of Smad degradation and activity by Smurf2, an E3 ubiquitin ligase. *Proc Natl Acad Sci U S A* **98**(3): 974-9.
- Zhao, G. Q., Y. X. Chen, X. M. Liu, Z. Xu and X. Qi (2001). Mutation in Bmp7 exacerbates the phenotype of Bmp8a mutants in spermatogenesis and epididymis. *Dev Biol* **240**(1): 212-22.
- Zhong, W. B., C. Y. Wang, T. C. Chang and W. S. Lee (2003). Lovastatin induces apoptosis of anaplastic thyroid cancer cells via inhibition of protein geranylgeranylation and de novo protein synthesis. *Endocrinology* **144**(9): 3852-9.
- Zhou, B., L. Chen, X. Wu, J. Wang, Y. Yin and G. Zhu (2008). MH1 domain of SMAD4 binds N-terminal residues of the homeodomain of Hoxc9. *Biochim Biophys Acta* **1784**(5): 747-52.
- Zhuang, Z., P. Jian, L. Longjiang, H. Bo and X. Wenlin (2010). Oral cancer cells with different potential of lymphatic metastasis displayed distinct biologic behaviors and gene expression profiles. *J Oral Pathol Med* **39**(2): 168-75.
- Zimmerman, C. M., M. S. Kariapper and L. S. Mathews (1998). Smad proteins physically interact with calmodulin. *J Biol Chem* **273**(2): 677-80.
- Zuker, M. (2003). Mfold web server for nucleic acid folding and hybridization prediction. *Nucleic Acids Res.* **31**(13):3406-3415.

Electronic references:

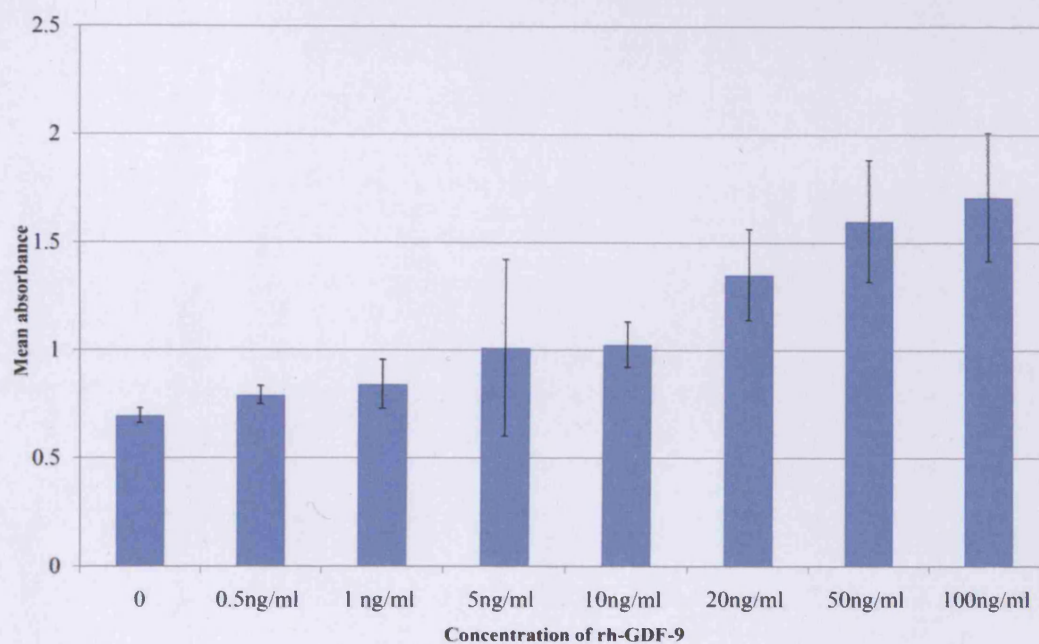
CR-UK 2007 - Prostate cancer mortality by age (2007)

(URL:<http://info.cancerresearchuk.org/cancerstats/types/prostate/mortality/>)

Simone Kaiser: Identification and Characterization of the Ion Channel TRPM8 in Prostate Cancer- Three categories of TNM stage.

(URL: <http://edoc.hu-berlin.de/dissertationen/kaiser-simone-2004-06-10/HTML/front.html>)

Appendix



	0 (n=3)	0.5ng/ml (n=3)	1ng/ml (n=3)	5ng/ml (n=3)	10ng/ml (n=3)	20ng/ml (n=3)	50ng/ml (n=3)	100ng/ml (n=3)
Mean	0.70	0.80	0.84	1.01	1.03	1.35	1.60	1.71
SD	0.04	0.04	0.11	0.41	0.11	0.21	0.28	0.30

Figure A1: Growth assay on PC-3 WT cells treated with varying concentrations of rh-GDF-9, following 4 days incubation. The cells were stained with crystal violet, and diluted with acetic acid before the absorption was measured using a spectrophotometer. The first concentration at which there was a statistically significant change in the absorbance and hence growth of the cells was 20ng/ml rh-GDF-9, $p=0.04$ compared to untreated control. 20ng/ml rh-GDF-9 was then selected as the concentration at which to treat the cells in all further functional assays. This data is representative of three independent repeats. Error bars represent standard deviation.